UNIVERSITY OF SOUTHAMPTON

Faculty of Environmental and Life Sciences

School of Biological Sciences

Elucidating the role of osteoblast-derived vascular endothelial growth factor in the regulation of bone development: Sexually dimorphic effects and cellular mechanisms

by

Alice Goring

Thesis for the degree of Doctor of Philosophy

August, 2019

University of Southampton

Abstract

Faculty of Environmental and Life Sciences

School of Biological Sciences

Thesis for the degree of Doctor of Philosophy

Elucidating the role of osteoblast-derived vascular endothelial growth factor in the regulation of bone development: Sexually dimorphic effects and cellular mechanisms

Alice Goring

Bone is highly vascularised and bone forming osteoblast-derived vascular endothelial growth factor (VEGF) has been reported to be a key regulator of bone development and bone repair. Sex differences during skeletal growth are well reported and this early divergence is thought to influence the onset and prevalence of degenerative bone pathologies in men and women with age. Although VEGF is critical during early bone development, little remains understood about the role that the vasculature plays in driving the sexual dimorphism in bone. Therefore, the main objective of my PhD was to improve understanding of the function of osteoblast-derived VEGF signalling in male and female bone development and mineralisation. For VEGF deletion in mature osteoblast cells, male and female mice carrying floxed alleles of VEGF and expressing Cre recombinase under the control of the osteocalcin promotor were compared and termed herein as OcnVEGFKO. The following aims were the focus of this thesis i) Quantification and validation of vascular phenotype within the bone cortex in male versus female adult OcnVEGFKO mice ii) Investigation of whole bone traits following osteoblast-VEGF deletion including bone geometry in males versus females, iii) Elucidation of the role of osteoblast-VEGF in prepubertal development and its direct effects on male and female osteoblast function and iv) Investigation into indirect effects of VEGF deletion in male and female osteoblasts on vascular endothelial cell function. High-resolution synchrotron computed tomography, histology and backscattered scanning electron microscopy at the tibiofibular junction revealed increased intracortical porosity (+2.73 fold increase, $p<0.0001$), increased vasculature (% blood vessel area; WT 0.54, OcnVEGFKO 3.6, $p=0.05$) and signs of widespread deficiency in matrix mineralisation in 16 week old male OcnVEGFKOs versus WT. In contrast, in female OcnVEGFKOs there were no notable alterations in intracortical porosity, vasculature or mineralisation, but an increase in lacunar density, volume and diameter versus WT. Comparable to the changes observed in 16 week old mice, analysis of 4 week old male and female tibia using SR CT identified increased intracortical canal volume in male OcnVEGFKOs versus WT only. Medium-resolution micro-CT enabled the quantification of changes in bone geometry along the whole tibial length. In 4 week old mice, bone architecture was significantly altered in male OcnVEGFKO versus WT. In 16 week old mice however, differences in bone geometry were identified in female OcnVEGFKO versus WT, but not in males. Trabecular measures were largely unaltered in 4 and 16 week old male and female OcnVEGFKOs versus WT. To assess the

directionality of VEGF signalling and its contribution to observed sexual dimorphisms, LOBs were isolated from male and female $Vegf^{fl/fl}$ mice *in vitro*. VEGF was deleted using Adenovirus-Cre (OBVEGFKO) to assess direct effects of VEGF deletion on OB function in males and females. OBVEGFKO had no significant effect on viability or alkaline phosphatase (ALP) elution in males or females versus WT. mRNA was extracted from OBVEGFKO and WT OBs and qPCR was utilised to measure changes in relative expression of mRNA. Negligible levels of *Vegfr2* expression was identified in male and female OBs, in comparison to the endothelial cell (EC) lysate positive control. Expression of *Ar, Esr1, Esr2, Rankl, Opg* and *Sost* was unchanged in male and female OBs as a result of VEGFKO. Indirect effects of OBVEGFKO on EC functions were investigated and WT and OBVEGFKO conditioned media was collected from OBs and used to treat mouse bone marrow endothelial cells (MBMECs). Additional sexual dimorphism was identified here, with differential expression of genes implicated in angiogenesis and osteogenesis in OBVEGFKO versus WT represented by fold changes, including *Igf-1* (female; +3.07, male; -2.33), *Hif1-α* (female; +1.22, male; -1.32), *Runx2* (female; +3.43, male; -1.55) and *Sos*t (female;+6.58, male; +3.21). Correlating with in vitro mechanistic findings of sexual dimorphism in endothelial cells driven by osteoblast-derived VEGF, immunohistochemistry of tibia sections revealed high levels of sclerostin, a potent inhibitor of bone mineralisation in male OcnVEGFKO and localised to CD31 positive cells at the tibiofibular junction. My results propose that osteoblast-derived VEGF regulates osteoblast matrix mineralisation directly and vascularisation indirectly, that this regulation is distinct to males and females and results in divergent physical bone traits between sexes. Importantly my cell culture studies have found that these dimorphic bone phenotypes are linked to alterations in endothelial cell gene expression which could be targeted clinically to improve bone mineralisation. Targeting vascular signals to modulate bone formation distinctly in males and females could therefore provide a more effective way to treat degenerative bone disease in our ageing population.

Table of Contents

List of Tables

List of Figures

List of Accompanying Materials

Video of rotating tibia (Figure 4.5): Increase in cortical porosity and the presence of woven bone at the tibiofibular junction fracture site in male OcnVEGFKO mice.

Research Thesis: Declaration of Authorship

Print name: Alice Goring

Title of thesis: Elucidating the role of osteoblast-derived vascular endothelial growth factor in the regulation of bone development: Sexually dimorphic effects and cellular mechanisms

I declare that this thesis and the work presented in it are my own and has been generated by me as the result of my own original research.

I confirm that:

1. This work was done wholly or mainly while in candidature for a research degree at this University;
2. Where any part of this thesis has previously been submitted for a degree or any other qualification at this University or any other institution, this has been clearly stated;
3. Where I have consulted the published work of others, this is always clearly attributed;
4. Where I have quoted from the work of others, the source is always given. With the exception of such quotations, this thesis is entirely my own work;
5. I have acknowledged all main sources of help;
6. Where the thesis is based on work done by myself jointly with others, I have made clear exactly what was done by others and what I have contributed myself;
7. Parts of this work have been published as:

Goring A, Sharma A, Javaheri B, Smith RCG, Kanczler JM, Boyde A, Hesse E, Ferrara N, Mahajan S, Olsen BR, Pitsillides AA, Schneider P, Oreffo ROC, Clarkin CE (2019) Regulation of the bone vascular network is sexually dimorphic. Journal of Bone and Mineral Research. DOI: 03.07.19.

Signature: Date:

Acknowledgements

Most importantly, I would like to thank my three supervisors; Dr Claire Clarkin, Professor Richard Oreffo and Dr Philipp Schneider. Your support, guidance and enthusiasm towards my project from the start of my PhD at Southampton until now has made it such an enjoyable process. I could not have done this PhD or learnt so much without you.

Special thanks to my principal supervisor Claire. Thank you for inviting me to join your lab group in the first place and for your endless help. Your kindness when you volunteered to chair the Hannah's Willberry Wonder Pony scientific panel in your rare free time will not be forgotten and Hannah would be proud to have someone like you so involved with her charity. I feel like I have made friends for life whilst being a part of the Clarkin lab and will miss you all when I leave.

Thanks also go to my funding body Versus Arthritis and the many amazing people and lab groups that I have collaborated with throughout this project. Much gratitude goes to Professor Alan Boyde for the BSE-SEM which has hugely contributed to this study, as well as for his knowledge and guidance throughout the project. I have really enjoyed learning from such an expert and feel inspired every time I leave Queen Mary thanks to your wisdom. Thanks go to Professor Eric Hesse for allowing me to work in his lab in Hamburg for a month to do the histology for this project. Special thanks go to Cordula Erdmann from the Hesse lab who taught me how to do the histology and Dr Simona Bolamperti who provided me with the protocol for CD31 staining, as well as the rest of the lab group for being so welcoming.

Thanks to Dr Behzad Javaheri and Professor Andrew Pitsillides at the Royal Veterinary College for your support throughout this project and in writing the paper. Behzad, I am immensely grateful for your hard work and help with the whole bone geometry measures and trabecular bone analysis, as well as your guidance and advice. I also would like to acknowledge the help of Dr Rosanna Smith in the probability distribution curves for the osteocyte lacunae. As well as this, Professor Janos Kanczler is gratefully thanked for his help with operating the Skyscan micro-CT scanner.

Not forgetting the members of the Clarkin group, past and present. Thank you Dr Juan Nunez for helping me with dissections and micro-CT when I first started and had no idea

where to begin. A huge thank you to Aikta Sharma, my partner in crime and ‘lab bestie’. In the two years you have been at Southampton, we have had so much fun and of course not forgetting the fact that you are very skilled at Raman Spectroscopy, which was a huge asset to the paper. Thanks also to Alisha Sharma for answering my CT queries as they arose.

Finally, I would like to thank my family and James for their love and support throughout my PhD. I would not have been able to do any of this without them and they all mean the world to me.

Especially, I would like to dedicate this thesis to my grandpa, John Cuthill, the only other scientist in my family and the one person I knew would always understand and read my work with fascination. He sadly died a month before handing this thesis in, so will never get to see me complete my PhD, but I know that he was immensely proud of my work and would have been in the front row for my graduation.

Definitions and Abbreviations

ACP – amorphous calcium phosphate
ALP – alkaline phosphatase
ANK - ankylosis protein
Ar – androgen receptor
ASARM - aspartic acid-rich motif
BCA - bicinchoninic acid protein assay
BGLAP – Bone Gamma-carboxyglutamic Acid-containing Protein
Bgn - biglycan
BMD – bone mineral density
BMP - bone morphogenic proteins
BMU – basic multicellular unit
bp – base pairs
BrdU – bromodeoxyuridine cell proliferation marker
BS/TV - bone surface area
BSE-SEM – backscattered electron scanning electron microscopy
BV – blood vessel
BV/TV - bone volume
cAMP – cyclic adenosine monophosphate
CAP - carbonated appetite
CCEC method – collagenase, collagenase, EDTA, collagenase osteoblast isolation method
CD31/PECAM - platelet cell adhesion molecule/cluster of differentiation 31
$CD31^{hi}$ – type H blood vessels
$CD31^{lo}$ – type L blood vessels
cGMP – cyclic guanosine monophosphate
CHD – coronary heart disease
CM – conditioned media
CSA – cross-sectional area
c-src - proto-oncogene tyrosine-protein kinase Src
Ct.Th - cortical thickness
DAPI - 4',6-diamidino-2-phenylindole blue fluorescent nuclei stain
dH_2O – distilled water
DLL4 - notch delta-like ligand 4
DLX5 - Distal-Less Homeobox 5
DMP1 - dentin matrix protein 1
EC – endothelial cell
ELISA - enzyme-linked immunosorbent assay
eNOS - endothelial nitric oxide synthase
Esr1/Esr2 – oestrogen receptor1/2
FGF – fibroblast growth factor
GAPDH - Glyceraldehyde 3-phosphate dehydrogenase
HCl – hydrochloric acid
HIF - hypoxia inducible factor-1
HSC – haematopoietic stem cell
HUVEC – human umbilical vein endothelial cells
IGF-1 – insulin-like growth factor – 1
Ihh – Indian hedgehog
IL – interleukin
iMax - maximum moment of inertia
iMin - minimum moment of inertia
J - predicted resistance to torsion

KO – knockout
Lc.Dm/Ca.Dm - osteocyte lacunar/intracortical canal diameter
Lc.Dn/Ca.Dn – osteocyte lacunar/intracortical canal density
Lc.V/Ca.V - osteocyte lacunar/intracortical canal volume
LOBs – long bone osteoblast cells
MBMEC – mouse bone marrow endothelial cell
MEM – minimum essential media
MEPE - matrix extracellular phosphoglycoprotein
mg – milligram
Micro-CT – micro computed tomography
ml – millilitre
mM – millimolar
MOI – multiplicity of infection
MSC – mesenchymal stem cell
MTA – material transfer agreement
MV – matrix vesicle
ng – nanogram
NO – nitric oxide
NPP1 - nucleotide pyrophosphate phosphodiesterase
NS – non significant
OA - osteoarthritis
OB – osteoblast
OBVEGFKO – *in vitro* deletion of VEGF
Ocn – osteocalcin
OcnVEGFKO – *in vivo* deletion of VEGF
OPG – osteoprotegerin
OPN - osteopontin
OSE - Osteoblast-specific cis-acting elements
Osx- osterix
PAF – platelet-activating factor
PBS – phosphate buffered saline
PDE – phosphodiesterase
PDGF - platelet derived growth factor
PFA – paraformaldehyde
PGF – placental growth factor
PGI2 - prostacyclin
PHEX - Phosphate regulating gene with homologies to endopeptidases on the X chromosome
Pi – inorganic phosphate
PMMA – Poly (methyl methacrylate)
PPARγ2 – peroxisome proliferator-activated receptor 72
PPi - pyrophosphate
PVDF - polyvinylidene difluoride
PYK2 - Proline-rich tyrosine kinase 2
qPCR – quantitative polymerase chain reaction
RANK – receptor activator of necrosis factor kappa beta
RANKL - receptor activator of nuclear factor kappa-B ligand
ROI – region of interest
RT-PCR – reverse transcription polymerase chain reaction
Runx2 - Runt-related transcription factor 2
SIBLING - small integrin-binding ligand N-linked glycosylated protein family
SLS – synchrotron light source
***Sost* –** gene encoding mouse sclerostin
SR CT – synchrotron-based micro-CT
SU5416 – semaxanib tyrosine kinase inhibitor

Tb.N – trabecular number
Tb.Th – trabecular thickness
TBST - tris-buffered saline (TBS) and tween-20
TGFβ – transforming growth factor beta
TNFα – tumour necrosis factor alpha
TRAP – tartrate-resistant acid phosphatase
Tymp - Thymidine Phosphorylase
µg – microgram
µl – microlitre
µM - micromolar
µm – micron
VCAM - Vascular cell adhesion protein 1
VEGF – vascular endothelial growth factor
VEGFR – VEGF receptor
XX – female sex chromosomes
XY – male sex chromosomes

Publications from this PhD project

Abstracts

Goring A, Sharma A, Javaheri B, Olsen BR, Pitsillides AA, Oreffo ROC, Schneider P, Clarkin CE (2019) Do sex hormones determine sexual dimorphism of the bone vasculature? **Oral poster presentation** at Bone Research Society meeting, Cardiff, September 2019.

Goring A, Boyde A, Pitsillides A, Ferrara N, Olsen BR, Oreffo ROC, Schneider P, Clarkin CE (2018) Increased sclerostin expression following OB-derived VEGF deletion. **Oral presentation** at Bone Research Society meeting, Winchester, June 2018. Winner of best oral presentation and new investigator award.

Goring A, Javaheri B, Boyde A, Pitsillides A, Ferrara N, Olsen BR, Oreffo ROC, Schneider P, Clarkin CE (2018) VEGF exerts sexually dimorphic effects on bone mass and architecture. **Oral poster presentation** at Bone Research Society meeting, Winchester, June 2018.

Goring A, Boyde A, Pitsillides A, Ferrara N, Olsen BR, Oreffo ROC, Schneider P, Clarkin CE (2018) Investigating a role for endothelial-derived growth factors in regulating bone mineralisation following osteoblast VEGF deletion. **Oral presentation** at Arthritis Research UK annual fellows meeting, Loughborough, March 2018. Winner of best oral presentation prize.

Goring A, Boyde A, Pitsillides A, Ferrara N, Olsen BR, Oreffo ROC, Schneider P, Clarkin CE (2018) Investigating a role for endothelial-derived growth factors in regulating bone mineralisation following osteoblast VEGF deletion. **Oral presentation** at Bone and Teeth Gordon Research Seminar and **poster presentation** at Gordon Research Conference. Galveston, Texas, January 2018.

Goring A, Núñez JA, Ferrara N, Olsen BR, Oreffo ROC, Schneider P, Clarkin CE (2017) Evidence for gender-specific vascular signalling in bone. **Oral poster presentation** at Bone Research Society Annual Meeting, Bristol, June 2017. Winner of new investigator award.

Goring A, Núñez JA, Ferrara N, Olsen BR, Hesse E, Oreffo ROC, Schneider P, Clarkin CE (2017) Evidence for resistance of endothelial cells to blockade of mature osteoblast-derived vascular endothelial growth factor. **New Investigator presentation and poster** at European

Calcified Tissue Society Annual Meeting. Salzburg, Austria, May 2017. Winner of best new investigator presentation prize.

Goring A, Oreffo ROC, Schneider P, Clarkin CE (2017) Investigating gender-specific vascular signals for bone repair. **Oral poster presentation** at Arthritis Research UK annual fellows meeting. Loughborough, April 2017. Winner of best poster prize.

Publications

Goring A and Sharma A, Emery R, Olsen BR, Boyde A, Pitsillides AA, Mahajan S, Oreffo ROC, Clarkin CE (2020) Raman spectroscopy reveals sexually dimorphic influence of osteoblast-derived VEGF on bone mineral and matrix composition. In preparation for submission to Matrix Biology.

Sharma A, **Goring A**, Staines K, Emery R, Pitsillides AA, Oreffo ROC, Mahajan S, Clarkin CE (2019) Raman spectroscopy links differentiating osteoblast matrix signatures to pro-angiogenic potential. Matrix Biology Plus. DOI: 20.11.19

Goring A, Sharma A, Javaheri B, Smith RCG, Kanczler JM, Boyde A, Hesse E, Ferrara N, Mahajan S, Olsen BR, Pitsillides AA, Schneider P, Oreffo ROC, Clarkin CE (2019) Regulation of the bone vascular network is sexually dimorphic. Journal of Bone and Mineral Research. DOI: 03.07.19.

Núñez JA, **Goring A**, Javaheri B, Razi H, Gomez-Nicola D, Hesse E, Pitsillides AA, Thurner PJ, Schneider P, Clarkin CE (2018). Regional diversity in the murine cortical vascular network is revealed by synchrotron X-ray tomography and is amplified with age. European Cells and Materials. 35: p. 281-299. doi:10.22203/eCM.v035a20.

Núñez JA, **Goring A**, Hesse E, Thurner PJ, Schneider P, Clarkin CE (2017) Simultaneous visualisation of calcified bone microstructure and intracortical vasculature using synchrotron X-ray phase contrast-enhanced tomography. Sci Rep, 7: p. 13289

Mosey H, Núñez JA, **Goring A**, Clarkin CE, Staines KA, Lee PD, Pitsillides A, Javaheri B (2017) *Sost* Deficiency does not Alter Bone's Lacunar or Vascular Porosity in Mice. Frontiers in materials. 4. 27. 10.3389/fmats.2017.00027.

Chapter 1 Introduction

1.1 Bone

1.1.1 Structure and function of bone

Bone makes up the framework of all vertebrates, with ligaments joining bones to adjacent bones and tendons connecting bones to muscle. It is a highly dynamic tissue and is vital to the constitution of the human skeleton, playing several essential roles in enabling survival. These include providing structural support, acting as a conduit for calcium, providing an environment for bone marrow, giving protection to delicate internal organs and facilitating movement (as reviewed by Taichman, 2005, Bilezikian et al., 2008). In order to do this, bones are tough, strong and resistant to a certain degree of repetitive strain without fatigue, as well as being light.

Structurally, bone is a composite material, consisting of both organic and inorganic material; 8% water, 22% proteins and 70% mineral (Augat and Schorlemmer, 2006). The organic protein component is called osteoid and 90% of this is made up of type I collagen. The stable structural composition of collagen ensures that it cannot be degraded by proteolytic enzymes and a triple helix formulated from three polypeptide chains constitutes each collagen molecule. The assembly of collagen molecules into overlapping, cross-linked fibrils makes collagen both flexible and strong. The remaining 10% of organic, non-collagenous protein components include; osteonectin, osteocalcin, osteopontin, bone sialoprotein and proteoglycans (reviewed by Maxie and Jubb, 2015).

The key mineral component of bone is hydroxyapatite, which combined with the flexible nature of collagen, ensures the skeleton remains strong and resists fragility fractures. Hydroxyapatite ($Ca_{10}(HPO_4)_6(OH)_2$) is produced from a combination of magnesium, calcium and phosphate ions which aggregate within the bone matrix, chemically combining and hardening (as reviewed by Martini et al., 2014).

During development and the production of primary bone there are different forms of bone that are present; namely immature woven bone and mature lamellar bone (figure 1.1). Woven bone is laid down quickly and because of this, there is no structure in the way in

which the collagen fibres are organised. Osteocytes are irregularly spaced and woven bone is frequently broken down and replaced in remodelling. This type of bone is commonly seen in early development, fracture calluses or diseased bone (reviewed by Martínez-Reina et al., 2018, Clarke, 2008). Woven bone is weak, due to the fact it is formed as a result of osteoblasts producing osteoid very rapidly. Lamellar bone on the other hand, is highly structured and is composed of orderly collagen fibrils of similar width (reviewed by Kini and Nandeesh, 2012) and evenly spaced osteocytes. Lamellar bone is laid down much more slowly and replaces woven bone during primary bone development. It is a stronger type of bone and therefore much more resistant to loading and fracture as a result (Boyde, 1980a, Boyde, 1980b). The vast majority of the healthy skeleton is made up of lamellar bone (reviewed by Clarke, 2008).

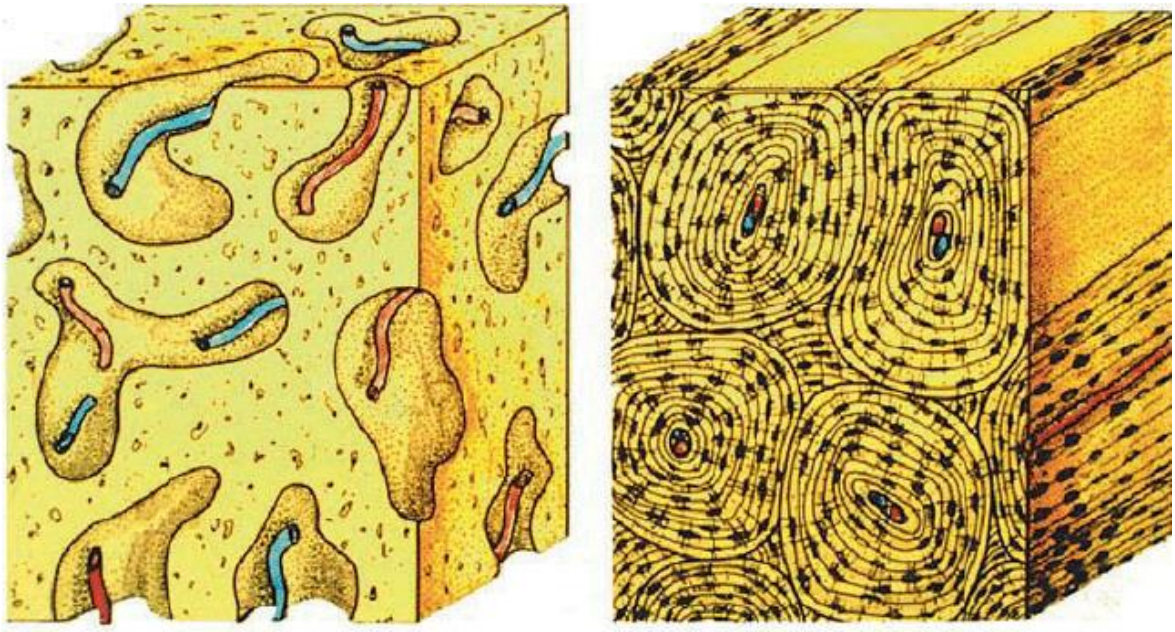

Figure 1.1: Structural composition of woven bone versus lamellar bone. A cartoon representation. Woven bone is bone is laid down very quickly during development, fracture healing or in disease. Osteocytes are irregularly spaced and vasculature is disorganised. Lamellar bone is made up of highly structured collagen fibrils, with osteocytes embedded amongst them in an orderly formation. It is much stronger and replaces woven bone (Khurana, 2009).

1.1.1.1 Composition and functionality of the long bones and the skull

Once formed, the human skeleton consists of both long bones (tibia, femur and humerus) and flat bones (skull, scapula mandible and ileum; reviewed by Moreira et al., 2019). Long bones and flat bones have distinct structural properties which enable them to fulfil their specific and contrasting skeletal functions. Endochondral ossification is the dominant form of development for the majority of mammalian skeletons and a vital component of long bone formation (Gerber and Ferrara, 2000). Unlike intramembranous ossification, endochondral ossification involves a cartilage intermediate phase (chapter 1.3.1). The flat bones of the skull however, are formed directly from connective tissue in a process called intramembranous ossification (Ferrara et al., 2003, Yang et al., 2012, Ortega et al., 2004, Kronenberg, 2003, Kini and Nandeesh, 2012).

In long bones such as the tibia, the metaphysis or the transition zone is located between the epiphysis which is found at both ends of the long bone and the diaphysis. The diaphysis is a hollow body of bone comprising the central shaft of the tibia and contains bone marrow and adipose tissue. A small layer of cartilage called the epiphyseal layer separates the epiphysis from the metaphysis and diaphysis in the tibia (Moreira et al., 2019).

The majority of the tibia is comprised of cortical bone (figure 1.2), with the tibia diaphysis and specifically the tibiofibular junction consisting purely of this bone type. Cortical bone or compact bone forms the dense, tough (Rodriguez-Florez et al., 2015) outer layer of the skeleton and makes up 80% of the body's bone composition. This gives it its strong mechanical properties (Clarke, 2008, Burr, 2010, Moreira et al., 2019). The presence of cortical bone in the skeleton is essential for lower limb physiological loading and therefore is required to be tough in order to withstand the pressure that the bone is subjected to (Mirzaali et al., 2016). The performance of the skeleton as a supportive structure is highly dependent of the composition and density of cortical bone, something that is altered as we age (Augat and Schorlemmer, 2006). Cortical bone is bordered by the periosteal surface on the outside and the endosteal surface on the inside (reviewed by Khurana, 2009) and contains osteoblasts, osteoclasts, nerves and blood vessels (Kini and Nandeesh, 2012). These blood vessels within long bone cortices pass through Volkmann's canals and Haversian canals which are found within osteons (Chapter 1.3.2).

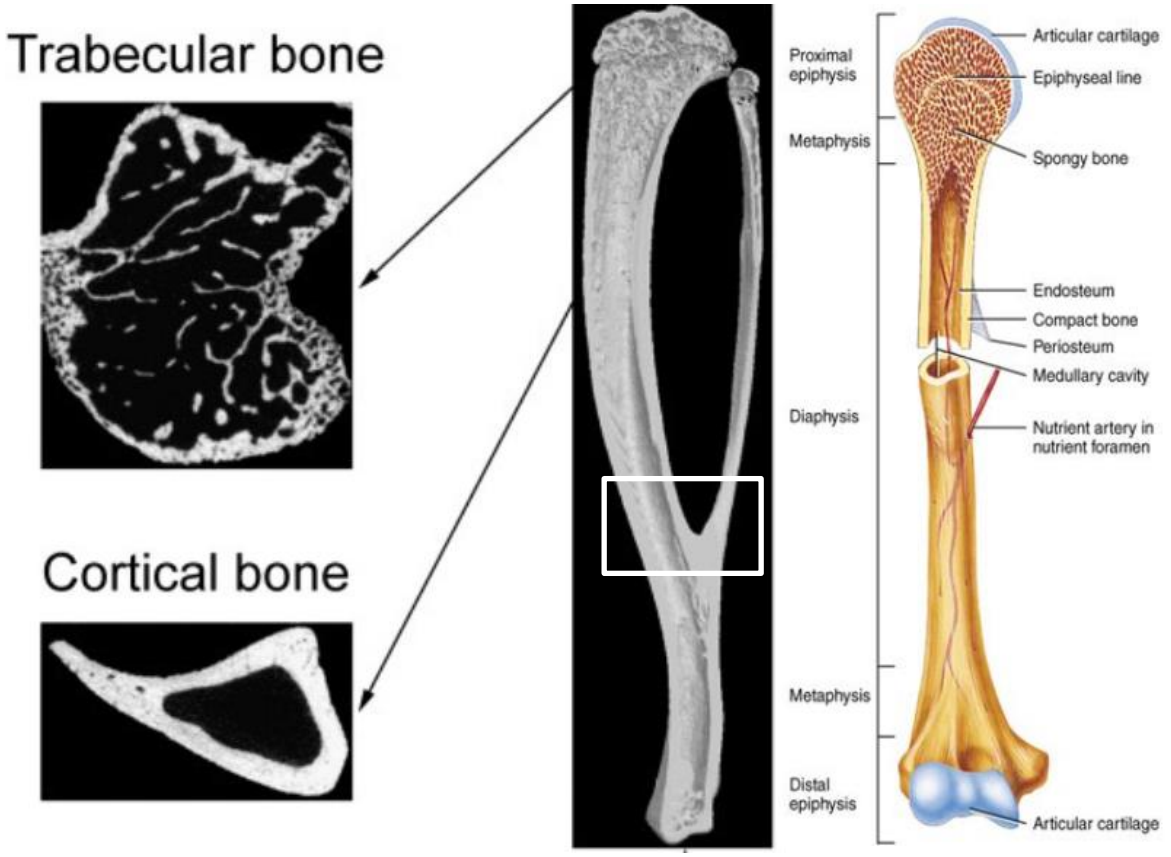

Figure 1.2: The structure of a long bone. The distribution of trabecular and cortical bone in the tibia. The tibiofibular junction (white box) and the diaphysis of the tibia are made up purely of cortical bone. The proximal ends of the tibia contain trabecular bone. The long bone consists of the epiphysis, metaphysis and diaphysis. The growth plate is located at the both the proximal and distal ends of the long bone. Image adapted from (Sugiyama et al., 2011) and 'bone tissue and the skeleton'. Accessed 27.07.19.

The proximal metaphysis as well as the proximal epiphysis of the tibia and other long bones is made from trabecular bone, which is easily identified by its honeycomb-like structure (figure 1.2). Trabecular bone forms 20% of the skeleton and it is characterised structurally by interlinked rods and plates. Unlike cortical bone, only 15-25% of trabecular bone is calcified and therefore it has very different structural properties (Moreira et al., 2019). The balance between trabecular and cortical bone is dependent on the type and function of the bone (Clarke, 2008, Moreira et al., 2019). Branches of trabecular bone are no more than 0.2-0.4mm in diameter, to ensure that diffusion of nutrients to the osteons can occur. Osteons are not always present and in this case the trabecular bone consists of a few layers of mature lamellae bone, osteocytes and mineralised bone matrix (Khurana, 2009). When present, trabecular osteons are called packets; they are much smaller than that of cortical

bone and are an ellipsoid shape (reviewed by Dempster, 2006). The bone itself is separated from the bone marrow by an endosteal layer, which contains a large number of osteoclasts and osteoblasts, meaning that this bone subtype is particularly metabolically active (Khurana, 2009).

The skull is an incredibly important part of the human skeleton, encasing the brain and providing a strong foundation for four out of the five senses; sight, smell, taste and hearing (reviewed by White and Folkens, 2005). The skull is structurally comprised of a layer of trabecular bone between two layers of cortical bone. The combined properties of both bone types ensure that the skeleton is both tough and light (Khurana, 2009). The fibrous joints that separate the frontal and parietal regions of the skull and provide a good reference point for intracranial measurement are called sutures. These sutures act as a region of growth during development, as well as providing flexibility during childbirth (reviewed by Chai, 2015).

1.1.1.2 Bone microstructure and intracortical porosity

Porosity is a measure of how much of the bone is empty space. The degree of porosity can be altered by ageing, disease or loading. Porosity is present in both trabecular and cortical bone, serving different functions in each bone subtype. In trabecular bone, voids within the bone create room for the bone marrow. In cortical bone however, the pores provide room for the intricate network of blood vessels and population of osteocytes which reside within them (Renders et al., 2007). Within these areas of no mineralisation, reside Haversian (Havers) or Volkmann's canals (chapter 1.3.2), enabling blood flow through the bone and sustaining the viability of cell types such as osteocytes (Bonewald, 2011).

Mechanical studies from as early as 1977 have shown that increased porosity is indicative of a decrease in bone strength and stiffness (Carter and Hayes, 1977). Indeed, it has been proven that increased cortical porosity in human femurs results in a 76% decrease in bone strength (Schneider et al., 2007b). Porosity has also been revealed to be sensitive to loading, with regional differences in cortical bone porosity identified. In the femoral neck, it has been shown that there are higher levels of porosity in the superior versus the inferior region. This is thought to be due to the differences in mechanical strain that these specific regions have to withstand. Where the superior region has to resist tension, the inferior

region has to undergo compressive load (Bell et al., 1999) and therefore the bone has had to adapt accordingly, showing the dynamic capabilities of bone.

Changes start to occur in the composition of the bone from the age of 27 onwards and there is a 15% increase in cortical porosity of the femur from the age of 40 to the age of 80 (Zebaze and Seeman, 2015; figure 1.3). 70% of this bone loss is associated with ageing and is characterised by an increase in porosity in cortical, as opposed to trabecular bone.

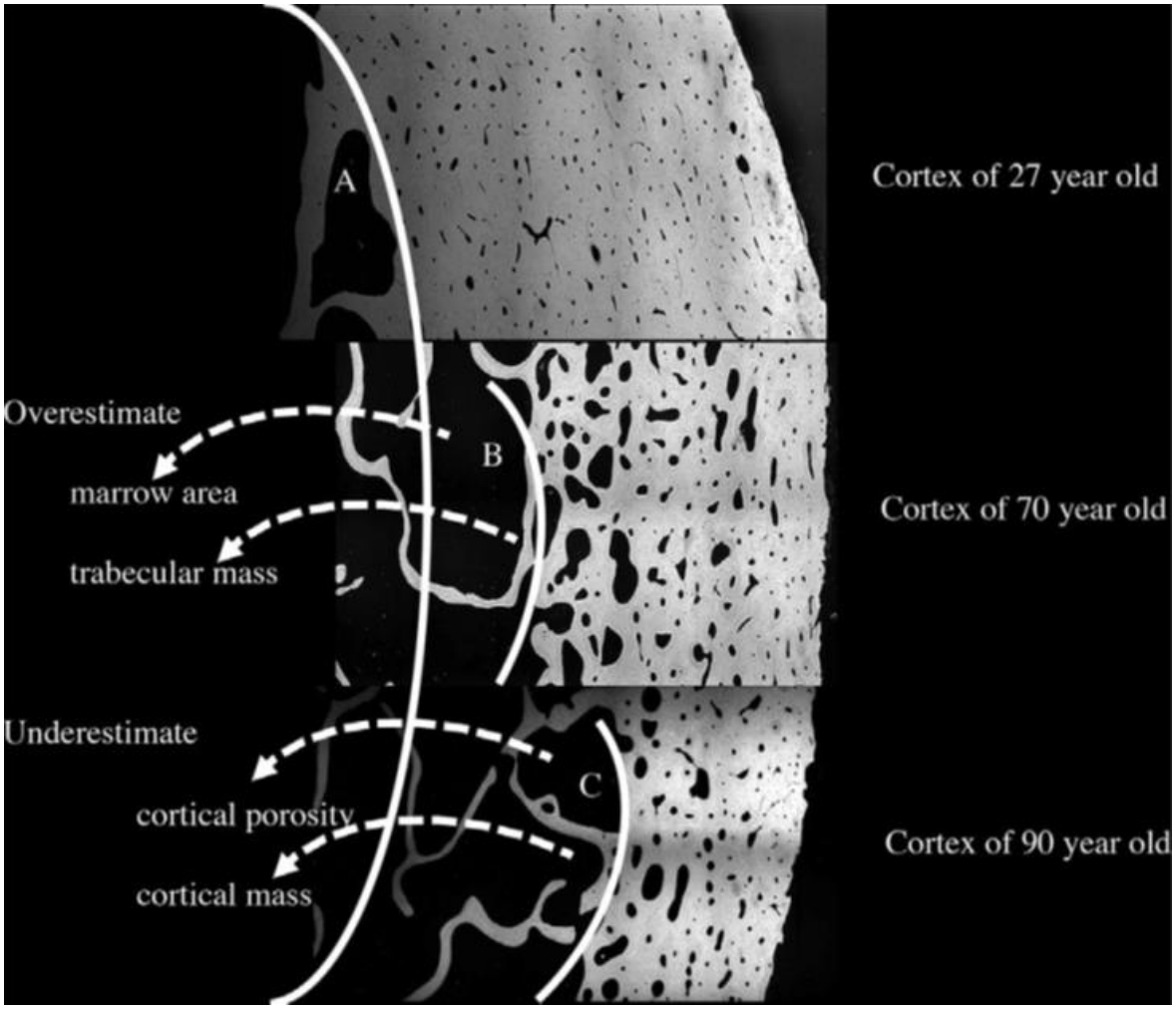

Figure 1.3: Changes in cortical porosity in the human skeleton with age. From the age of 27, there are noticeable increases in cortical porosity. In turn, this causes a decrease in cortical bone mass (Zebaze and Seeman, 2015).

There are several techniques which are commonly used for the analysis of porosity, with micro computed tomography (micro-CT) being particularly widely used and significantly increasing our understanding of bone microstructure. Unlike other analysis techniques such as histology, micro-CT is a highly sensitive but non-destructive imaging technique, enabling the production of 3D projections of both trabecular and cortical bone porosity when performed at a high enough resolution (Palacio-Mancheno et al., 2014). High resolution synchrotron-based micro computed tomography (SR CT) uses a high-flux proton beam to produce high resolution and high signal-to -noise 3D images of the microstructure and ultrastructure of bones at speed. The first trabecular bone images produced using SR CT were obtained in 1999 and since then SR CT has been a technique which has advanced and is becoming more commonly used for the study of bone microstructure and porosity, which before was unable to be visualised due to low the resolution of images (Salomé et al., 1999, Nuzzo et al., 2002).

1.1.2 Osteoblast cells

The three key bone cells whose interactions are pivotal in the maintenance of bone health, integrity and function are osteoblasts, osteoclasts and osteocytes (Khurana, 2009). In mature adults, 4-6% of bone cells are osteoblasts. Osteoblasts are typically cuboidal in shape and are well adapted for their role in the synthesis of proteins, with a large nucleus, rough endoplasmic reticulum, Golgi apparatus and secretory vesicles as important parts of their structure (Hochberg et al., 2014, Florencio-Silva et al., 2015). Adhesion junctions, tight junctions and gap junctions enable the communications between not only cells of the same subtype, but bone marrow cells and bone lining cells found on the surface of the bone too (reviewed by Hochberg et al., 2014). Osteoblasts frequently undergo apoptosis and display short life-spans, living between 1-200 days (Zhao et al., 2000, Bilezikian et al., 2008).

Osteoblast cells are produced from multipotent mesenchymal cells and differentiate into progenitor cells committed to the osteoblast lineage, which are located in the perivascular tissue, periosteum, endosteum, Haversian canals, Volkmann canals and bone marrow (Khurana, 2009). Mature osteoblasts are involved in the production of bone matrix and their functionality is essential for bone development, bone turnover and bone repair. On reaching the end of the process of bone production, 60-70% of cells will undergo apoptosis and die. Osteoblast cells that are left will differentiate into inactive bone lining cells or

become osteocytes and will not proliferate further (as reviewed by Manolagas, 2000, Hochberg et al., 2014).

1.1.2.1 Processes by which bone forms

The development of our skeleton or ossification in humans, takes place from embryonic weeks 6-7 until the mid-twenties in most individuals (reviewed by Breeland, 2019). Over millions of years, ossification of the primary skeleton has evolved and thus it is known that cells from different lineages are responsible for the development of different regions of the vertebrate skeleton (reviewed by Berendsen and Olsen, 2015). The three cell types involved in this process are; 1) neural crest cells which make up the craniofacial bones in the face, the skull and the dentin in our teeth, 2) the paraxial mesoderm which gives rise to the remaining posterior craniofacial bones and a large proportion of the axial skeleton (including the vertebrae, sacrum, coccyx, ribs and sternum), and finally 3) the cells which are located in the lateral plate mesoderm which are needed for limb bone development (Olsen, 2006, Berendsen and Olsen, 2015).

The osteoblast as a bone producing cell plays a key role in bone formation and calcification. During bone formation, organic aspects of the bone matrix are produced by the secretion of collagen (predominantly type I) and proteoglycans from osteoblast cells (reviewed by Jensen et al., 2010, Khurana, 2009). Once secreted, this is subsequently processed and the type I collagen acts as a template for the formation of microfibrils, fibrils and fibres. The collagen matrix matures and inclusion of hydroxyapatite crystals into the new bone matrix takes place, a process which is controlled by alkaline phosphatase (ALP) enzyme activity (Niedermair et al., 2018). Osteoblast cells play a key role in the regulation of bone formation.

1.1.2.2 Osteoblast differentiation

During development, stem cells will take several routes and mesenchymal cells will either differentiate into bone producing osteoblast cells, chondrocytes, myoblasts or adipocytes. This fate is determined largely by Wnt signalling pathways. If Wnt signalling stimulates increased levels of beta-catenin by preventing its degradation, mesenchymal cells will differentiate into osteoblasts (figure 1.4) and the transcription of genes which are required for differentiation of other cell types will be inhibited (reviewed by Olsen, 2006). The

importance of beta-catenin in this process of osteoblast differentiation has been illustrated in knockout studies, where there is a direct impact on osteoblast function, differentiation and early skeletal development (Hill et al., 2005). If beta-catenin is not inactivated by the Wnt signalling pathway, the mesenchymal cells will differentiate into chondrocytes as opposed to osteoblasts (Olsen, 2006). The commitment of the putative mesenchymal stem cells to a specific lineage is solidified by the selective expression of master transcriptional regulators, including peroxisome proliferator-activated receptor 72 (PPARγ2; stimulates adipogenesis) (Issemann and Green, 1990), SOX9 (promotes chondrocyte development) (de Crombrugghe et al., 2000) and Runt-related transcription factor 2 (RUNX2) required for osteoblast differentiation and bone development (Ducy et al., 1997).

Early *in vitro* studies have proven instrumental in furthering our understanding of the mechanisms involved in the control of osteoblast differentiation. In culture, osteoblasts can be characterised by the presence of mineralised extracellular matrix. Early studies looking at key regulators of osteoblast differentiation identified two cis-acting elements which may play a pivotal role. Osteoblast-specific cis-acting elements (OSEs) OSE1 and OSE2 were shown to upregulate the activity of osteoblast promotors in differentiated osteoblasts. Positioned in the promotor of the osteocalcin gene, it was suggested that both of these elements have an important role in the regulation of osteoblast differentiation (Ducy and Karsenty, 1995). Following this finding, it was possible to identify and characterise Cbfa1 or Runx2 as it is commonly known as, which is expressed in mesenchymal cells. It was these preliminary studies which first identified Runx2 as the primary osteoblast-specific transcription factor, with a focus on its important role in the control of osteoblast differentiation (Ducy et al., 1997).

Homozygous mutation of Runx2 *in vivo* has further improved our understanding of its functionality. Mice with this genetic alteration did not survive postnatally and examination of the phenotype identified a skeleton comprised of avascular cartilage only, with no sign of any ossification (Komori et al., 1997). Mice which have a mutation in Runx2 also have no osteoclasts and therefore this suggests that osteoblasts are perhaps a prerequisite of osteoclast differentiation (Ducy, 2000). This reiterates the importance of Runx2 in the process of osteogenesis and osteoblast differentiation, which in turn plays a role in osteoclast differentiation.

The involvement of Runx2 in the control of osteoblast-expressing genes which are crucial to osteoblast differentiation has been known for many years (Ducy, 2000). This includes osterix (Osx), which together with Runx2 is essential in early bone development, the differentiation of osteoblast progenitors into mature cells and matrix mineralisation (Nakashima et al., 2002, Clarkin and Olsen, 2010, Bosworth and Downes, 2011, Parfitt, 1994, Niedermair et al., 2018).

Another key player in the control of osteoblast differentiation is osteocalcin. The functionality of osteocalcin was initially identified by the use of an animal model devoid of osteocalcin. These osteocalcin-null mice showed increased bone mass, suggesting that activated osteocalcin is involved in the inhibition of osteoblast functionality (Ducy et al., 1996). Osteocalcin is produced specifically by osteoblasts and is of particular interest due to the nature and specificity of the animal knockout in this study. The gene encoding osteocalcin (BGLAP) can be found on chromosome 1, position 1q25-q31 (as reviewed by Zoch et al., 2016, Moser and van der Eerden, 2018, Hu and Olsen, 2016). Osteocalcin is a mature peptide and a marker of mature osteoblast differentiation produced by cleavage of an endoplasmic reticulum sequence and a pro-sequence, as well as γ-carboxylation of position 17, 21 and 24 glutamic acids (Boskey et al., 1998).

Aside from the important roles of Runx2 and osteocalcin, the commitment of cells to the osteoblast lineage is thought to be further regulated by growth factors. Indian hedgehog (Ihh) is produced by chondrocytes and its role in the development of the skeleton and osteoblast differentiation, as well as the control of chondrocyte proliferation has been established by silencing *Ihh* (St-Jacques et al., 1999). Other growth regulatory growth factors involved in the development of bone include bone morphogenic proteins (BMPs), which are key regulators of osteogenesis via osteoblast differentiation, bone development and bone growth (Mukherjee and Rotwein, 2009). It has been shown BMP family members are able to upregulate the expression of Runx2 in culture (Ducy et al., 1997), which could explain the effect that it has on osteoblast cells. Transforming growth factor-beta (TGF-β) signalling has been shown to enhance osteoblast differentiation *in vivo* by promoting the transition from progenitor cells. In turn, it inhibits osteoclast differentiation which is reliant on the release of receptor activator of nuclear factor kappa-B ligand (RANKL) from osteoblast cells (Yasui et al., 2011). ALP is an enzyme produced by osteoblasts and an early indicator of osteoblast differentiation (reviewed by Florencio-Silva et al., 2015, Bosworth

and Downes, 2011). As a result, levels of ALP eluted from osteoblast cells are often used as a useful measure of osteoblast differentiation *in vitro*. Finally, the fibroblast growth factor (FGF) family has been shown to be equally important in the control of osteoblast differentiation and bone development (Marie et al., 2002).

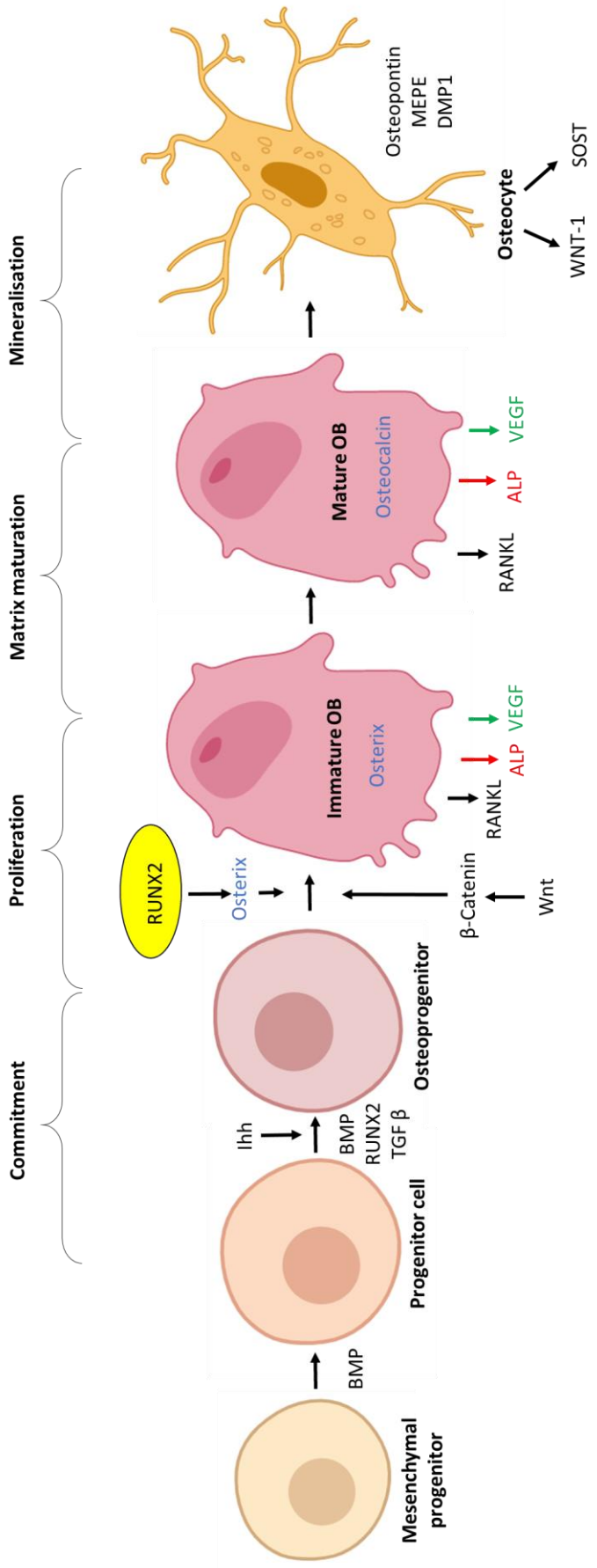

Figure 1.4: The development of an osteoblast from early osteoblast commitment, to proliferation, matrix maturation and mineralisation. Wnt and beta-catenin are involved in the early commitment of progenitor cells to the osteoblast lineage. Up-regulation of Runx2 activates osteoblast differentiation. Image created and based on diagram by Soltanoff et al, 2009.

1.1.2.3 Factors produced by osteoblasts

Non-collagenous proteins produced by osteoblasts include osteocalcin, osteopontin, bone sialoprotein and osteonectin. Osteoblasts also secrete a wide range of cytokines and growth factors, namely; interleukin-6, interleukin-11, vascular endothelial growth factor (VEGF), TGFβ, BMPs, platelet derived growth factors (PDGFs) and insulin-like growth factors (IGFs) (reviewed by Khurana, 2009). These growth factors use autocrine and / or paracrine signaling pathways to communicate with receptors on their own surface or neighbouring cells. Importantly, RANKL is also secreted by osteoblast cells, important for the survival and differentiation of osteoclasts (Yasui et al., 2011).

1.1.3 Osteocytes and bone lining cells

When osteoblast cells have fulfilled their role in the production of new bone matrix, there are three possible fates. These are; cell death by apoptosis, conversion into a bone lining cell or terminal differentiation into an osteocyte after becoming embedded in the bone matrix (Jilka et al., 1999). Osteocytes are mechanosensory cells, sensing changes in strain and subsequently influencing the activity of osteoblasts (bone production) and osteoclasts (bone resorption) in remodelling (reviewed by Dempster, 2006). Osteocytes are highly abundant within the bone matrix and have life spans reported to be as long as 20 years (Bilezikian et al., 2008, Zhao et al., 2000). Ultimately osteocyte cells undergo apoptosis, which is suggested to be as a result of 'leakiness' of nuclear pores, an imbalance in free radicals within the body or due to dysfunctional autophagy (Manolagas and Parfitt, 2010, Pursiheimo et al., 2009). In mature adults, osteocytes make up 90-95% of bone cells (Lanyon, 1993), but although theories regarding their functionality have been generated over the past 100 years, in comparison to osteoblasts and osteoclasts there is still much to be understood.

Osteocytes have an average volume of 455µm^3 (McCreadie et al., 2004) and with the advances in high-resolution micro CT scanning and scanning electron microscopy (SEM) enabling the production of 3D imagery of these bone cells, it is hoped that understanding of osteocyte function will improve. As shown in *in vitro* experiments, the expression of several key markers is altered following the evolution of osteocytes from osteoblasts. This includes reduction in levels of ALP and upregulation of casein kinase II and osteocalcin (Mikuni-Takagaki et al., 1995).

Each osteocyte is comprised of roughly 50 dendritic processes (figure 1.5) which attach to the cell surface and are encased within tiny canaliculi, adjoined by gap junctions which are made of connexin (Doty, 1981, Bonewald, 1999). These dendritic processes enable osteocytes to dynamically connect to and communicate with other osteocytes, cells on surface of the bone and the bone marrow (Kamioka et al., 2001). Osteocytes respond to strain and dependent on the frequency, duration and strength of the strain will influence bone production and resorption by altering the differentiation of osteoblasts and osteoclasts (Lanyon, 1993). Osteocytes have also been identified as the main cell expressing sclerostin (*Sost*), a negative regulator of osteogenesis. It is thought that via production of sclerostin, it is possible for osteocytes to regulate the differentiation of osteoblast progenitor cells into mature osteoblast cells and alter their activity (Winkler et al., 2003). Sclerostin is also involved in the control of matrix mineralisation. Osteocytes secrete Wnt-1, which is shown to induce bone mineralisation and this is regulated by the release of sclerostin from osteocytes, which impedes matrix mineralisation due to its inhibitory effect on the Wnt pathway (Joeng et al., 2017). Osteocyte cells also express proteins such as dentin matrix protein 1 (DMP1), Phosphate regulating gene with homologies to endopeptidases on the X chromosome (PHEX) and matrix extracellular phosphoglycoprotein (MEPE) which are thought to be important in the control of hydroxyapatite production during mineralisation (Feng et al., 2006, He and George, 2004). Thus, osteocytes have an important job in the maintenance of bone homeostasis and matrix mineralisation.

Microcracks which occur in close proximity to the osteocyte are also enough to initiate osteocyte apoptosis, which following communications with the bone surface can subsequently initiate a cascade of bone remodelling (Burr et al., 1985). Besides from this, osteocytes rarely undergo apoptosis and in comparison to osteoblasts and osteoclasts, they are cells with a long life-span and ordinarily will stay alive until bone remodelling takes place (reviewed by Bilezikian et al., 2008).

In healthy bone, there are a large amount of dendritic processes connected to the osteocyte and angled towards the vasculature, where they interact with endothelial cells (Prasadam et al., 2014). Osteocytes are regularly and evenly distributed within the bone matrix. In diseased osteoporotic bone, dendrites are poorly organised and levels of connectivity reduced, jeopardising the mechanosensory function of the osteocyte. A large

increase or decrease in dendrite connectivity therefore has a significant effect on bone mechanics and it is important that a consistent equilibrium is maintained to ensure that our bones stay healthy (reviewed by Marcus, 2008). Disruptions to osteocyte functionality are also caused by aging, where apoptosis is potentially the consequential effect of damage to the gap junctions and dendritic connections, resulting in empty osteocyte lacunae which can be identified by histology (Tiede-Lewis et al., 2017).

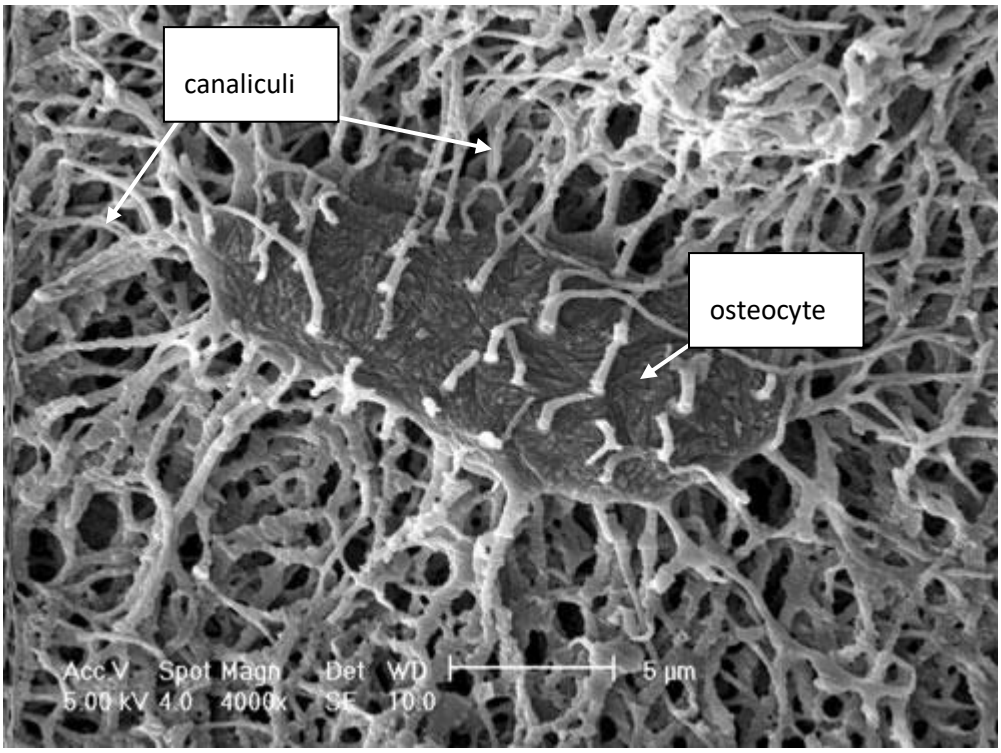

Figure 1.5: Osteocytes within the bone matrix. Osteocytes are mechanosensory cells with long processes called canaliculi attached to the cell surface. SEM image extracted and annotated from a paper by Lynda Bonewald (Bonewald and Wacker, 2013). Scale bar = 5µm

The separation between the calcified bone tissue and the bone marrow is formed by elongated, flattened bone lining cells. They are produced by the differentiation of osteoblast cells which have terminated osteogenesis but have not undergone apoptosis or formed osteocytes. These cells play an important role in bone resorption by using collagenase to prepare the surfaces of the bone and remove remaining unmineralised collagen in preparation for osteoclastic activity (Hauge et al., 2001). This cleaning process is shown to bridge bone resorption and bone production, facilitating the transition

between the two phases. Following bone remodelling, a new layer of smooth collagen is laid down by lining cells (Everts et al., 2002).

Not only do lining cells protect the surface of the bone, they are also involved in communications. It is suggested that they have a role in the movement of calcium to and from the bone via gap junctions which facilitate communications with other cell types such as osteoblasts and osteoclasts as well as between other lining cells. Unlike osteocytes, they are not terminally differentiated and the lining cells are able to re-activate themselves and change their morphology to become osteoblast cells once more (Hauge et al., 2001).

1.1.4 Osteoclasts

Osteoclasts are large, multinucleated cells with monocyte/macrophage ancestry (Takahashi et al., 1988). As per osteoblasts, osteoclasts have short life-spans and ordinarily live between 1-25 days. It is thought that production of RANKL (*Tnfsf11*) by osteoblasts is required for differentiation of osteoclast precursor cells into mature osteoclasts, with bone resorption capabilities (figure 1.6). RANKL is part of the tumour necrosis factor (TNF) family of cytokines and can act as a membrane-bound protein, or be shed as a soluble protein. The RANK receptor is located on myeloid cells (Marks and Seifert, 1985, Xiong et al., 2018) and osteoclast differentiation is controlled by the presence of decoy receptor osteoprotegrin (OPG), which binds RANKL to decrease the rate of osteoclast differentiation (Chambers, 2000).

There is experimental evidence to suggest however, that osteoblasts are not the only source of RANKL (Collin-Osdoby et al., 2001). In fact, when osteoblast cells were ablated, there was no effect on both the number of osteoclast cells, resorption or the secretion of RANKL providing further evidence to support this theory (Corral et al., 1998, Galli et al., 2009). Indeed, it has been suggested that chondrocytes, osteocytes (Silvestrini et al., 2005), lymphocytes (Kanematsu et al., 2000) and endothelial cells (Collin-Osdoby et al., 2001) are involved in the secretion of RANKL (O'Brien, 2010, Xiong et al., 2015). As well as expressing RANKL, human vascular endothelial cells have also been shown to produce OPG and in the presence of pro-inflammatory cytokines including TNF-α and IL-1α, it has been shown that the expression of both OPG and RANKL is upregulated (Collin-Osdoby et al., 2001).

Several additional cytokines, growth factors and hormones have also been proven to be required in the control of osteoclast differentiation during cell development. Macrophage colony stimulating factor is involved in the upregulation of proliferation and differentiation of osteoclast precursor cells (Yoshida et al., 1990) and IL-1, TNF-α (Pfeilschifter et al., 1989) and IL-6 (Roodman, 1992) are thought to upregulate osteoclast differentiation. The role of macrophage colony stimulating factor was confirmed by knockout studies, in which the genetic modification resulted in a complete lack of osteoclast cells required for bone resorption (Yoshida et al., 1990). On the other hand, cell culture experiments have proven that both IL-4 and IFN-γ suppress the differentiation of osteoclast cells (Lacey et al., 1995). Another inhibitory protein is TGF-β, which upregulates the expression of the calcitonin and vitronectin receptor in the down regulation of osteoclast proliferation. Therefore, bone resorption remains a closely regulated process (Orcel et al., 1990).

Attachment of osteoclasts to the bone matrix is facilitated by integrins, making an area called the sealing zone in the small gap in-between the two adjoining surfaces. αvβ1, α2β1 and αvβ3 are all integrins which are expressed by osteocytes. αvβ3 is the most commonly expressed integrin, with very high levels present in the resorbing osteoclast and in turn αvβ3 interacts with several extracellular matrix proteins including vitronectin, bone sialoprotein and osteopontin. The recruitment and localisation of phosphatidylinositol 3-kinase, proto-oncogene tyrosine-protein kinase Src (c-Src), Proline-rich tyrosine kinase 2 (PYK2) and p130cas to the sealing zone of the osteocyte during resorption, which is initiated by interactions with integrins such as αvβ3, suggests that they also play an important role in adhesion during the resorption process (Duong et al., 2000). Production of an actin ring ensures that there is an enclosed space for bone degradation and a proton pump and chloride channel creates an acidic environment of low pH in which mineral is dissolved (Lakkakorpi et al., 1989, Hochberg et al., 2014). The osteoclast has a ruffled border (Baron, 1989) which is essential for bone resorption and formed by exocytosis following the merging of osteoclasts and the bone surface. Acidified vesicles containing proteolytic enzymes and the osteoclasts themselves adjoin and enable the breakdown of organic and inorganic bone components. This border is sustained throughout resorption due to the tight equilibrium maintained between endocytosis and exocytosis (Stenbeck and Horton, 2000, Jensen et al., 2010). Proteolytic enzymes such as cathepsin K are secreted in the process of osteolysis during osteoclast matrix degradation (reviewed by Charles and

Aliprantis, 2014). Osteoclast activity is tightly coupled to osteoblast activity in healthy, young individuals to ensure that bone mass stays constant and disruption in this balance can lead to the onset of degenerative bone diseases such as osteoporosis (reviewed by Wallace et al., 2015).

Tartrate-resistant acid phosphatase (TRAP) is a well-known osteoclast marker and is secreted by osteoclast cells during bone resorption. It is particularly highly expressed in times of high bone turnover (Andersson and Ek-Rylander, 1995) and has been shown to play a role in the development of the growth plate and metaphysis of long bones (Blumer et al., 2012).

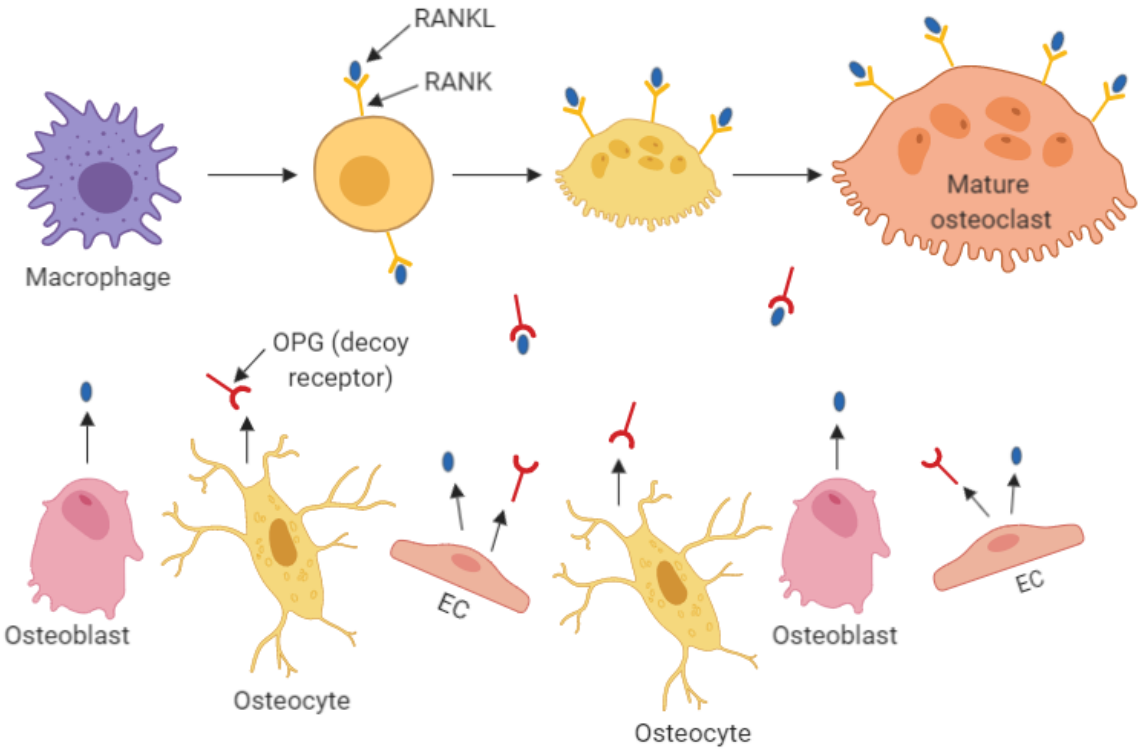

Figure 1.6: Osteoclast maturation from a macrophage to a mature cell. Osteoblast cells and endothelial cells (ECs) produce RANKL, which binds to RANK receptors on osteoclast progenitor cells. In some cases, RANKL will bind to OPG which is produced by osteocyte cells and also expressed by ECs. OPG acts as a decoy receptor and binds to RANKL to prevent it binding to RANK on the surface of osteoclast cells. RANKL promotes the maturation of the osteoclast from a monocyte to a mature osteoclast (image based on research by Silvestrini et al., 2005, Collin-Osdoby et al., 2001).

Recent studies have shown that the capabilities of an osteoclast involve much more than purely their important role in bone resorption. Osteoclasts are able to engulf microorganisms which has characteristically been shown to cause an up-regulation in bone resorption in response (Trouillet-Assant et al., 2015). Osteoclasts are also able to present antigens and respond to signals from inflammatory cytokines (Li et al., 2010). As well as this, osteoclasts have been shown to have further roles in the regulation of osteoblast differentiation, T-cell activation, the hematopoietic cell niche and tumour cell proliferation in bone (as reviewed by Charles and Aliprantis, 2014).

1.1.5 Bone modelling

The careful sculpting of the 213 bones which constitute the adult human skeleton is called 'modelling' (reviewed by Dempster, 2006, Khurana, 2009). In the 1960s, Frost identified the importance of bone modelling in growth and the dictation of the size and shape of the skeleton (Frost, 1963, Frost, 1969). Modelling is known to be involved in the shaping of the adult skeleton in response to loading or mechanical strain. It is a process that is more infrequent than remodelling; changes are steady and bone resorption is not tightly coupled to bone production, which means that the bone actively changes shape due to the lack of equilibrium between osteoblast cells and osteoclast cells (reviewed by Khurana, 2009, Kini and Nandeesh, 2012).

Modelling does not purely involve the deposition of new bone by osteoblasts, however. It has been suggested following the discussion of unpublished results performed by Boyce in a review article, that knockout studies have shown that RANKL/RANK/NF-κB are essential for the process of bone modelling, especially in the preliminary few weeks of life (Boyce and Xing, 2008). This is unsurprising, given the known role of RANK and RANKL communications in the development of osteoclasts (Marks and Seifert, 1985, Xiong et al., 2018, Dougall et al., 1999). Indeed, it was suggested that deletion of RANKL/RANK/NF-κB caused mice to have a thickened region of hypertrophic cartilage, due to the fact that osteoclasts were not present to degrade the cartilage, as well as developing osteopetrosis (Boyce and Xing, 2008). Cdc42 is involved in the control of osteoclast proliferation and is regulated by RANKL. It has been found that when Cdc42 is deleted from mature osteoclasts in mice, femur are of an abnormal shape due to reduced bone resorption and thus

modelling is dysfunctional. Cdc42 is therefore important in this process of modelling, where bones are sculpted and shaped (Ito et al., 2010).

In 1892, Wolff's law was introduced which denotes that the skeleton models and remodels itself as a result of the changing mechanical pressures that it has to withstand. It is now known that during periods of bone post-natal growth, modelling is especially active and it is thought to be altered as a result of the combined influence of nutrition, genetics, hormones and strain (Steenbock and Herting, 1955, Bingham and Raisz, 1974, Raisz and Bingham, 1972, Biewener et al., 1986). It has been suggested that bones model to ensure an equal balance of strain throughout their structure and modelling is thought to be location-specific (Biewener et al., 1986). Without the influence of strain, studies using denervated rat tibia have shown that the bone fails to develop properly. Bone mass is decreased and the tibial curvature is not present, showing the importance of strain such as exercise for healthy skeletal development (Lanyon, 1980).

1.1.6 Bone remodelling

In developed bone, the continual renewing and replacement of mineralised tissue is referred to as 'remodelling' and this is a process which happens throughout life (Dempster, 2006, Khurana, 2009). Studies have shown that both human and mouse bones react comparatively to a change in load by remodelling (Lanyon et al., 1975, Rubin and Lanyon, 1984). Unlike modelling, if the load that the bone is subjected to remains constant, the activity of osteoclasts and osteoblasts is tightly coupled and therefore the end volume of bone remains the same. Remodelling also plays a role in the maintenance of calcium homeostasis and it is involved in repairing damaged bone in juvenile and adult bone alike (Wang et al., 1998). Bones are able to adapt and progressively change as a result of different hormonal, mechanical or environmental pressures that they may be subjected to and bone has a specific lifespan to enable it to fulfil its mechanical or structural function efficiently. Beyond this time old bone must be replaced (Parfitt, 1994, Forwood and Turner, 1995, Frost, 1963, Frost, 1987). Remodelling activity is tightly regulated to ensure homeostasis and adequate bone strength.

A basic multicellular unit (BMU) has been proposed as being responsible for remodelling of cortical bone (figure 1.7). This intricate structure contains osteoclasts at the front, in a

cutting cone formation to remove old bone (Parfitt, 1994). Bone resorption is kick-started by the binding of osteoblast secreted RANKL to the RANK receptor on myeloid cells, stimulating osteoclast maturation (Marks and Seifert, 1985, Xiong et al., 2018).

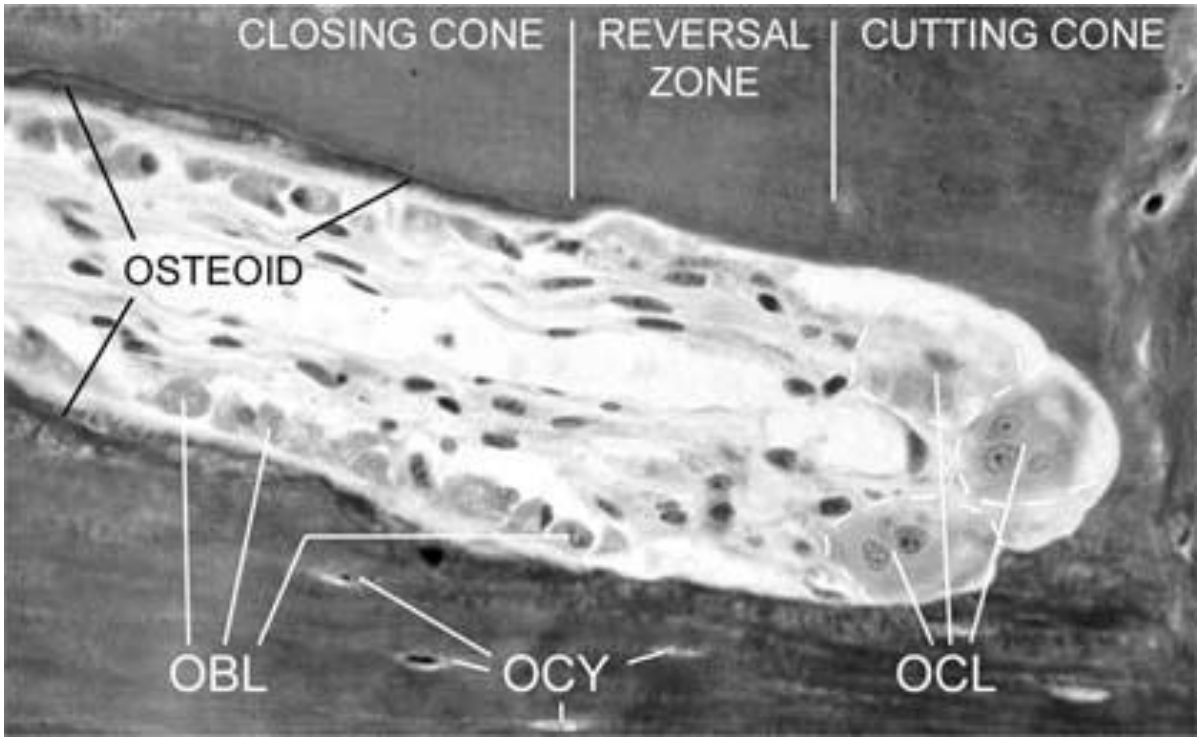

Figure 1.7: Structural organisation of a BMU responsible for bone remodelling. The osteoclasts (OCL) at the front create a cutting cone and the osteoblasts (OBL) at the back fill the gaps with osteoid which will be later mineralised. The osteocytes (OCY) are old osteoblasts that have become embedded within the bone matrix, remaining adjoined to the bone. Image of a human BMU taken from Smit et al., 2002.

Osteoblasts are found directly behind osteoclasts in the BMU, forming the closing cone which will lay down new bone. Runx2 and Osx are involved in the differentiation of mesenchymal progenitor cells into mature osteoblasts and mature osteoblasts subsequently produce collagen type I and osteocalcin (Parfitt, 1994, Niedermair et al., 2018). The gap in between the cutting and closing cone is filled with nerves, connective tissue and blood vessels creating a very specialised structure (Parfitt, 1994) and it is bone

production by osteoblast cells that takes the longest during the 2-8 month life-span of the BMU (reviewed by Kini and Nandeesh, 2012).

During the catabolic phase of fracture healing, there is 'coupled' remodelling which involves a cycle of osteoclast and osteoblast activity. Immature woven bone formed during initial bone mineralisation is resorbed by osteoclasts and secondary bone is laid down by osteoblast cells (Holstein et al., 2013, Melnyk et al., 2008). Remodelling of the newly formed bone is carried out, with the production of RANKL by osteoblast cells up-regulating the activity of osteoclasts, which shape and reform cortical and trabecular bone to its original pre-injury morphology (Flick et al., 2003). Vasodilation to increase the blood supply and inflammatory cytokines to the fracture site is one of the first responses following a bone injury. Here, blood supply is subsequently returned to normal levels by the remodelling and pruning of vessels, completing the healing process (Holstein et al., 2013, Melnyk et al., 2008).

In mice, the remodelling process is thought to be slightly different to humans where it has been suggested that a BMU is involved in the regulation of bone turnover. Mice do not have Haversian canals but contain their primary canals throughout their lifetime, due to the fact that their bones do not undergo spontaneous remodelling (Cooper et al., 2016, Sietsema, 1995). In mice, the highest levels of growth occur between 3 and 6 weeks of age. Changes in the bones of mice therefore occur via periosteal resorption by osteoclasts, which is paired with endosteal osteoblast activity in which new bone is laid down. Like in humans, this is a closely regulated process and in adult bones an equilibrium must be maintained in order to prevent net bone loss (Martin et al., 1998). It has been suggested that the size of the porosity in mice is directly comparable and scalable to the size of the cortical porosity in humans (Jowsey, 1966).

1.1.6.1 Dysfunctional remodelling

Remodelling is shown to play an essential role in the maintenance of bone health and also in bone healing following fracture. A close equilibrium between osteoclast activity and osteoblast activity is heavily important in this process and a disruption in the balance can have adverse effects. An increase in intracortical porosity has been identified with age and it is thought that this is as a result of dysfunctional remodelling (Núñez et al., 2018). In humans, remodelling is known to be much more active in menopausal women and to a

lesser extent in men of a similar age (as reviewed by Pacifici et al., 1989, Clarke, 2008), suggesting that the decrease in concentration of oestrogen at this stage of a woman's life has a large influence in the control of bone remodelling. In fact, oestrogen has been shown to prevent the apoptosis of osteoclasts, maintaining the tight equilibrium between osteoclast and osteoblast activity (Hughes et al., 1996). An *in vivo* study using ovariectomised pigs has shown that oestrogen supresses the activity of osteoclasts, maintaining bone homeostasis in females. Oestrogen is involved in the regulation of bone strength and removal of the ovaries meant that the pigs no longer produced oestrogen, mimicking menopause in humans (Pufe et al., 2007). As a result, there are disruptions in bone remodelling in post-menopausal women and this is due to bone being broken down by osteoclasts faster than it is being laid down by osteoblasts. Disruptions in bone remodelling are shown in post-menopausal osteoporosis and result in a net decrease in bone mass due to the poor regulation of osteoclastic activity (Albright, 1947b, Albright, 1947a, Balasch, 2003).

Osteoporosis is a degenerative bone disease which is characterised by highly porous, brittle bones and affected twenty-two million women and 5.5 million men in the EU in 2010 (Hernlund et al., 2013). It is particularly prevalent in the ageing population, where there is more bone resorption than there is bone production, causing changes in the structure of the bone and a decrease in bone mass due to dysfunctional remodelling. As a result, fragility fractures are characteristically associated with osteoporosis and are bone fractures which are the result of low-impact trauma (Pietri and Lucarini, 2007). In osteoporotic animal models, it has been shown that several key features of the bone healing process are inhibited. This includes impaired matrix production, callus formation and callus remodelling (Stuermer et al., 2010, Thormann et al., 2014, Alt et al., 2013). In 5-10% of cases, there is the occurrence of non-union fractures in which fracture healing is further impaired and surgical intervention is required (Gómez-Barrena et al., 2015). Subsequently, not only are osteoporosis sufferers more prone to fracture due to dysfunctional remodelling which makes bones incredibly porous, they are less able to recover and therefore osteoporosis can ultimately lead to mortality.

Other bone diseases which are prevalent as a result of disruptions in bone remodelling include renal osteodystrophy, Paget's disease, osteopetrosis and rickets. Renal osteodystrophy is characterised by either high (hyperparathyroidism) or low

(hypoparathyroidism) bone turnover rates. Irregular bone morphology, the formation of osteoid and fibrosis are common signs. In contrast, Paget's disease typically has a high bone turnover due to an increase in bone resorption and bone production. This results in the deposition of woven bone and bones are commonly populated with lesions (Siris and Feldman, 1997, Singer, 2009). Osteopetrosis is caused by a deformity in osteoclast activity, which results in a higher bone density in comparison to controls (reviewed by Tolar et al., 2004). Rickets is often associated with low levels of vitamin D. This in turn, increases RANKL secretion by osteoblasts and subsequently the differentiation of osteoclast cells. At the same time the differentiation of osteoblast progenitors is supressed and as a result, bone turnover is upregulated. This gives the individual a much higher risk of fracture and ultimately, osteoporosis (Anderson et al., 2008, Feng and McDonald, 2011).

1.1.7 Bone mineralisation

The most abundant component in the composition of the skeleton is mineral, making up 70% of our bones (reviewed by Augat and Schorlemmer, 2006). A combination of calcium (Ca), phosphorous (P), carbonate (CO_3), sodium (Na), water (H_2O), nitrogen (N), carbon (C) and potassium (K) makes up this mineral and the exact proportions of each is dependent on the function of the bone. The skull is made up of compact bone and has been shown to have much higher levels of Ca, P, CO_3 and Na, but much lower levels of H_2O, N, C and K in comparison to bones such as the ilium in the pelvis which contains high proportions of trabecular bone (Agna et al., 1958). It has been suggested that bone in fact contains ~99% of the bodies calcium reserves, ~85% of the bodies phosphorous, ~90% of total sodium and ~50% of total body magnesium (Avioli and Krane, 1998). The important interactions between calcium and phosphate in the process of bone mineralisation have been studied for many years and it is known therefore that hydrolysis of calcium phosphate produces octocalcium phosphate, the intermediate bone mineral form (Biltz and Pellegrino, 1977).

After the first phase of bone matrix synthesis, osteoblasts enter the mineralising phase, in which there is ultimately invasion of hydroxyapatite crystals into the newly formed matrix which prior to this is in an immature state and consists purely of unmineralised collagen fibrils (Rey et al., 1996, Ecarot-Charrier et al., 1988). The distinct mechanisms by which this occurs remain debated in the literature, however it is thought that mineralisation is separated into vesicular and fibrillar stages.

The mineralisation of the extracellular matrix (ECM) occurs via the actions of matrix vesicles (MVs), which evidence suggests are formed by the budding of chondrocyte and pre-mineralised osteoblast cell membranes (Majeska and Wuthier, 1975). MVs hold both phosphate and calcium ions which are bound by proteins and lipids within the vesicle. The process of mineralisation begins by the upregulation of phosphatases within the MV itself, which include; ALP, adenosine triphosphatase (ATP) and PHOSPHO1 (reviewed by Anderson, 2003). ALP is involved in the promotion of mineralisation by hydrolysing pyrophosphate (PP_i), an inhibitor of bone mineralisation, to produce inorganic phosphate (P_i). This is a process which is tightly regulated in order to ensure that sufficient levels of mineralisation are activated at the correct time (Narisawa et al., 1997, Johnson et al., 2000). ALP works alongside nucleotide pyrophosphate phosphodiesterase (NPP1) and ankylosis protein (ANK), which conversely are involved in the inhibition of mineralisation and act to maintain this balance. Studies have found that NPP1 and ANK promote the production of PP_i, negatively regulating bone mineralisation (Harmey et al., 2004).

Following the vascularisation of the bone cortex, the mitochondria of the hypoxic cells located in the collagen matrix become abundant in oxygen, Pi and calcium species, triggering their release into the cytosol of the MV (Shapiro et al., 1988). Transporters which are located in the vesicle membrane include annexin II, V and VI and it is proposed that they are able to act as calcium channels for the movement of calcium into and out of the MV. Calcium then chelates with Pi to produce the first mineral deposits (Kapustin et al., 2011).

The role of ALP in matrix mineralisation was investigated further by a study in which ALP was ablated. This surprisingly showed that the production of mineral and hydroxyapatite was still taking place within MVs, suggesting that ALP works alongside other regulators of mineralisation, which are able to compensate for the loss of ALP. It was hypothesised that PHOSPHO1 was likely to play a role in this (Anderson et al., 2004). It has subsequently been shown that homozygous deletion of PHOSPHO1 causes skeletal deformities such as osteomalacia and increased fracture risk (Huesa et al., 2011), a phenotype which has since been confirmed in *Phospho1* knockout studies which identified patchy osteomalacia and arrested mineralisation fronts by use of SEM (Boyde et al., 2017). It is thought that PHOSPHO1 is able to stimulate mineralisation by producing Pi from phospholipids such as phosphocholine and phosphoethanolamine (Roberts et al., 2004, Roberts et al., 2007), as

well as interacting with other regulators of bone mineralisation such as ALP. The abnormalities in bone mineralisation seen here were therefore hypothesised to be due to PHOSPHO1 ablation causing a decrease in ALP and subsequently reducing the levels of mineralisation by upregulating PP_i (Huesa et al., 2011). Double ablation or inhibition of both PHOSPHO1 and ALP has been shown to inhibit mineralisation nearly entirely, emphasising the importance of the combined actions of both components in osteoblast and chondrocyte matrix mineralisation (Yadav et al., 2011). *In vivo* and *ex vivo* studies have since verified the close communications between PHOSPHO1 and ALP, which are essential in the mineralisation of bone (Huesa et al., 2015).

MVs have been shown to interact with and bind to the proteoglycans in the pre-existing bone matrix. Not only do annexins in the cell membrane facilitate the movement of calcium ions, annexin V is thought to be particularly significant in the upregulation of calcium phosphate formation within the MV in the process of bone mineralisation (Genge et al., 2008). It is the interactions between calcium and phosphate ions following nucleation which results in the formation of hydroxyapatite crystals (Avioli and Krane, 1998). Subsequently, this leads the fibrillar stage, in which the MVs fill to bursting point with calcium and phosphate ions and on bursting, hydroxyapatite populates the bone matrix and embeds itself between collagen fibrils (reviewed by Florencio-Silva et al., 2015).

The fibrillar stage of mineralisation is thought to be regulated by members of the small integrin-binding ligand N-linked glycosylated (SIBLING) family of proteins, which include MEPE, DMP1 and osteopontin (OPN) (Fisher and Fedarko, 2003, Qin et al., 2001). MEPE is expressed in hypertrophic chondrocytes and is thought to bind to hydroxyapatite to regulate matrix mineralisation via its acidic, serine and aspartic acid-rich motif (ASARM), which can be found in the C terminus (Addison et al., 2008). ASARM is only able to negatively regulate mineralisation if serine is in its phosphorylated state (Rowe et al., 2000, Martin et al., 2008), which could potentially be linked to a decrease in key endothelial cell markers following its phosphorylation. The activity of MEPE can be controlled by the cleavage of ASARM (Staines et al., 2012, Martin et al., 2008) and it has been identified that when serine is not phosphorylated in ASARM, matrix mineralisation is up-regulated (Staines et al., 2012).

Remodelling is separated into two phases. Initially during primary remodelling, there is incredibly quick mineralisation of osteoid. This is followed by secondary remodelling in

which mineral is embedded into the bone matrix much more slowly. EphrinB2 plays a known role in the control of osteoblast differentiation, however until very recently the role of osteocyte-derived EphrinB2 in mineralisation was unknown. To investigate this further, EphrinB2 has been ablated in osteocytes and it has been shown that transgenic knockout mice have dysfunctional secondary mineralisation which has been linked to an up-regulation in autophagosomes. Therefore, it is suggestive that autophagic events within osteocytes may be responsible for the control of secondary bone mineralisation and that primary and secondary remodelling are regulated by individual mechanisms (Vrahnas et al., 2019).

The role of sclerostin in the mineralisation of bone has been demonstrated by the use of anti-sclerostin antibodies, which are able to bind to sclerostin and silence its activity. Following ovariectomy there is, like in the menopause, an increase in bone loss. Anti-sclerostin causes a reduction in osteoclast activity and an up-regulation in osteoblast activity, increasing the mineralising surface. Therefore, when activated, sclerostin is involved in the inhibition of mineralisation (Ominsky et al., 2010, Veverka et al., 2009). The mechanism by which it functions is via the up-regulation of MEPE-ASARM, which has been shown to inhibit mineralisation in its phosphorylated form (Atkins et al., 2011).

1.2 Endothelium

1.2.1 Vascular derived endothelial cells

The first isolation of human umbilical vein-derived endothelial cells (HUVECs) in cell culture was as early as 1973, where they were shown to grow in monolayers for up to five months (Jaffe et al., 1973). This was pioneering work in the characterisation of the vascular endothelial cell, which provided a platform for future studies and investigations into endothelial cell function, a cell type which has since been shown to have a vast surface area of 1 to 7 m^2 in the human adult and is largely heterogeneic (Cines et al., 1998).

Vasculogenesis is the process in which blood vessels are produced from mesodermal endothelial cell progenitors known as angioblasts and hemangioblasts during the early stages of development (Risau and Flamme, 1995, Tsuji-Tamura and Ogawa, 2018). Semi-permeable vascular endothelial cells form a degree of separation between the blood and the smooth muscles of the blood vessel, which are able to undergo vasoconstriction and vasodilation in response to specific stimuli (Collin-Osdoby, 1994). Early work on the characterisation of endothelial cells suggested that their key role was purely as a barrier and described them as 'nucleated cellophane' (Florey, 1966). It has since been shown that these cells which line our blood vessels are highly dynamic and active in the maintenance of health, with many important and complex functions.

Over the past 40 years, our knowledge on vascular endothelial cells has evolved beyond measure. From the tiniest capillaries to the largest organs such as the heart, vascular endothelial cells line every artery, vein and capillary in the body (as reviewed by Rajendran et al., 2013). In fact, so important that endothelial cells have been referred to as 'building blocks of the nutrient transport network', a perfect summary of their role (Grosso et al., 2017). Key functions of vascular endothelial cells include; the regulation of a haemostatic balance, leukocyte interaction during inflammation, control of blood clotting and coagulation, maintenance of vascular tone and angiogenesis, tissue morphogenesis and organ development (Rajendran et al., 2013, Ramasamy, 2017). A good blood supply is also vitally required for the transport of oxygen around the body and therefore without functioning vascular endothelial cells, there would be hypoxia, cell apoptosis and ultimately death (Grosso et al., 2017).

The activity and function of vascular endothelial cells is altered by the binding of growth factors, lipid transporting particles, metabolites and hormones to receptors which are situated on the cell membrane. Endothelial cells have been shown to play an important role in the control of blood flow and regulate vasodilation by the release of nitric oxide (NO) and prostacyclin (PGI2) and also control vasoconstriction by the release of endothelin (ET) and platelet-activating factor (PAF). Not only is vasodilation important in inflammation, it can also be initiated by an increase in blood flow, which causes the release of endothelial nitric oxide synthase (eNOS) as a result of an up-regulation in shear stress (Cines et al., 1998).

Dysfunctional vascular endothelium is a key marker of disease and is associated with the onset of a vast range of pathologies, including; cancers (including tumour growth and metastasis), stroke, heart disease, diabetes and kidney failure (Rajendran et al., 2013). This is often as a result of the presence of free radicals, which can make the endothelium become excessively and unselectively permeable, allowing the movement of toxins across its cell membrane and negatively influencing the balance of NO (Rubanyi and Vanhoutte, 1986).

1.2.2 Angiogenesis

Angiogenesis occurs after initial blood vessels have been laid down during endochondral ossification and is a process in which new vasculature is produced from pre-existing blood vessels to make an extensive network, enabling blood flow around the body and within our skeletal system (Risau, 1997). Vascular endothelial cells are the main cell type involved in the production of these new vessels and in order to do this, they must proliferate, migrate, form tubules and finally organise themselves to create a sealed passageway for the flow of to specific areas of the body (as reviewed by Portal-Núñez et al., 2012). In bone, angiogenesis is the main process by which the complex vascular network is formed to enable the transport of oxygen, nutrients, growth factors and hormones to the bone cells (reviewed by Tong et al., 2019).

There are two key forms of angiogenesis; the sprouting of new capillaries from pre-formed vessels or splitting of existing vessels to form new capillaries, a process also known as intusception. Sprouting and intusception have been known to occur simultaneously in the

angiogenesis of organs such as the heart during late organogenesis. At the tip of the sprout, there is an elongation of endothelial cells in the direction of neighbouring cells which are producers of pro-angiogenic factor VEGF. Intusception on the other hand, occurs in organs such as the lungs in which the vessels have wide channels and a sudden up-regulation of endothelial cell proliferation within the lumen prompts the separation of new capillaries from pre-existing vessels (Risau, 1997).

A balanced and closely regulated relationship between angiogenesis and osteogenesis is required for optimal bone health, strength and repair (Trueta and Trias, 1961, Trueta and Buhr, 1963, Kusumbe et al., 2014b). One of the main inducers of angiogenesis is hypoxia, which up-regulates the expression of hypoxia inducible factor-1 (HIF1) and subsequently the expression of potent mitogen VEGF by osteoblasts (Cramer et al., 2004). There is compelling evidence to suggest that VEGF produced by bone-derived osteoblast cells interacts with vascular endothelial cells in a paracrine manner to up-regulate angiogenesis and the division of vascular endothelial cells, ensuring that it is tightly coupled with bone production (Muller et al., 1997, Breier and Risau, 1996, Gerstenfeld and Einhorn, 2006). A recent study has suggested that blood vessels are then able to control cell differentiation, growth and tissue regeneration via paracrine signals with neighbouring tissues (Ramasamy et al., 2016). Exercise has also proven to initiate angiogenesis in bone, in response to the mechanical loading incurred (Matsuzaki et al., 2007).

Equally, the influence of Angiopoietin in the regulation of angiogenesis must not be underestimated, with an identified role in angiogenesis during both osteogenesis and fracture healing. Acting in a different way to VEGF, when VEGF is not present Angiopoietin 2 initiates vessel destabilisation and retraction (Holash et al., 1999). In the presence of VEGF however, it has been shown that Angiopoietin 2 up-regulates the migration (Witzenbichler et al., 1998) and sprouting (Koblizek et al., 1998) of endothelial cells .

Notch signalling has proven to be important in the formation of the leading “tip” and following “stalk” endothelial cells, which communicate with each other in order for angiogenesis to take place (Gerhardt et al., 2003). Following the binding of VEGF to VEGF receptor 2 (VEGFR2) on endothelial cells, there is an increase in Notch Delta-like ligand 4 (DLL4), which subsequently binds to Notch1 receptors on endothelial cells. This in turn acts to limit the rate of angiogenesis by reducing the levels of VEGFR2 on these vascular

endothelial cells and inhibits disproportionate tip selection, only allowing a leading tip to contain the high levels of VEGFR2 required for angiogenesis (Noguera-Troise et al., 2006, Claxton and Fruttiger, 2004, Sainson et al., 2005). It is thought that the timing, intensity and robustness of these choices is influenced by tetraspanin, which magnifies VEGF signalling during endothelial cell tip selection in angiogenesis (Page et al., 2019).

The role of angiogenesis in fracture healing has been acknowledged for many years (Trueta and Trias, 1961, Trueta and Buhr, 1963), but the mechanisms involved have remained unclear until more recently. It is now known that the tight coupling between osteogenesis and angiogenesis takes place via a positive feedback loop, in which osteoblast cells produce growth factors including PDGF and VEGF (Harada et al., 1994, Wang et al., 1996) to upregulate angiogenesis via vascular endothelial cells (Risau, 1997). In turn, vascular endothelial cells produce up-regulators of osteogenesis such as BMP-2 and BMP-4, Wnt5a and Notch signaling which enhance the proliferation and differentiation of osteoprogenitor cells (as reviewed by Liu and Castillo, 2018, Grosso et al., 2017). Following fracture, osteoprogenitor cells and newly formed vessels produced by angiogenesis will enter the site of the bone injury together, dependent on each other and work together to drive bone regeneration (Hausman et al., 2001, Kurdy et al., 1996). Angiogenesis is known to be important in the healing of big bone injuries too, in a process called distraction osteogenesis, where osteogenesis must be fully activated in order for bone healing to take place. Studies have shown that local injection of endothelial cell progenitor cell exosomes into the location of injury accelerated bone regeneration and distraction osteogenesis by the upregulation of angiogenesis (Jia et al., 2019).

The functions of angiogenesis are not all helpful to the body however, as the sprouting of new blood vessels is also involved in the progression of cancer. A rich blood supply formed by blood vessel sprouting for delivery of oxygen and nutrients provides the perfect microenvironment for tumour growth. VEGF as a promotor of angiogenesis plays a large role in this process, proven in experimentation using VEGF neutralising antibodies which were able to suppress glioma tumour growth (Breier and Risau, 1996). Aggressive tumours require high levels of oxygen in order to proliferate and therefore a common characteristic of solid tumours is hypoxia (Vaupel et al., 2004), an up-regulator of angiogenesis via the combined actions of VEGF and Angiopoietin 2 which initiate the proliferation of vascular endothelial cells. New vascular networks unlike those in healthy angiogenesis are

structurally and functionally abnormal, but nevertheless promote metastases and increase the likeliness of resistance to treatment (reviewed by Schito, 2019, Schito and Semenza, 2016).

1.2.2.1 Biological effects of VEGF

VEGF is a major stimulator of vasculogenesis and early studies have shown that receptors are located on angioblasts, with adequate levels of growth factor binding required for angioblast differentiation to occur (Risau, 1997). VEGF is also a potent mitogen (Muller et al., 1997) and its main function is as an inducer of angiogenesis, playing a key role in the communication between bone cells and endothelial cells (Risau, 1997). This in turn promotes the migration, proliferation and survival of endothelial cells (reviewed by Hoeben et al., 2004).

Overexpression or under expression of VEGF can have serious consequences and a great amount of information on the precise functionality of this growth factor has been gained by performing knockout studies. It has been shown that a global deletion of VEGF is lethal and this has severely limited the progression of our knowledge on the role of VEGF in later developmental processes. Studies have shown that even one missing VEGF-A allele causes mortality between embryonic day 11 and embryonic day 12. Post-mortem unsurprisingly identified that these mice had abnormal vasculature, as well as cardiovascular deformities and poorly developed forebrains (Carmeliet et al., 1996, Ferrara et al., 1996). VEGF is therefore vital for survival and the development of a healthy blood supply.

1.2.2.2 Isoforms of VEGF

VEGF was first recognised as ‘vascular permeability factor’, following its identification in tumour cells (Senger et al., 1983). Subsequently, it was Ferrara et al. who characterised vascular endothelial growth factor (VEGF) and named it as a result of its observed interactions with endothelial cells (Ferrara and Henzel, 1989). VEGF was shown to be undistinguishable from vascular permeability factor and it was therefore concluded that they were the same (Leung et al., 1989).

Six subtypes of VEGF make up the VEGF family of homodimers in humans, namely VEGF-A, VEGF-B, VEGF-C, VEGF-D, VEGF-E and placenta growth factor (Ferrara et al., 1996, Achen

et al., 1998, Jeltsch et al., 1997, McMahon, 2000, Olofsson et al., 1996, Petrova et al., 1999). The most commonly recognised subtype of VEGF is VEGF-A, which is arguably the most important promotor of blood vessel formation. VEGF-A has five key isoforms which are 121, 145, 165, 189 and 206 amino acids long in humans. Each one of these isoforms is one amino acid less in mice than it is in humans and they are produced as a result of alternative splicing of exons 6 and 7 (Park et al., 1993, Poltorak et al., 1997).

VEGF-A binds to VEGF receptors (VEGFR-1 and VEGFR-2), which are located on vascular endothelial cells (Terman et al., 1991, Shibuya et al., 1990). The first isoform of VEGF-A ever classified by Ferrara et al. was $VEGF_{165}$, which was shown to act as a potent mitogen and to up-regulate proliferation in vascular endothelial cells (Ferrara and Henzel, 1989). Since, it has been discovered that $VEGF_{165}$ (a 45kDa homodimer) is important for the survival of endothelial cells, migration, growth and vascular permeability. It has also been shown to play a role in the onset of pathologies, including cancers. $VEGF_{165}$ has an affinity for heparin and is the only isoform to bind both neuropilin-1 and neuropilin-2. $VEGF_{189}$ and $VEGF_{206}$ are also able to bind to heparin via heparin binding domains and this means that unlike $VEGF_{121}$ which is able to move freely, they are confined to the extracellular matrix (Lange et al., 2003, Bates et al., 2002, Woolard et al., 2004, Cohen et al., 1995, Poltorak et al., 1997).

The other five VEGF subtypes which make up the VEGF family are not as well documented in the literature, but each have specific functions due to their different affinities to each of the VEGF receptors. PDGF and VEGF-B bind to VEGFR-1, whereas VEGF-D and VEGF-E bind to VEGFR-2 and VEGF-C binds to VEGFR-2 and VEGFR-3 (as reviewed by Holmes and Zachary, 2005). Unlike deletion of VEGF-A, ablation of VEGF-B is not lethal but has enabled us to discover that VEGF-B has a role as an endothelial mitogen, with a specific function in the regulation of blood vessels which supply the heart (Bellomo et al., 2000). VEGF-C can be isolated in the ovaries, intestine, thyroid gland, heart and placenta and is often localised to sprouting lymphatic vessels (Chen et al., 1999, Li and Eriksson, 2001). It has since been shown to promote lymphatic function and therefore has been investigated as a potential treatment for inflammatory bowel diseases (D'Alessio et al., 2014). Although not to the same extent as VEGF-A, VEGF-D is also involved in the upregulation of angiogenesis and also lymphangiogenesis (Rissanen et al., 2003). VEGF-E is encoded in the genome of the Orf parapox virus, which is known to stimulate angiogenesis and infect mainly farm animals, but occasionally humans. Like other VEGF subtypes, it is therefore important in

angiogenesis (Lyttle et al., 1994). Finally, the roles of PDGF appear to be diverse and it is known to play an important part in; gastrulation, neural crest development, organogenesis (lung and intestine), cell migration, development of the skin, growth of the testes and spermatogenesis, maintenance of kidney health, lens development, glial cell development, cardiovascular development, haematopoiesis and the onset of some cancers and tumours (as reviewed by Andrae et al., 2008).

1.2.2.3 VEGF receptors

VEGF binds to receptor tyrosine kinases; VEGFR-1, VEGFR-2 and VEGFR-3 (Achen et al., 1998, Joukov et al., 1996, van der Geer et al., 1994, Shibuya, 1995, Terman et al., 1992). Despite the fact that the affinity of VEGF-A to VEGFR-1 is 10-fold greater than it is for VEGFR-2, interactions with VEGFR-2 are most documented in the literature and it is the key receptor involved in the up-regulation of signalling pathways due to its enhanced tyrosine kinase activity. VEGFR-1 sequesters VEGF by binding it in competition with VEGFR-2 (Takahashi and Shibuya, 2005, Olsson et al., 2006). Where VEGFR-1 and VEGFR-2 are both expressed purely on vascular endothelial cells, VEGFR-3 can be found on endothelial cells in the lymphatic system (Kaipainen et al., 1995).

Following binding of VEGF to the receptors, homodimerisation initiates tyrosine phosphorylation and signal transduction particles gather, which are involved in the activation of specific cellular responses to VEGF (reviewed by Stuttfeld and Ballmer-Hofer, 2009). This includes the regulation of pathways such as the MAP kinase, PI3K, Src and Rac, which all rely on the binding of VEGF with its receptor for their activation (Koch and Claesson-Welsh, 2012).

Knockout studies have also improved our understanding of the role of VEGF receptors, specifically VEGFR-1 and VEGFR-2. When VEGFR-2 (Flk-1) is deleted, mice do not survive past embryonic days 8.5-9.5. These mice have dysfunctions in the differentiation of endothelial and hematopoietic stem cells and are therefore unable to live (Shalaby et al., 1997, Shalaby et al., 1995). A global deletion of VEGFR-1 (Flt-1) impairs the development of healthy vasculature (Fong et al., 1995).

1.3 Vascular endothelial cells in bone

1.3.1 Endochondral ossification

The invasion of blood vessels into the bone cortex is an important part of both intramembranous and endochondral ossification (reviewed by Gerber and Ferrara, 2000). As previously mentioned, where intramembranous ossification produces new bone without an intermediate stage, endochondral ossification is a multi-step process involving a cartilage intermediate phase. Endochondral ossification is incredibly important in the process of long bone formation and takes place at diaphyseal and epiphyseal ossification points (Ortega et al., 2004). If beta-catenin is not activated by the Wnt signalling pathway, mesenchymal cells will differentiate into chondrocytes which begin to secrete cartilage components for construction of the ECM (Akiyama et al., 2004, Mak et al., 2006, Tamamura et al., 2005). This process is called hypertrophy and the chondrocytes grow in size as it takes place. Hypertrophic chondrocytes can be found in the epiphyseal growth plate at the end of growing long bones and express mRNA for VEGF, which plays a key role in endochondral ossification and vascularisation of the cortices, a prerequisite for bone formation (Ferrara et al., 2003, Gerber and Ferrara, 2000).

Early studies by Gerber et al. have shown that blocking VEGF negatively impacts endochondral ossification and inhibits mineralisation. Using mFlt(1-3)-IgG to block VEGF in 24 day old mice, the specific effect of global VEGF silencing on bone growth and blood vessel invasion into the cartilage was looked at in further depth. Blocking VEGF showed a huge adverse effect on the formation of blood vessels in the growth plate, the expansion of hypertrophic chondrocyte zone and also on the development of the trabecular bone as a result of the mutation (Gerber et al., 1999a). This is supported by Olsen et al. who show that mice that only have the $VEGF_{120}$ isoform survive but have defects in both the early and later stages of vascular invasion into the cartilage, with possible additional adverse effects on the maturation of chondrocytes (Zelzer et al., 2002). Increasing evidence suggests therefore that not only is VEGF required for the vascularisation of the primary ossification centre and the development of bone, it is also essential for the survival of chondrocytes (Zelzer et al., 2004).

The formation of the cartilage intermediate is an important transition phase as it provides a solid platform for bone production. Close communications between these hypertrophic chondrocytes and endothelial cells ensures that the processes of vasculogenesis and ossification are in synch (Lewinson and Silbermann, 1992). In the jaw, early studies identified the next stages of endochondral ossification to be slightly different. Here it is thought that there is fusion of hypertrophic chondrocytes and the cells do not die, but once the cartilage template is degraded, they are involved in the production of new bone (Silbermann and Frommer, 1972). In the long bones, it is thought that chondrocytes eventually undergo apoptosis and there is degradation of the transverse septa cartilage components directly adjacent to these cells. This creates space for the invasion of osteoclasts, osteoblast precursors, bone marrow cells and blood vessels, all of which are essential in bone and bone marrow cavity formation (Mackie et al., 2008, Gibson, 1998). Osteoblasts deposit new bone on the cartilage foundations and secrete matrix components which include type I collagen. Osteoclasts help to further degrade the avascular cartilage and work in parallel with osteoblasts to maintain homeostasis. These osteoclasts have been isolated to the ends of branching capillaries and the endothelial cells, therefore they work together with osteoblasts to sculpt the bone (Streeten and Brandi, 1990). It has been found that endochondral ossification is reliant on the close coupling of angiogenesis and osteogenesis by immature (osterix-expressing) osteoblastic precursors (Maes et al., 2010).

An adequate blood supply to the bones is essential for human survival and therefore the replacement of avascular cartilage with blood vessels, osteocytes and bone matrix is a vital part of endochondral ossification. Although it has been indicated that the secretion of cartilage components by chondrocytes comes prior to the penetration of the vascular network into the avascular cartilage (Lewinson and Silbermann, 1992, Gibson, 1998), there is conflicting evidence which implies that blood vessels are one of the first structures to be laid down in endochondral ossification, before cartilage formation occurs (Dilling et al., 2010). It has been suggested that during the sprouting of the vasculature towards the hypertrophic cartilage, immature osteoblasts will ‘piggy back’ onto the pre-existing vessels, with VEGF amongst other factors acting as a migratory signal (Maes et al., 2010). This area of uncertainty regarding the precise timing of vascular invasion in bone development would prove valuable to clarify in the future as in order to treat diseases that have vascular

phenotypes, the mechanisms involved in the development of this network of blood vessels must be fully understood.

1.3.2 Haversian systems

In 1678, Leeuwenhoek was the first person to identify canals within the bone microstructure, using microscopy (Enlow, 1962). However, it was Clopton Havers who then went on to describe the structure of these canals in increased detail. This pioneering work was famously titled 'Osteologia nova' and as a result of his findings, the structures found within cortical Haversian systems (osteons) in adult bone are referred to now as Haversian canals (figure 1.8) (reviewed by Dempster, 2006).

Haversian canals are a branched network of lamellae lined canals in which vessels and nerve filaments pass through (Currey, 1960). They take up an organised longitudinal row formation in the bone and their density is thought to increase with age (Cohen and Harris, 1958, Tappen, 1977, Stout et al., 1999). In cortical bone, microscopy has shown that these lamellae form concentric circles around the blood vessel. Branching is regulated by the presence of transverse Volkmann's arteries, which are much shorter vessels that connect Haversian arteries to the periosteal arteries and ensure adequate blood flow to the outside of the human skeleton (Ramasamy, 2017, Kim et al., 2015). Regional differences in this branching have been identified, with large and branched Haversian canals in the endosteal region and small and linear Haversian canals with increased lamellae in the periosteal region (Kim et al., 2015). The average global diameter of a Haversian canal in females is approximately 0.055mm, however occasionally 'giant' canals are identified in the bone cortex with a much larger diameter of over 0.385mm. The density of these canals in the anterior region is proven to be increased two fold in human fracture subjects, suggesting that their presence increases the likelihood of a fragility fracture and therefore has a negative impact on bone integrity (Bell et al., 1999).

In addition to the primary blood vessel canals laid down during bone development when bone is rapidly growing, secondary canals which can be found within Haversian canals are produced during bone turnover in large adult vertebrates such as humans (Frost, 1963). These secondary Haversian systems are formed when bone is resorbed and replaced by new lamellae in response to previously described stimuli in the process of remodelling

(Enlow, 1962). In contrast to primary canals where there are no amorphous cement lines bordering the osteon and lamellae runs smoothly with the bone surface to encase the blood vessel canals before branching, secondary Haversian systems have a tight circular formation, with osteocytes and resorption lacunae embedded amongst the lamellae. The canaliculi present on the surface of osteocytes within lacunae enables communications through the dense cortical bone, between osteocytes and Haversian canals. Separation of the Haversian system with the rest of the bone is established as a result of cement lines (Martiniaková et al., 2007).

The porous nature of our bones subsequently enables them to be vascularised, unlike cartilage which is completely avascular (reviewed by Marenzana and Arnett, 2013). Contrasting humans, smaller vertebrates such as mice have a complex network of blood vessels canals, but have no Haversian canals and bones do not undergo secondary modelling (Cooper et al., 2016). Rats have been used as a model for structural characterisation of Haversian canals in the past, however the presence of secondary Haversian system remodelling in these vertebrates remains debated in the literature. Although Haversian systems show to be existent in Wistar rats, historical studies using the white rat have shown that the presence of osteons is much rarer than in larger organisms such as rabbits, dogs and monkeys (Kim et al., 2015, Duranova et al., 2014). Regardless of the size of the animal however, a complex network of vasculature will still exist (Enlow, 1962).

The reasoning behind this lack of Haversian canals in small rodents is unclear, however it could be hypothesised that this is due to the fact that rodents have a much lower cortical thickness in comparison to larger vertebrates and therefore diffusion distances to the nearest tissue are much lower. In wild type mice, the average thickness of the cortical bone diaphysis is 0.21mm, however this increases with the size of the vertebrate and has been shown to be 0.38mm in dogs, which is nearly doubled (Bagi et al., 2011). The density of osteocyte lacunae in relation to the distance from a Haversian canal in humans also as much as doubles when you compare numbers in close proximity to those further away, suggesting that higher numbers are required in the absence of a close Haversian canal (Hannah et al., 2010). Therefore, perhaps smaller rodents such as mice are able to compensate for the lack of Haversian systems using their intricate organisation of blood vessel canals and osteocyte lacunae, as well as shorter diffusion distances. The answer

remains un-investigated, however mice are commonly used as model animals for investigations into the vasculature nevertheless due to the physiology and mechanism of action by which their vessels work being otherwise directly comparable to humans.

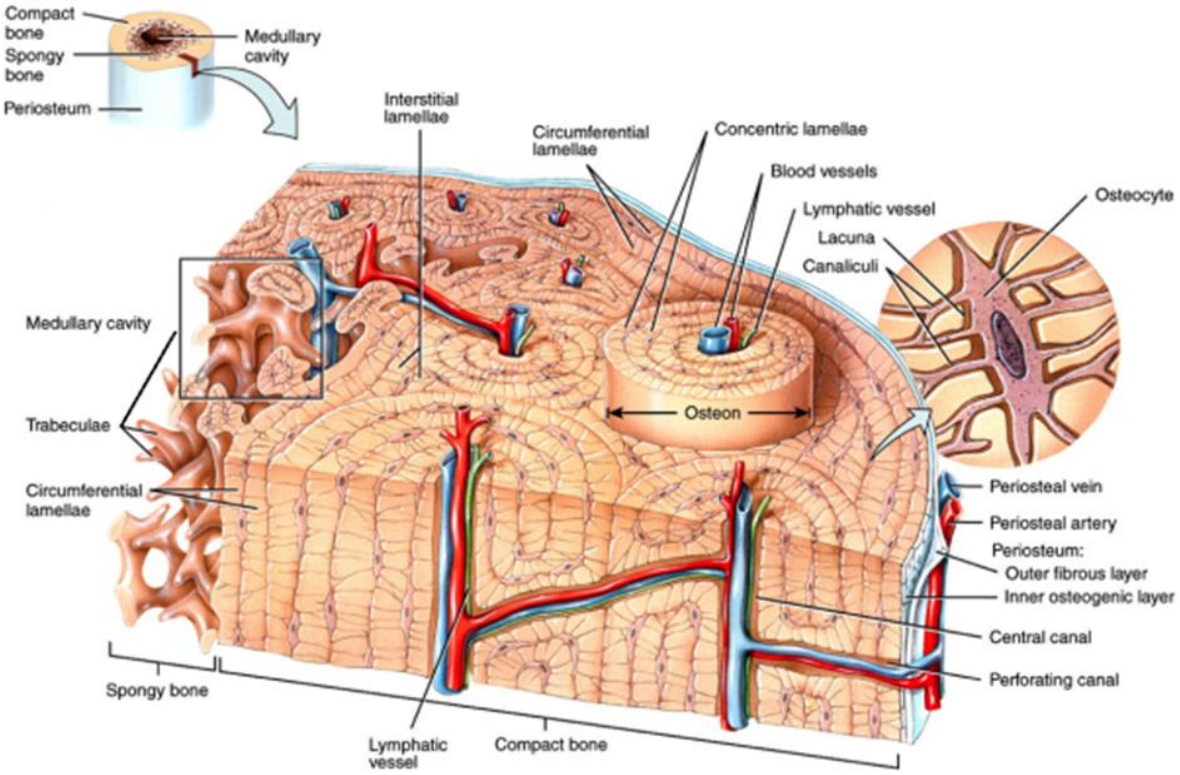

Figure 1.8: Typical bone morphology highlighting the vascular structures embedded within the bone mineral and Haversian canals. Osteons are made of layers of lamellae which have lacunae in which Haversian canals and Volkmann's canals pass through. The microenvironment within the bone shown here is essential for the maintenance of bone health (Tortora and Derrickson, 2014).

1.3.3 Circulation

10% of our cardiac output is delivered to the bones via these blood vessels that are housed within canals (reviewed by Marenzana and Arnett, 2013). Throughout the vertebrate skeleton a good blood supply is vital for the transportation of osteoclast and osteoblast progenitor stem cells and calcium which are key components in bone mineralisation, as well as the movement of oxygen, nutrients, regulatory growth factors and cytokines. A healthy vascular network within bone is also required for removal of metabolic waste

products which includes carbon dioxide and acid (Ray et al., 1967, Gross et al., 1979). The local microenvironment that surrounds the blood vessel defines it within the skeletal system and therefore, it is possible to have blood vessel heterogeneity in one organ alone, where blood vessels have distinct properties and 'niches' (Itkin et al., 2016).

From as early as 1953 where surgeons gave an insight into the organisation of vasculature within the femoral head, vasculature within bone was shown to be essential for human survival (Trueta and Harrison, 1953). One of the earliest papers written about the blood supply in the tibiofibular junction, described how the anterior tibial and inferior medial genicular arteries branch out to form the periosteal network in the rabbit. It detailed how the principal nutrient artery runs within the tibia and is formed from the anterior tibial artery. From the nutrient artery, the blood is moved to the small irregular shaped blood vessels that make up the bone marrow, before branching out into the cortical vasculature within the bone cortex (Brookes and Harrison, 1957, Brookes, 1963). In the past 60 years our knowledge has been expanded to give us a much more in depth understanding of the complex network of blood vessels that exist within our bones. Most recently, data has been published which describes the presence of small trans-cortical vessels which originate in the bone marrow within both murine and human long bones. They are thought to act as channels for 80% of the arterial blood supply and therefore play an important role in maintaining the key functions of bone vasculature (Grüneboom et al., 2019).

There has shown to be a reduction in the blood supply to our bones in degenerative bone diseases, with a recent study showing that in comparison to pre-menopausal women, post-menopausal osteoporotic women have significantly less CD31 positive Endomucin^{hi} vessels (Zhu et al., 2019, Wang et al., 2017). The decrease in blood flow and therefore osteogenesis during both ageing and disease has been associated with a reduction in Notch signalling by bone endothelial cells (Ramasamy et al., 2016).

1.3.4 VEGF in bone

Although we already knew about the angiogenic properties of VEGF, prior to 1994 the origin of this growth factor was unknown. In 1994 for the first time, scientists were able to trace the expression of VEGF mRNA to adult rat tibia bone tissue and osteoblast cells derived from rat calvaria (Harada et al., 1994). Osteoblast cells are the major producers of

VEGF, which plays a pivotal role in bone development (Wang et al., 1996) and is closely involved with the coupling of osteogenesis and angiogenesis (Muller et al., 1997, Breier and Risau, 1996, Gerstenfeld and Einhorn, 2006). Osteoblasts produce VEGF in response to mechanical strain, hypoxia, oestrogen, insulin-like growth factor, prostaglandins, TGF-β, FGF-2 and 1,25-dihydroxyvitamin D_3 (figure 1.9) (Spector et al., 2001, Lin et al., 2004, Wang et al., 1996, Harada et al., 1994, Kodama et al., 2004). In early studies it was shown that the expression and production of VEGF by osteoblast cells was rapidly induced by PGE_2 specifically, which is a known up-regulator of osteogenesis (Harada et al., 1994). One of the key environmental inducers of VEGF and angiogenesis is hypoxia, which causes raised levels of HIF-1 as a survival mechanism. Transcription of several genes that play a part in angiogenesis and glycolysis is activated during hypoxia, the most notable being VEGF (Lin et al., 2004) and there is compelling evidence to suggest that HIF-1α must be present in osteoblast cells in order for sufficient angiogenesis to take place (Wan et al., 2008).

Much of the current information that we have regarding the functions, properties and expression of VEGF in bone has been understood as a result of different knockout studies that have been performed. The premature death of these mice following a global deletion *of Vegf* has meant that studying the effect of a *Vegf* deletion on skeletal development has been incredibly challenging prior to the emergence of studies in which *Vegf* is conditionally deleted in specific cell types (Ferrara et al., 1996). In one of the preliminary *Vegf* knockout studies, partial disruption of VEGF signalling was achieved using inducible Cre-loxP, where *Vegf* was deleted in Cre positive cells following intraperitoneal injection of IFN-α at postnatal day 3, 5 and 7, resulting in a total or partial *Vegf* knockout in the liver, spleen, heart, thymus, kidney, brain, skeletal muscle and bone marrow. The result was an increased death rate and compromised growth in new born mice. When VEGF was almost completely silenced on a global scale with mFlt(1-3)-IgG VEGF receptor protein, the effects were much more profound and in the majority of cases caused mortality and a large reduction in the size of the liver, kidneys and heart in particular (Gerber et al., 1999a). The limitations of knockouts in which VEGF signalling is disrupted in multiple cell types are apparent and therefore in order to understand the precise effect of VEGF on bone health, strength and repair it was clear that VEGF deletion must be targeted to more specific cell types.

To find out more about the expression and functionality of VEGF, experiments have been undertaken by Olsen et al. using Cre-Lox mice to perform an osteoblast specific deletion of

VEGF. The conditional knockout of VEGF in osteoblast cells does not cause mortality and as a result, in this study it was possible to look at older mice than those used previously following a global knockout. Results have shown that osteoblast differentiation is decreased and adipocyte differentiation is increased when VEGF is knocked out specifically in osteoblastic bone cells using an Osx-Cre specific promotor. It was found that intracrine pathways are involved in the maintaining the equilibrium between osteogenesis and angiogenesis, with conditional deletion of VEGF causing a reduction in bone mass similar to the phenotype seen in people with osteoporosis (Liu et al., 2012).

As well as its known role in the regulation of osteogenesis and angiogenesis, VEGF is also important in endochondral bone formation during early development. It has been identified that chondrocytes are able to produce VEGF, which is heavily involved in the vascularisation of the avascular cartilage (Gerber et al., 1999b). Knockout studies using a mouse model in which $VEGF_{120}$ ($VEGF_{121}$ in humans) is silenced have highlighted this isoform specifically as having an important role in this regulation of endochondral ossification, specifically in the regulation of chondrocyte and osteoblastic activity (Zelzer et al., 2002).

From early development and throughout life, VEGF controls the tight balance between the production and breakdown of bone. In elderly women however, levels of oestrogen are greatly reduced as a result of the menopause. The effect of this reduction in oestrogen on the levels and activity of VEGF has been studied by using an ovariectomised Gottingen miniature pig animal model. Fifteen months after removal of the ovaries, vertebral concentrations of VEGF were 27% lower than levels seen in control pigs. Oestrogen is therefore involved in the regulation of bone strength, by controlling levels of VEGF by using paracrine signalling paths (Pufe et al., 2007).

In bone, VEGF has also been implemented in fracture healing and following a conditional osteoblast-specific VEGF knockout, the replacement of the initial cartilage filled callus structure with bone was inhibited. This is an important transition stage in bone healing and gives us an insight into what may be malfunctioning during the fracture healing of osteoporotic bones in humans, which have comparable physiology and genes to mice (Hu and Olsen, 2016).

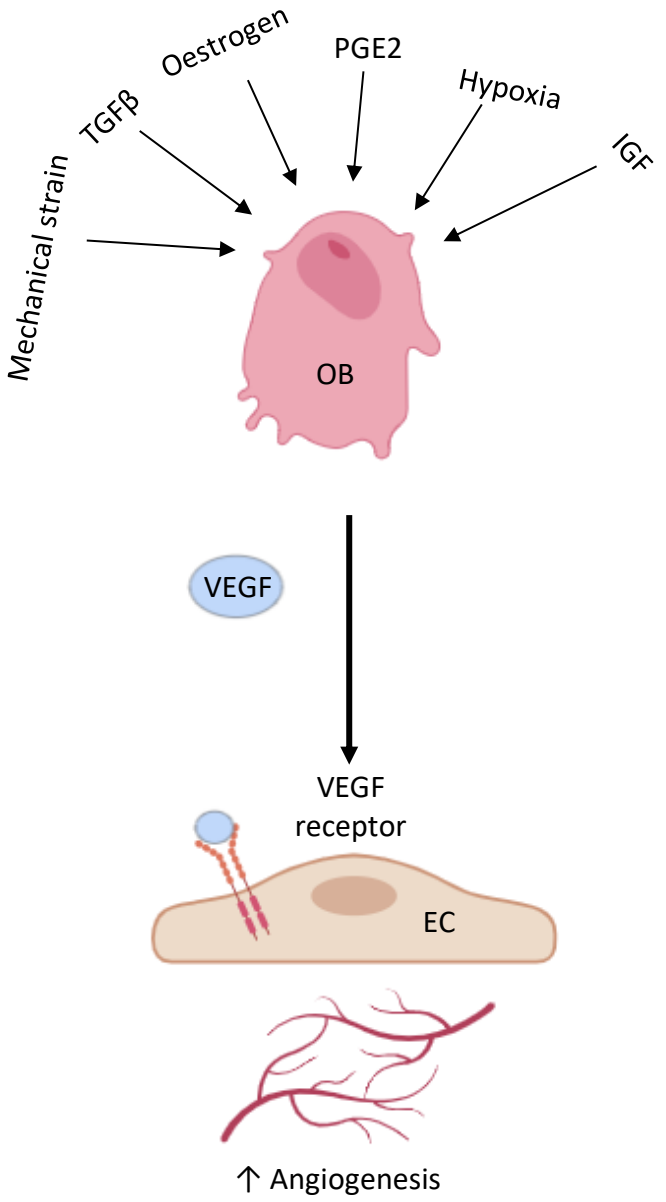

Figure 1.9: Osteoblasts (OBs) produce vascular endothelial growth factor (VEGF) in response to many different stimuli. This includes hypoxia, oestrogen, transforming growth factor beta (TGFβ), prostaglandin E2 (PGE2), mechanical strain and insulin-like growth factor (IGF). VEGF binds to VEGF receptors commonly found on endothelial cells (ECs). This in turn, will induce angiogenesis.

1.3.4.1 Signal transduction

To further improve our understanding of VEGF and its role in healthy and diseased humans, knowledge on the pathways in which VEGF signals is vital. Evidence suggests that VEGF interacts with osteoblast cells both directly; using intracrine and autocrine signalling and indirectly using paracrine signalling methods. This is a subject area that requires further research and clarity. Contradictions that exist in the literature may be due to the fact that VEGF producing cells of different ages and maturity are being used for experiments, or that cells from different origins are being used, altering the expression of VEGF receptors.

Intracrine signalling is where signalling molecules have a direct effect within the cells that produced them and is in affect an internal autocrine signalling pathway. It therefore does not involve or require interactions with receptors on the surface of the cell. Recently, intracrine VEGF signalling has been shown to control the balance between the differentiation of adipocytes and osteoblasts (Liu et al., 2012). Intracellularly, VEGF works in tandem with Lamin A and they both interact with their respective transcription factors RUNX2 and PPARγ to maintain the homeostasis of osteoblast and adipocyte differentiation (Berendsen and Olsen, 2014).

It has been suggested that the maintenance of homeostasis in blood vessels is controlled by internal autocrine signalling. This has been shown using a specific intracellular VEGF knockout in endothelial cells. Here, extracellular levels of the ligand are unaffected, but there is mortality in 65% of mice as a result of cardiac complications. The intracrine role of VEGF has been confirmed by the fact that only membrane soluble VEGF antagonists are able to have any kind of effect. Although endothelial cell viability is heavily implicated, angiogenesis is seemingly unaffected by this intracellular silencing of VEGF (Lee et al., 2007). This therefore suggests that perhaps cell viability and angiogenesis in endothelial cells are regulated by two distinct pathways. The fact that angiogenesis is taking place still despite the deletion of intracellular VEGF supports a paracrine pathway for the maintenance of angiogenesis.

VEGF is also proven to signal via these internal autocrine pathways in the regulation of haematopoietic stem cell (HSC) survival. Following deletion of VEGF from haematopoietic HSCs, HSC viability, differentiation and colony formation is decreased. Using an inhibitor to

bind to extracellular VEGF had no effect on the survival of HSCs, suggesting that it is internal VEGF which is involved in the control of HSC viability (Gerber et al., 2002).

Autocrine signalling is another way in which molecules signal directly to the cells that produce them and involves the secretion of a ligand, which subsequently binds to receptors on the cell that produced it to induce an effect. The localisation of VEGF receptors to specific cell types is debated in the literature, but clarification could help us to determine the signalling pathways involved in osteogenesis. Previous studies in our lab and by other groups have suggested that osteoblasts do not have the VEGF receptors on their cell surface needed to engage in autocrine signalling and therefore signal with other cell types such as endothelial cells via paracrine signalling pathways (Clarkin et al., 2008a). In contrast however, other studies have implied that osteoblasts do have VEGF receptors on their surface and they are able to directly regulate their own function (Hu and Olsen, 2016).

Further evidence shows that not only do endothelial cells produce VEGF, they also have VEGFR1 receptors on the abluminal side of their structure and VEGFR2 receptors on the luminal side (Stefanini et al., 2009). Although VEGF positive feedback loops in endothelial cells have shown to have important purposes in maintaining health, overstimulation of these pathways have been linked to haemangioma tumours and therefore can be very dangerous (Hamlat et al., 2005, Lee et al., 2007).

Historically, VEGF has primarily been considered to be a protein which uses paracrine signalling to indirectly regulate vasculogenesis and angiogenesis (Carmeliet et al., 1996, Wang et al., 2007). Preliminary studies suggested that VEGF was able to influence the function of other cell types, namely endothelial cells (Berse et al., 1992). In as early as 1994, paracrine signalling pathways were linked to the regulation of healthy angiogenesis (Harada et al., 1994). Parenchymal cells synthesise VEGF, which interacts with receptors on endothelial cells by paracrine signalling to enable the ligand to regulate these functions *in vivo* (Fong et al., 1995). A study using primary human osteoblast cells showed that crosstalk between osteoblasts and endothelial cells used VEGF paracrine signalling, rather than autocrine signalling to promote osteogenesis. It has been shown that VEGF only affects osteoblast differentiation when there is a co-culture of osteoblasts and endothelial cells and therefore VEGF signals in a paracrine manner during osteogenesis. The data suggests

that VEGF produced by osteoblasts in response to environmental cues, does not act directly on osteoblast cells in autocrine signalling pathways (Clarkin et al., 2008a).

Paracrine signalling has also been shown to be of high importance in bone healing due to the fact that VEGF functions as an osteogenic growth factor, plays a key role in angiogenesis and acts as a pro-inflammatory signalling molecule. Here, VEGF controls osteoblast activity by facilitating paracrine interactions between osteoblasts, endothelial cells and haematopoietic cells. Deletion of VEGFR2 in osteoblast cells upregulated the mineralization and maturation of cells of the osteoblast lineage, providing evidence towards the utilisation of this paracrine signalling pathway during fracture repair. This suggests that osteoblastic-VEGF does not bind to VEGF receptors on the osteoblast cell surface its function in bone healing (Hu and Olsen, 2016). The diverse range of cells that produce VEGF provides further evidence for VEGF paracrine interactions, which involve a vast array of different target cells throughout the body to induce a more global effect (Sison et al., 2010, Dias et al., 2001).

VEGF synthesised by bone mesenchymal stem cells (BMSCs) has been shown to communicate using paracrine signalling pathways to regulate osteoclast differentiation (Liu et al., 2012). VEGF has also been found to play a paracrine role in osteoclast development (Niida et al., 1999, Niida et al., 2005). Chondrocyte VEGF is shown to regulate the migration of osteoclasts to the area surrounding the growth plate, which is important in the process of ossification (Zelzer et al., 2004). During development, VEGF therefore is able to stimulate osteoclast activity by regulating the movement of these destruction cells via paracrine signalling pathways and as a result influence angiogenesis, ossification and remodelling (Engsig et al., 2000).

1.3.5 Endothelial subtypes

The molecular, morphological and functional differences in the endothelium of skeletal capillaries results in the classification of two subtypes of blood vessel; type H and type L (Kusumbe et al., 2014b). Type H vessels are characterised by the expression of high levels of CD31 and are mainly found in growing regions of the long bones between the growth plate and the endosteum (Liu and Castillo, 2018, Ramasamy, 2017). Type H vessels are adjoined to each other via their distal end and align in a columnar formation (Sivaraj and Adams, 2016). These vessels have been shown to give out specific signals to

osteoprogenitors that are found in close proximity to the bone vasculature, controlling the growth of nearby vessels and ensuring that the process of angiogenesis and osteogenesis is tightly coupled. To ensure this tight-coupling, an adequate blood flow to type H capillaries is essential (Ramasamy et al., 2016, Kusumbe et al., 2014b). In ageing and in certain diseases such as osteoporosis, it has been shown that blood vessels within bone are of poorer quality and this is associated with an increase in porosity (Marenzana and Arnett, 2013). There is a reduction in type H vascular endothelial cells specifically and this is directly correlated with reduced levels of osteoprogenitor cells. This compromises the coupling between osteogenesis and angiogenesis (Liu and Castillo, 2018, Kusumbe et al., 2014b).

Conversely, type L blood vessels are found within the bone marrow space. Unlike type H vessels, they are multidirectional and form a branched capillary network which interacts with the central vein, but not arteries (figure 1.10). This means that the part of the bone in which they reside is particularly hypoxic (Sivaraj and Adams, 2016).

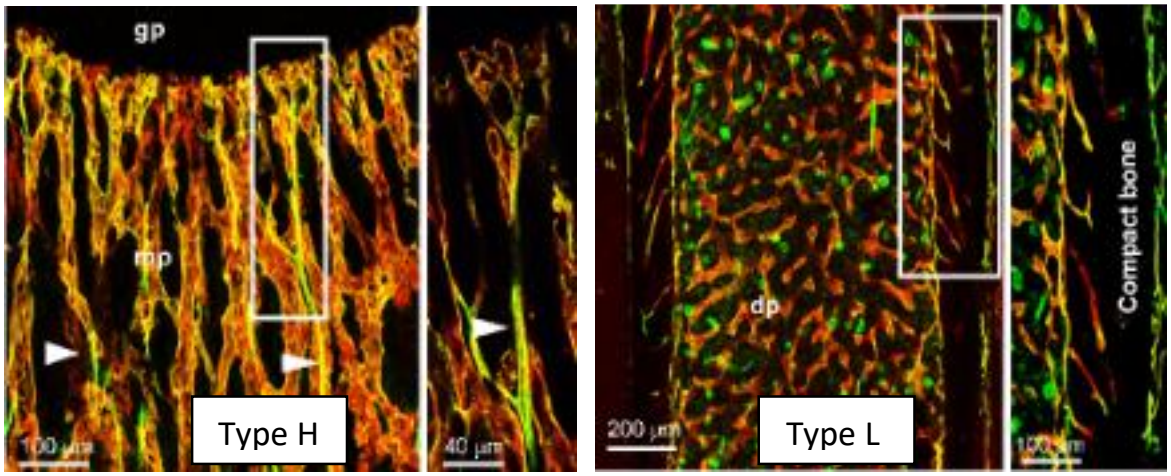

Figure 1.10: Identification of type columnar type H vessels ($CD31^{hi}$) and branched type L vessels ($CD31^{lo}$) blood vessels within compact bone. Type H and L vessels are visually divergent. Figure taken from paper by Sivaraj et al (Sivaraj and Adams, 2016).

1.3.6 Studying the vasculature in bone

The intricate study of the blood vessels within calcified tissue has proved problematic for decades, due to the fact that the vessels are encased within the hard bone mineral and are therefore not visible to the human eye and cannot be visualised by x-ray, or low-resolution micro-CT. Histology and immunohistochemistry is also a delicate procedure as vessel lumens are especially thin. Often these procedures will require bones to be decalcified, which can be an aggressive treatment for the bone and its intracortical canals, resulting in the loss of vasculature. Due to improvements in analysis techniques and micro-CT scanning resolutions however, there have been significant advances in the characterisation of vessels within bone.

Until recent years, the resolution of micro-CT scans has not been high enough to perform in-depth analyses of changes in cortical porosity by separating the osteocyte lacunae from the blood vessel canals in both aged bones and disease models (figure 1.11). This has hampered our understanding of bone pathologies considerably. Bone vasculature is deeply embedded within calcified tissue, which has made the imaging of the blood vessel canals which penetrate the bone matrix somewhat challenging.

Experiments in which the measurements of osteocyte lacunae and blood vessel canals were actively compared when scanning the same bone at two different resolutions of 1µm versus 4µm voxel size have shown that volumetric measurements were underestimated in the case of canals, or not detected in the case of lacunae, at the resolution of 4µm. It has been suggested that a resolution of at least 1-2µm is required for the accurate analysis of blood vessel canals and an even higher resolution of 1µm or greater needed for the interrogation of smaller osteocyte lacunae (Palacio-Mancheno et al., 2014). A scan of this resolution using a desktop scanner would take 8 hours to image one bone, proving costly and making it difficult to achieve high enough n numbers within an acceptable time scale. A scan of a comparable spatial resolution at a synchrotron light source (SR-CT) would take just minutes, enabling the scanning of whole data sets within 24 hours and therefore the use of synchrotron scanning is being increasingly favoured.

The first experiments which enabled the visualisation of vasculature within their intracortical canals using a desktop micro-CT scanner were facilitated by perfusing the blood vessels with an x-ray absorbing contrast agent, typically barium sulphate (Schneider

et al., 2009b, Fei et al., 2010, Roche et al., 2012). Not only did perfusion with barium sulphate enable quantification of the vasculature, it made the vessels visible to the human eye (Schneider et al., 2009b). One downside however, is that we do not know the exact effect of these contrast agents on the vasculature and there is the risk that vessels can be distorted following treatment. Due to advances in technology and SR-CT scanning capabilities, a study carried out in our lab using phase-contrast enhanced tomography has shown that for the first time it is now possible to visualise vessels within blood vessel canals without the use of a contrast agent such as barium sulphate. Using different voxel sizes as a form of comparison it was shown that at the lowest resolution of 1.3µm, vessels were not visible within the canals. A resolution of 0.65µm enabled the identification of larger vessels, however a much higher resolution of 0.325µm was required to image the much smaller intracortical capillaries within the tough bone mineral matrix (Núñez et al., 2017). This research marks huge advances in the imaging capabilities of bone, especially seeing as the 3D separation of blood vessel canals from osteocyte lacunae is still a relatively novel concept in the study of degenerative bone disease.

With a SR (or desktop) scanning resolution of ≤1µm, it has been possible to extract a negative imprint of calcified tissue and produce an accurate a cast of the blood vessel canals and osteocyte lacunae within bone (Núñez et al., 2018, Schneider et al., 2007b). This is a technique which is emerging as highly valuable for the analysis of both aging animal models and transgenic models of disease (Mosey et al., 2017, Núñez et al., 2018, Boyde et al., 2017, Goring et al., 2019). At times however, the close proximity of the blood vessel canals to the osteocyte lacunae in bones with extreme vascular phenotypes has raised challenges in the separation of canals from lacunae. This is a caveat which must be overcome in order to investigate the vasculature using micro-CT in more detail.

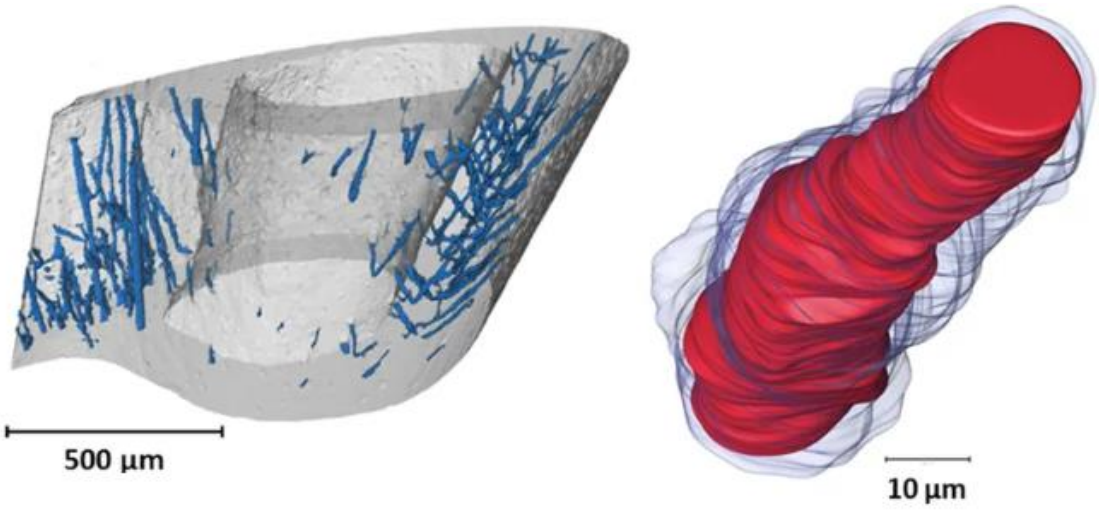

Figure 1.11: Interrogation of blood vessel canals within cortical bone by using high-resolution, synchrotron based micro-CT. With a micro-CT resolution of 1.3µm (left image), it is possible separate and quantify blood vessel canals within cortical bone. It has also been identified that it is possible to visualise blood vessels (right image) within these canals at a synchrotron resolution of 0.325µm (Núñez et al., 2017).

In vitro, the study of bone endothelial cells is equally as challenging due to the difficulties in isolating primary endothelial cells from bone. Where the isolation of primary osteoblast cells from bone has been well characterised (Taylor et al., 2014), the extraction of endothelial cells from bone has proven more difficult and therefore bone marrow endothelial cells get used frequently for *in vitro* experimentation as a substitute (Liu et al., 2014, Masek and Sweetenham, 1994).

1.4 Sexual dimorphism

1.4.1 Development

Sexual dimorphism is defined by the occurrence of inherent differences between males and females within a singular species. It is undeniable that sex hormones must play a considerable role in the expression of phenotypic divergences between males and females, however it is also evident from the literature that other factors may influence any differences observed. One of these contributing factors which plays a role from the early stages of blastocyst formation is genetics. Sex differences in the gene expression of thousands of genes present in the bovine blastocyst have been identified, before the presence of sex hormones and the development of the ovaries or testes (Bermejo-Alvarez et al., 2010). Subsequent studies using bovines have identified the precise timing for the onset of these sex differences in gene expression, suggesting that the onset of differential genetic expression occurs during the morula-blastocyst transition at 144 hours post-fertilisation and that this is influenced by apoptosis (Oliveira et al., 2016). In the first trimester of pregnancy, additional divergences in the transcriptome of the placenta have been identified between males and females (Gonzalez et al., 2018). Sex hormone independent dimorphisms between males and females have also been identified in somatic cells and these differences are said to be regulated by sex chromosomes (Callewaert et al., 2009).

In males (XY), genes located on the Y chromosome will be present and in females (XX) genes located on the X chromosome will be present, with the expression of these X-linked genes in males and females dependent on quantity of X chromosomes and the influence of parental genetics. During the sixth week of gestation, the SRY gene on the male Y chromosome is involved in the differentiation of the male gonads, which are undifferentiated prior to this (Jost, 1953 , Larsen, 2003). Historically, it was found that SRY on a 14kb genomic fragment was able to initiate the formation of the testes in an otherwise female embryo and this experiment has helped to further characterise the function of this SRY gene in embryo development (Koopman et al., 1991). By the eighth week of gestation in males, the Leydig cells are able to produce testosterone and this is upregulated between pre-natal week 10 and week 20 (Lipsett et al., 1966, Larsen, 2003, Smail et al., 1981). By

week 24 of gestation testosterone levels are low once more and they remain low until puberty (Hayward, 2003).

Following fertilisation, if high levels of testosterone are not present at week six of embryo development, females are formed as the default sex. In females however, the ovaries are not differentiated until the seventh week of gestation and the levels of oestrogen remain low for most of development (Larsen, 2003). Experiments performed using a female pig model have found that low and almost undetectable levels of oestrogen were present in the blastocyst (Ying et al., 2000). It is well characterised that prior to puberty, the levels of female sex hormones in the body remains low. It has been shown in studies which look at human females that from 30 months prior to puberty to 6 months post-puberty, levels of oestrogen steroid hormone oestradiol increase by over four-fold (Biro et al., 2014).

In humans, the average age for the onset of puberty is 11 in females and 12 in males. During this phase, hypothalamus-pituitary feedback loops using the gonadotropins luteinizing hormone and follicle stimulating hormone activate the maturation of the ovaries and testes, which begin to produce oestrogen and testosterone respectively (Blakemore et al., 2010, Laurent et al., 2014). Although the biological processes and enzymes responsible for reaching sexual maturity are comparable between species such as humans and mice, the onset of puberty is species-dependent, with mice reaching sexual maturity at 8.5 to 9 weeks of age (Drickamer, 1981).

1.4.2 Vasculature

Although not extensively investigated in the literature, sexual dimorphisms have been recognised in blood flow, endothelial cell function and cardiovascular function. It has been identified that basal levels of hand blood flow, finger blood flow and skin perfusion are significantly higher in men than in women (Cooke et al., 1990). It is also known that females have higher levels of vasodilation and a lesser fight or flight response in comparison to males. As well as this, females have been shown to have a reduced resting blood pressure and lower systolic blood pressure during intense exercise. This is thought to be due to different mechanisms controlling the balance of cardiac output and blood pressure between sexes. With age, there is a gradual reduction in heart rate and this is shown to be much more steady in females when comparing them with their male counterparts (Wheatley et al., 2014).

Further studies have been carried out in an attempt to explain these differences observed in vasodilation. In response to shear stress, mediators are released from endothelial cells to initiate vasodilation. Following the deletion of eNOS, it has been shown that males and females show divergence in the mediators which are produced to initiate flow-induced vasodilation. Ordinarily one of these mediators would be NO, however with a depletion of NO, males and females are able to compensate in a sex-specific manner. Where males will subsequently release prostaglandins in response to shear stress, females release endothelium-derived hyperpolarizing factor. Both of these factors cause relaxation and dilation of the vasculature (Sun et al., 1999, Wu et al., 2001, Huang et al., 2001a). This dimorphism is thought to be regulated by the difference in sex hormones in males and females, with oestrogen promoting the expression of endothelium-derived hyperpolarising factor and ovariectomised mice using prostaglandins to promote vasodilation in response to shear stress (Huang et al., 2001b).

Phosphodiesterases (PDEs) are involved in the breakdown of cyclic adenosine monophosphate (cAMP) and cyclic guanosine monophosphate (cGMP) which are important in in the maintenance of blood vessels as a barrier. Intrinsic variances in levels of PDE1A and PDE3B mRNA are present in males and females and therefore silencing of PDE3 causes a dimorphic effect on vascular endothelial cells in their role as a barrier. Microvessel permeability is shown to be lower in male versus female veins and arteries as a result of these sex differences (Wang et al., 2010).

In terms of pathologies, it has been identified that males are more prone to increased severity pulmonary vascular disease than females, despite the fact that pulmonary hypertension is more common in females. In attempt to explain this phenomenon, differences in the control of vascular tone in males and females have been investigated. It has been shown that silencing of NOS results in inhibition of PDE5, which in turn upregulates vasodilation to a greater extent in females than males (de Wijs-Meijler et al., 2017). Coronary heart disease (CHD) is also a major cause of death in post-menopausal women in particular and they suffer from it up to 10 years later than males. This is particularly severe in females with diabetes, where there is a 50% greater likelihood of suffering from CHD due to narrowed vessels and increased activity of inflammatory factors in the construction of atherosclerosis plaques (reviewed by Maas and Appelman, 2010).

In the context of bone specifically, very few sex differences in intracortical canals have been identified and documented. This could be due to the fact that studies rarely look at both males and females, or because few differences exist. It has been shown however, that females have bigger Haversian canals and males have thicker osteon walls (Havill et al., 2013). The exact mechanism behind this has not been deciphered, however it highlights the importance of looking at both males and females when interrogating bone and vascular phenotypes.

1.4.3 Bone

There are several existing skeletal sexual dimorphisms which come as no surprise, due to the child bearing capabilities of women and the differential expression of sex hormones during and after puberty. The skeletal architecture of women has evolved to ensure that they have larger pelvises in comparison to men; notably the posterior space, angulation of sacrum, biischial breadth and subpubic angle are most divergent (Tague, 1992).

Conversely, during healthy bone development changes in bone geometry are more pronounced in males in comparison to females (Hu and Olsen, 2016, Kusumbe et al., 2014a, Costa et al., 2009, Martin, 2002). Males produce a larger skeleton which is thought to protect them from fracture in later life (Seeman, 2001, Martin, 2002, Seeman, 2002, Callewaert et al., 2010a). On average, men are characteristically taller than women as a result of the differential influence of oestrogen and testosterone on longitudinal bone growth at the growth plate. Oestrogen is known to initiate the closing of the growth plate cartilage, a process which occurs later in men (Joakimsen et al., 1998, Meyer et al., 1993, Perry et al., 2008). Men have longer, thicker bones with a higher bone mass and it has been suggested by a study undertaken in Norway that height is a contributing factor to an increased fracture risk (Joakimsen et al., 1998).

Furthermore, it has been proposed in this study that weight gain has shown to seemingly protect males from hip fractures and females from fractures of the leg (Joakimsen et al., 1998, Meyer et al., 1993), observations which perhaps require further investigation. Due to high levels of periosteal expansion, men have wider bones than females relative to bone length and unlike in females, the cortical bone continues to grow into middle age (Laurent et al., 2019). Healthy men in their 20s and 30s have been shown to have higher % cortical

porosity in comparison to females, a difference which was negated in subjects over 50 (Burghardt et al., 2010).

In mice, peak bone growth is identified when mice are between 3 to 5 weeks old and it is said to be 40% higher in males, when compared to females of matching ages. This has been linked to up-regulation of *Igf-1* in male mice. In comparison to males, in early puberty oestrogen prevents bone growth, confirmed by ovariectomy which up-regulated the accumulation of new bone during early puberty. *Igf-1* has been shown to work independently to sex hormones here and this has been confirmed by removal of the gonads in these studies (Callewaert et al., 2009). Therefore, although sex hormones are clearly playing a role during male and female skeletal development in this mouse model, it is possible that other factors such as *Igf-1* are acting independently to these hormones in regulating the expression of dimorphic bone phenotypes.

Using human cadaveric bones, direct comparison of bone strength in males and female at areas of equal stiffness have shown that the proximal femur in males was 158% stronger versus females, with a de-coupling of strength and stiffness which could potentially be attributed to sexual divergence in porosity measures (Patton et al., 2019). It is possible that sexual divergences in the structure and geometry of bone are influenced by a combination of hormonal, genetic, biological or environmental factors and thus experiments which look at both males and females in order to define the mechanisms behind observed sex-dependent differences in aging or disease are hugely valuable.

1.4.4 Bone pathologies

There is a recognised difference in age-related fracture risk between men and women, which has been associated with dimorphisms in the regulation of bone growth and development that males and females are subjected to post-puberty (figure 1.12). Prior to the menopause in females, the UK fracture incident rate is higher in males (200 per 10,000) than females (40 per 10,000) between the ages of 15 and 24. In post-menopausal women and in the aged population, these statistics are altered, with 22% more females than males suffering from a fracture over the age of 85 (Donaldson et al., 1990). This study has been supported by subsequent analysis in different regions of the UK (Johansen et al., 1997). In females there is an increase in bone remodelling over the age of 50 due to a loss of oestrogen during menopause, whereas in males testosterone levels remain static for longer

and gradually decline later in life (Lindsay, 1982, Lindsay, 1987, Balasch, 2003, Riggs and Melton, 1995).

It has been shown that removal of the ovaries in female primates induces a decline in the bone mass density (BMD) and bone mass of the trabecular bone (Iwamoto et al., 2009). Following an orchidectomy in male rats, bone formation is shown to be decreased and bone resorption upregulated, albeit mildly (Danielsen et al., 1992). In another study, BMD has also been found to be reduced in rats following orchidectomy (Ryu et al., 2015). The lack of comparisons between male and female animals of comparative ages and species makes it hard to make comparisons between both sexes, however it is clear from the literature that sex hormones do have an influence on the quantity and quality of both trabecular and cortical bone. The extent to which sexual dimorphisms in bone integrity and structure are controlled by hormones and other factors such as genetics or environmental influences remains unclear due to the small number of studies in which males and females are actively compared.

Due to the known role of oestrogen in the regulation of bone remodelling, it is well documented that women that have been through menopause are at much higher risk of developing osteoporosis (Albright, 1947b, Albright, 1947a, Lindsay, 1982, Lindsay, 1987) and are often the focus of osteoporosis research. It has been shown that aged women are much more likely to fall than men, a phenomenon which remains unclear but could be explained by the fact that males retain their high peak muscle mass better than females. This in turn, will increase the risk of osteoporotic fracture in females (Burns et al., 2016, Nordström et al., 2011). Although doctors, sufferers and the general public still think of osteoporosis as a disease which predominantly affects women, the effect on men must not be underestimated. Due to an increase in life expectancy, much more attention is now being paid to men who have the disease and typically suffer from osteoporotic fractures ten years later than women (Jennings et al., 2010, Schuit et al., 2004). It has been shown that one third of all osteoporotic hip fractures in the world affect men (Gullberg et al., 1997). In males, they are often much more severe and there is a 37.5% mortality rate within a year following hip fracture, which is much higher than their female counterparts (Cooper et al., 1992, Jones et al., 1996, O'Neill et al., 1996). Despite the high risk of post-fracture mortality however, osteoporosis is a bone pathology that is still highly underdiagnosed and undertreated in the male population (Jennings et al., 2010, Laurent et al., 2019).

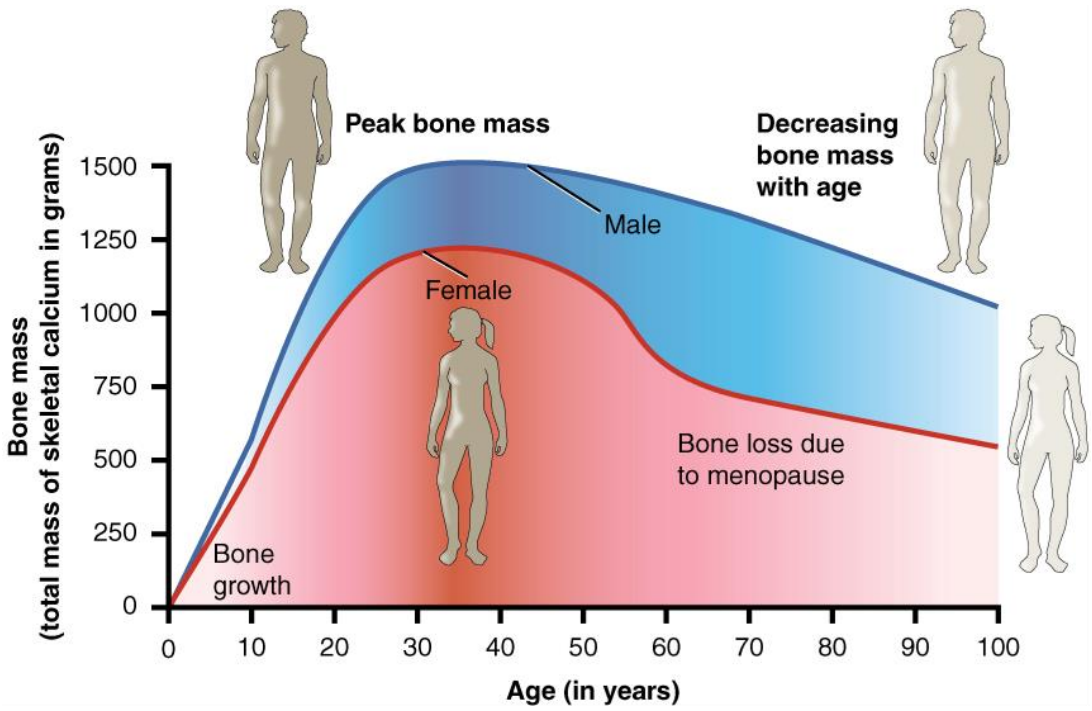

Figure 1.12: Sexual dimorphisms in bone loss, increases with age. Bone loss occurs rapidly in females after the menopause due to decreased levels of oestrogen, which has a role in maintaining bone density. Bone loss in males occurs much more gradually at a later age (Young et al., 2003).

1.5 Project approach, hypothesis and aims

Given the importance of osteoblast-derived VEGF in the coupling of endothelial and osteoblast behaviour and the sexual dimorphism founded during bone development and sustained in disease, my thesis aim is to better understand the role VEGF signalling in males and females during bone development and mineralisation.

Hypothesis: Osteoblast-derived VEGF regulates bone development and mineralisation distinctly in males and females.

Aim 1: Quantification and validation of vascular phenotypes following osteoblast-*Vegf* deletion

*Osteoblast-derived Vegf will be deleted in osteocalcin expressing cells in vivo (Ocn*VEGFKO*) and tibiofibular cortical microstructure analysed in mice at 16 weeks of age*

- High resolution synchrotron-based micro-CT for bone architecture determination
- Validation of blood vessels within canals using histology
- Backscattered scanning electron microscopy to investigate the vasculature (BS-SEM)

Aim 2: Elucidation of physical bone traits following osteoblast-*Vegf* deletion

*Whole tibial analysis of Ocn*VEGFKO *at 16 weeks of age will be undertaken*

- Gross measurements of bones using well known growth determinants
- Craniometric measurements using medium-resolution micro-CT
- Trabecular bone analysis using medium-resolution micro-CT
- Assessment of tibial geometry
- Investigations into bone mineralisation using backscattered electron scanning electron microscopy (BSE-SEM)

Aim 3: Investigating the role of VEGF expression in prepubertal development and osteoblast function

Whole tibial analysis of $_{Ocn}$VEGFKO at 4 weeks of age

- High resolution micro-CT in *4 week old prepubertal mice*
- Trabecular bone analysis using medium-resolution micro-CT
- Whole Geometry measurements of the tibia

Osteoblast-derived *Vegf* will be deleted in male and female long bone osteoblasts (OB) *in vitro* (OBVEGFKO).

- *In vitro* effects of *Vegf* deletion in male and female osteoblasts (VEGF enzyme-linked immunosorbent assay (ELISA) to confirm knockdown, ALP, viability, quantitative polymerase chain reaction (qPCR), western blot)

Aim 4: Investigating indirect effects of osteoblast *Vegf* deletion in males and females on endothelial cell function

OBVEGFKO cell media from male and female bones will be collected and added to endothelial cell cultures

Conditioned media (CM) experiments

- Viability, BrdU, gene expression, angiogenic array and osteogenic array

Osteoblast-derived Vegf will be deleted in vivo ($_{Ocn}$VEGFKO) and CD31/sclerostin/VEGFR2 expressing cells immunolabelled

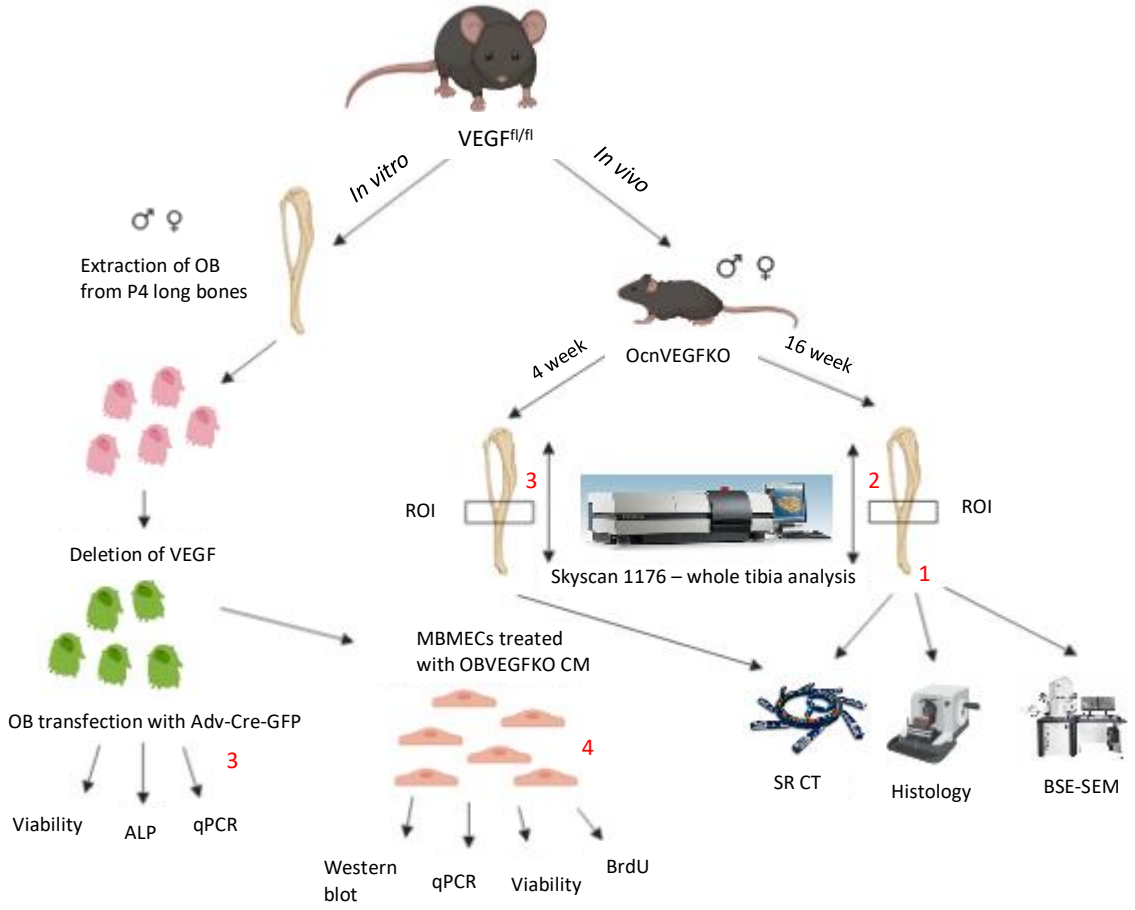

Figure 1.13: Workflow of analysis techniques used in this PhD to study the effect of an osteoblast-derived *Vegf* deletion. Following *in vivo* deletion of *Vegf* in male and female mice, micro-CT, histology and BSE-SEM was used to interrogate the bone phenotype at the tibiofibular junction (Aim 1). Skyscan 1176 was used to scan the entire bone for measures of bone geometry and trabecular bone analysis (Aim 2). This was performed mainly using 16 week old mice, however micro-CT analysis was also performed on pre-pubertal 4 week old mice (Aim 3). For *in vitro* deletion of *Vegf*, osteoblast cells were extracted from male and female P4 *Vegf*$^{fl/fl}$ mice and treated with adenovirus-cre. qPCR, western blot, ALP elution/stain and viability assays were then carried out on KO and WT osteoblast cells (Aim 3). Conditioned media from transfected OBs was used to treat mouse bone marrow endothelial cells (MBMECs). Bromodeoxyuridine (BrDU) proliferation assay, viability assays, qPCR and western blots were then carried out to look at the indirect effect of VEGF deletion in osteoblasts on MBMECs (Aim 4). PhD aims 1-4 detailed on this schematic (red numbers).

Chapter 2 Methodology

This chapter contains information on general methodologies used throughout this PhD. Full methodologies for more specific techniques are detailed in correlating individual results chapters. Information on the sources of specific materials used for the methods described can be found in appendix A and details on the composition of solutions in appendix B.

2.1 *In vivo* deletion of *Vegf*

2.1.1 Animal derivation

In order to produce second generation *Vegfa* knockout mice *in vivo* (referred to as $_{Ocn}$VEGFKOs), homozygous *Vegf*$^{fl/fl}$ mice (Genentech, San Fransisco) were mated with hemizygous Ocn-Cre mice. The offspring produced from this breeding are first generation *Vegf*$^{fl/fl}$, with a single allele of Ocn-Cre (Jacksons lab, Maine). These offspring are then mated back to *Vegf*$^{fl/fl}$ mice to produce second generation *Vegf* $^{fl/fl}$; Ocn-Cre, the transgenic mice that will be used in this study (figure 2.1).

Second generation $_{Ocn}$VEGFKO and WT mice (*Vegf* $^{fl/fl}$) were bred. Heterozygote mice were also produced as a result of breeding, but were not utilised for experiments described in this thesis. LoxP sites flank the gene of interest, which in this case is *Vegf*, allowing genetic recombination to occur between these two sites in the presence of Cre recombinase. This enabled bone-specific deletion of *Vegf* (Zhang et al., 2002).

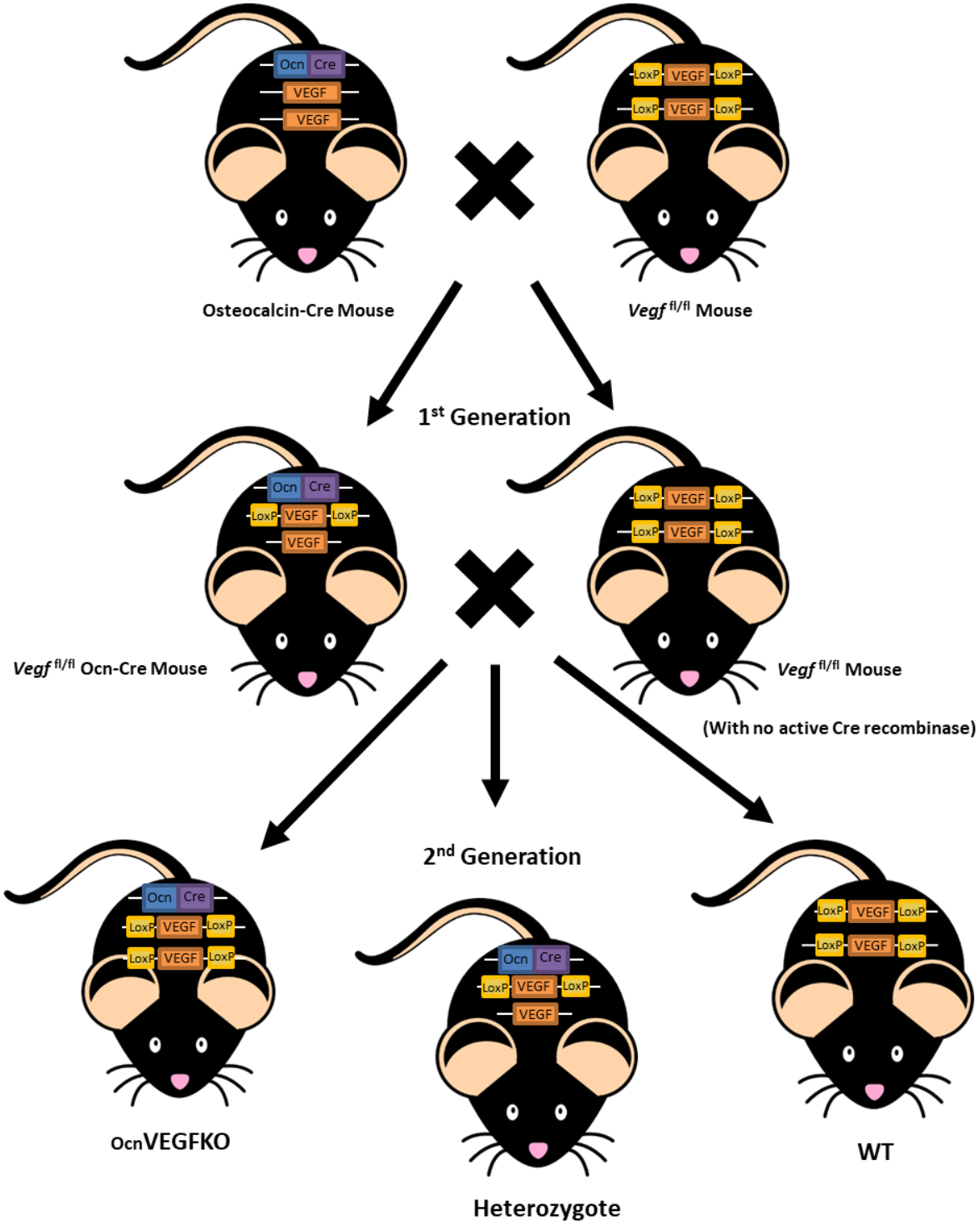

Figure 2.1: Production of 1st and 2nd generation *Vegf* knockout mice following genetic recombination between LoxP sites in the presence of Cre recombinase (Ocn-Cre). VEGF Is flanked by LoxP. Ocn-Cre drives the deletion of VEGF in mature osteoblast cells. OcnVEGFKO, heterozygote and WT mice are produced as a result of two generations of breeding.

2.1.2 Genotyping

Animals were culled by schedule 1 cervical dislocation at 4 or 16 weeks and use of tissue was carried out in compliance with the Animals Act, 1986. For maintenance of the Ocn-Cre and first generation colonies for breeding purposes, genotyping was performed using ear tips collected by animal house technicians in accordance with Home Office regulations. Mice were genotyped to determine whether they were Cre positive or Cre negative, as previously described in the literature (Liu et al., 2012). For genotyping of second generation mice, a segment of tail was dissected after the mouse was culled. This tissue contained a small amount of bone, which was essential for determining bone-specific *Vegfa* deletion. Cre and *Vegf* forward and reverse primers that were used to make up the PCR mastermix are detailed in appendix C.1.

2.1.2.1 Genomic DNA extraction

250ul of lysis buffer (1M Tris pH8, 5M NaCl, 0.5M EDTA pH8, 10% (w/v) SDS and dH_2O) with 20mg/ml proteinase K was added to the ear tips or tail tips. Samples were incubated with the lysis buffer at 50°C for an hour and afterwards were vortexed, to ensure that the entire tissue had been broken down sufficiently. Samples were spun in a centrifuge for 15 minutes at 17,000 x *g*. The supernatant was removed from the Eppendorf tubes and added to fresh tubes containing 30µl 5M NaCl. Tubes were inverted and spun at 17,000 x *g* for a further 15 minutes. The supernatant was mixed with equal volumes with 100% (v/v) ethanol and the tube was gently shaken, revealing thin strands of DNA. Samples were then spun at 17,000 x *g* for 30 minutes. Following this, the ethanol was poured out of the Eppendorf, leaving the DNA pellet within the tube. 500µl of 70% (v/v) ethanol was then added and the samples spun as per previous conditions. After removing the tubes from the centrifuge, the ethanol was removed, ensuring not to disrupt the pellet and 50µl of dH_2O was added. The quality and quantity of the genomic DNA within the samples was determined using a nanodrop. Samples were diluted with dH_2O to 20ng/µl before the PCR process.

2.1.2.2 End point PCR

In order to determine which samples were Cre positive and which samples were Cre negative, an 18μl volume of PCR mix (5X green buffer, MgCl2, GoTaq DNA polymerase, dNTPs and Cre forward/reverse primers) and 2μl volume of extracted DNA was combined. If Cre positive, a band was present at 411 base pairs (bp) on the 1.5% (w/v) agarose gel (figure 2.2). This process was used for both genotyping of first generation mice for maintenance of the breeding colony and for first-stage genotyping of second generation mice.

The second generation samples which were Cre positive were then separated and tested further to determine whether they were heterozygous or homozygous OcnVEGFKO strains, using VEGF forward and reverse primers. The PCR product was run on a 2% (w/v) agarose gel. Mutant homozygous OcnVEGFKO mice have one band only, visible at 148bp (figure 2.3). Heterozygote *Vegfa* flox/+ shows one band at 148bp and one band at 100 bp below (Gerber et al., 1999a). Wild type, Cre negative mice will be referred to as WT.

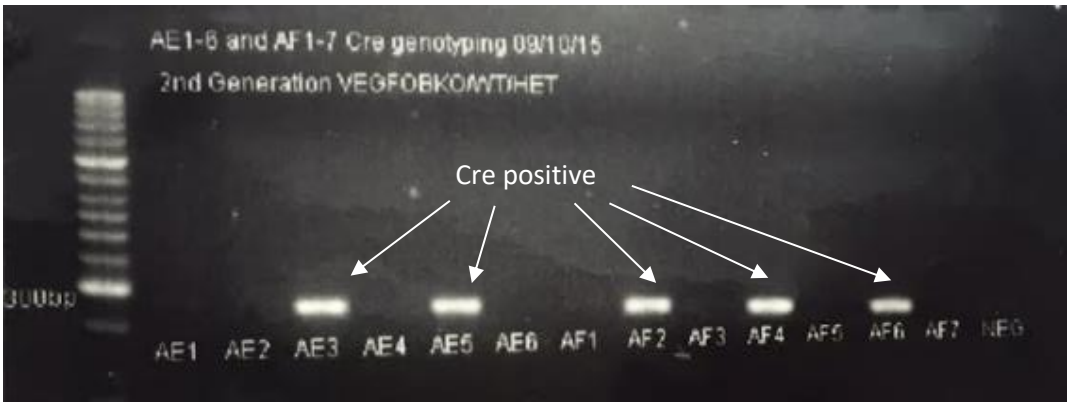

Figure 2.2: Identification of Cre positive and wild type samples. White bands present on the agarose gel at 411bp show the samples which are Cre positive (AE3, AE5, AF2, AF4 and AF6). The wild type *Vegf* $^{fl/fl}$ samples have no band visible. Negative control (NEG) confirms the validity of results. Genotyping to determine Cre positive samples is performed on both first and second generation mice.

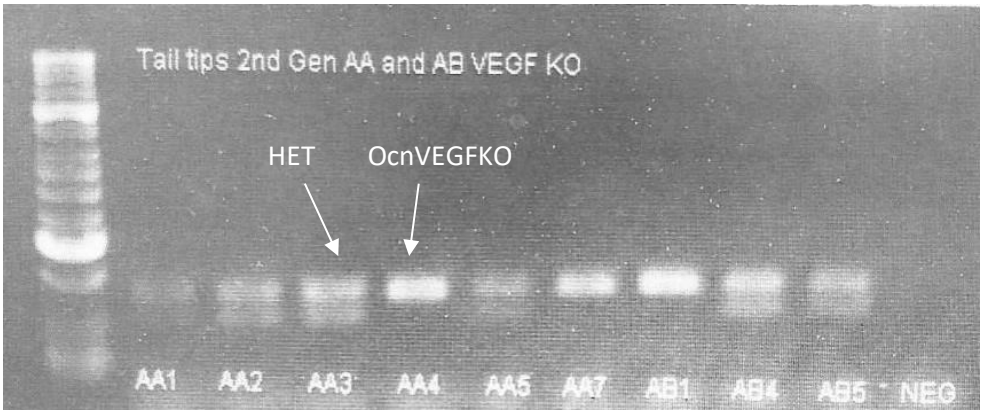

Figure 2.3: Identification of second generation mutants (OcnVEGFKO mice) and heterozygotes. Subjects with one band on the agarose gel are classified as OcnVEGFKO mice (AA4, AA7, AB1), in which *Vegf* has been knocked out specifically in osteoblast cells. Subjects with a double band are classified as heterozygotes.

2.2 Quantitative PCR

For lysis of RNA from osteoblast and mouse bone marrow endothelial cells, buffer RLT from the RNeasy Qiagen kit was utilised and purification of RNA was performed as per the manufacturers' instructions. For lysis of RNA from calvaria, to confirm the deletion of bone-derived *Vegf*, snap frozen calvaria were ground into a fine powder using a pestle and mortar on dry ice. Individual equipment was used for WT and OcnVEGFKO calvaria to ensure that there was no cross-contamination between genotypes. Buffer RLT was added to the calvaria powder and the solution pushed through a needle and syringe as per the manufacturer's instructions, to ensure total lysis. Concentrations of RNA (ng/µl) were measured using the nanodrop reader. The GoScript Reverse Transcriptase kit was used for the reverse transcription of RNA and for first-strand cDNA synthesis, 500ng of RNA per sample was used.

To investigate individual gene expression, Luna Universal qPCR mastermix was used. *Vegf, Vegfr2*, *Opg*, receptor activator of tumour necrosis factor kappa-B ligand (*Rankl*), androgen receptor (*Ar*), estrogen receptor 1 (*Esr1*), estrogen receptor 2 (*Esr2*), osteocalcin (Ocn), *Vegf* and *Sost* primers were required for qPCR. Glyceraldehyde 3-phosphate dehydrogenase (*Gapdh*) was used as a housekeeping control and forward and reverse sequences are recorded in appendix C.2, along with their annealing temperatures. 12.5ng of cDNA was used per triplicate.

For examinations into the expression of a large range of different genes in mouse bone marrow endothelial cells (MBMECs), the endothelial and osteogenesis Qiagen RT Profiler PCR array was used. qPCR was performed using a Step One Plus RTPCR machine. Further details on this process can be found in chapter 6.2.2.

2.3 Micro-computed tomography

For detailed analysis of bone structure and geometry, medium (18μm) and high (0.65μm) resolution micro-CT was used. Following schedule 1 cervical dislocation, the long bones were dissected from 4 and 16 week old OcnVEGFKO, heterozygote and WT mice for analysis. Skulls were collected from 16 week old mice for comparative analysis of a non-weight bearing bone.

2.3.1 Sample preparation

Right tibia/fibula were utilised for μCT for both resolutions and fine dissection ensured the removal of all muscle and tissue from the bone surface. Tibiae were inserted into individual sterilin tubes and fixed with 4% (v/v) paraformaldehyde (PFA) at 4°C for 48 hours on a tube roller. PFA was removed and dH_2O used to wash the bones, before adding 70% (v/v) ethanol for long-term storage. Prior to scanning, tibiae were secured in wax within individual Eppendorf tubes to prevent sample movement.

Dissection of the entire mouse head ensured that the skull remained intact for scanning and subsequent analysis. Heads were frozen on dry ice and stored at -80°C in 50ml universal tubes until scanning. Ear punches were used to ID mice for scanning.

2.3.2 High-resolution micro-CT

For high-resolution scans, 4 and 16 week old tibiae were prepared for synchrotron-based CT (SR CT) at a voxel size of 0.65μm, conducted at the TOMCAT beamline of the Swiss Light Source (Villigen, Switzerland), following previously published methods (Núñez et al., 2018). Here, electrons are excited to near light speeds within an electron accelerator in a circular orbit, which is maintained by magnetic fields. Electromagnetic radiation or synchrotron light is then directed into a beam and used to scan samples, producing very high-resolution scans. In this case, 300 reconstructed high-resolution CT slices from the tibiofibular junction were used for each animal. More information regarding the region of interest used for SR CT scans, quantification methodology and separation of osteocyte lacunae from blood vessel canals is detailed in chapter 3.2.1.

2.3.3 Medium resolution scans

The Skyscan1176 system (Bruker microCT, Kontich, Belgium) at Southampton General Hospital was used to scan the entire tibia and skulls; X-ray tube potential of 45kVp, X-ray tube current of 556µA, integration time of 375ms and voxel size of 18µm. Cross-sectional tomography projection images of the tibia and skull were reconstructed using Bruker software's (Kontich, Belgium) NRecon programme. In depth detail of skull measurement methodologies, bone geometry analysis, calculation of BMD and trabecular bone analysis can be found in chapter 4.2.

2.4 Histology

Histology was performed at Hamburg UKE, in the laboratory of Professor Eric Hesse (Saito et al., 2019), in order to validate the presence and morphology of blood vessels within the blood vessel canals and osteocytes within the lacunae. It also enabled a closer look at the quality of bone and mineralisation at the tibiofibular junction. 16 week old mice were used for this study, producing an n number of at least four WT and OcnVEGFKO bones for both males and females. The contralateral leg to those that were used for micro-CT was used here in order to create a direct comparison.

2.4.1 Sample preparation

Prior to histology, tibia were fixed in 4% (v/v) PFA for 48 hours and then stored in 70% (v/v) ethanol. Bones were prepared for dehydration in the AutoTechnicon machine by removing the foot and the muscle using forceps and a scalpel. Liston bone cutting forceps were used to make a cut that was just above the tibiofibular junction. Filter paper soaked in 70% (v/v) ethanol was put inside the cassette to prevent the drying out of tissue. Cassettes were put into 70% (v/v) ethanol for storage, before being automatically transferred from 70% to 99% (v/v) ethanol inside the AutoTechnicon machine.

Following dehydration, bones were soaked for 24 hours in each of the two methyl methacrylate (MMA) infiltration solutions (900ml MMA, 3.3g benzoyl peroxide (BPO), 100ml nonylphenol) at 4°C. The bones were then put into snap cap glass vials with the foot end pointing upwards and embedded in MMA. MMA was produced by adding 100ml of embedding solution (900ml MMA, 6.6g BPO, 100ml nonylphenol) to 400 µL of N-N Dimethyl-P-toluidine. Once embedded in MMA, glass vials were put into a 4°C fridge overnight, to allow the MMA to set.

Blocks were removed from the Eppendorf tubes and ground down using Meta Serv 250 Grinder-Polisher so that the cutting surface was flat. 10µm sections were cut in order to trim the bone until the region just below the junction where the tibia and fibula meet was reached. Once at the region of interest, 5µm sections were cut and 6 sections were put onto each slide. One drop of 80% (v/v) isopropanol solution was put onto each section to stretch it and prevent folds. A plastic cover slip was placed over the sections and they were

pressed in an incubator at 40°C overnight, before staining. Further detail on the histological stains used can be found in results chapter 3.2.2.

2.5 Scanning electron microscopy

PMMA blocks created for histology were polished and uncoated surfaces imaged using a Zeiss EVO MA10 SEM operated at 20 kV and 49 Pa chamber pressure with a four quadrant backscattered electron (BSE) detector. Samples were re-polished to new levels and in new planes and re-imaged as necessary. All BSE-SEM was performed in collaboration with Professor Alan Boyde at Queen Mary University.

2.5.1 Sample preparation

PMMA blocks which were embedded in Hamburg for histology using previously detailed methodology (chapter 2.4.1) were used for BSE-SEM. Using P600 and P1200 grades of silicon carbide abrasive papers lubricated with water, excess PMMA was removed to expose section planes (LS, TS and oblique). The exposed surfaces were polished further using P2400 and P4000 grade abrasive paper. More information on the methodology used for etching, tri-iodide staining of soft tissue and erosion of calcified tissue can be found in the specific results chapter (3.2.3).

2.6 Cell culture

All primary isolations and tissue culture procedures were carried out using standard aseptic techniques in a class II safety cabinet. Cultures were maintained in an incubator at 37°C with 95% air/ 5% CO_2. The use of animal tissue was carried out under the compliance with Home Office regulations. Long bone osteoblast cells (LOBs) were extracted from postnatal day 4 *Vegf* $^{fl/fl}$ mice as described fully in chapter 5.2.2. MBMECs used for tissue culture were purchased due to the known difficulty of extracting primary endothelial cells (appendix A).

2.6.1 Trypsinising, splitting and counting cells

Media was removed from cells and 5ml sterile phosphate buffered saline (PBS) added to each flask to wash. After removal of PBS, 3ml trypsin-EDTA was added to each flask and cells were incubated for one minute. Once the cells were detached from the bottom, equal volumes of 10% (v/v) FBS media was added to each flask (3ml). The contents of each flask was centrifuged for 5 minutes at a speed of 350 x *g*. The supernatant was removed and the pellet resuspended in 1ml of media. Number of cells per ml were counted using a haemocytometer and dilutions were made accordingly.

The same process was carried out for splitting cells, except cells were not counted. Following centrifugation, the pellet was resuspended in the basal media that corresponded with the osteoblast or EC cell type. Cells were transferred from one T25 flask to one T75 flask. Following this, cells were grown until confluent and then split again, one-in-three into T75 flasks.

2.6.2 Protein assay

Six well plates were used to plate LOBs at a density of 250,000 osteoblast cells per well. Male and female cells were separated and cells were left to become confluent for two days before treating with the adenovirus. Adv-Cre and Adv-GFP was added to the respective wells, to make a final volume of 1000µL per well.

Prior to cell lysis using the Pierce bicinchoninic acid (BCA) protein assay kit, 2 mg/ml bovine serum albumin (BSA) stock was diluted with water to make nine 100 µl standards of concentrations: 0, 0.025, 0.125, 0.25, 0.5, 0.75, 1.0, 1.5 and 2.0 mg/ml. BCA solution for use

in the protein assay was made up with 2156µl of reagent A and 44µl of regent B in a 1:50 ratio.

Following collection and storage of the conditioned media, stopping buffer (0.4mM Na_3VO_4 in PBS) was added to the wells and directly removed. 250µl lysis buffer (96.35mM Tris HCl pH6.8, 10% (v/v) glycerol, 2% (w/v) SDS, 1mM Na_3VO_4) was added to the centre of each well. A syringe was used to scrape the cells off the bottom of the wells and the lysate was stored in Eppendorf tubes at -80°C until use.

Caps were placed on the Eppendorf lids before boiling the protein at 95°C in a heat block for 5 minutes. 5µl of each sample (standards, adenovirus treated and control treated) followed by 100µl of BCA (1:50 ratio) was put into wells of a 96 well plate and duplicates were made of each one. The microplate was wrapped in cling film and incubated at 37°C for 30 minutes. A spectrophotometer with a 570 nm filter was used to read the absorbance and unknown concentrations were calculated using the standard curve created.

2.6.3 Cell viability

Cells were plated at 2,500 cells per well and left to adhere to the bottom of the wells for 24 hours. 1% (v/v) FBS alpha MEM was used to starve the cells of growth media for 24 hours prior to treatment of cells with various different conditions for 24 hours each. Following incubation with 100µl of the respective treatments for 24 hours, 100 µl (1:1 ratio) of Cell Titer-Glo 2.0 Assay was added to each of the wells for 10 minutes. The contents was then transferred to a white plate and read using the preloaded Cell Titer-Glo protocol on the plate reader. The GloMax®-Multi detection system (Promega, UK) was used to measure luminescence.

2.7 Enzymatic assays

2.7.1 ALP activity

LOBS were plated at a density of 50,000 cells per well and left for two days to reach confluence before being treated with the adenovirus as described. A final volume of 500µL was added to each well. Cells isolated from male *Vegf* $^{fl/fl}$ pups were separated from those isolated from females and grown in individual flasks to enable sex comparisons to be made. ALP is one of the most recognised markers of bone formation and it is eluted by differentiating osteoblast cells (Tobiume et al., 1997).

2.7.2 ALP elution assay

Prior to running an elution assay, culture medium was removed and frozen at -80°C. Osteoblast cells were washed once with PBS and then fixed with 100% (v/v) ethanol for 1 minute. The cells were then washed with distilled water, twice.

Standards of known concentration, ranging from 0mM to 0.25 mM, were produced using P-nitrophenol solution diluted with working solution (see appendix B).

P-nitrophenyl phosphate (1mg/ml) was added to the working solution. 500µl of working solution was added to each well and incubated at 37°C for 30 minutes.

Following incubation, the contents of each well was transferred to a 96 well plate. Two 200µl duplicates from each well of eluted solution were plated out. Duplicates of each standard were also transferred to the 96 well plate. After a minute, the plate reader was used to measure the absorbance at a wavelength of 405nm. Unknown concentrations were calculated by comparing the absorbance of each sample to the absorbance of standards with known concentrations in the standard curve.

2.8 Western blot

10µl of 6x blue/orange loading dye and 11.9µl of mercaptoethanol was added to each pre-boiled (see methods 2.6.2) protein lysate. 1 X running buffer was poured into the centre of the two 4-12% (w/v) Bis-Tris protein gels (NuPAGE), which were clamped in place within the electrophoresis chamber. 7.5µg of protein lysate was loaded into each well of the gel and the gels run at 150V until the bands were almost at the bottom.

The membrane (Amersham™ Hybond®) was soaked in mercaptoethanol, followed by dH_2O, followed by 1% (v/v) transfer buffer for 5 minutes each prior to usage. The gel and nitrocellulose membrane was inserted into the transfer cell, with sponges and filter paper either side (figure 2.4). The cell was clamped in place and filled with 1% (v/v) transfer buffer for the transfer of the protein onto the blotting membranes, which took place at a current of 58 mA.

Following the transfer, the membranes were blocked in 3% (w/v) milk in 1 X tris-buffered saline and tween-20 (TBST) for one hour at room temperature on a shaker. Membranes were incubated in rabbit monoclonal antibody (mAb) VEGFR2 primary antibody or GAPDH as a loading control overnight at 4°C on a shaker. The membrane was washed 8 times in 1X TBST (TBS pH7.4 + Tween-20) the following morning and incubated with goat anti-rabbit IgG horseradish peroxidase (HRP) in the dark for 1 hour (1:10000 dilution in 0.2% (w/v) non-fat milk). The membrane was then washed a further 8 times in 1X TBST.

ECL blotting reagents 1 and 2 were combined in equal volumes. A few drops were put onto the protein membrane for one minute. The blotting reagents were then removed and the membranes put into the cassette (protein side up). Westerns were developed in the dark room using Polymax developer and fixer, along with film (Amersham hyperfilm ECL). The film was cut to size and put onto the membrane within the cassette for one minute. The film was then transferred into the developer, until bands became visible. The film was subsequently transferred into water and then fixer.

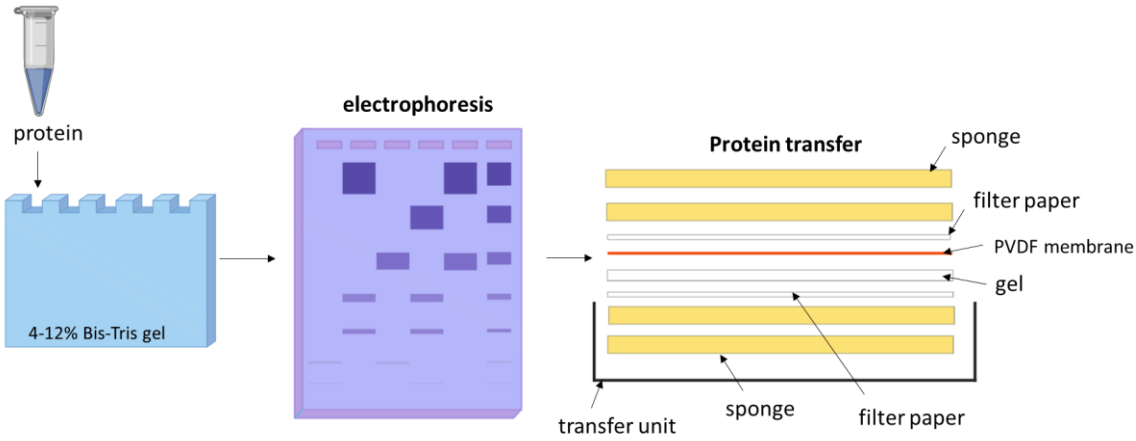

Figure 2.4: Western blotting methodology. Protein lysate was loaded into each well of the gel. The gel was run and proteins separated, before carefully moving the gel into the transfer unit. Two sponges were put into the bottom of the transfer using first, followed by filter paper, the gel, the polyvinylidene difluoride (PVDF) membrane, more filter paper and two more sponges.

2.9 Statistical analysis

For micro-CT analysis in which direct comparisons between both sex and genotype were made, two-way ANOVA was employed. This type of statistical analysis was selected based on the advice of reviewers, following submission of work from this PhD project to the Journal of Bone and Mineral Research (Goring et al., 2019). Two-way ANOVA was calculated using GraphPad Prism version 6.0 for Windows (GraphPad Software, La Jolla, CA, USA). Post-hoc analysis was performed using Tukey's multiple comparison test on GraphPad Prism.

For WT versus OBVEGFKO *in vitro* comparisons, one-tailed paired students t-tests were undertaken between littermate animals, with WT representing *Vegf*$^{fl/fl}$ mice. Excel was used to calculate p values.

All data included in this thesis is always recorded as the mean value ± the standard error of mean (SEM).

Chapter 3 Results I – Quantification and validation of vascular phenotypes following osteoblast-*Vegf* deletion

3.1 Introduction

Due to global deletion of as little one allele of VEGF causing rapid mortality during gestation (Carmeliet et al., 1996, Ferrara et al., 1996), until the introduction of conditional *Vegf* knockout models, the study of the specific role of VEGF in the development of the adult skeleton was challenging. What was known was based on a study in which a soluble receptor protein was utilised to partially silence VEGF (Gerber et al., 1999a) and a study in which tetraploid embryos and embryonic stem cells were combined to produce embryos in which VEGF was genetically modified (Zelzer et al., 2002). These studies showed the importance of VEGF in the vascularisation of the cartilage during endochondral ossification. However, with one study only partially silencing VEGF at day 24 (Gerber et al., 1999a) and the other studying the effect of mice only expressing the $VEGF_{120}$ isoform at embryonic day 17.5 (Zelzer et al., 2002), it was still not possible to look at the role of VEGF in the development of juvenile to adult animal models. Conditional knockout studies are therefore invaluable for investigations into the precise role of VEGF in the maintenance of bone health.

Since the generation of the first Cre transgenic mouse strain by the Clemens lab (Zhang et al., 2002), conditional deletion of genes from specific cell types has been an attractive way to study skeletal development. In this PhD, a bone-specific deletion of *Vegfa* was performed, where VEGF was deleted specifically in osteocalcin expressing bone cells using LoxP genetic recombination. The specificity of *Vegf* knockdown in osteoblast lineage cells using the Cre-Lox system has been well cited in the literature and therefore has proven to be both targeted and effective. Despite levels of *Vegfa* deletion as high as 70% being shown by qPCR in studies by other lab groups (Liu et al., 2012), it is thought that even these results underestimate the true efficiency of *Vegf* deletion by Osx-Cre in this case, due to the fact that the bone will also contain non-osteoblastic cells such as endothelial cells. Additional

studies using the Osx-Cre promotor have used both antibodies against VEGF and ZsGreen to trace the efficiency of *Vegf* deletion in osteoblast lineage cells, identifying significant deletion of VEGF from osteoblast cells (Hu and Olsen, 2016). Using TD tomato mice, it has also been found that bone-specific *Vegf* deletion is not present in the muscle but that *Vegf* is successfully deleted in both woven and cortical bone using the Osx-Cre promotor and thus the deletion is highly specific to bone cells (Buettmann et al., 2019).

Both Osx and Ocn are osteoblast cell markers, however where Osx is an early osteoblast marker, Ocn is a marker of mature osteoblast differentiation (Boskey et al., 1998). Although the majority of studies in which *Vegf* has been conditionally deleted in bone cells have used the Osx-Cre promotor (Hu and Olsen, 2016, Buettmann et al., 2019, Liu et al., 2012), osteoblast-specific deletion using a Ocn-Cre promotor has also been investigated in previous studies. In one study in which *Igf1* was deleted, Lac Z/ALP reporter mice were mated with Ocn-Cre mice in order to assess the efficiency of genetic recombination present. Following the successful deletion of the gene of interest, LacZ was excised and ALP levels were increased. This double reporter of Cre recombination confirmed Ocn-Cre specific deletion of *Igf1* in transgenic calvaria, but not the bladder, heart or skeletal muscle. This was confirmed by PCR (Zhang et al., 2002) and therefore combined with studies using the Osx-Cre promotor, there is a large amount of evidence to suggest that genetic recombination using Osx-Cre and Ocn-Cre is highly specific to bone-derived cells. Ocn-Cre was selected specifically for this work due to the specific interest into the effect of *Vegf* deletion in mature osteoblasts and based on the evidence presented in the literature appeared to be a robust transgenic mouse line to use for this study.

Previous investigations in which VEGF has been deleted specifically in osteoblast cells using an Osterix-Cre promotor have only looked at 8 week old males, focusing on changes in trabecular bone. Here, it was found that conditional deletion of VEGF caused enhanced adipogenesis and reduced osteogenesis, as well as a reduction in bone mass (Liu et al., 2012). Osteoporosis is a degenerative bone disease which is characterised by a reduction in bone mass (as reviewed by Zebaze and Seeman, 2015). Therefore, this bone phenotype produced as a result of conditional VEGF deletion greatly resembled that of an osteoporosis sufferer. In osteoporosis, it has been shown that there is a 60% reduction of circulating levels of VEGF (Senel et al., 2013) and therefore conditional deletion of *Vegf* in osteoblast

cells creates a valuable model for the study of degenerative bone disease such as osteoporosis.

The Olsen lab has previously used the Osterix-Cre mouse model to study the important role of VEGF in bone healing, where it was found to regulate osteoblast differentiation via paracrine pathways. For this study, 9-12 week old male mice were used (Hu and Olsen, 2016). Some studies have focussed their research into bone phenotypes on females due to the fact that degenerative bone diseases and namely osteoporosis are typically associated with post-menopausal women (Yeh et al., 1996). Therefore it was of great interest in this PhD project to carry out investigations into the effect of conditional *Vegf* deletion on adult animals, where both males and females are studied. The study of both sexes was also an important part of this study, especially given the basal skeletal differences observed in healthy individuals (Seeman, 2001, Martin, 2002, Seeman, 2002, Callewaert et al., 2010a).

For many years the focus of studies into degenerative bone disease has been on trabecular bone (Liu et al., 2012, Pufe et al., 2003, Albright, 1947b, Riggs and Melton, 1986), despite the fact that 70% of age-related bone loss is cortical (Zebaze et al., 2010, Zebaze and Seeman, 2015). In studies which have been undertaken, cortical bone microstructure and ultrastructure following a conditional deletion of *Vegf* in bone is yet to be investigated due to limitations in scanning resolutions. Advances in technology and the use of high-resolution synchrotron-based micro-CT to assess bone phenotype has changed this, enabling 3D porosity analysis and the separation of osteocyte lacunae from blood vessel canals in animal models of ageing and disease (Núñez et al., 2017, Núñez et al., 2018, Schneider et al., 2009b).

In line with ARRIVE guidelines, the N number used for SR CT was based on power calculations, determined from total cortical porosity (%) measurements (WT 4.92+/-1.74 and OcnVEGFKO 18.2 +/-6.09). This indicated that with a 95% power at p 0.01 we should be able to detect a significant difference with n = 3 and therefore was deemed adequate for this investigation. These animal numbers (n=3/4) were also in line with landmark publications by Bjorn Olsen using Osx-Cre/*Vegf* $^{fl/fl}$ (Liu et al., 2012).

The tibiofibular junction was chosen as a point of focus due to the fact that it is a skeletal site where the bone is predominantly cortical, enabling analysis of the intracortical vasculature specifically. It is a region which has been the focus of previous studies (McKeon

et al., 2012, Brookes and Harrison, 1957, Núñez et al., 2017) and a well cited location for the occurrence of fracture (Sferopoulos, 2010, Sundaram et al., 2018, Jianhong Pan, 2018). The tibiofibular junction has been used as a region of interest in past studies from as early as 1957 (McKeon et al., 2012, Brookes and Harrison, 1957) and is therefore an important area of the tibia to investigate. The tibiofibular junction also acts as a reference point when positioning the µCT scanner prior to image acquisition, ensuring that scans are comparable and of the same location along the tibia length.

Studies rarely look at bone phenotypes in both sexes, cortical bone is rarely the focus of these investigations and adult mice are used infrequently. It would therefore prove interesting to determine the effect of the deletion of *Vegfa* from mature osteoblast cells (OcnVEGFKO) on the cortical bone phenotype in adult males and females. With an inherent interest in the vasculature, the study of the intracortical blood vessels in this mouse model was also a focus of this chapter. Micro-CT, histology and BSE-SEM was used to look at the effect of an OcnVEGFKO on the cortical bone and vascular phenotype in 16 week old mature male and female tibia.

The aim of this first results chapter was to quantify and validate the vascular phenotype following osteoblast-*Vegf* deletion.

Osteoblast-derived Vegf will be deleted in osteocalcin expressing cells in vivo (OcnVEGFKO) and tibiofibular cortical microstructure analysed in mice at 16 weeks of age

- High resolution synchrotron-based micro-CT for bone architecture determination
- Validation of blood vessels within canals using histology
- BSE-SEM to investigate the vasculature

3.2 Methodology

3.2.1 High resolution micro-CT

3.2.1.1 Region of interest

For more more in-depth analysis, it was important to select a region of interest (ROI). Scanning at a high resolution produces a large amount of data and as a result it would not be possible or time efficient to scan the entire tibia, as you can when performing low resolution scans. SR CT scans were centred around the tibiofibular junction. The area of the tibia selected as the ROI for subsequent analysis (Figure 3.1) consisted of 300 SR CT slices scanned at 0.65µm. The start of this ROI was at the point in which the tibia joined the fibula and the resulting 299 slices were distal of this landmark.

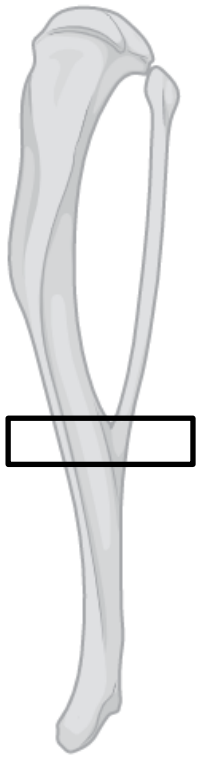

Figure 3.1: Selection of the tibiofibular junction as the ROI for high resolution micro-CT. ROI used for analysis identified on tibia and included 300 slices distal of the tibiofibular junction.

3.2.1.2 Quantification of volume porosity

SR CT was performed at the synchrotron light source (SLS), Zurich at a resolution of 0.65µm voxel size and reconstructed on site. Porosity was extracted using ImageJ by thresholding two copies of the 300 slice stack and inverting one copy. The 'keep largest region' function was used and the stack eroded (12 times) and dilated (13 times) to create the mask. The image calculator plugin 'AND' function was then used to combine the two images, leaving just the porosity within the cortical bone (Figure 3.2). The image stack for the mask and the porosity was saved for future analysis. Volumetric measurements of porosity were extracted using the particle analysis function in ImageJ. The % cortical porosity was calculated by calculating the volume porosity as a function of the total mask volume.

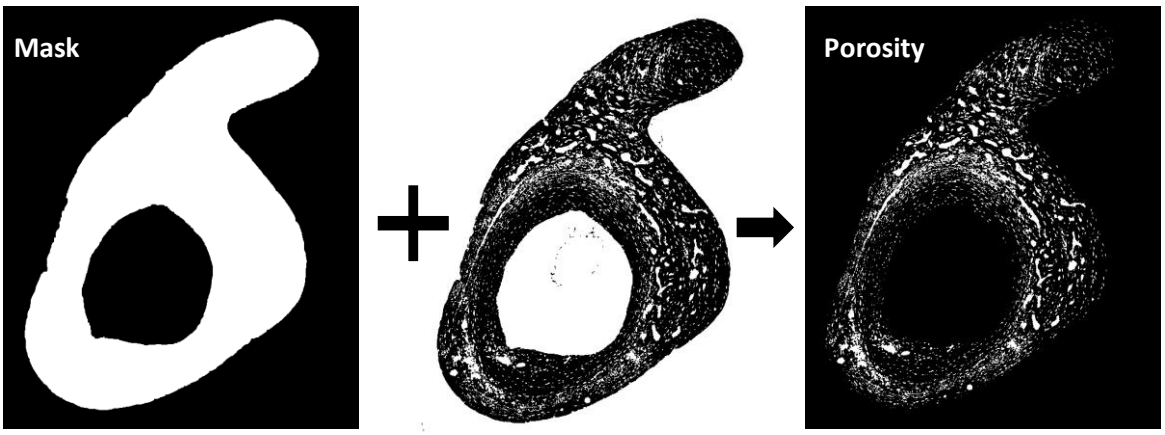

Figure 3.2: Workflow of cortical porosity extraction. The mask was combined with the original image, using the image calculator plugin 'AND' function. This enabled extraction of the cortical porosity.

3.2.1.3 Separation and quantification of osteocyte lacunae and blood vessel canals

Extracted cortical porosity slices were imported into Avizo (9.3.0; ThermoFisher Scientific), which was used for separation of osteocyte lacunae from vascular canals and the definition of threshold values. The volume threshold was chosen for each animal by increasing the volume selection in small increments until the first vascular canal was visible amongst the lacunae in the 3D reconstruction.

Table 3.1: Individual threshold values defining the separation of osteocyte lacunae and intracortical canals for 16 week old animals.

	Female ID	Threshold (μm^3)	Male ID	Threshold (μm^3)
WT	**1**	1922	**1**	1922
	2	1785	**2**	1648
	3	1648	**3**	1648
OcnVEGFKO	**1**	6591	**1**	6041
	2	2472	**2**	9337
	3	1648	**3**	7140

The sieve analysis function was used to dictate the particle volume range selected and the label analysis function measured the total volume of the specific particle selection (open image file-interactive thresholding-label analysis-sieve analysis-label analysis-volume rendering).

Particles smaller than 27.4 μm^3 were considered as noise. Particles volumetrically larger than noise, but smaller than the individual threshold values which separate the lacunae and the canals were categorised as osteocyte lacunae. Characteristically, a global size threshold was employed for the separation of osteocyte lacunae and vascular canals based on particle volume, as previous studies have shown minimal variation in the range of mean osteocyte volumes between subjects (Mosey et al., 2017, Javaheri et al., 2015, Carriero et al., 2014). In this instance, when a global threshold size of 1510μm^3 was used to separate

osteocyte lacunae from intracortical canals based on disseminations of cortical porosity in WT animals, the vascular fraction within OcnVEGFKO bones appeared to include a proportion of large osteocyte lacunae. This challenge was overcome by using individual size thresholds to separate osteocyte lacunae and intracortical canals. Thresholds were carefully selected and set just below the volume of the smallest intracortical canal for each animal (Table 3.1). It therefore should be noted that subsequent measures of the canal volume fraction in the OcnVEGFKO male and female animals include these 'attached' lacunar volumes. As a result, they were referred to in this study as intracortical canals. More in depth analysis of the number, volume and diameter of osteocyte lacunae and vascular canals was performed using the 'Analyse Particles' function in ImageJ.

Probability density distributions of osteocyte lacunae by Dr Rosanna Smith enabled determination of the different volumes of osteocyte lacunae within this fraction. Distributions for each animal were estimated using the ggplot2 (R Core Development Team, 2011, Wickham, 2016) package (version 2.2.1) in R (version 3.3.3) (Wickham, 2016), using a default bandwidth and 2048 estimate points. In male OcnVEGFKO animals, the volume associated with the threshold separating the two distinct populations of lacunae shown in the plot (low and high volume) was determined. Although the separation point between low and high volume osteocyte lacunae was more subtle, corresponding values were found for male and female WT and female OcnVEGFKO animals. This enabled comparisons of the proportion of osteocyte lacunae in the smaller fraction following OcnVEGFKO in males and females.

3.2.2 Histological staining

3.2.2.1 Giemsa stain

Giemsa stain enables the identification of erythrocytes, blood platelets and nuclei and was therefore used in this study for the identification of blood vessels within canals. The slides containing bone cross-sections embedded in polymethyl methacrylate (PMMA) were put into Cellosolve acetate solvent (2-ethoxyethanol) and subsequently hydrated in decreasing concentrations of ethanol, until reaching full hydration in dH_2O (2 minutes each). Giemsa stock solution was combined with dH_2O (1:10) and the solution used to cover slides for 1 hour at 37°C. Increasing the incubation temperature to 60°C reduced the time in which it took for slides to be stained, however it also reduced the quality of the stain and therefore 37°C was maintained throughout. 1% (v/v) acetic acid in dH_2O was used as a differentiating agent (30 seconds). Slides were then quickly dehydrated and transferred from 50% (v/v) ethanol solution to increasing concentrations of ethanol, until 100% (v/v) was reached. They were then put in Xylene solutions I-III for 5 minutes each. They were mounted with coverslips and DPX mountant, dabbing the sides of the slide to remove excess.

3.2.2.2 Pentachrome stain

Movat's Pentachrome stain enabled investigations into both the vasculature within the canals and the mineralisation state of the bone. The slides were put into Cellosolve and subsequently hydrated in decreasing concentrations of ethanol, until reaching full hydration in dH_2O (2 minutes each). Slides were put into a solution of Alcian Blue for 15 minutes, followed by a 5 minute wash in running tap water. The sections were next submerged in alkaline alcohol (90ml 80% (v/v) ethanol and 10ml 25% (v/v) ammonia) for 60 minutes and washed in tap water for 10 minutes and then dipped in dH_2O. Slides were put into Iron haematoxylin for 15 minutes, followed by a wash with dH_2O. Brilliant Crocein was used to cover the slides for 8 minutes, followed by a 0.5% (v/v) acetic acid in dH_2O. 5% (v/v) phosphotungstic acid was added to the slides until bone pink and blue colouring was visible and they were then put into 0.5% (v/v) acetic acid. After three 5 minute treatments with absolute ethanol, the slides were put into saffron solution for 40 minutes. They were then put into absolute ethanol for an additional three times for 5 minutes each, before being put into Xylene solutions I-III for 5 minutes each. They were mounted with coverslips and DPX mountant.

3.2.2.3 Image analysis

Once the slides were stained with Giemsa and Movat's pentachrome stain, global quantification of % filled canals was performed to calculate the percentage of canals that contained a blood vessel. The pentachrome stain enabled identification of blood vessels most precisely, so it was these slides that were used for the quantification. Local analysis of % fill of blood vessel canals in posterior and anterior regions was also performed, due to published findings by Núñez et al. which suggest that the posterior region of the bone has a higher vascular canal volume density than the anterior region (Núñez et al., 2018). Anterior and posterior regions were defined using the guidelines shown in figure 3.3a. Blood vessel area was calculated using the freehand selection tool on ImageJ (CTRL+M; for area measurements). The 'count' function on ImageJ also enabled the osteocytes to be counted, in order to calculate the % fill osteocyte lacunae and the number of osteocytes per mm^2. Further detail of this methodology can be seen in figure 3.3b.

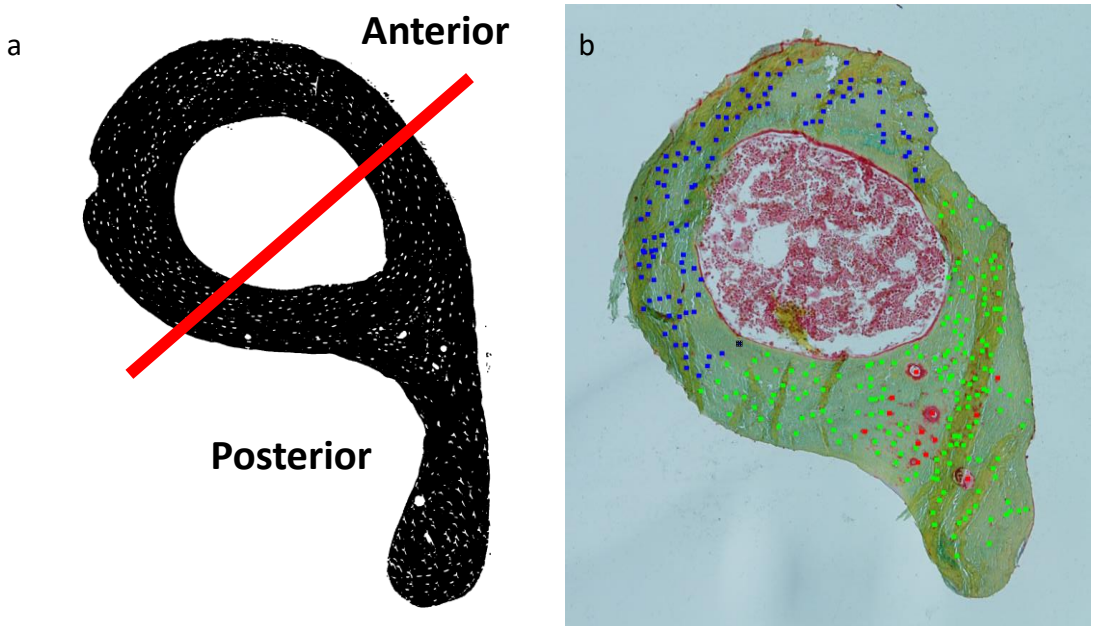

Figure 3.3: Defining the anterior and posterior regions in murine cortical bone. For analysis of histological images, the tibiofibular junction cross-section was split into anterior and posterior halves (a). Histological cross sections were analysed using the 'count' function in ImageJ. The anterior osteocytes that have been counted are labelled in blue, the posterior osteocytes in bright green and the blood vessels in red (b).

3.2.3 BSE-SEM

3.2.3.1 Etching

In order to take a closer look at the microstructure of OcnVEGFKO bones, with a particular interest in the vasculature, the exposed surface of the tibia which was embedded in PMMA was lightly etched by application of DFG icon-etch dentistry gel (Boyde et al., 2017). This is a silicic acid gel containing phosphoric acid which can be applied precisely to selected areas. Etch times used were 30 to 120 seconds. The etchant was washed off with distilled water, dried, and re-examined in the SEM. The depth of penetration with this regime was only a few microns, so that the same sample could be re-polished to a new level.

3.2.3.2 Tri-iodide staining of soft tissue

The surface of polished blocks, etched preparations and 'casts' were stained using either an aqueous solution of iodine in ammonium iodide ('triiodide') or dry using iodine vapour (Boyde et al., 2017, Boyde et al., 2014). Both of these procedures stain cells and matrix to a depth of a few microns, allowing the visualisation of blood vessels and other cellular components of bone.

3.2.3.3 Erosion of calcified tissue

The same samples were treated to remove bone matrix and mineral by treatment with 2N HCl and 7% (v/v) chlorine sodium hypochlorite solutions (thin bleach) in succession. Bone samples were subsequently washed with water and dried. This erosion procedure removes bulk bone in normally calcified tissue and solely leaves the space outside the bone as a solid PMMA cast. This includes the periosteum, and space inside the bone including the medullary cavity and any blood vessel canals which may be present. Casts of the lacunar-canalicular space are washed away except for lacunae nearest to free bone surfaces which remain anchored in position.

3.3 Results

3.3.1 Deletion of mature bone-derived *Vegf* increased cortical porosity in 16 week old male mice

A large proportion of current research is focussed on the effect of a *Vegf* knockout on developing female mice, but very few studies compare both sexes and look at mature subjects. The role of VEGF in maintaining bone integrity in mature males and females distinctly is therefore not fully understood. In order to study the skeletal functions of osteoblast-produced VEGF in further detail, *Vegfa* was conditionally deleted from mature osteoblast cells. The deletion of *Vegf* was determined by both genotyping, using genomic DNA extracted from mouse tail tips as described in the methodology (chapter 2.1.2) and by qPCR following the reverse transcription of RNA extracted from 16 week old murine calvaria (methods chapter 2.2). qPCR outputs supported genotyping results, showing a 72.5% decrease in detectable levels of *Vegf* in male and female OcnVEGFKO mice versus WT controls (appendix D.1).

For interrogation of the microstructure at the tibiofibular junction in WT and OcnVEGFKO mice, high resolution SR CT was used. Here, high spatial resolutions in the order of 1µm and better can be achieved at high image quality levels and intracortical microstructures such as the intracortical canal network or osteocyte lacunae can be resolved within a few minutes of scanning time (Schneider et al., 2007a, Schneider et al., 2013, Mader et al., 2013, Dong et al., 2013). SR CT at the tibiofibular junction enabled analysis of the microstructure and ultrastructure of transgenic tibia both quickly and at a high resolution (0.65µm voxel size), greatly enhancing the information extracted in comparison to medium resolution scans using a desktop scanner (Schneider et al., 2009a). As a result, for the first time in this model of disease, cortical porosity was able to be visualised clearly and subsequently quantified in 3D.

The 16 week old mice used in this chapter have been through puberty and subsequently have fully developed skeletons. Using SR CT, differences in cortical porosity between subjects were instantly visible at a higher resolution and somewhat surprisingly, male OcnVEGFKO bones had a particularly striking porous phenotype which was characterised by

the presence of large, irregularly shaped cavities (figure 3.4). This was consistent throughout every repeat (figure 3.5).

Until now and due to the bias towards using female animals for research into degenerative bone disease, this sexual dimorphism had not been identified. Therefore, this preliminary finding emphasised the importance of looking at both males and females throughout this PhD project.

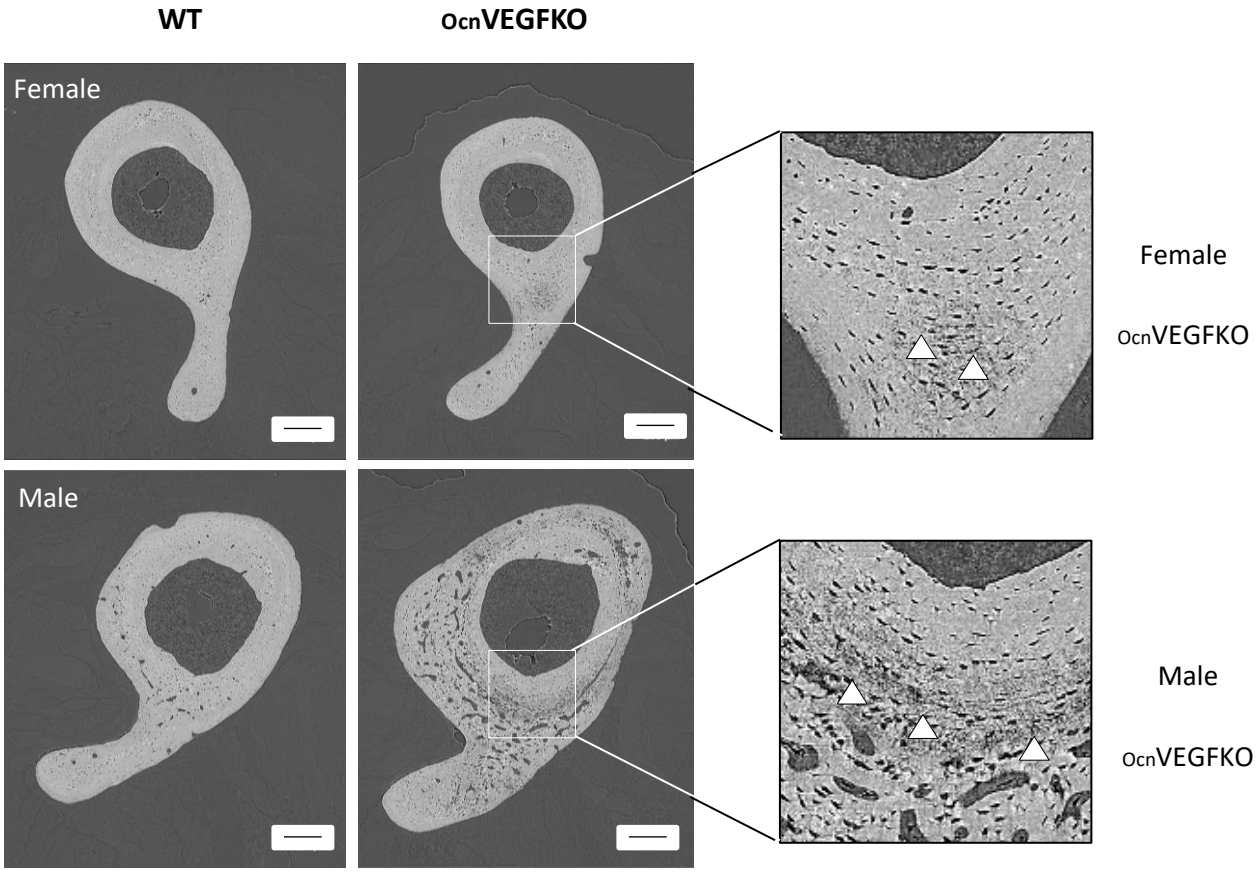

Figure 3.4: Conditional deletion of *Vegf* alters cortical porosity in adult tibiae, particularly in males. High resolution, synchrotron X-ray computed tomography (SR CT; 0.65µm) slices from female and male WT and OcnVEGFKO mice revealed poorly mineralised areas of cortical bone at posterior region of tibiofibular junction (white arrows) and differences in cortical porosity between male and female OcnVEGFKO. Scale bar = 200µm.

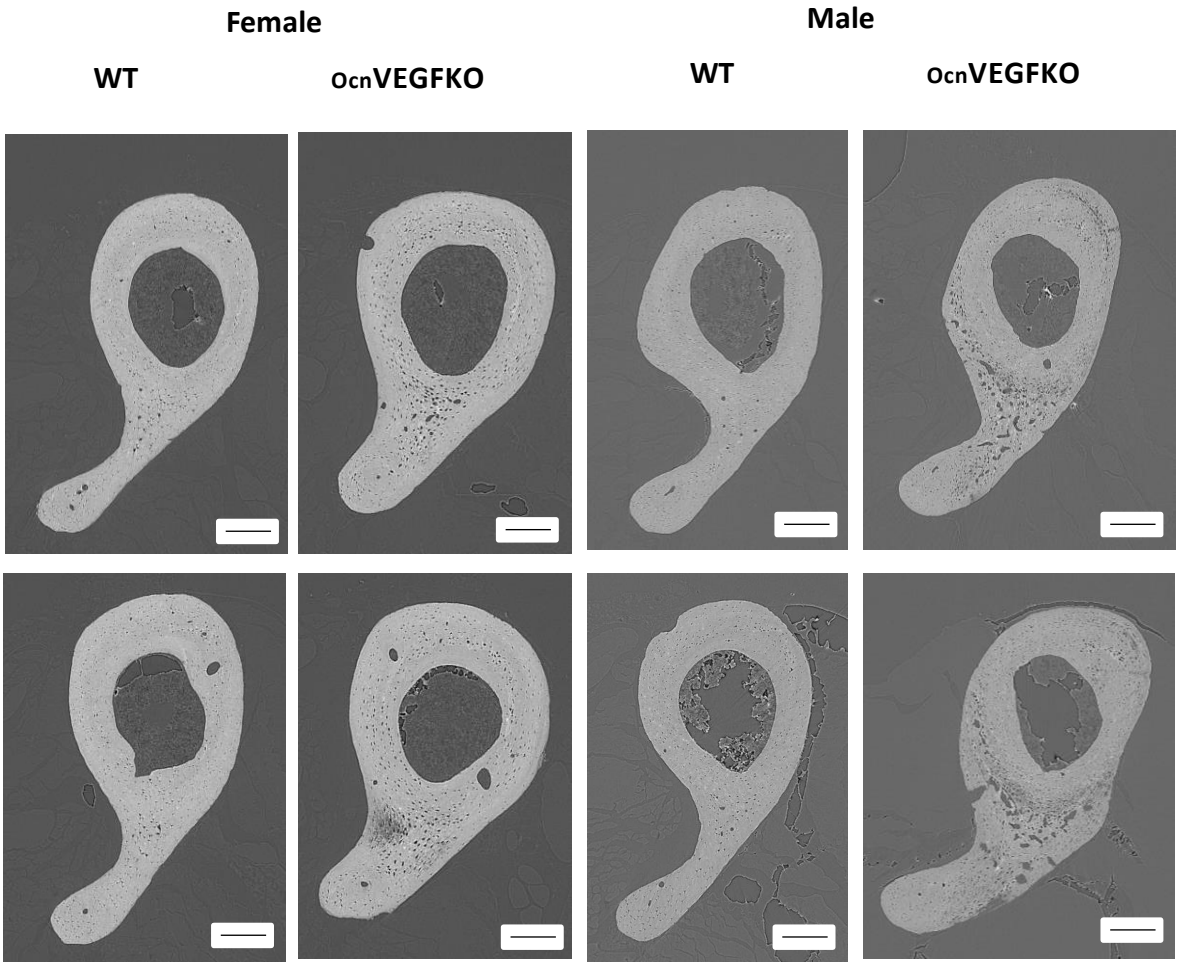

Figure 3.5: Individual animal repeats to illustrate that conditional deletion of *Vegf* alters cortical porosity in adult tibiae consistently in both males and females. Individual slices taken from SR CT scans (0.65µm) of each 16 week old animal at the tibiofibular junction. Severe increased cortical porosity observed in male OcnVEGFKO mice, particularly in the posterior region of the tibiofibular junction. Two additional repeats displayed to illustrate reproducibility of the phenotype observed. Scale bar = 200µm.

Quantification of % volume intracortical porosity from high-resolution scans, showed severe cortical porosity at the tibiofibular junction, especially in male OcnVEGFKO mice versus WT controls (2.73 fold increase, p<0.0001). Although there was an increase in intracortical porosity following OcnVEGFKO in females, this was not significant versus WT (0.51 fold increase, p=NS). When comparing female OcnVEGFKO versus male OcnVEGFKO however, there was a significant increase in intracortical porosity (1.82 fold increase, p<0.0001), providing further evidence for sexual dimorphisms in tibial microstructure following OcnVEGFKO (figure 3.6).

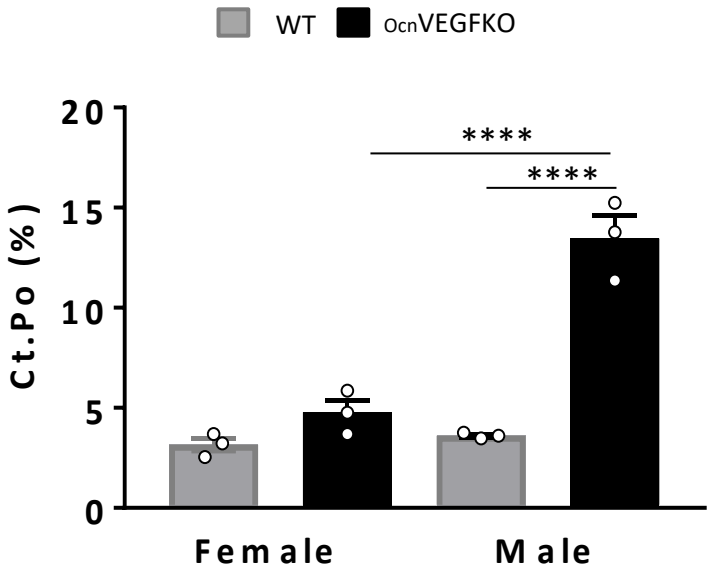

Figure 3.6: Deletion of osteoblast-derived *Vegf* increases intracortical porosity in males. In female OcnVEGFKO, there was an increase in volume cortical porosity versus WT littermate controls, however this was not significant. In males, there was a large significant increase in volume cortical porosity in OcnVEGFKO versus WT. Male OcnVEGFKOs also had a significantly higher volume cortical porosity than female OcnVEGFKOs (error bars indicate mean value ± SEM, n=3 females and 3 males from individual litters p<0.0001**** using two-way ANOVA).

3.3.2 High-resolution synchrotron-based micro-CT identified sexual dimorphisms in lacunar and vascular canal phenotypes in 16 week old mice following deletion of mature osteoblast-derived *Vegf*

In order to further interrogate sex differences observed in measurements of cortical porosity at the tibiofibular junction, a negative imprint of the calcified bone tissue was extracted from high-resolution CT image stacks. This allowed investigations into the effect of OcnVEGFKO on the number, volume and diameter of intracortical canals and osteocyte lacunae using Aviso 9.0 for analysis. A number of studies have previously applied this principle to human (Cooper et al., 2003, Cooper et al., 2007) and rodent bone samples (Núñez et al., 2017, Núñez et al., 2018, Britz et al., 2010, Britz et al., 2012, Schneider et al., 2007b, Schneider et al., 2013, Thurner et al., 2010). Due to the explained limitations of micro-CT used in previous studies however, this is not a technique which has been applied to VEGFKO models in the past and therefore was of significant interest for this study.

As aforementioned in the methods (3.2.1.3), individual threshold values were employed for the separation of osteocyte lacunae and intracortical canals due to the variations observed in the size of porosity fractions between OcnVEGFKO repeats. These abnormally shaped lacunae were disorganised and joined to the canals as a result of their close proximity (figure 3.7). Particle sizes below 27.4 μm^3 were defined as noise, correlating with previous studies in which confocal laser scanning microscopy and high resolution µCT were used to interrogate porosity and osteocyte lacunae were found to be no smaller than 28μm^3 (McCreadie et al., 2004, Carriero et al., 2014). The mean separation threshold used for WT and OcnVEGFKO females was significantly lower than the thresholds used for OcnVEGFKO males in which the 'clumping' of canals and lacunae was particularly prominent (figure 3.8).

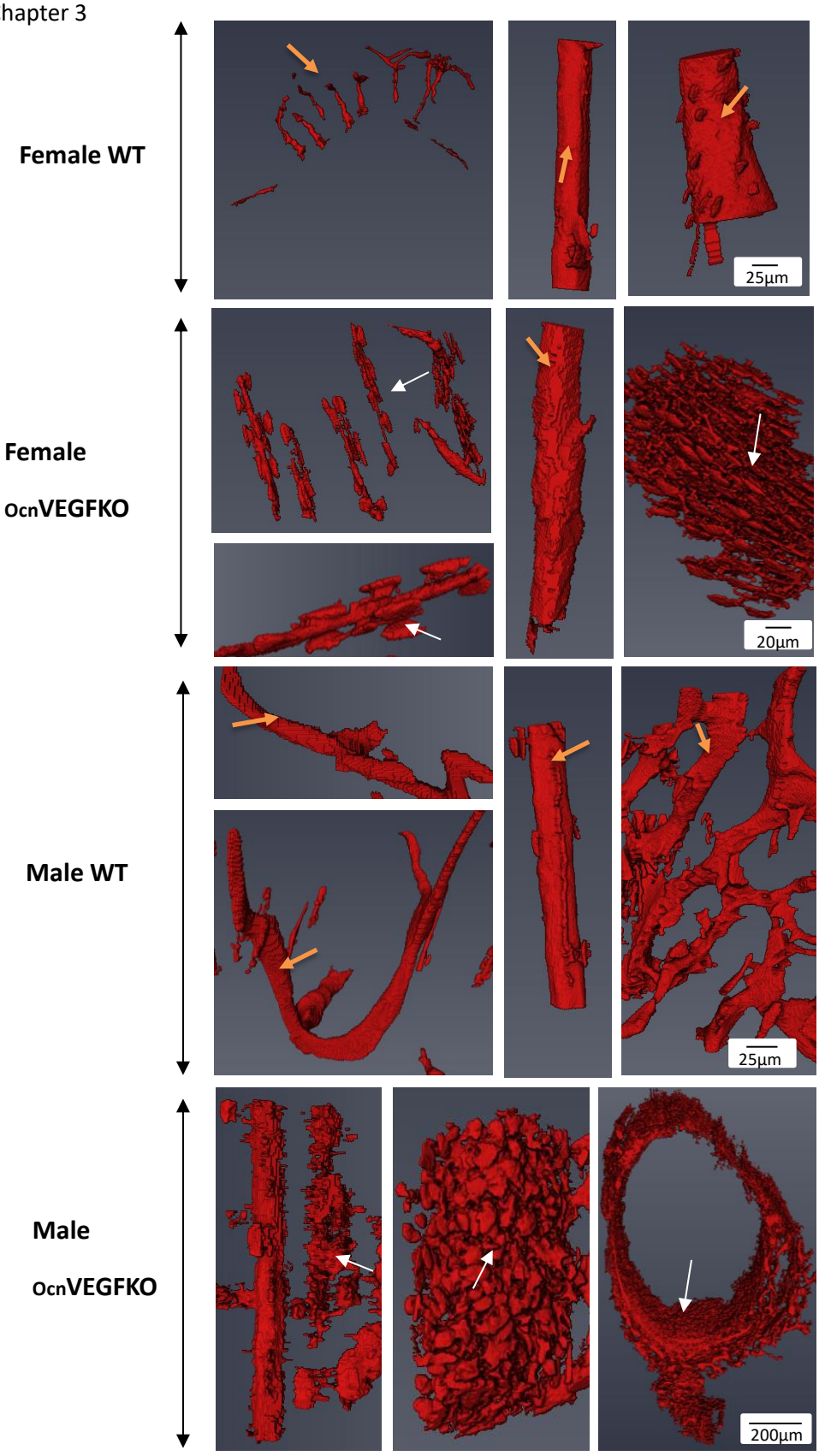

Figure 3.7: Osteocyte lacunae adjoined to intracortical canals in 16 week old OcnVEGFKO mice. Small, medium and large (left to right) intracortical porosity. Following OcnVEGFKO and particularly in males, canals, osteocytes and large intracortical porosity (white arrows) has been identified by Aviso 9.0 software as one large piece of porosity in the vascular canal compartment. Orange arrows denote healthy looking canals.

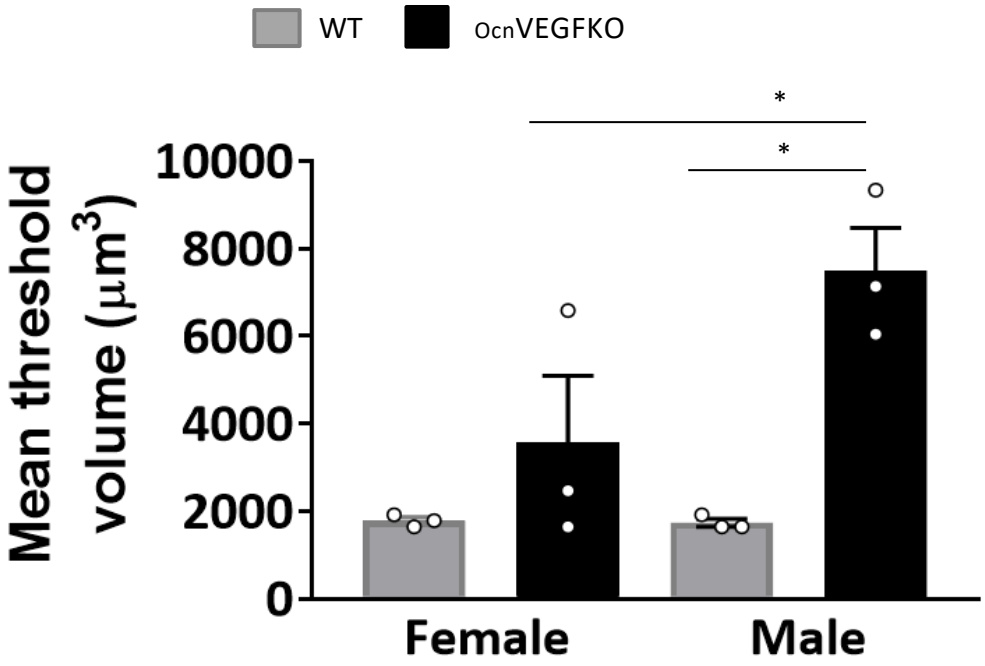

Figure 3.8: Sexual dimorphism in osteocyte/intracortical canal separation thresholds. Average separation threshold is just below the volume of the smallest intracortical canal for each individual bone (values and error bars indicate mean value ± SEM, n = 3 females and n=3 males, $p<0.05$* using t-test).

Using these individual separation thresholds, it was possible to produce 3D representations of the osteocyte lacunae (yellow) and intracortical canals (red) as two different subtypes of the intracortical porosity (figure 3.9). In male WT, female WT and female OcnVEGFKO, the ratios of osteocyte lacunae to intracortical canals were fairly consistent. In WT females, 75.8% of the total pore volume represented osteocyte lacunae and 22.0% intracortical canals (figure 3.10a). In WT males 75.4% of the pore volume consisted of osteocyte lacunae and 23.1% intracortical canals (figure 3.10b). In OcnVEGFKO females (figure 3.10a), the ratio of lacunae versus canals was comparable to WT values. Once again however, it was the OcnVEGFKO males which were dimorphic and there was almost a complete switch in the proportions of osteocyte lacunae to intracortical canals. Here, 76.1% of the total porosity was made up of intracortical canals and only 22.3% composed of osteocyte lacunae (the rest defined as noise; figure 3.10b). Importantly, in OcnVEGFKO animals, some osteocyte lacunae contributed to the canal volume fraction due to their intimate proximity (i.e. direct connection) to the intracortical canals (figure 3.7).

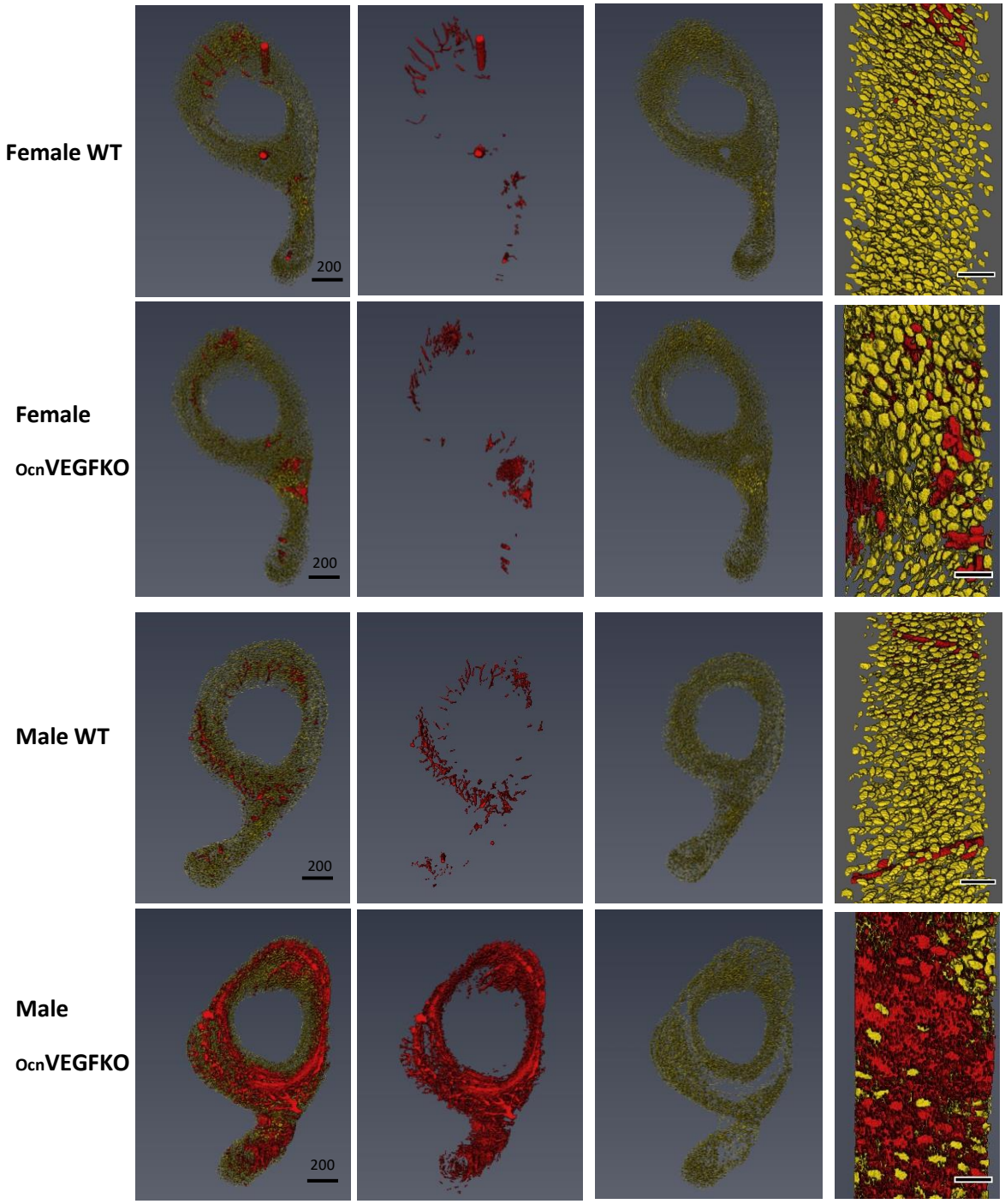

Figure 3.9: Separation of osteocyte lacunae and intracortical canals in males and females. 3D renderings of osteocyte lacunae (yellow) and intracortical canals (red) from female and male, WT and OcnVEGFKO mice (16 weeks-old) following SR CT scans (0.65µm voxel size). Scale bar = 50µm unless otherwise stated. All measurements recorded in µm.

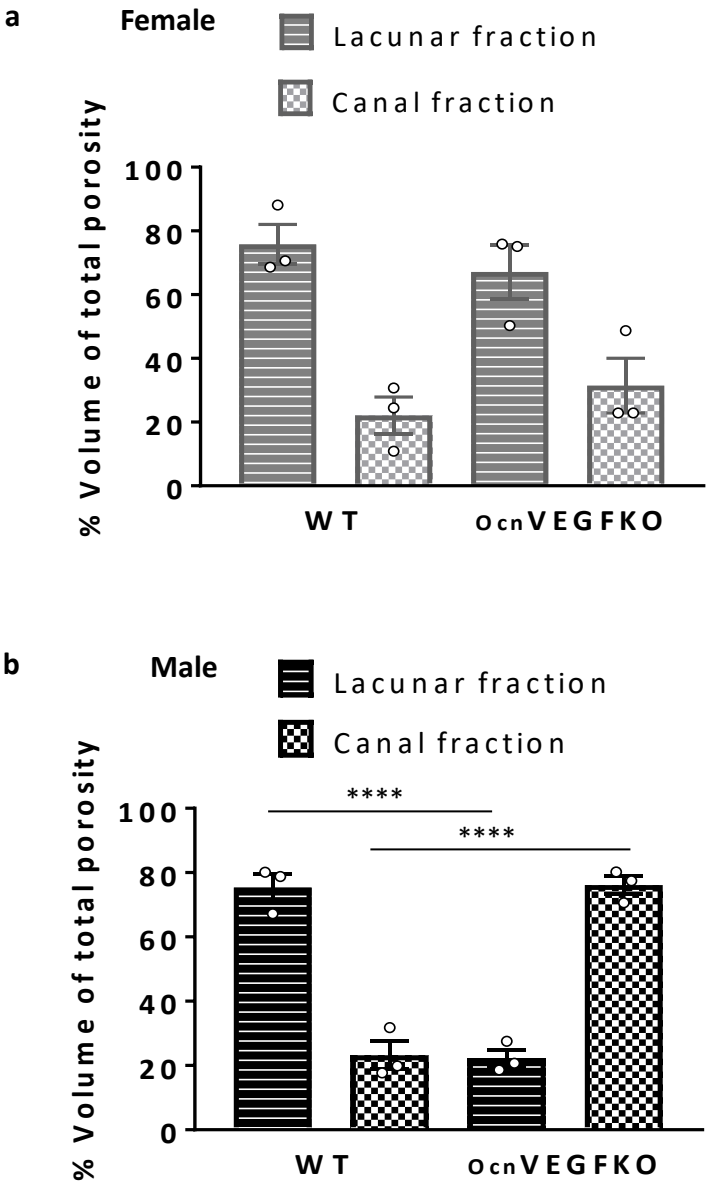

Figure 3.10: Proportion of intracortical porosity made of osteocyte lacunae and blood vessel canals. In female animals (a), osteocyte lacunae made up the highest fraction of the intracortical porosity for both WT and OcnVEGFKO. In males (b) % pores constituting the lacunar fraction was decreased and intracortical canal fraction was increased in OcnVEGFKO versus WT. Error bars indicate mean value ± SEM, n=3 females and 3 males from individual litters $p<0.0001$**** using two-way ANOVA.

In order to further understand the bone phenotype, individual canal and lacunar fractions were quantified and values compared to look at the effect of sex and OcnVEGFKO. In female OcnVEGFKO mice, there was a significant increase in lacunar number density (standardised to mask volume - Lc.Dn; figure 3.11a), mean lacunar volume (Lc.V; figure 3.11b) and lacunar diameter (Lc.Dm; figure 3.11c), in comparison to WT animals. No significant differences were shown in the lacunar number density or mean lacunar volume in male OcnVEGFKO mice, but a significant decrease in lacunar diameter was identified (figure 3.11c).

To investigate the distribution of lacunae sizes that are used to calculate the mean lacunae volume, a particle distribution analysis was carried out, using the lacunar volumes obtained from the particle analyser function in ImageJ. In both female (figure 3.11d) and male (figure 3.11e) WT groups, there is a large peak in the probability density curve at just above 200 μm^3. In females, following the deletion of bone-derived VEGF, the distribution curve was much broader and there was a greater variance in lacunar volume recorded between each animal. In stark contrast, in male OcnVEGFKOs, the probability density curve had a bimodal distribution and two individual populations of osteocyte lacunae were identified. The presence of a large quantity of smaller osteocyte lacunae could explain the lack of significance in the mean volume cortical porosity results following the deletion of osteoblast-derived VEGF in males, as it is possible that the smaller osteocyte population could skew the mean volume. Statistical analysis confirmed that the proportion of osteocyte lacunae in the smaller volume population was significantly larger in OcnVEGFKO males than in both male WT ($p=0.007$) and female OcnVEGFKO mice ($p=0.015$). Unlike in males, no significant differences in proportions of osteocyte lacunae sizes were shown in female OcnVEGFKO, when comparing with female WT animals (Raw data: Appendix D.2).

Above the individual threshold values, porosity was labelled as intracortical canals. Quantification of the canal fraction indicated a significant decrease in the canal number density (Ca.Dn; figure 3.11f) and a significant increase in mean canal volume (Ca.V; figure 3.11g) in male OcnVEGFKOs versus WT controls. The mean canal diameter (Ca.Dm; figure 3.11h) was unchanged, however. This suggested that there were not as many, significantly larger intracortical canals in male OcnVEGFKO mice. Given the differences in mean threshold values in males, this increase in canal volume was unsurprising ($7507\mu m^3$ in OcnVEGFKO males versus $1739\mu m^3$ in WT males). In females however, no significant changes in intracortical canal number, volume or diameter were observed.

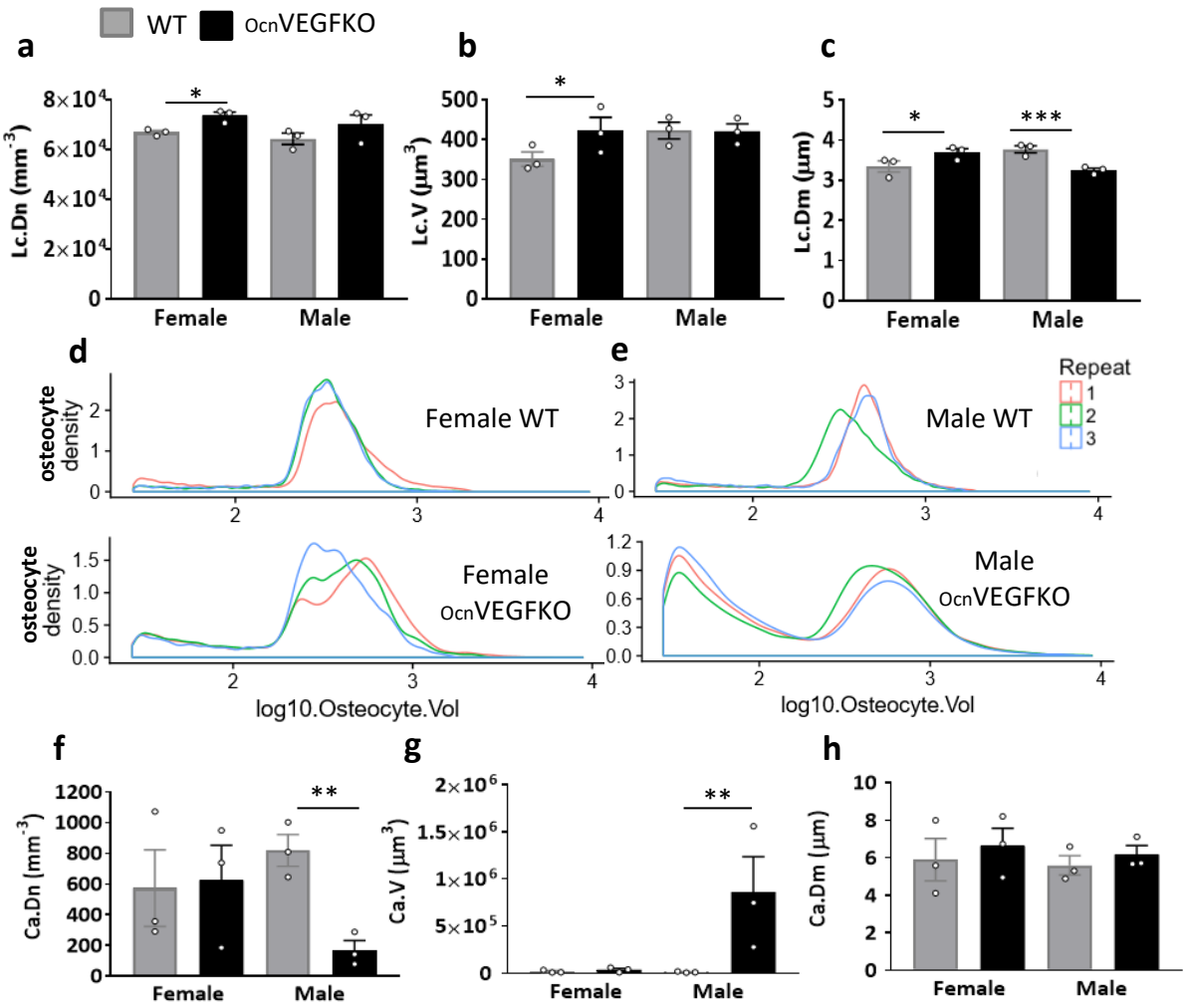

Figure 3.11: Deletion of osteoblast-derived *Vegf* significantly increases intracortical canal volume in males. Measurements taken of regularly sized osteocyte lacunae show an increase in lacuna number density (Lc.Dn; a), mean lacunar volume (Lc.V; b) and mean lacunar diameter (Lc.Dm; c) in female OBVEGFKO versus WT. In males, there was a decrease in mean lacunar diameter (Lc.Dm; c) following knockout of OBVEGF. The probability density of osteocytes of different volumes for females (d) and males (e) are shown by graphs on a logarithmic scale, which were created using the free language and environment for statistical computing and graphics R (https://cran.r-project.org/). Each coloured line represents one animal. Number of intracortical canals greater than the lacunar threshold (see methods) is significantly decreased in male OcnVEGFKO (Ca.Dn; f). An increase in mean canal volume was seen following OcnVEGFKO (Ca.V; g), however no change in mean canal diameter was observed in male OcnVEGFKO (Ca.Dm; h). Error bars indicate mean value ± SEM, n=3 females and 3 males from individual litters p<0.05*, p<0.01**, p<0.001***, p<0.0001**** using two-way ANOVA.

3.3.3 Deletion of osteoblast-derived *Vegf* affects blood vessel morphology and osteocyte phenotype specifically in 16 week old male mice

Giemsa and pentachrome staining of sections from the mouse tibiofibular junction, using the contralateral legs to those used for micro-CT enabled the identification of blood vessels within the intracortical canals in females and males (figure 3.12a). Although pentachrome sections were predominantly used for quantification purposes, Giemsa stains enabled visualisation of blood vessels and erythrocytes and acted as an ideal second point of validation.

In order to be able to carry out sex comparisons, stained sections were used for histological analysis in females. Both the Giemsa and the pentachrome stains showed a degree of disorganisation in female OcnVEGFKO bones versus WT controls (figure 3.12a and 3.13), however this was not nearly as prominent as the strong phenotype observed in males (figure 3.12a and 3.14). This correlated with synchrotron scans in which there was an increase in cortical porosity following OcnVEGFKO in females, which was non-significant. A high canal occupancy was identified (figure 3.12b) and quantification using the histological sections from 8 female mutant and wild type bones showed that an average of 92.4% (± 2%, n = 8) of the blood vessel canals were filled with a blood vessel. There were no significant differences identified between female OcnVEGFKO and WT sections. Meanwhile, there were no significant changes in the area of vascular canals (figure 3.12c). In females, there was no significant increase in osteocyte number (figure 3.12d) and no significant changes in the proportion of total osteocytes present in the posterior region in female OcnVEGFKO versus WT. Osteocytes were evenly distributed in the anterior and posterior of the cross sections (posterior; female OcnVEGFKO, 66%; female WT, 65%, NS).

In both Giemsa and pentachrome stained sections, blood vessels in male OcnVEGFKO bones were strikingly disorganised (figure 3.12a and 3.14). Using a pentachrome stain, it was possible to distinguish between non-mineralised (red) and mineralised components (green) of the bone. Here, large areas of poorly mineralised osteoid were visible around the blood vessels and osteocytes, partly explaining the raised volume cortical porosity identified specifically in male OcnVEGFKO mice following SR CT analysis. In comparison, the organisation of osteocytes and blood vessels in WT animals appeared to be more

structured across the bone cortex and there was no osteoid present around the osteocytes or blood vessels.

Correlating with what has been previously identified in the literature (Núñez et al., 2018), in males the majority of blood vessels (69% WT and 70% OcnVEGFKO) were found in the posterior region of the tibia. Quantification of histology validated the presence of blood vessels within the canals and the percentage of filled blood vessel canals was 85.4% (± 2%, n = 8) in males, with only a very small proportion of them empty (figure 3.12b). Even so, it is highly likely that *in vivo* the small number of empty canals were filled and that histological processing was responsible for the loss of the vessel from within the canal. The percentage canal occupancy was not significantly different in OcnVEGFKO versus WT controls. There was however, a significant increase in vessel area in OcnVEGFKO males versus WT (3.12c) and a significant increase in osteocyte number (3.12d). There was also a significant increase in the proportion of total number of osteocytes present in the posterior region in male OcnVEGFKO versus WT (posterior; Male OcnVEGFKO, 74%; Male WT, 54%, $p<0.05$). As per the vasculature, in male OcnVEGFKO, a greater proportion of osteocytes were present in the posterior region in comparison to the quantities counted in the anterior region.

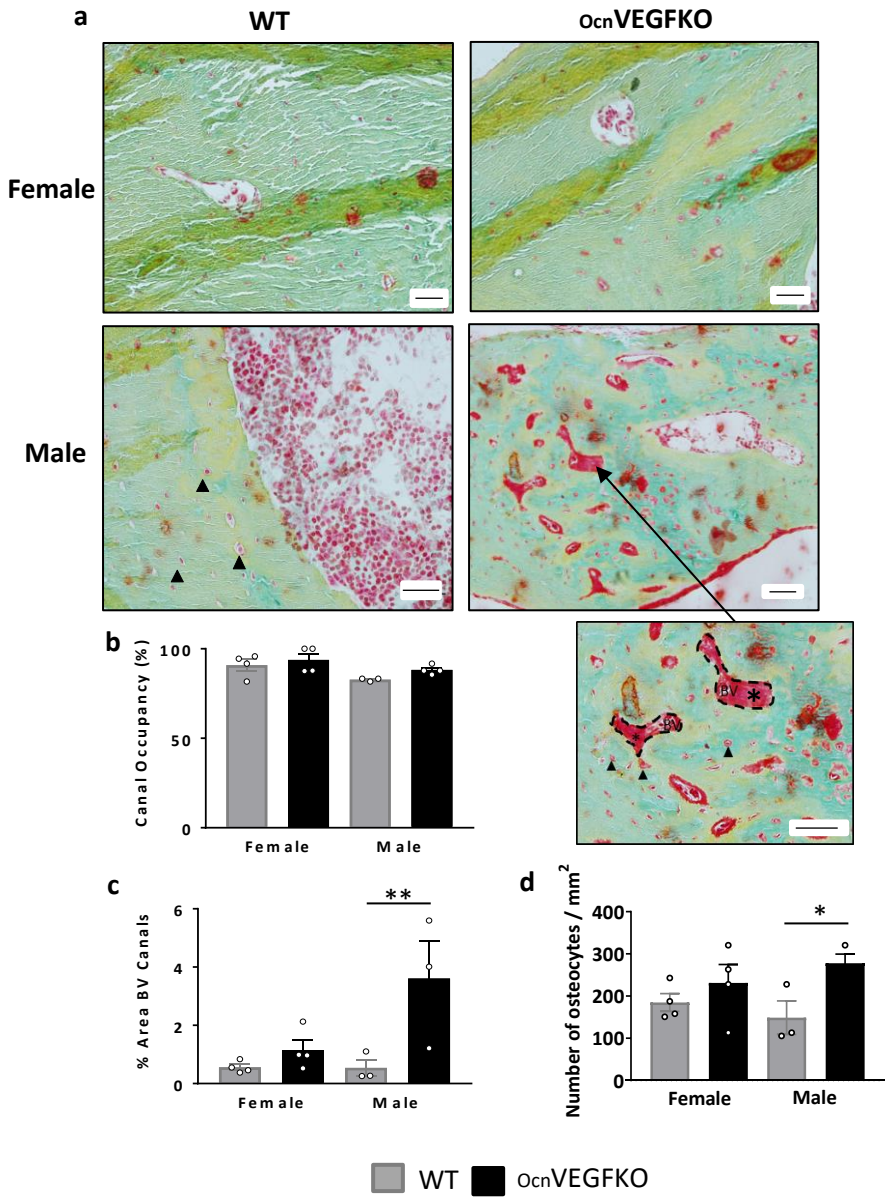

Figure 3.12: OcnVEGFKO increases the area of blood vessel canals in mature male mice specifically. No large or obvious alterations in osteocyte or blood vessel morphology following OcnVEGFKO in females versus WT (a). In pentachrome stained male OcnVEGFKO sections however, there was large amounts of unmineralised osteoid (*) surrounding blood vessel canals (hatched lines) and osteocytes (black arrows). Analysis of stained sections showed there was a high level of vascular canal occupancy (b), which remained unchanged in OcnVEGFKO versus WT animals. In male OcnVEGFKO versus WT %, area blood vessel (BV) canals was significantly increased (c). Osteocyte number was significantly increased in both males (d; error bars indicate mean value ± SEM, n=4 female and n=3 male mice from individual litters, $p<0.01$** using ANOVA). Scale bar = 20µm.

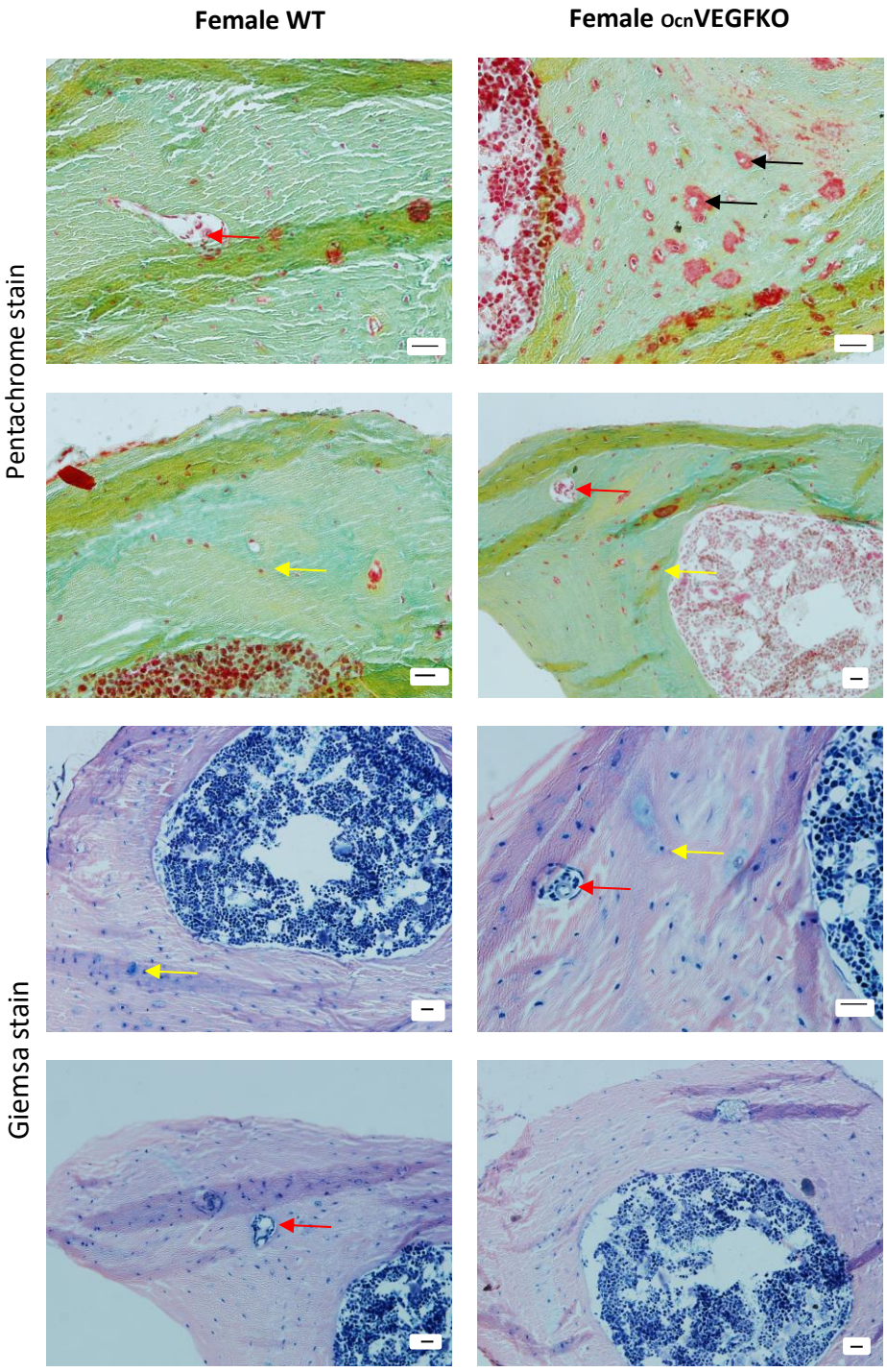

Figure 3.13: Using Giemsa and pentachrome histological stains to interrogate the vasculature in 16 week old WT and OcnVEGFKO female mice. Following deletion of *Vegf* in female mice, the pentachrome stain shows a small increase in osteoid (red stain) surrounding the osteocytes within lacunae (black arrows). Other than this, no abnormalities can be detected in the vasculature (red arrows) or osteocytes (yellow arrows). Scale bar = 20µm.

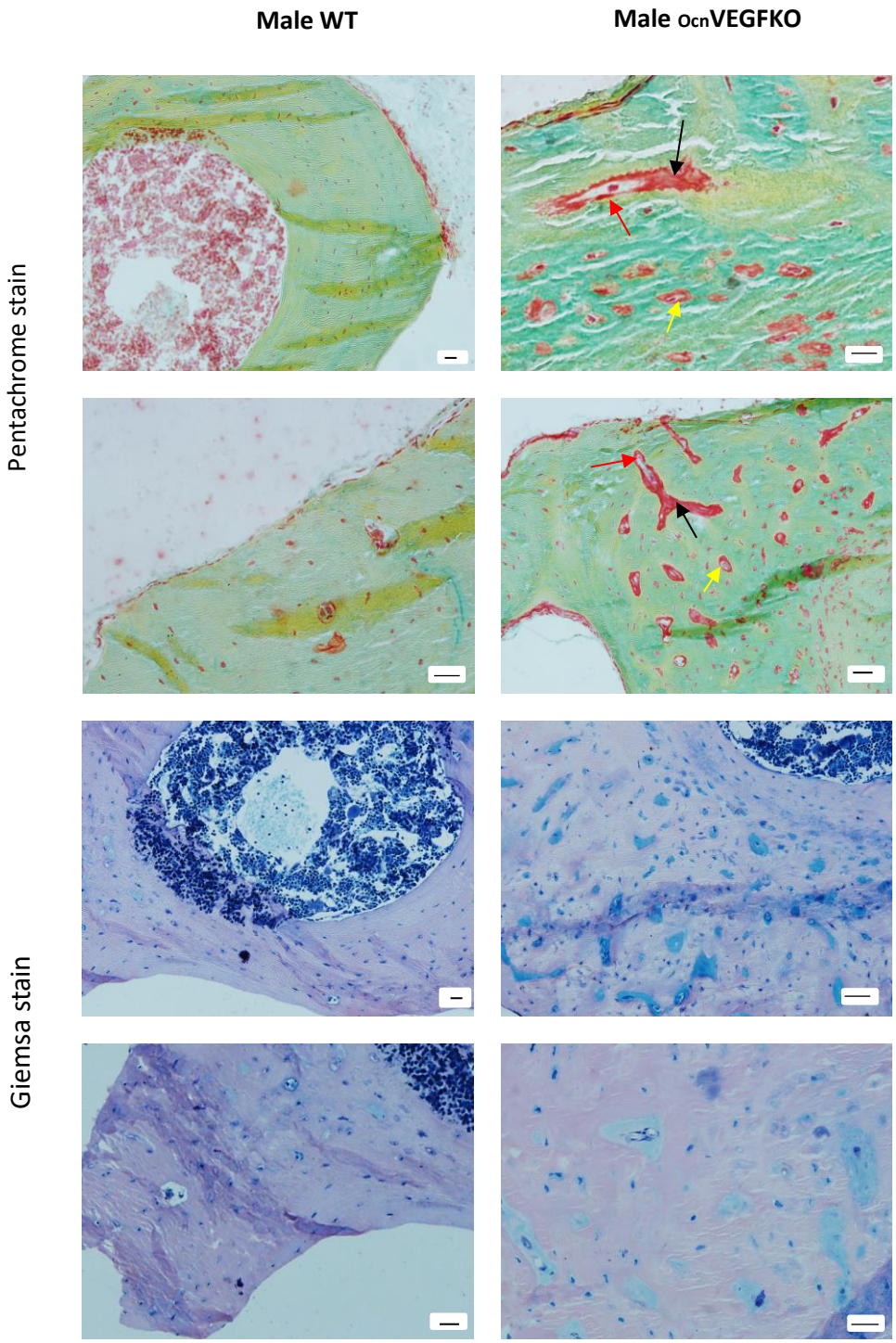

Figure 3.14: Using Giemsa and pentachrome stains to interrogate the vasculature in 16 week old WT and OcnVEGFKO male mice. Following deletion of *Vegf* in males, the pentachrome stain shows a large increase in osteoid (red stain; black arrows) surrounding the osteocytes (yellow arrows) and blood vessels (red arrows), making the canals abnormal in shape. This is mirrored in the Giemsa stained sections, where vessels and osteocytes appear to be overcrowded and disorganised. Scale bar = 20µm.

3.3.4 Increase in vasculature and disorganisation of the bone matrix following deletion of bone-derived VEGF validated by BSE-SEM

To further investigate the osteocyte/vascular phenotype and the poor mineralisation, which is shown to be particularly severe in male OcnVEGFKOs, BSE-SEM was used. This technique allowed the fine scrutiny of these transgenic tibia and a level of detail which is shown to be greatly enhanced. By treating PMMA blocks containing tibiae with iodine vapour or tri-iodide, it was possible to identify fine cellular detail within the bone cortex at the tibiofibular junction in females (figure 3.15a) and males (figure 3.16a), such as the blood vessel lumens within canals. Increased magnification also enabled closer inspection of blood vessels within blood vessel canals in females (figure 3.15b) and males (figure 3.16b). In females, deletion of osteoblast-derived *Vegf* resulted in a minimal increase in woven bone (mid-grey) versus WT, with small amounts surrounding the osteocytes and vessels (3.15c), but no large notable abnormalities. Similarly to the pentachrome stained sections, in male SEM images of OcnVEGFKOs, the osteoid appeared to make up a major component of the blood vessel canal space compartments (figure 3.16c; mid-grey). As a result, blood vessel canals were abnormal in size and morphology in comparison to male WTs, with blood vessels filling only part of the canal. Osteocytes were also surrounded by osteoid within the lacunae and this was suggestive of disruptions in healthy bone mineralisation in male OcnVEGFKOs, something which will be investigated further in subsequent chapters.

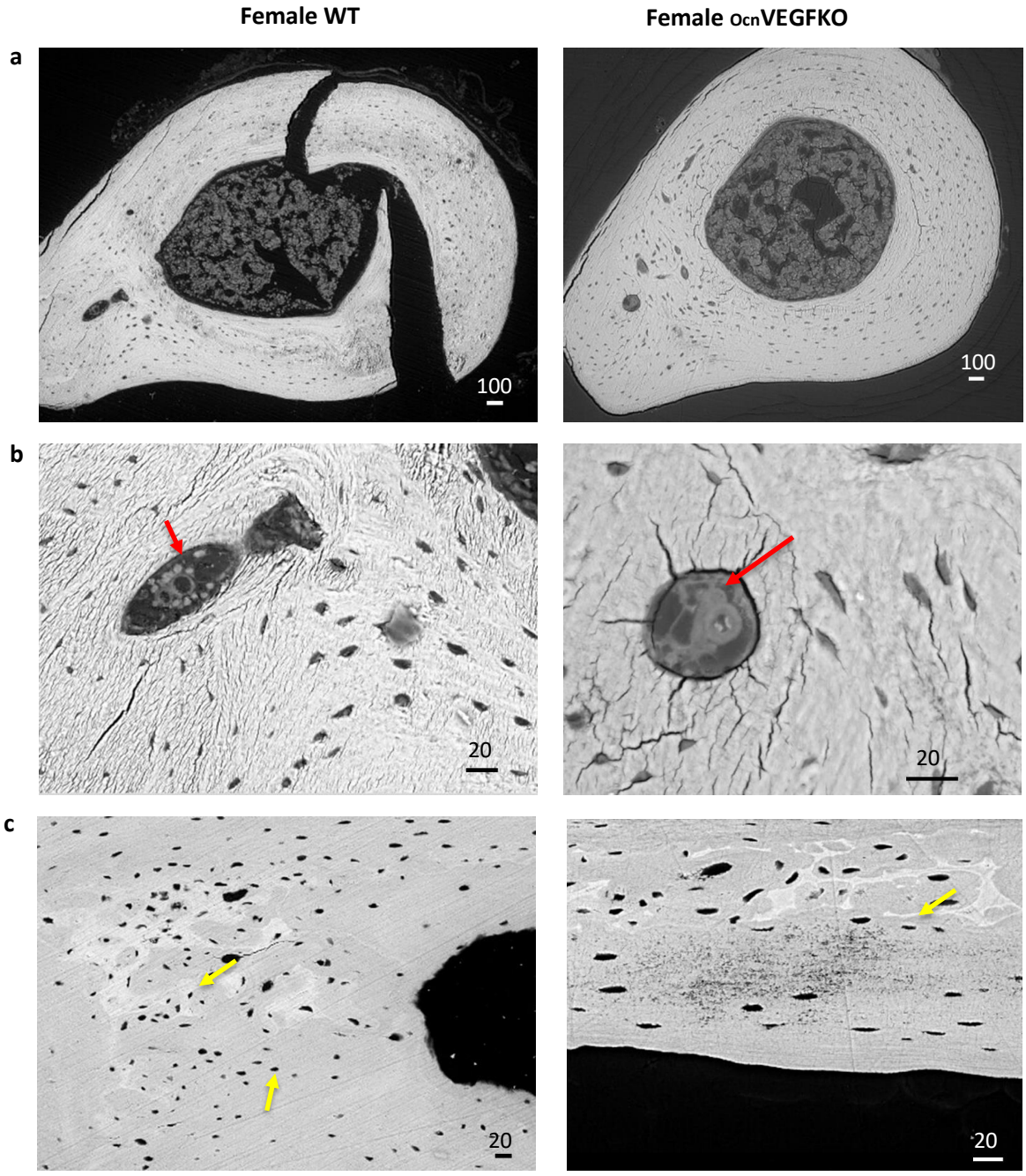

Figure 3.15: No changes in the vasculature of 16 week old female tibia following OcnVEGFKO. Following the deletion of *Vegf* in females, BSE-SEM was carried out at the tibiofibular junction in 16 week old mice. Staining with iodine vapour enabled the cellular detail to be picked up (a), including blood vessels within the canals (red arrows; b) and osteocytes (yellow arrows). Low levels of woven bone visible in OcnVEGFKO versus WT (c). Scale bars detailed in µm.

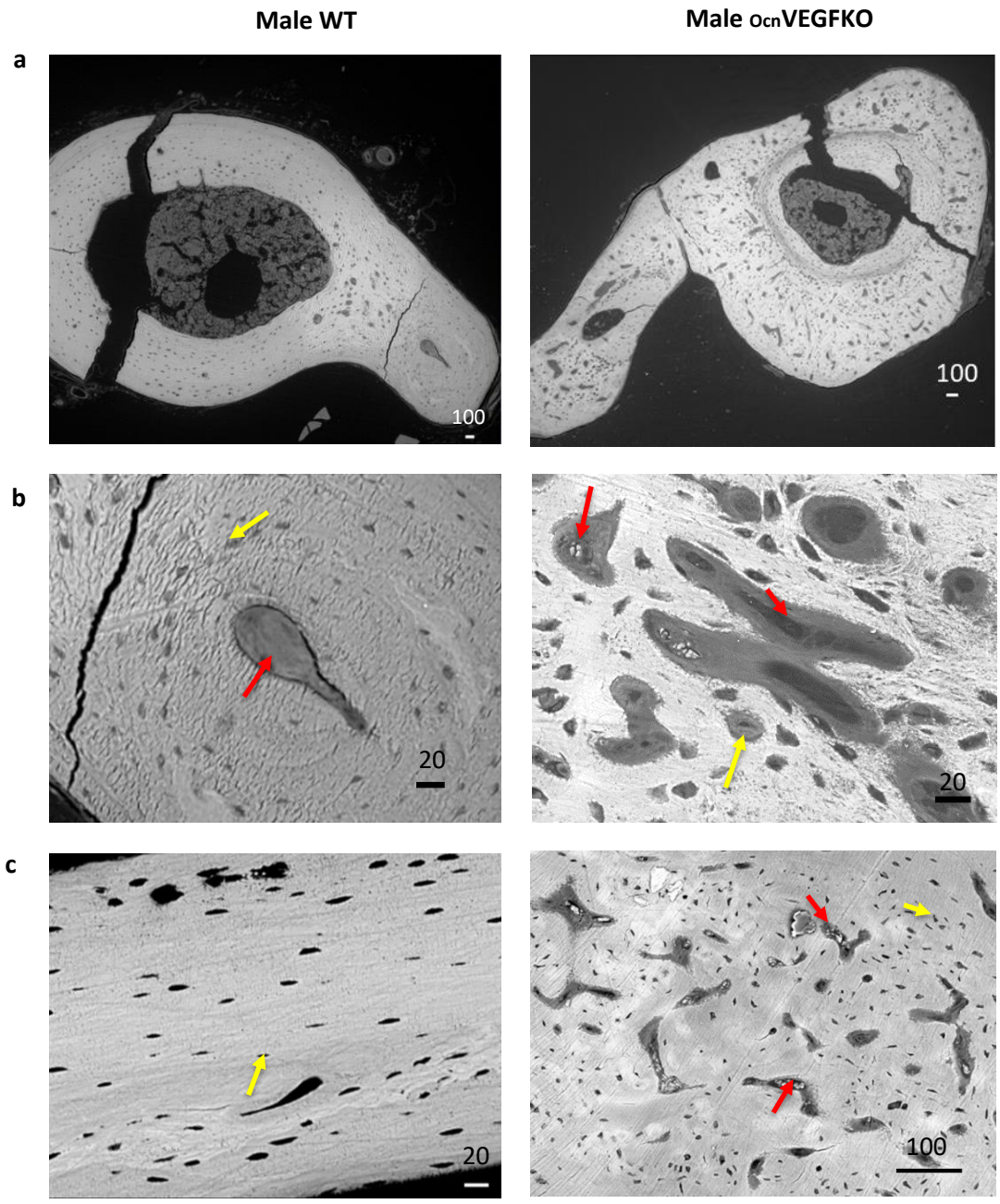

Figure 3.16: Increased osteoid surrounding the vasculature and reduced bone quality in male 16 week old tibia following OcnVEGFKO. Following the deletion of *Vegf* in males, BSE-SEM was carried out at the tibiofibular junction in 16 week old mice. Staining with iodine vapour, enabled the cellular detail to be picked up (a), including blood vessels within the canals (red arrows; b) and osteocytes (yellow arrows). Canals appeared to be abnormal in shape and filled with osteoid, suggesting poor mineralisation in OcnVEGFKO bones. In WT animals, osteocytes looked organised (c) and no osteoid was visible. Scale bars detailed in µm.

Using DFG Icon dentistry gel to etch away at the surface of the calcified bone and subsequently treating the blocks with ammonium triiodide, it was possible to pick up cellular detail within the cast of osteocyte lacunae and blood vessel canals that remained (figure 3.17). Further erosion of bone mineral with a more severe treatment of HCl and bleach facilitated a much deeper erosion (figure 3.18). No differences were observed in female WT versus female OcnVEGFKO; canals and lacunae were regularly spaced and organised. Conversely and correlating with the porous phenotype identified by SR CT, in male OcnVEGFKO bones the bone cortex was overcrowded with blood vessel canals. These canals were poorly organised, overlapping and in close proximity to osteocyte lacunae. Due to the seemingly poor mineralisation around the marrow cavity, PMMA was retained in male OcnVEGFKOs in this region. It was hypothesised that this area of the tibiofibular junction contained woven bone, which has not mineralised properly (figure 3.18).

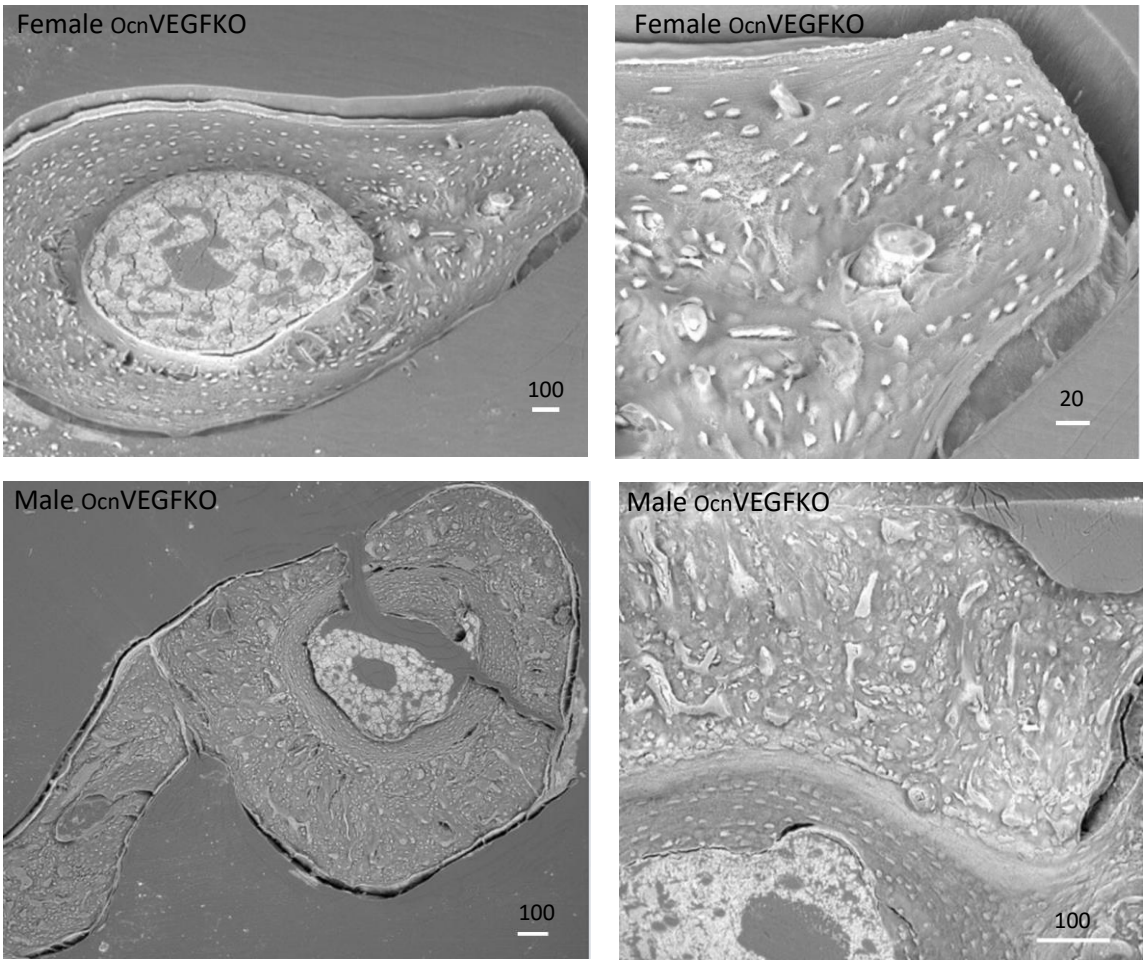

Figure 3.17: Icon etch dentistry gel reveals cast of blood vessel canals and osteocyte lacunae. Female and male OcnVEGFKO mice were compared by performing BSE-SEM on 16 week old tibia treated with DFG Icon etch dentistry gel. The differences between the female OcnVEGFKO and male OcnVEGFKO were substantial, with males appearing to have increased and abnormal vasculature, often overlapping. Scale bars detailed in µm.

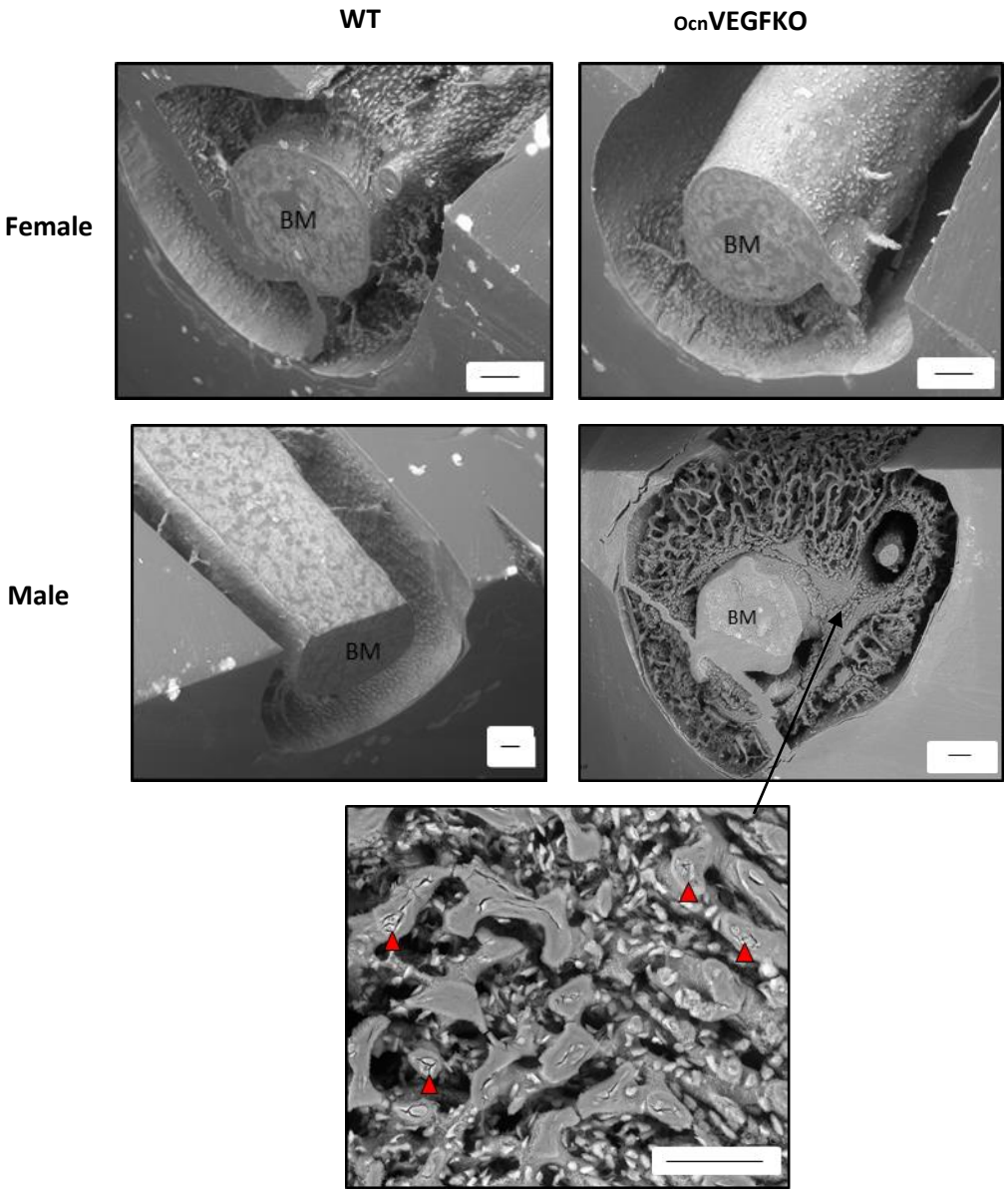

Figure 3.18: Increased vasculature in male 16 week old tibia following OcnVEGFKO. In OcnVEGFKO male bones, increased vascularisation (red arrows) was present and visible in SEM images following treatment with HCl and thin bleach. The close proximity and overlapping of the osteocytes surrounding the bone marrow (BM) and the poor mineralisation, results in large amounts of PMMA remaining. Scale bar=100µm.

3.4 Discussion

Using a conditional *in vivo Vegf* knockout mouse model to investigate the role of VEGF in the maintenance of both male and female adult bone health, the current studies have shown for the first time that VEGF produced by mature osteoblast cells is sexually dimorphic in its effect on intracortical vasculature. *Vegf* conditional knockout models are a relatively new concept in the literature, only having been studied by a small handful of labs previously (Zhang et al., 2002, Hu and Olsen, 2016, Buettmann et al., 2019, Liu et al., 2012). This is partially due to requiring a material transfer agreement (MTA) with Genentech in order to breed this mouse model for research purposes, which few labs possess.

In the work detailed in this chapter, the surprising phenotype identified by a substantial increase in intracortical porosity in males following OcnVEGFKO was noticeable from the first CT scan. The importance of looking at both sexes in a study investigating bone and vascular phenotypes was therefore realised. Due to the prevalence of degenerative bone disease amongst post-menopausal woman, males are often forgotten during analysis of disease phenotype (McCreadie et al., 2004, Senel et al., 2013, Pufe et al., 2003). It is therefore possible that a lack of comparisons between sexes in such studies has meant that underlying dimorphisms between males and females may have been missed in the past.

This increase in intracortical porosity in 16 week old male OcnVEGFKOs was characterised by SR CT (0.65µm) initially. Further interrogation performed following the segmentation of osteocyte lacunae and intracortical canals showed an increased volume in intracortical canals (fewer and larger) in male OcnVEGFKO versus WT controls. These canals were abnormal in shape and were adjoined to osteocyte lacunae, which meant that a large amount of osteocyte lacunae were picked up in the intracortical canal fraction. It is possible that low resolutions of micro-CT used for previous investigations could have hidden sex differences in bone phenotype and intracortical porosity due to being unable to extract intracortical porosity (Liu et al., 2012).

The determining factor which was causing these osteoblasts to reside in such close proximity to the vasculature was initially unclear. Previous studies suggested that osteocyte dendrites attach to blood vessels in the regulation of angiogenesis (Prasadam et al., 2014). It has been proposed that the apoptosis of osteocytes may be responsible for the decreased bone mass observed in osteoporosis (Bonewald, 2004). Equally, in age-induced

osteoporosis it has also been shown that there are reduced numbers of osteocytes, as well as disorganisation of canaliculi (Kobayashi et al., 2015). In this current study however, there is an increase in osteocyte density in female OcnVEGFKOs shown by SR CT analysis and an increase in osteocyte number in both males and females shown by histology. It was suggested in additional investigations that osteocytes were able to halt remodelling and that the bone formation rate was inversely proportional to the density of osteocytes (Qiu et al., 2002). Given that intracortical porosity was increased in both sexes to an extent, but significantly in males following OcnVEGFKO, it can be predicted that the bone forming rate in these mice is disproportionately lower than bone resorption as per previous VEGF KO studies (Liu et al., 2012). This would therefore help to explain the increase in osteocyte density quantified as a result of *Vegf* deletion.

The most probable explanation behind the adjoined canals and lacunae in male OcnVEGFKO however, is a lack of mineralisation in the bone cortex. SR CT at a resolution of 0.65µm is only able to pick up calcified tissue and therefore it is possible that the osteocytes were embedded within woven bone or regions of poor mineralisation in male OcnVEGFKO, giving the appearance of large volumes of intracortical porosity via SR CT (Schneider et al., 2007b, Schneider et al., 2009b). Indeed, a histological pentachrome stain of 16 week old tibiofibular junction sections has identified areas of osteoid surrounding blood vessels within canals in OcnVEGFKO males specifically. Woven bone is laid down very quickly in very early development and the first stage of bone healing. It is of poor quality and low strength in comparison to tough lamellar bone and will be investigated in more depth in subsequent chapters.

It has been previously found that the size of osteocyte lacunae is comparable to the level of matrix mineralisation. In male OcnVEGFKO bones, there was a population of smaller osteocyte lacunae visible that was not present in either male WT or female tibia. Perhaps therefore, further indication of poor mineralisation in this area of the tibia is the fact that there is this population of small osteocyte lacunae which has been identified as a result of the deletion of OcnVEGF in males. In adult humans it has been shown that as matrix production decreases, osteocytes decrease in volume and therefore in areas of poor mineralisation there would be less matrix production, as well as smaller osteocytes (Marotti, 1977, Frost, 1961). As a result, the mineralisation state of these male and female OcnVEGFKO bones will be further investigated in subsequent chapters.

By using a combination of SR CT, histology and BSE-SEM, it was possible to identify and characterise a strong vascular phenotype in males following the deletion of osteoblast-derived *Vegf*. VEGF is well known to be a potent inducer of angiogenesis (Risau, 1997, Tombran-Tink and Barnstable, 2004) and as a result it was initially expected that deletion of *Vegf* would cause a reduction in the vascularisation of the cortex. It has been shown in previous studies that ovariectomy prompted a 15% decrease in the number of CD31 positive cells and reduced levels of VEGF (Pufe et al., 2007, Roche et al., 2012). Therefore, a similar outcome and reduction in the vasculature was expected here and the subsequent results obtained were somewhat surprising.

This increase in the volume of intracortical canals in male OcnVEGFKOs was supported by histology, where a pentachrome stain not only confirmed a high % fill of blood vessel canal, but a significant increase in blood vessel area in OcnVEGFKO male mice versus WT littermate controls. SEM also showed an increase in intracortical vascular canals following OcnVEGFKO in males, in comparison to WT controls. Blood vessels appeared to be extremely disorganised, misshapen and surrounded by large amounts of osteoid, validated by the retention of a large amount of PMMA surrounding the vessels and osteocyte lacunae in the male OcnVEGFKO versus WT following treatment with bleach. Erosion of the mineralised bone matrix also further identified that osteocytes were both irregularly spaced and overlapping. The reasoning behind this strong vascular phenotype specifically in 16 week old male OcnVEGFKO mice was unclear. Increased angiogenesis, vascular disorganisation and leakiness is associated frequently with cancer and tumours, however this ordinarily goes hand in hand with increased levels of *VEGF* expression as opposed to decreased levels (Morikawa et al., 2002, McDonald and Foss, 2000). Like in cancer however, in male OcnVEGFKOs histology and SEM has highlighted that the blood vessels appear to be disorganised and of irregular morphology. It is therefore possible that they are potentially not functioning properly as a result. If blood vessels are indeed not functioning correctly, they will not be able to efficiently fill their role in the maintenance of bone health. The vascular phenotype here is unexplained and will be investigated further *in vitro,* in the final chapter of this thesis.

It is not clear whether this phenotype which is particularly evident in males is isolated to the changes in cortical porosity and the vasculature observed here, or whether OcnVEGFKO affects the geometry of the entire tibia and other physical bone traits. Characterisation of

gross and whole tibia phenotypes, as well as further investigations into the mineralisation state of the bone in males and females was therefore an important next step and will be addressed in the subsequent chapter.

Chapter 4 Results II – Elucidation of physical bone traits following osteoblast-*Vegf* deletion

4.1 Introduction

Following the identification of a notable vascular phenotype as a result of OcnVEGFKO, particularly in males, a number of different bone parameters were subsequently examined in 16 week old male and female mice. It was previously found that VEGF controls healthy growth plate morphology (Gerber et al., 1999a) and in other studies deletion of VEGF induced a reduction in both weight and body size (Hu and Olsen, 2016). Therefore, investigations into growth in this study which focuses on the effect of OcnVEGFKO on adult (16 week old) mice were of importance.

Analysis included measurements of the skull, the whole tibia and matrix mineralisation. The skull was primarily utilised as unlike the long bones, it has a different origin and is formed via intramembranous ossification during development (reviewed by Ferrara et al., 2003, Yang et al., 2012, Ortega et al., 2004, Kronenberg, 2003, Kini and Nandeesh, 2012). Both bone types are heavily adapted to fulfil their individual functions and whereas the skull is not designed to bare constant load in its role where it protects the brain, one of the key functions of the long bones is to facilitate locomotion and support the load of the rest of the body without breaking. By studying the effect of OcnVEGFKO in the skull therefore, it was envisaged this would elucidate the effect of loading on the occurrence of a bone phenotype and subsequent sex differences which have been observed in knockout mice.

It has been found previously that disuse of limbs as a result of prolonged bed rest results in a readjustment of the mineral components of the skeleton, with increased mineral in the skull and decreased mineral in load bearing bones (Leblanc et al., 1990). Subsequent studies performed in microgravity, which mimics unloading, have identified that this shift in mineral distribution is associated with alterations in perfusion. The decrease in the perfusion of blood to the long bones here was complemented by an increase in perfusion to the skull, suggesting that bone remodelling is strongly influenced by both blood flow and loading (Colleran et al., 2000). Subsequently, it has also been identified that damage to the spinal cord is associated with a decrease in blood vessel volume (Ding et al., 2012). The

mineral density and blood supply to the long bones therefore appears to be strongly associated with loading, with unloading affecting the skull and the long bones in contrasting ways. The skull measurements using micro-CT data from both male and female OcnVEGFKO versus WT mice were therefore of great interest here.

Where the use of a desktop scanner is not sufficient for in depth analysis of the bone microstructure, it is entirely sufficient for the analysis of whole bone traits and can be used for the scanning of the skull or the entire tibia where the fine structural detail is not required. Whole bone analysis of bone phenotypes has proven valuable in past studies (Mosey et al., 2017, Berwick et al., 2017) and it enables a comparison in geometrical measurements at different points along the length of the tibia, as opposed to purely focusing on the tibiofibular junction. Analysis of micro-CT scans enables the quantification of the hydroxyapatite content within the tibia and the subsequent calculation of BMD, a known measure in the study of degenerative bone diseases such as osteoporosis in which levels of hydroxyapatite are shifted to the left of normal and correlate with an decrease in bone mass (Roschger et al., 2001).

VEGF has been shown to play a significant role in the control of mineralisation, which involves the incorporation of hydroxyapatite into the bone matrix. This has been supported by data which shows that during bone mineralisation, VEGF reaches its peak levels of expression (Deckers et al., 2000). As well as its role in the mineralisation of bone, VEGF also plays such a significant part in the invasion of blood vessels into the cartilage during endochondral ossification (Gerber et al., 1999a). Given the accrued information on the increased and abnormal porosity and vasculature within the cortex of the OcnVEGFKO mice used for this study, a more in depth study of the mineralisation state of male and female OcnVEGFKO bones was of great interest. Previous investigations have successfully analysed changes in the mineralisation state of bone using BSE-SEM and therefore similar analysis techniques will be used to look at both male and female bones in this study (Boyde, 1980a, Boyde et al., 2017).

The aforementioned bias towards the analysis of trabecular bone measures when studying bone pathologies, has meant that multiple investigations into this bone subtype have been documented in the literature (Liu et al., 2012, Pufe et al., 2003, Albright, 1947b, Riggs and Melton, 1986). This could be due to the fact that trabecular bone is particularly metabolically active and roughly 25% of the total volume of trabecular bone is replaced on

an annual basis, as opposed to 3% in cortical bone (Parfitt, 1994). The interrogation of cortical bone phenotypes is therefore lacking in the literature and given the known influence of cortical bone in degenerative bone disease, it was the main focus of this study (Zebaze et al., 2010, Zebaze and Seeman, 2015). For completeness and sex comparison purposes however, basic measures of trabecular bone were undertaken. The majority of studies into changes in trabecular bone look at one sex only and therefore this will enable correlations with past work to be made. In this chapter therefore, notable physical bone traits identified following the deletion of osteoblast-derived *Vegf* in male and female 16 week old mice were investigated. Craniometric measurements, measurements of bone geometry (including BMD) and BSE-SEM were used in order to do this. As well as this, the trabecular bone measures were analysed for completeness of the phenotypic analysis.

The aim of this chapter was to elucidate physical bone traits following osteoblast-*Vegf* deletion.

Aim 2: Elucidation of physical bone traits following osteoblast-*Vegf* deletion

Whole tibial analysis of $_{Ocn}$*VEGFKO at 16 weeks of age will be undertaken*

- Gross measurements of bones using well known growth determinants
- Craniometric measurements using medium-resolution micro-CT
- Trabecular bone analysis using medium-resolution micro-CT
- Investigations into bone mineralisation using BSE-SEM
- Assessment of tibial geometry

4.2 Methodology

4.2.1 Gross anatomical measurements

Immediately after culling the 16 week old mice, measures of tail length and weight were obtained (n=6-8 male and females from 5 individual litters). Tail length was recorded using a calliper to measure from the base of the tail to the tip of the tail. Weight was measured by placing the mouse into a container directly after culling and using a scientific scales to determine the weight. Taking these measures directly after the mice were culled made the data obtained more accurate as the mouse was not moving, which would make the recording of these results difficult.

4.2.2 Skull measurements

Skulls of 16 week old mice (n=4) were scanned at 18µm voxel size using Skyscan 1176. VGSTUDIO MAX (Volume Graphics, Heidelberg, Germany) was used to create 3D reconstructions of the skull scans. 2D images were imported into ImageJ for quantitative bone morphometry, using the measure function (figure 4.1).

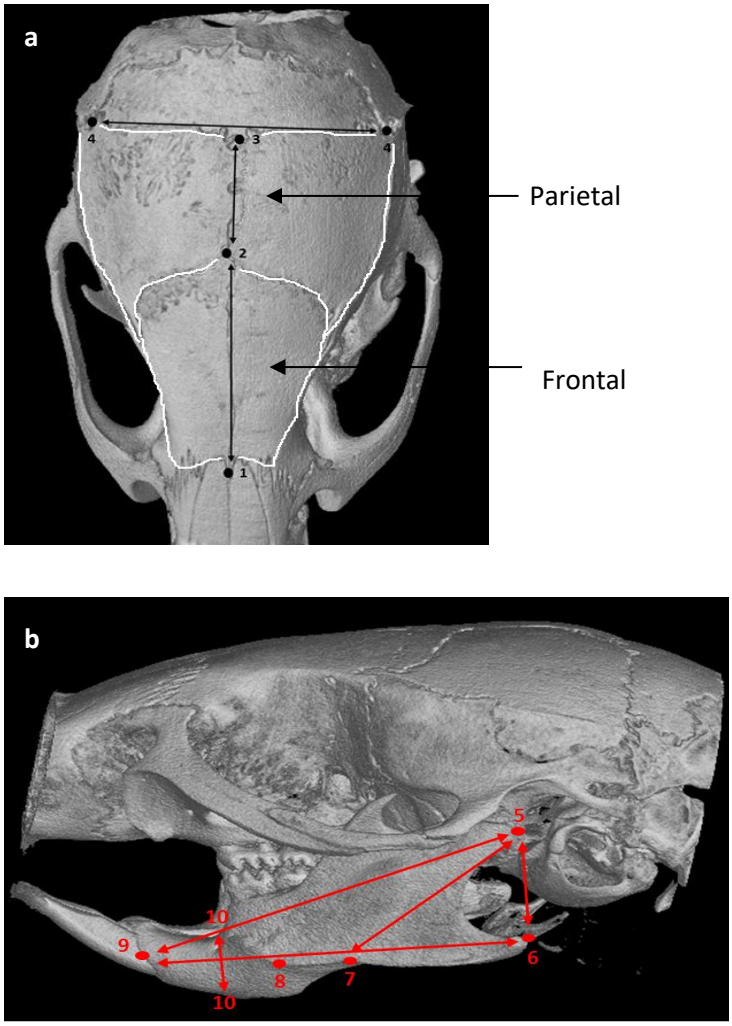

Figure 4.1: Effects of sex on skull phenotype following VEGF deletion. Craniometric measurements of 16 week old male and female WT and OcnVEGFKO were taken from reconstructed Skyscan1172 micro-CT images (18µm). The schematic (a, b) shows the landmarks used to take cranial measurements; 1–2: frontal length, 2–3: parietal length, 4-4: bitemporal distance, 5-6: posterior mandible height, 5-7: condylar axis, 5-9: effective mandible length, 6-9: mandible plain, 7-8: mandible axis, 10-10: anterior mandible height (Javaheri et al., 2016).

4.2.3 Measurements of bone geometry

Medium resolution CT scans (18µm) were analysed for quantification of bone geometry in male and female 16 week old mice (n=4). CTAn (Version 1.10) by Bruker was used to select upper and lower limits at the proximal and distal end of the tibia for whole bone analysis, ensuring that this was standardised for all animals. The tibia was visually inspected slice by slice from the knee to foot and the slice before the tibia was no longer visible at the proximal and distal ends of the were used as 'top' and 'bottom' slices of the stack

respectively. The number of slices between these two boundaries was used to calculate the length of the bone (number of slices x thickness of each slice; 0.018mm in this case). The fibula was digitally removed at the regions in which it was separated from the tibia, using the subtractive ROI function on CTAn. This enables you to draw around the tibia along the length of the selection and save this new data set which excludes the fibula as the volume of interest (VOI).

The new VOI image sequence was imported into ImageJ. The scale was adjusted by inserting a pixel height, width and depth of 0.018mm into image J. A lower threshold of 80 and upper threshold of 255 was used to separate bone from non-bone. The BoneJ, slice geometry plugin in ImageJ was utilised for interrogation of the entire tibia. Results were generated by slice geometry in an excel format, displaying iMin (minimum moment of inertia), iMax (maximum moment of inertia), Ct.Th (cortical thickness) and CSA (cross-sectional area) for each slice. Two extra parameters were calculated from these data: ellipticity (bone shape) = iMax/iMin and J (predicted resistance to torsion) = iMax+iMin.

Imin and Imax define the least and greatest distributions of mass across the minor and major axes respectively, thus acting as a measure of rigidity. Measurements are dependent on the accurate positioning of centroids, which is done automatically by BoneJ and values are a measure of the area around the minor (Imin) and major (Imax) axis. J describes the torsional rigidity of the bone and is calculated from the Imin and Imax values. Ellipticity is the measure of divergence of an ellipse from a perfect circle. For measures of Ct.Th, BoneJ fits many different spheres within the cortical bone mask and the average diameter of the sphere per slice is recorded. CSA is the calculation of the cortical bone area per slice.

To enable the results to be plotted as a graph, the % of tibia length was calculated for each slice. This was depicted by inserting the following equation at the top of a new column next to the first slice number and dragging it down until reaching the final slice number, to apply to the entire length of the bone (N.B. the number highlighted in yellow depicts the total number of slices analysed, so is different for each individual bone depending on its length):

% tibia length = ((1/(D985 - D2)) * ($D2 - D2))*100

The top and bottom 10% of the tibia was excluded from whole bone analysis and graphs were plotted by Dr Behzad Javaheri at the Royal Veterinary College, using R (Mosey et al., 2017).

4.2.4 Bone mass density calculations

BMD was calculated for 16 week old mice (n=4) by scanning a low and a high density phantom of known hydroxyapatite content and BMD (0.25g.cm^{-3} and 0.75g.cm^{-3}), using the same conditions mentioned previously for whole bone analysis (chapter 2.3.3). The VOI of each phantom was opened in CTAn and the 'toggle VOI view', followed by 'from dataset' was selected. The x-ray attenuation coefficient mean total for each phantom was calculated in CTAn (File>Preferences>Histogram>AttenuationCoefficient>OK). The two attenuation coefficient values were then used to calculate the BMD for each animal. Tibia VOI files were opened individually and the known BMD's of the two phantoms (0.25g.cm^{-3} and 0.75g.cm^{-3}), as well as the low (0.022) and high (0.051) attenuation coefficients calculated previously were inserted into CTAn (File>Preferences>Histogram>Calibrate). An equation is then produced by CTAn for the calculation of BMD for each tibia (BMD = ((AC-0.0075)/0.058) in this case). The BMD script generated by Dr Behzad Javaheri was subsequently imported into CTAn. The threshold was set at 80-255 and the script ran, calculating the BMD for each individual slice of tibia.

CTvox (2.0) was used to determine bone threshold density within the tibia, by loading the bone density heat map function and using a standardised opacity for each bone.

4.2.5 Trabecular analysis

In 16 week old mice (n=4 female WT, female OcnVEGFKO, male OcnVEGFKO and n=5 male WT), trabecular measures of bone volume (BV/TV), bone surface area (BS/TV), trabecular thickness (Tb.Th) and trabecular number (Tb.N) were investigated for completeness. For morphometric trabecular analysis, appearance of the trabecular bridge that connected the two primary spongiosa bone islands was set as a reference point for the analysis of proximal tibia metaphyseal trabecular bone; 10% of the total bone length from this point (towards the diaphysis) was utilised. Quantification of trabecular bone was performed by Dr Behzad Javaheri.

4.2.6 BSE-SEM

4.2.6.1 Sample maceration

WT and OcnVEGFKO male and female femur were macerated and rendered anorganic by prolonged treatment with 7% (v/v) chlorine sodium hypochlorite solutions. This removed all cells and non-mineralised matrix components to show the 3D morphology of the previously mineralised tissue. Femur were subsequently washed and dried. Both the periosteal and endosteal surfaces were studied with 20kV BSE SEM in collaboration with Professor Alan Boyde, as detailed previously.

4.3 Results

4.3.1 Absence of gross anatomical alterations observed following the deletion of bone-derived VEGF

Weight and tail length are well known measures of healthy development in mice (Rhees and Atchley, 2000, Chen et al., 1999) and have proven valuable for comparative analysis of growth rates (Interlichia et al., 2010). In this instance, no gross anatomical alterations were observed between 16-week-old *Vegfa* osteocalcin conditional male and female knockout mice (OcnVEGFKO; figure 4.2a). The mice appeared from the outside, to all be physiologically normal and visually, there were no obvious differences in mobility between subjects. Following deletion of *Vegf,* there were no differences between male and female tail length versus WT (figure 4.2b). No weight differences were seen between genotypes of either sex, however unsurprisingly based on the knowledge around sexual dimorphisms in development, it was shown that male WT and OcnVEGFKOs were significantly heavier than female WTs and OcnVEGFKOs (figure 4.2c).

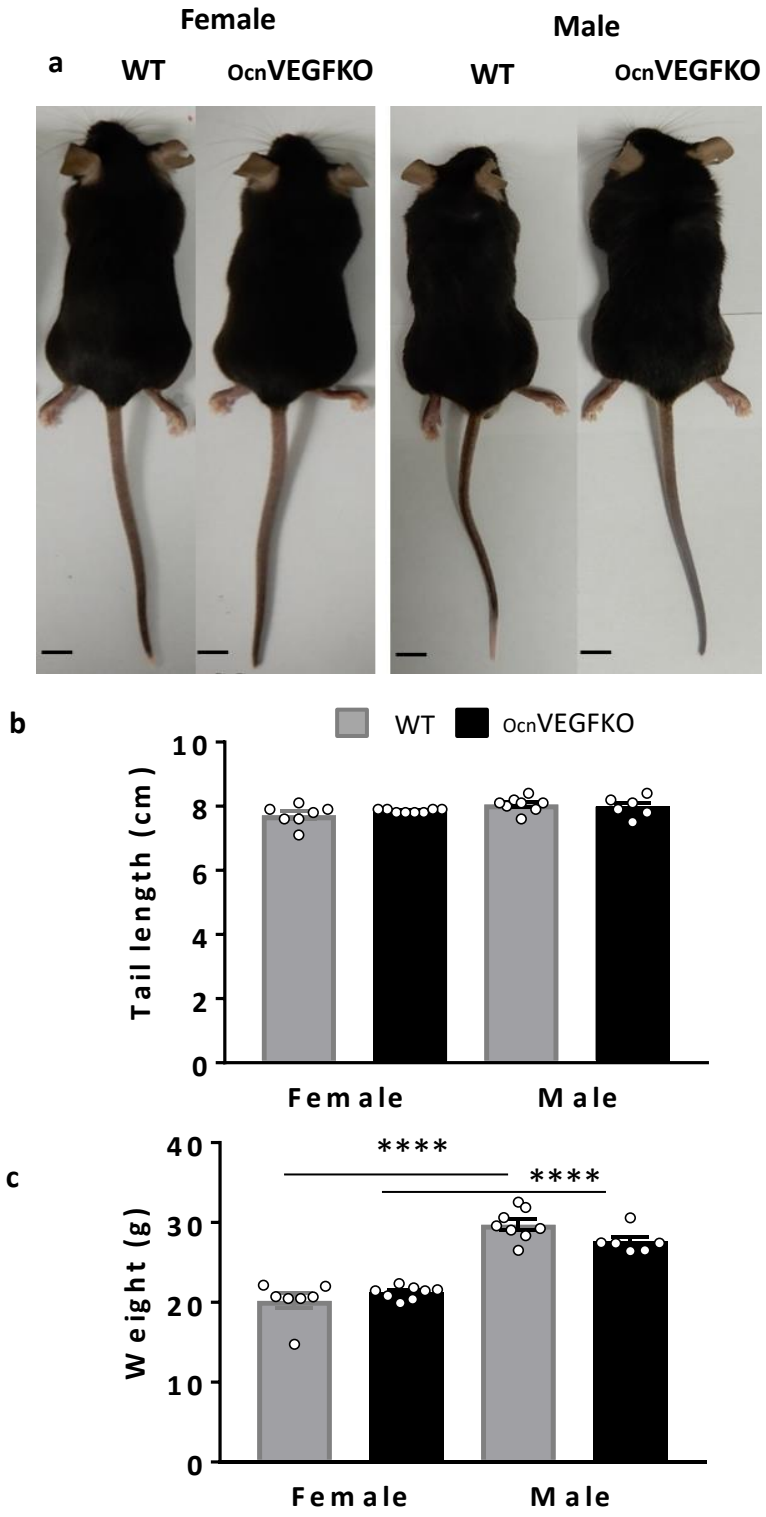

Figure 4.2: No significant differences in tail length or weight were observed when comparing OcnVEGFKO versus WT in males and females. No gross anatomical differences were visible in OcnVEGFKO or WT mice (a). No significant differences were seen in tail length following the deletion of OcnVEGF in males or females (b). Significant differences in weight were observed in female versus male animals (c), but not in OcnVEGFKO versus WT animals (n=6-8 animals from 5 individual litters, presented as mean measurements +/- SEM $p<0.05$*, $p<0.0001$**** using two-way ANOVA).

4.3.2 Deletion of bone-derived *Vegf* has no gross effects on the microstructure of the skull

In order to assess the overall effect of loading in long bones on the bone phenotype and any potential sexual dimorphisms expressed, cranial measurements of the skull dissected from 16 week old male and female, WT and OcnVEGFKO mice were taken. The skull does not have to withstand load and therefore, was considered to be an interesting part of the skeleton to study in this case. Ten cranial measurements made from medium-resolution µCT scans (18µm) in WT and OcnVEGFKO animals were used to investigate the skull phenotype. Across the entire skull, there were no obvious defects in ossification when comparing male versus female and OcnVEGFKO versus WT mice (figure 4.3). Craniometric measurements taken at the intramembranous mesoderm, intramembranous neural crest and mandible were largely unaltered in OcnVEGFKO versus WT males and females. In female OcnVEGFKOs, the frontal length was significantly less in comparison to WT counterparts. In males, the bi-temporal distance was significantly reduced in the OcnVEGFKO versus WT (table 4.1).

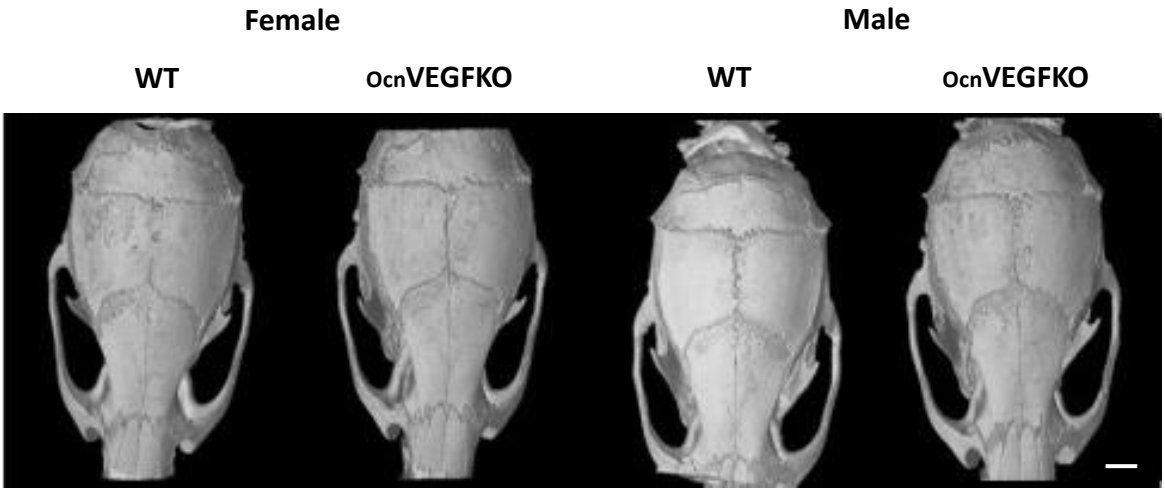

Figure 4.3: Skulls were scanned at medium resolution for cranial analysis. Reconstructed images were imported into CTVOX for 3D rendering, enabling the comparison of the anatomy of female and male, WT and OcnVEGFKO skulls from 16 week old mice. Scale bar = 2mm.

Table 4.1: Craniometric measurements for 16 week old male and female WT and OcnVEGFKO animals.

Craniometric measurements	Female WT	Female OcnVEGFKO	P value	Male WT	Male OcnVEGFKO	P value
	n=4	n=4	Female WT vs OcnVEGFKO	n=3	n=4	Male WT vs OcnVEGFKO
Intramembranous (neural crest)						
Frontal length (mm)	7.97 ± 0.16	7.41 ± 0.081	< 0.01	8.093 ± 0.045	7.79 ± 0.086	NS
Frontal area (mm^2)	33.52 ± 0.84	33.27 ± 0.82	NS	35.40 ± 0.30	33.97 ± 2.028	NS
	n=4	n=4	Female WT vs OcnVEGFKO	n=4	n=4	Male WT vs OcnVEGFKO
Intramembranous (mesoderm)						
Bitemporal distance (mm)	9.79 ± 0.038	9.67 ± 0.053	NS	9.84 ± 0.043	9.46 ± 0.084	< 0.01
Parietal length (mm)	4.29 ± 0.15	3.92 ± 0.12	NS	4.40 ± 0.081	4.24 ± 0.13	NS
Parietal area (mm^2)	54.017 ± 0.46	52.94 ± 0.75	NS	53.78 ± 1.075	54.73 ± 1.097	NS
	n=4	n=4	Female WT vs OcnVEGFKO	n=4	n=4	Male WT vs OcnVEGFKO
Mandible, intramembranous (neural crest)						
Effective mandible length (mm)	11.98 ± 0.24	11.72 ± 0.56	NS	13.65 ± 1.20	11.39 ± 0.31	NS
Mandible axis (mm)	2.49 ± 0.15	2.57 ± 0.21	NS	2.72 ± 0.26	2.18 ± 0.099	NS
Condylar axis (mm)	6.64 ± 0.20	6.53 ± 0.17	NS	7.63 ± 0.60	6.51 ± 0.21	NS
Anterior mandible height (mm)	1.92 ± 0.067	2.35 ± 0.45	NS	2.25 ± 0.20	2.40 ± 0.56	NS
Posterior mandible height (mm)	3.87 ± 0.10	4.10 ± 0.30	NS	4.98 ± 0.29	4.37 ± 0.056	NS

4.3.3 Deletion of bone-derived *Vegf* impacts long bone microstructure at the tibiofibular junction and epiphysis in 16 week old male mice

Following a conditional deletion of *Vegfa* in mature osteoblasts and using reconstructed medium resolution (18µm voxel size) micro-CT images (figure 4.4a), it was possible to accurately quantify differences in tibial length in 16 week old males and female OcnVEGFKO and WT mice. In male mice, there was an increase in tibial length following OcnVEGFKO, however no significant differences were identified in female OcnVEGFKO versus WT (figure 4.4b).

By scanning the whole tibia using the Skyscan 1176 at a resolution of 18µm, it was possible to visualise the region of interest for this study, as well as the entire tibia in 3D (figure 4.4a). In males specifically, there was severe and extensive porosity at the tibiofibular junction and epiphysis which was visible following OcnVEGFKO. In one male OcnVEGFKO bone in particular, the tibia was fractured and a callus structure was visible where the bone had attempted to regenerate and not succeeded, filling the callus with poorly mineralised woven bone (figure 4.5). There were also sexual dimorphisms in bone threshold density at the tibiofibular junction (figure 4.6). Following deletion of OcnVEGF in males, there was an increase in bone threshold density in comparison to WT controls, which could be the result of a potential compensatory mechanism. In females, OcnVEGFKO prompts a decrease in bone threshold density, a reversal of the observed changes observed in males.

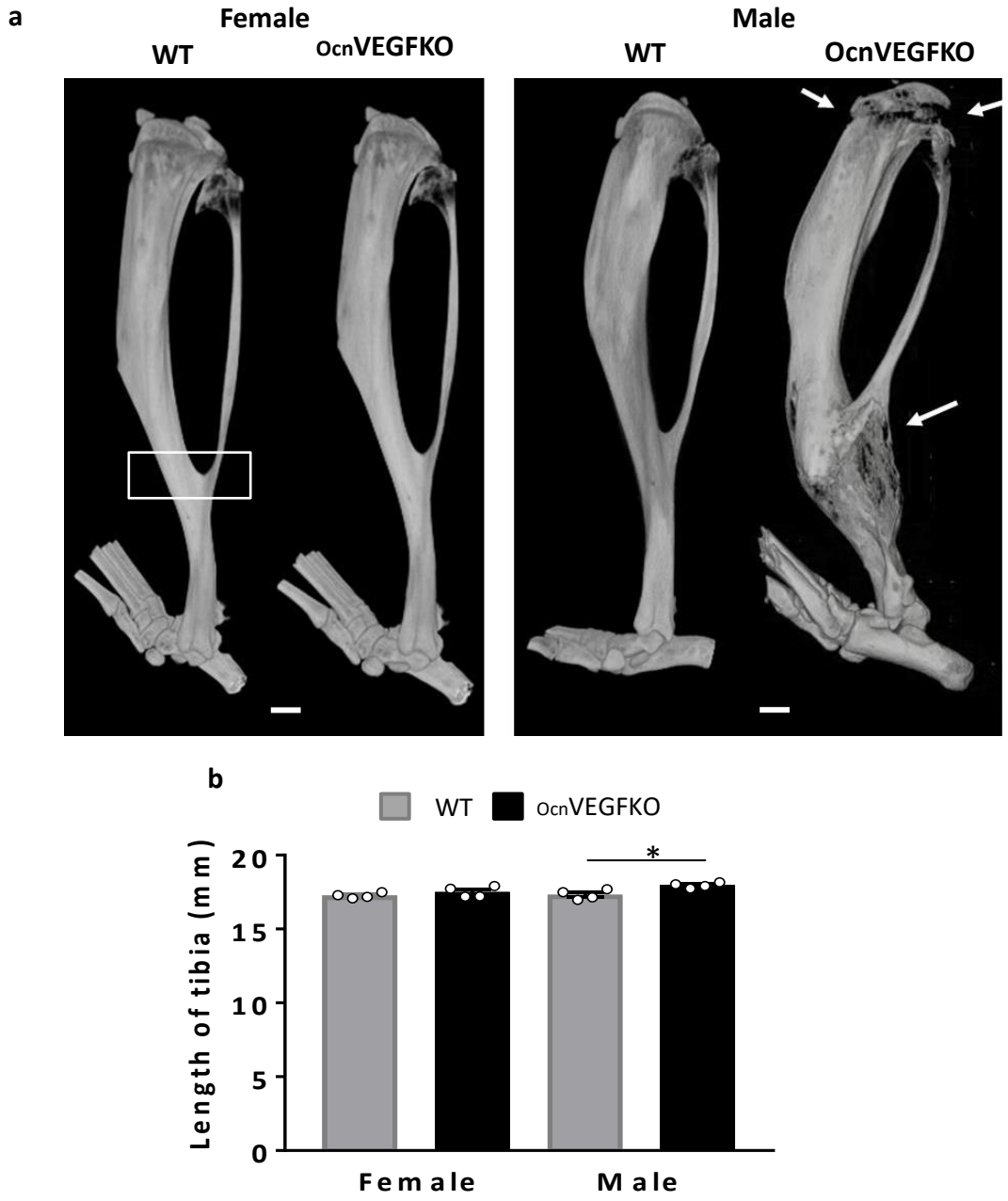

Figure 4.4: Whole bone scans of the entire tibia at 18 microns enabled scrutiny of overall bone morphometry following OcnVEGFKO in 16 week old mice. The region of interest used for this PhD is identified on the female WT tibia (tibiofibular junction; white box). Although female WT, female OcnVEGFKO and male WT bones appear comparable in structure, the male OcnVEGFKO tibia presented here has been fractured previously and was unable to sufficiently heal. Extensive porosity is identified at the tibiofibular junction and the epiphysis specifically (arrows; a). In males, tibial length was increased following OcnVEGFKO (b; n=4 males and 4 females from individual litters presented as mean ± SEM $p<0.05$* using two-way ANOVA). Scale bar = 1mm.

Figure 4.5: Increase in cortical porosity and the presence of woven bone at the tibiofibular junction fracture site in male OcnVEGFKO. Video shows a rotation of the whole tibia of a 16 week old male mouse. Dysfunctional fracture healing is observed at the epiphysis and the tibiofibular junction (see video).

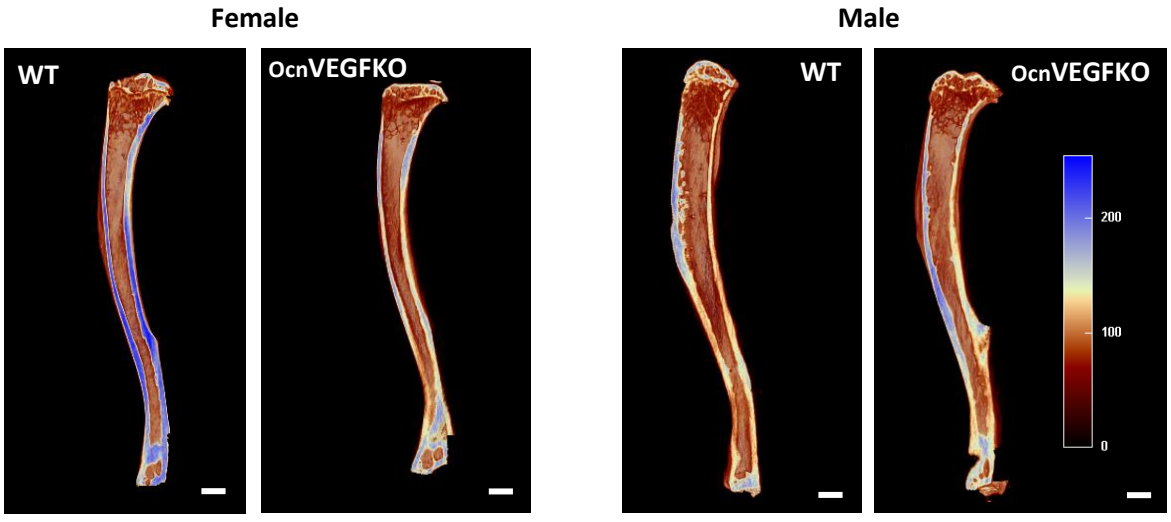

Figure 4.6: Sexual dimorphisms identified in bone density heat maps following OcnVEGFKO. Longitudinal tibial cross sections created using CTvox, show a decrease in bone density in OcnVEGFKO females and an increase in bone density in OcnVEGFKO males. Heat map scale plotted from 0 (brown; low threshold density) to 255 (blue; high threshold density). Scale bar = 1mm.

4.3.4 Adult males conserve tibial geometry and shape following deletion of *Vegf* from mature osteoblast cells

For analyses of changes in shape and geometry along the entire tibia in both males and females, medium-resolution (18µm) scans were used. Fractured bones such as those shown above in figure 4.5 were not used for this quantification. Measures including CSA, Imin, Imax and Ct.Th, ellipticity, J and BMD were quantified. A graphical heat map was used to present statistical significance of these measures between 10% and 90% along the tibial length (figure 4.7a).

Surprisingly and unlike previous studies in which cortical bone phenotypes were seen in males only, here the only significant differences were observed when comparing female OcnVEGFKO and WT (figure 4.7a and 4.7b). The tibiofibular junction was situated at ~60% along the tibial length and it was in this region in particular (or just above/below) that a vast amount of significance was seen. In females, ellipticity was significantly higher in WT compared to OcnVEGFKO at 50% along the tibia (just below the junction) and higher in OcnVEGFKO in the distal area of the tibia (appendix D.4a). Imax (appendix D.4b) was higher in WT than OcnVEGFKO at every significant point in females, as was Imin (appendix D.4c). J (figure 4.7b) and cortical thickness (appendix D.4d) were also higher in the WT animals versus OcnVEGFKO animals in all areas of significance. Although BMD was higher in the female WT than female OcnVEGFKO subjects (figure 4.7b), this was not statistically significant.

There did appear to be differences in geometry and shape following OcnVEGFKO when looking at the graphs plotted for males (figure 4.7 and appendix D.4), however statistical analysis showed that shape and geometry were not significantly compromised due to large amounts of variability between OcnVEGFKO repeats. Ellipticity was higher in OcnVEGFKO than WT around the tibiofibular junction area (appendix D.4a), however this was not significant (figure 4.7a). Equally, cortical thickness was higher in OcnVEGFKO mice versus WT (appendix D.4d), but this was also non-significant. BMD in males following OcnVEGFKO was also non-significant. Overall, these findings suggest that where males compromise their cortical bone porosity following OcnVEGFKO, geometry and mechanical properties of the tibia are preserved. Females were able to maintain their cortical porosity, but compromise bone geometry following OcnVEGFKO.

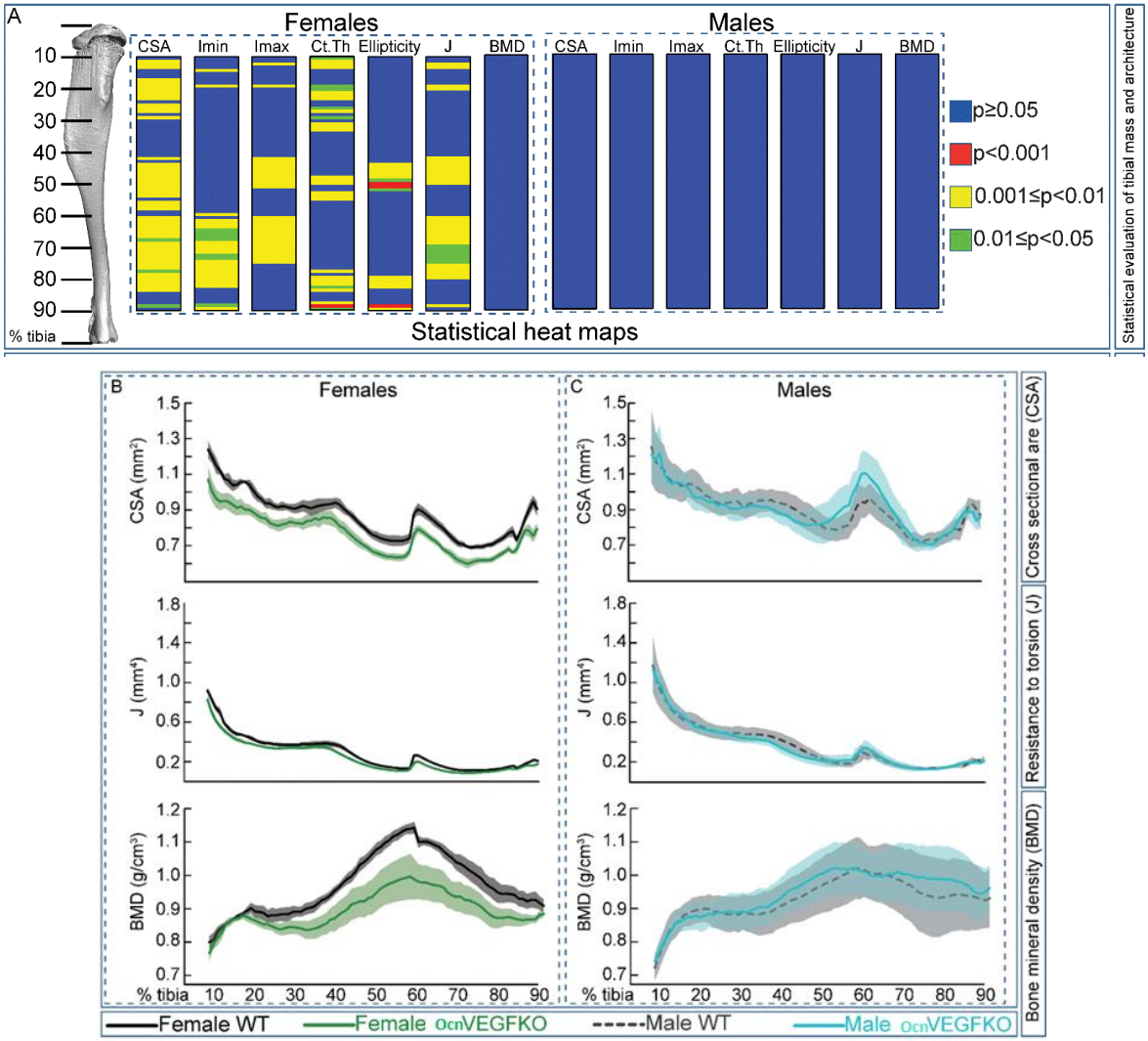

Figure 4.7: Significant alterations in tibial geometry following bone-derived *Vegf* deletion is evident only in females. Minimum and maximum second moments of inertia (Imin and Imax respectively), cross-sectional area, resistance to torsion (J), ellipticity, cortical thickness and BMD of male and female OcnVEGFKO tibiae versus WT at 16 weeks of age (a). Graphical heat map summarises statistical differences (using ANOVA) at specific matched locations along the tibial length (10 to 90%), representative of overall effect of genotype. Red $p \leq 0.0001$, yellow $p \leq 0.001$-0.01, green $p \leq 0.01$-0.05 and blue ≥ 0.05. Line graphs represent means for female (b) and male (c) WT versus OcnVEGFKO ± SEM (n=4 female and 4 male mice from individual litters).

Given the sex differences identified already following SR CT, BSE-SEM and histology, male and female statistical comparisons were made for bone geometry measurements in addition to the genotype comparisons. This identified that female bones were significantly thicker than male bones at several points above and below the tibiofibular junction in WT animals. These basal sex differences in tibia thickness were not present in male and female OcnVEGFKO mice at the same specific regions. CSA, iMin, iMax, Ct.Th and J were significantly greater in male OcnVEGFKO bones in comparison to females at several different points along the length of the tibia. Ellipticity was the only exemption as it was significantly lower in male versus female OcnVEGFKO animals at approximately 80% along the tibial length (Figure 4.8). There were no significant differences in BMD when comparing female and male tibia.

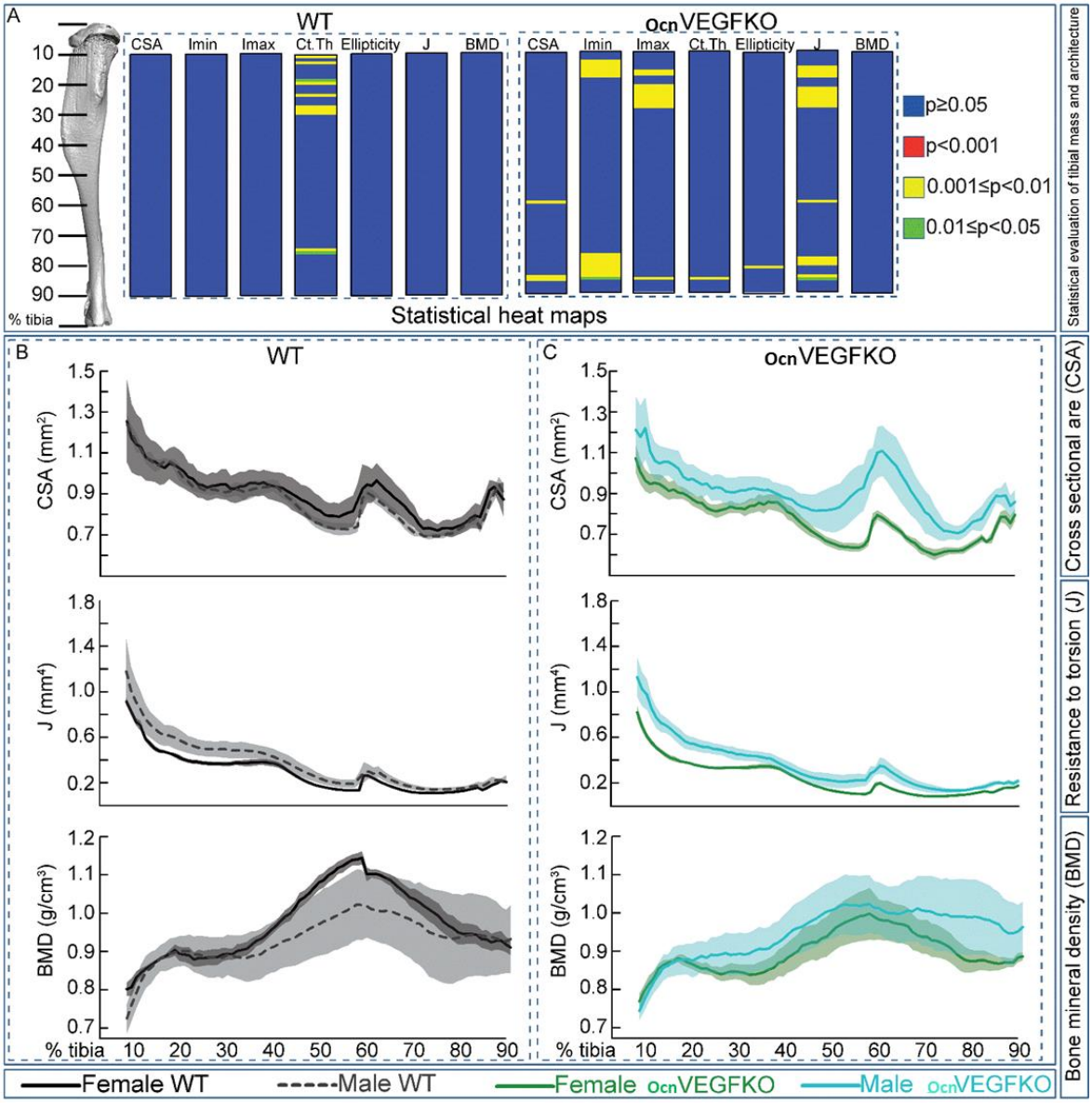

Figure 4.8: Sex differences evident along the tibial length in 16 week old WT and OcnVEGFKO bones. Graphical heat map summarises statistical differences between female versus male subjects within WT and OcnVEGFKO groups at specific matched locations along the tibial length (a). Yellow p≤0.001-0.01, green p≤0.01-0.05 and blue ≥0.05. Line graphs represent means for WT (b) and OcnVEGFKO (c) females versus males ± SEM (n=4 males and females from individual litters). Statistics performed using ANOVA.

4.3.5 Effects of deletion of bone-derived *Vegf* on trabecular bone parameters in male and female 16 week old mice

For completeness, measurements of trabecular bone were taken. Due to the fact that trabecular bone has been studied extensively in the past when investigating degenerative bone disease, the aim of this analysis was to get a brief overview of any sexual dimorphisms that may be present within the trabecular bone for discussion purposes (figure 4.9). In 16 week old male and female animals, no significant differences in BV/TV (figure 4.9b), BS/TV (figure 4.9c) or Tb.Th (figure 4.9d) were identified. The only significant finding was a decrease in Tb.N (figure 4.9e) in female $_{Ocn}$VEGFKO versus WT.

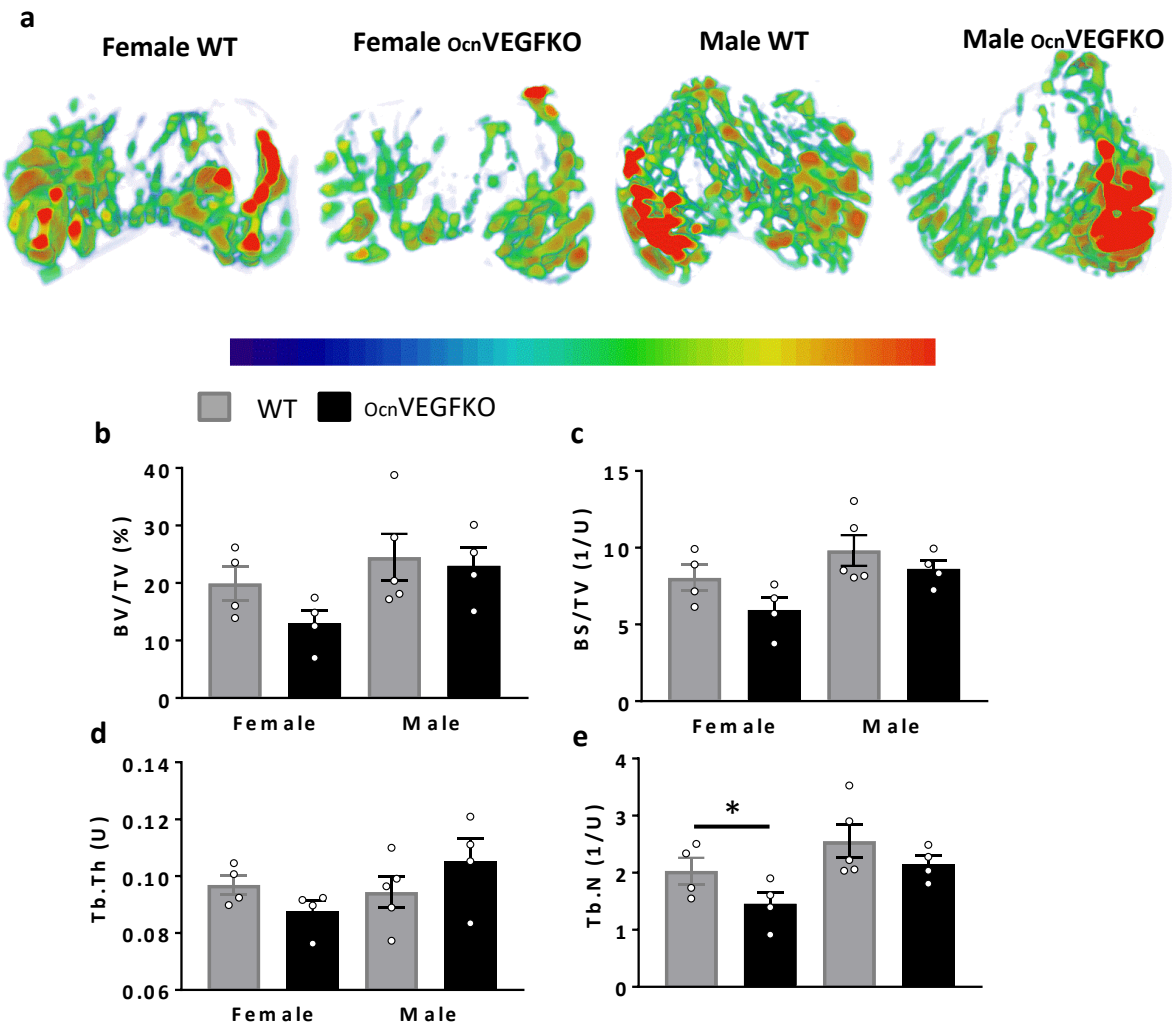

Figure 4.9: Minimal changes in trabecular measurements in 16 week male and female mice following OcnVEGFKO. Trabecular thickness for 16 week old male, female, WT and OcnVEGFKO tibiae is displayed as a heatmap with blue representing the thinnest trabeculae and red representing the thickest trabeculae (a). In 16 week old mice, no differences in % bone volume (b; BV/TV), bone surface area (c; BS/TV) and trabecular thickness (d; Tb.Th) were observed. A significant decrease in trabecular number was identified in female animals only, following OcnVEGFKO (e). Error bars indicate mean value ± SEM, $p<0.05$*, using two way ANOVA. N=4 female WT, female OcnVEGFKO and male OcnVEGFKO and n=5 male WT.

4.3.6 Deletion of *Vegf* in mature osteoblasts impacts mineralisation of the bone matrix, particularly in mature 16 week old male mice

BSE-SEM was performed for further inspection of the mineralisation state of the bone following OcnVEGFKO in both sexes. In female tibia, a small amount of woven bone was identified following OcnVEGFKO (figure 4.10a), however other than this very few differences could be seen when comparing with female WTs (figure 3.15). In male OcnVEGFKO tibia (4.10b,c), large areas of woven bone were visible versus WT (figure 3.16), supporting previous observations that these knockout bones contain expansive regions of poor mineralisation.

In order to look deeper into the mineralisation state of the cortical bone following the deletion of osteoblast-derived *Vegf* and to complement the information gained from pentachrome histological stains, 16 week old male and female femur were macerated. This enabled the study of the periosteal and endosteal surfaces of the bone (figure 4.11), by removing the cells and non-mineralised matrix. When comparing the female WT and female OcnVEGFKO, normal remodelling was observed. On the posterior surfaces, wall to wall resorption was visible in WT (figure 4.12a) and OcnVEGFKO (figure 4.13a) femur and this is part of the modelling process which takes place in healthy bone. During this process, bone is removed from the posterior outside surface, before being deposited on the endosteal surface. On the endosteal surface of the female WT (figure 4.12b), the bone morphology was typical of a mineralising front; lots of blood vessel canal openings were present and healthy modelling and bone-forming mineralisation taking place. In the OcnVEGFKO femur, the endosteal surface (figure 4.13b) was also mineralising and modelling, with light resorption taking place in parallel. The newly formed canal openings appeared healthy in appearance, with no indication of osteoid within them.

When comparing BSE-SEM from male WT (figure 4.14a) and male OcnVEGFKO (figure 4.15a) macerated femur, no differences were identified in the morphology of the periosteal surface. In both bones, the periosteal surface appeared to be undergoing active resorption and bone remodelling throughout. In the male WT (figure 4.14b), modelling bone formation and mineralisation was taking place on the endosteal surface, with light resorption. In OcnVEGFKO (figure 4.15b) bones and on the endosteal

surface, vascular canals were surrounded by bone which was undergoing resorption. Most notable however, were the osteoid seams and areas of deficient mineralisation surrounding the opening of the blood vessel canals in this male OcnVEGFKO. On closer inspection (figure 4.16a and 4.16b), an arrested mineralising front could be identified. The mineralised surface surrounding the blood vessel canals was incomplete and there was a failure to mineralise on the forwards facing surface of the osteocyte. This is an observation which was not present in female bones of either genotype, or in male WT femur and validates the results obtained from the pentachrome histological stain which showed large levels of osteoid and poor mineralisation surrounding osteocytes and blood vessel canals.

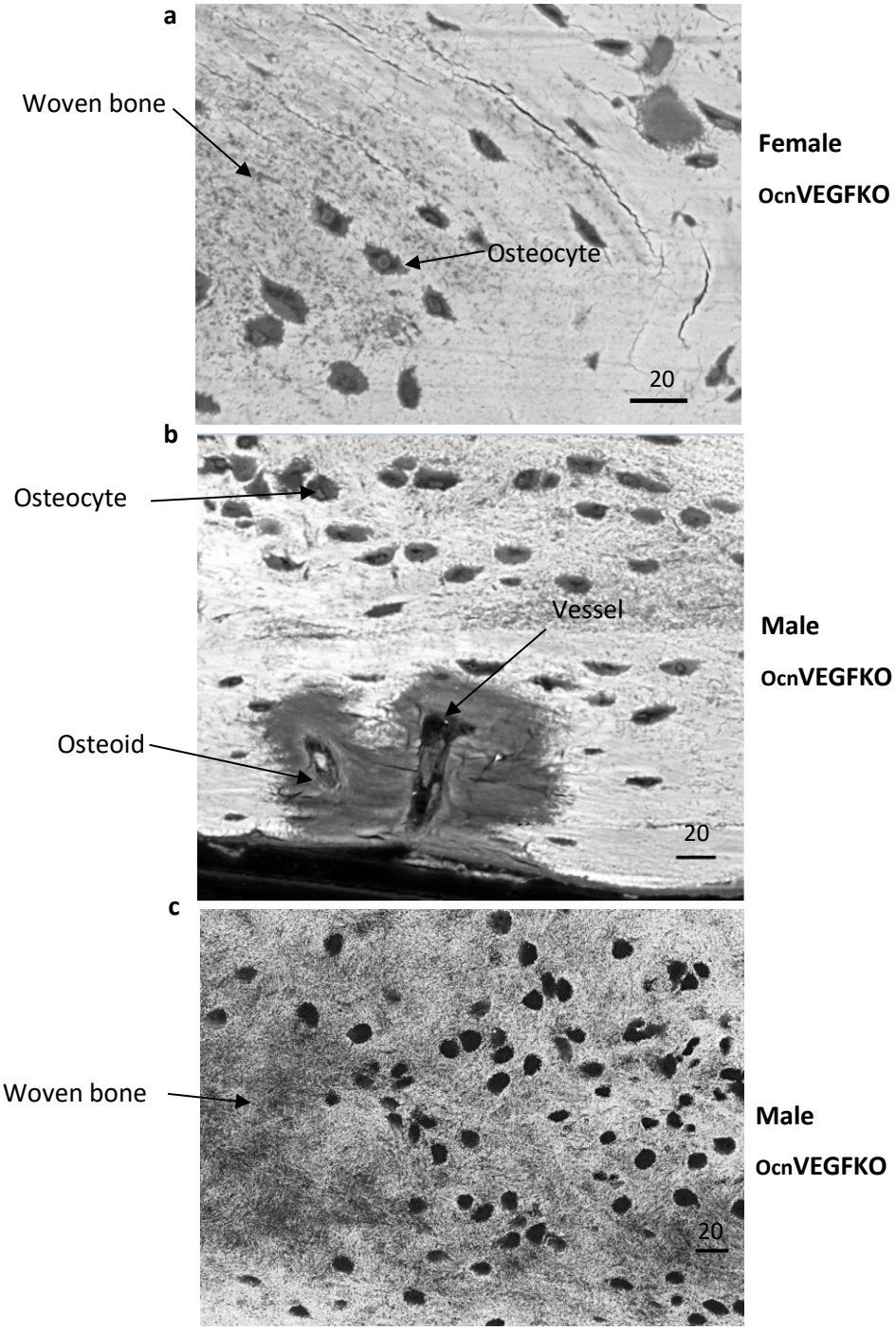

Figure 4.10: High levels of woven bone visible in BSE-SEM images following the deletion of *Vegf* in mature osteoblasts. Shaded grey tones depict large areas of woven bone at the tibiofibular junction region in male 16 week old female OcnVEGFKO (a) and male OcnVEGFKO (b,c) mice. All measurements for scale bars are detailed in μm.

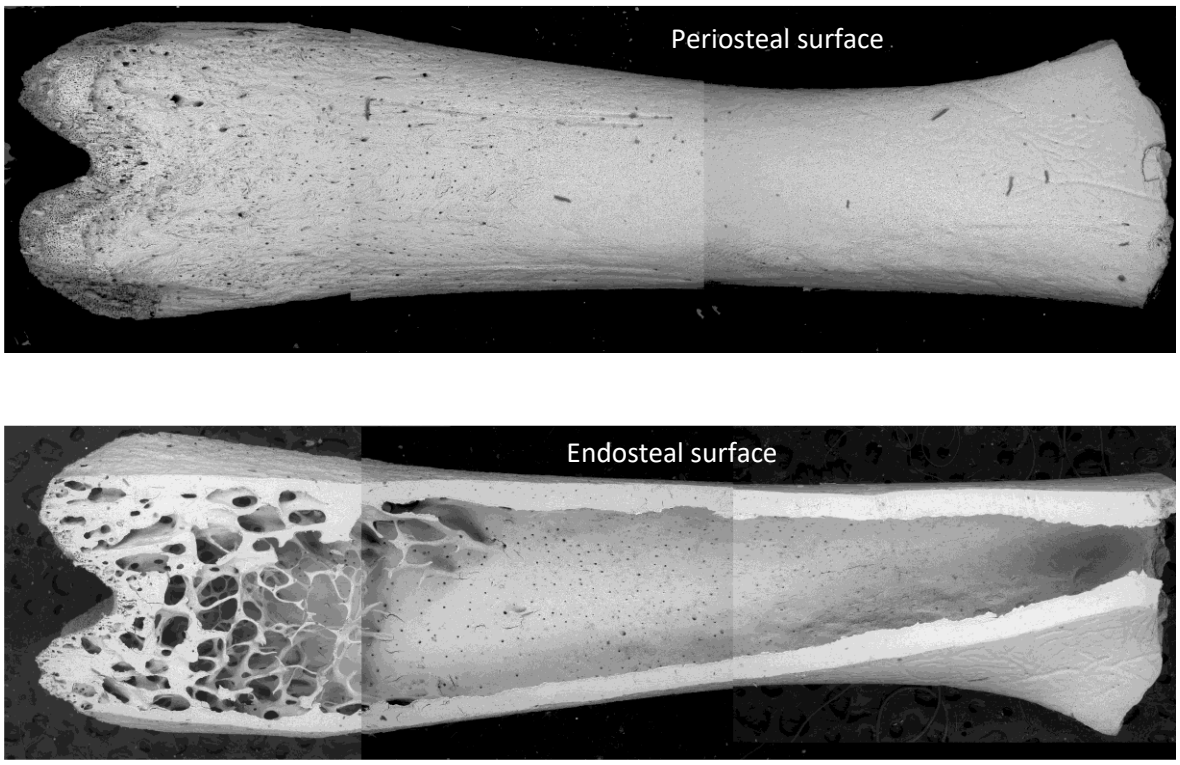

Figure 4.11: Mature 16 week old femur were macerated to enable interrogation of the periosteal and endosteal surfaces by use of BSE-SEM. Defining the periosteal and endosteal surfaces of the macerated femur (male OcnVEGFKO used as an example). Characteristically, active bone resorption takes place on the periosteal surface and deposition of new bone and mineralisation takes place on the endosteal surface.

Female WT

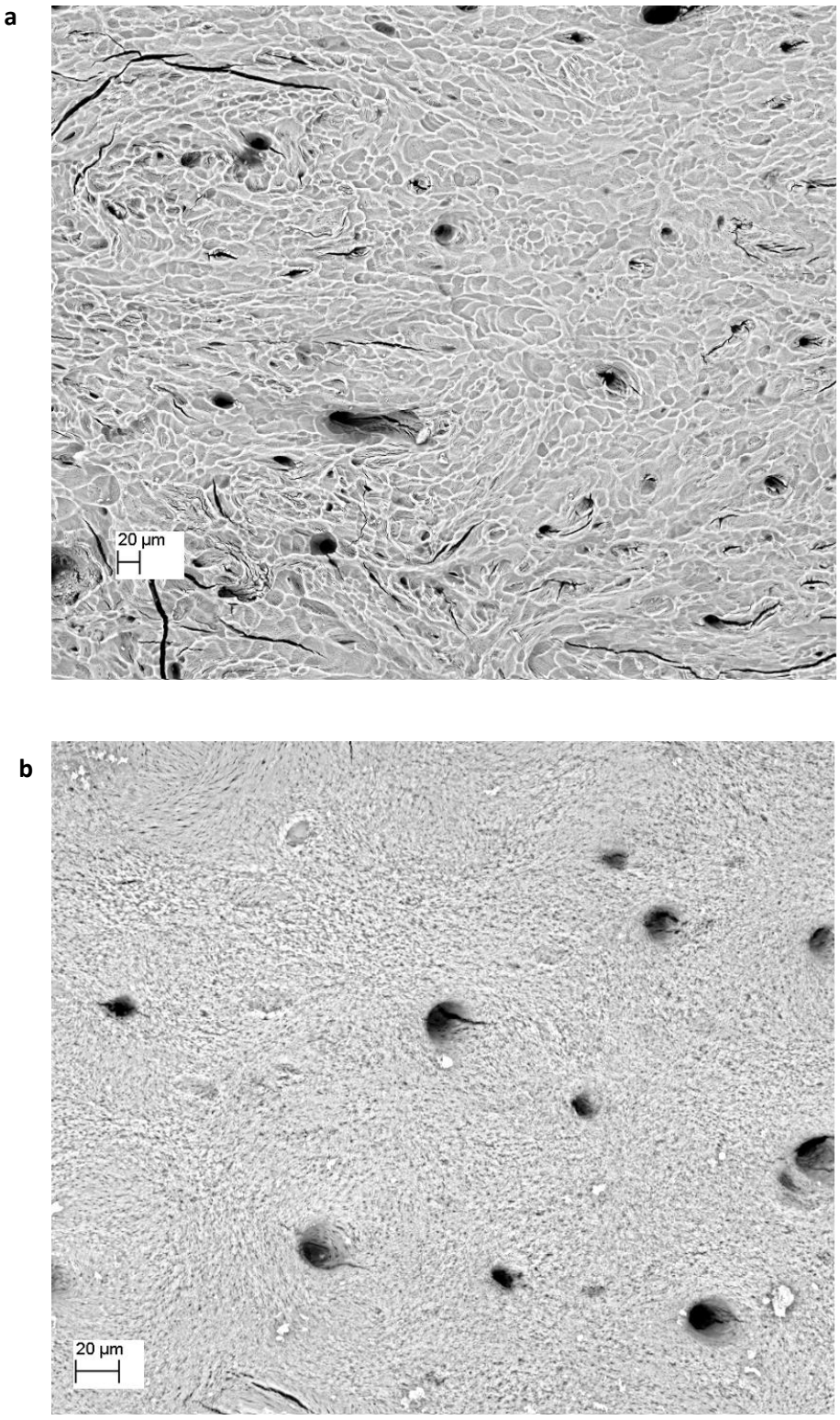

Figure 4.12: Bone resorption shown by BSE-SEM imaging following maceration of mature 16 week old female WT femurs. Healthy bone resorption visible on the periosteal surface of the female WT femur (a). Multiple canal openings visible on the endosteal surface of the female WT femur and identification of mineralising front bone modelling morphology (b). Scale bars are measured in µm.

Female OcnVEGFKO

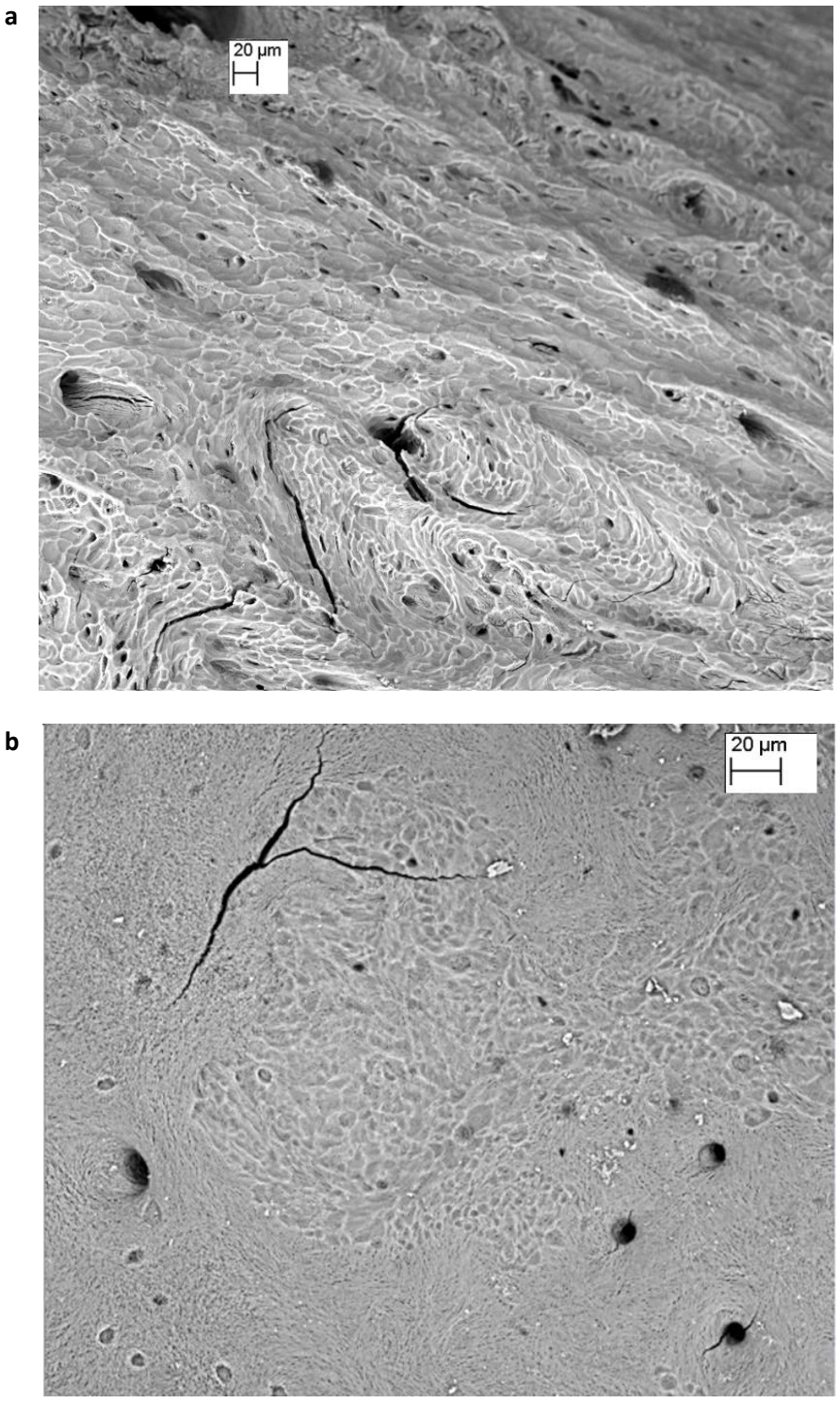

Figure 4.13: Bone resorption shown by BSE-SEM imaging following OcnVEGFKO in mature 16 week old macerated female femurs. Healthy bone resorption visible on the periosteal surface of the female OcnVEGFKO femur (a). On the endosteal surface of female OcnVEGFKO there is a mineralising front morphology and bone formation, with small areas of resorption present. Canals do not appear to have osteoid within them (b). Scale bars are measured in µm.

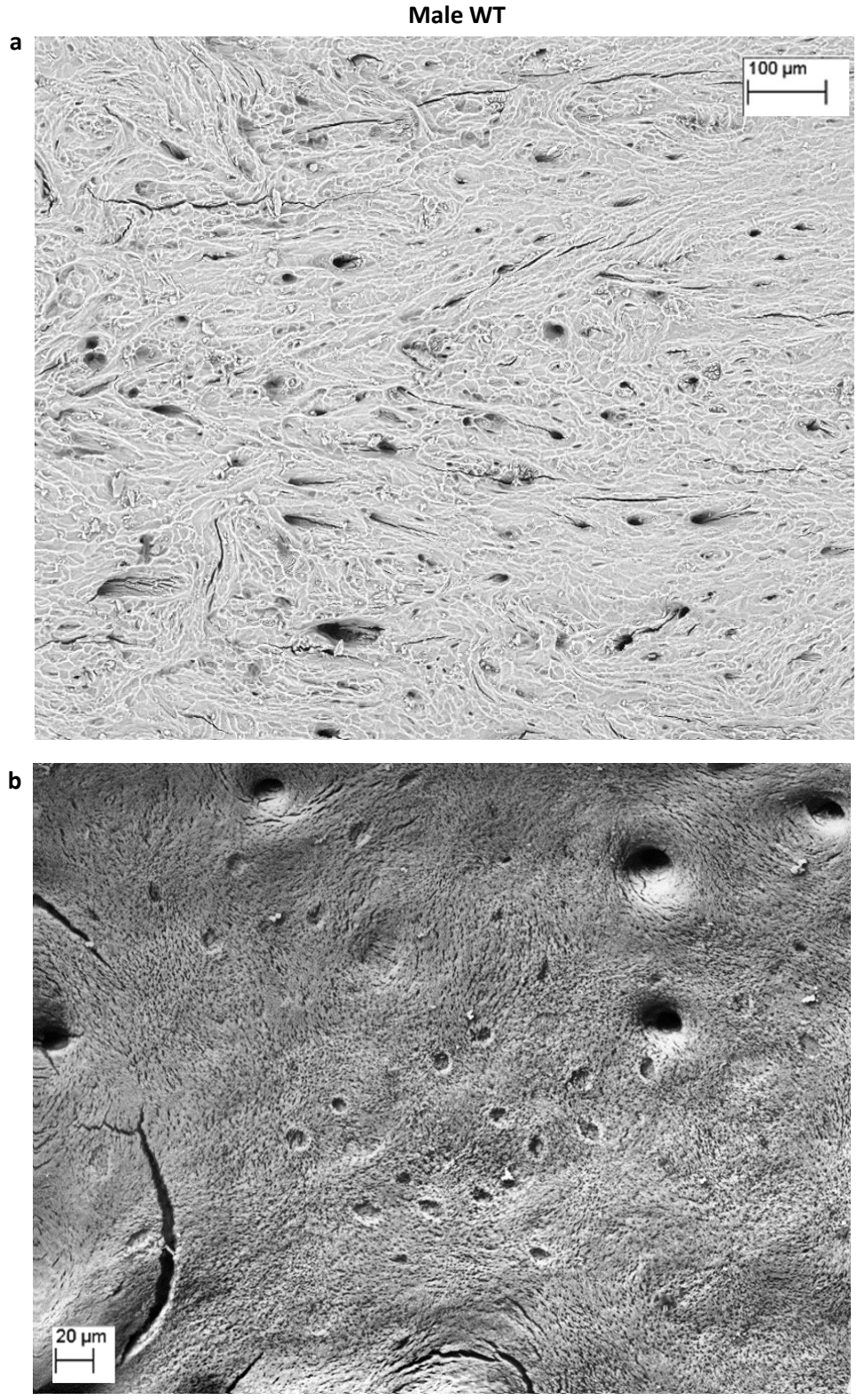

Figure 4.14: Bone resorption shown by BSE-SEM imaging in WT 16 week old macerated male femurs. Healthy bone resorption visible on the periosteal surface of the male WT femur (a). Multiple canal openings visible on the endosteal surface of the male WT femur and mild resorption, as well as modelling mineralisation and deposition of new bone (b). Scale bars are measured in µm.

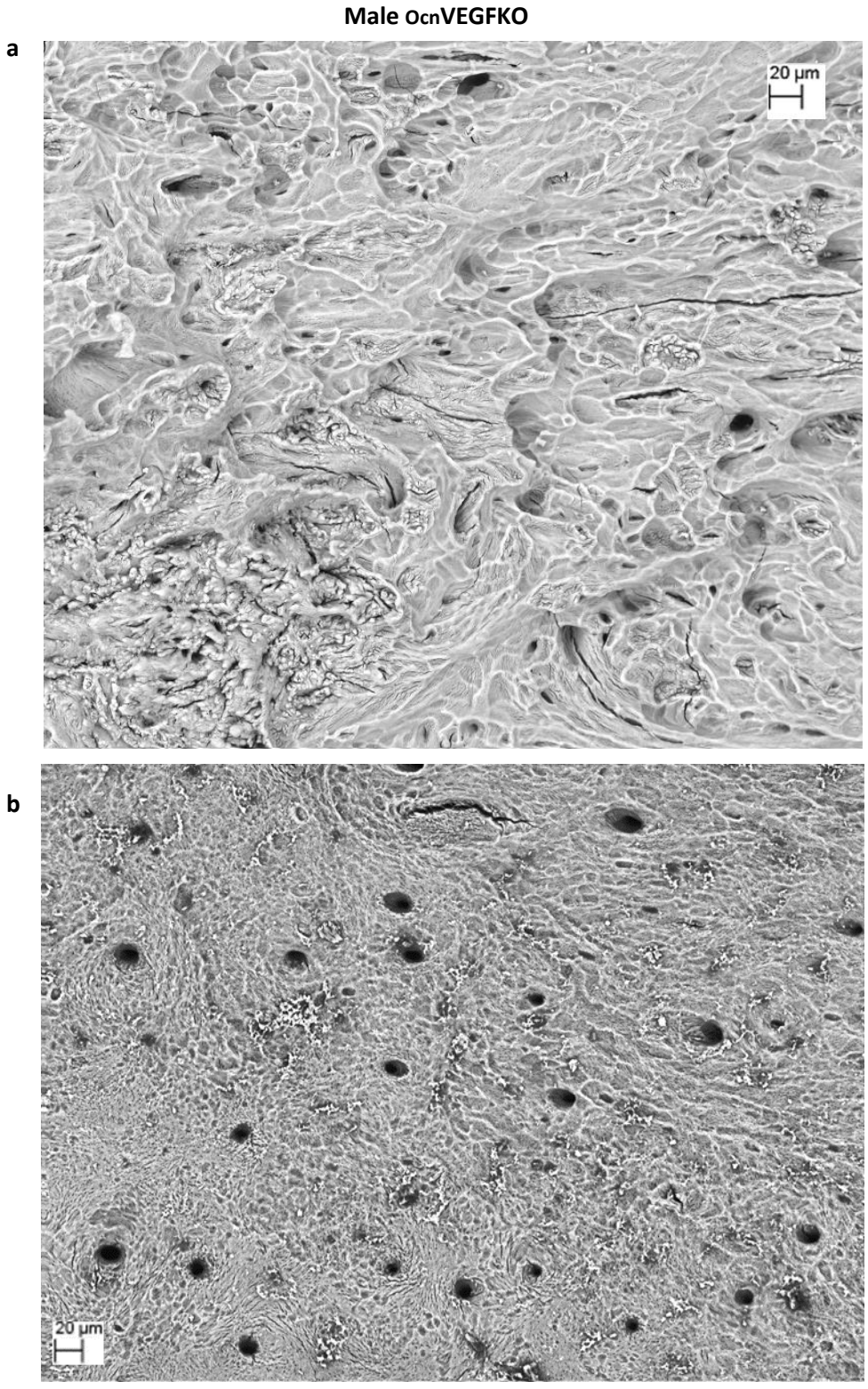

Figure 4.15: Identification of osteoid canals of macerated 16 week old male femur by BSE-SEM. Bone resorption taking place on the periosteal surface of the male OcnVEGFKO femur (a). In male OcnVEGFKO, osteoid is present within the canals on the endosteal surface, suggestive of poor mineralisation (b). Scale bars are measured in µm.

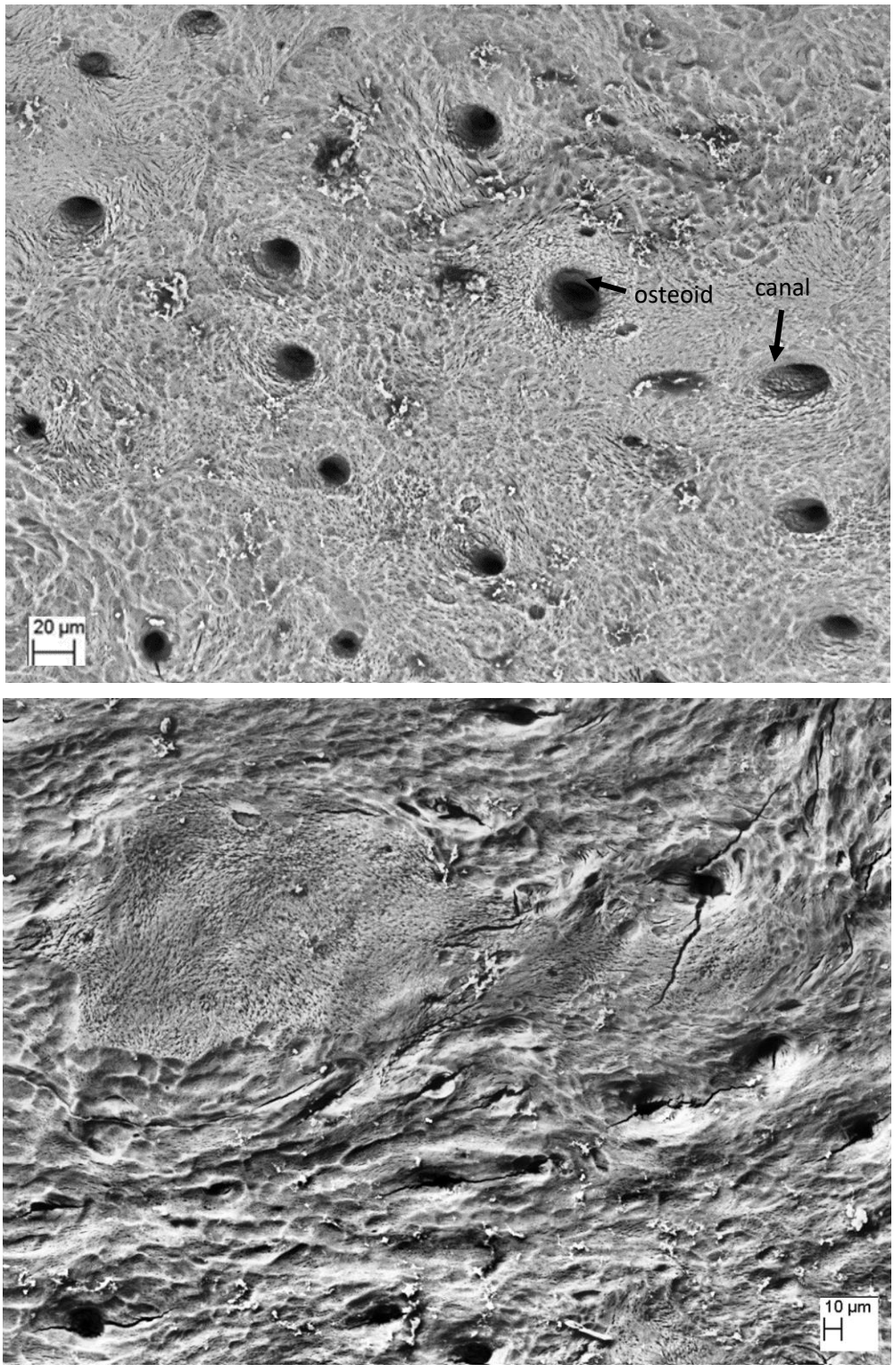

Figure 4.16: BSE-SEM has identified osteoid within multiple blood vessel canals on the endosteal surface in mature male OcnVEGFKO mice following maceration. BSE-SEM has identified non-mineralised osteoid within blood vessel canals following maceration of the femur. Mineralisation appears to be arrested, with mineral depositions starting to accumulate around vascular inlets.

4.4 Discussion

Unlike in previous studies in which deletion of *Vegf* in osteoblasts under the control of an Osterix-Cre promotor caused notable changes in body size and skeletal size via x-ray (Hu and Olsen, 2016, Liu et al., 2012), there were no obvious gross phenotypic observations in male or female mature mice following OcnVEGFKO here. Visually, mice appeared healthy and following analysis, there were no significant differences in OcnVEGFKO versus WT for either weight or tail length, which is a known measure of growth. As expected, males were significantly heavier than females in both WT and OcnVEGFKO subjects, a characteristic which is comparable in human men. Oestrogen is involved in the initiation of the closing of growth plate cartilage in women and thus males are physiologically larger in both their skeleton and their build in comparison to females (Joakimsen et al., 1998, Meyer et al., 1993, Perry et al., 2008). Human men have been shown to have 40% more muscle in their upper bodies and 33% more muscle in their lower bodies in comparison to women due to the up regulatory effect of testosterone on growth hormones (Janssen et al., 2000). A similar difference in bone growth and body mass is therefore expected when comparing male and female mice, who share gene regulation and many other biological systems with humans.

The sexual divergence identified in the long bones of 16 week old OcnVEGFKO versus WT mice was not replicated in the skull, with one male and one female significant result recorded from twenty intracranial measurements. For both of these results, the OcnVEGFKO cranial measurement was significantly lower than the correlating WT value. Based on the literature regarding the effect of loading on the mineral composition and blood supply to the skull and long bones, this would suggest that there could be a small increase in OcnVEGFKO mouse long bone loading versus WT, which would then correlate with a small reduction in cranial measurements in OcnVEGFKO. If this was correct, based on the literature this would also result in an increased blood supply to the long bones (Leblanc et al., 1990, Colleran et al., 2000, Ding et al., 2012). Skull measurements are mainly insignificant however and loading has not been investigated in this study, so therefore this theory would need to be tested further. The skull is a bone which does not have to withstand load and therefore the lack of gross observations in the skull phenotype suggested that the phenotype observed in OcnVEGFKO animals is associated with loading.

Initial CT scans of both male and female OcnVEGFKO bones identified a bad fracture in one of the OcnVEGFKO male mice and following 3D reconstructions of CT scans, it was clear that the fracture repair process in this mouse was dysfunctional. The callus surrounding the fracture site contained thin bone which was woven in appearance and had seemingly attempted to heal itself, but had not succeeded at the time of culling. Recent work has suggested that VEGF-A from early osteoblast lineage cells (osterix positive) is essential for both angiogenesis and the rapid formation of immature woven bone post-fracture. It is also heavily involved in controlling the filling of the cartilage filled callus with bone (Buettmann et al., 2019) and therefore following OcnVEGFKO, the lack of healing in this male mouse correlated with what is already known about the requirement of VEGF in the process of fracture repair.

The main gross difference observed in 16 week old OcnVEGFKO tibia was in males, where the average tibia length was significantly greater in comparison to WT. Opposing what has been identified here, mice that purely have $VEGF_{120}$ isoform have a much reduced tibia length (Maes et al., 2002). For the male mice used in this PhD, the reasoning behind the increase in tibia length in OcnVEGFKOs was unclear. It is also likely that the differences between previous studies are seen because this deletion of *Vegf* in this study occurs in mature osteoblast cells, as opposed to immature osteoblast cells. Therefore, it is probable that a later stage of bone development is affected in comparison to past work. The length of our bones is defined by several factors including the closing of the growth plate, chondrocyte size, chondrocyte proliferation rate and the rate of matrix production. The closing of the growth plate is a process which is known to occur later in life in males versus females and thus, perhaps there are alterations in this process when *Vegf* is deleted in mature male osteoblasts (Joakimsen et al., 1998, Meyer et al., 1993, Perry et al., 2008). VEGF is also known to play a known role in endochondral ossification (Ferrara et al., 2003, Gerber and Ferrara, 2000), which is dysfunctional in the absence of VEGF and this could be affecting the tibial length, which is increased in males.

Whole bone analysis measures of tibial geometry showed that despite the large increase in cortical porosity following the deletion of osteoblastic *Vegf* in males, they were able to maintain their overall geometry. Females on the other hand, compromised their geometry in order to maintain their porosity. In females, the tibiofibular junction was a region in which a vast number of changes in bone geometry took place. Thus, was proven in both

this study and in work by others (McKeon et al., 2012, Brookes and Harrison, 1957, Sferopoulos, 2010, Sundaram et al., 2018, Jianhong Pan, 2018) that the tibiofibular junction is both a highly dynamic and valuable region of interest for the study of degenerative bone disease phenotypes. It was unclear why these divergences in geometry between both sexes were present, although it is known that basally males produce a larger skeleton which is thought to protect them from fracture in later life and that differences do therefore exist between males and females even in healthy individuals (Seeman, 2001, Martin, 2002, Seeman, 2002, Callewaert et al., 2010a). In this study, males were able to maintain their geometry in an apparent compensation for the lack of bone-derived *Vegf*, which following the analysis of volume cortical porosity was surprising. The mechanism behind this finding and particularly, the potential role of sex hormones in the maintenance of bone geometry will be investigated in subsequent chapters. As well as this, investigations into the directionality of VEGF signalling pathways in the control of bone health, will also interrogate any sexual dimorphic effects further and identify potential targets for the treatment of degenerative bone diseases.

In females the only measurement in which there were no significant changes following the deletion of *Vegf* was BMD, which equally remained unchanged in male $_{Ocn}$VEGFKOs. It has been shown previously that BMD is not directly associated with the concentration of circulating VEGF (Costa et al., 2009), potentially explaining this finding following the deletion of bone-derived *Vegf*.

Although trabecular bone is often the focus of studies into degenerative bone disease due to the fact that it is so metabolically active (Liu et al., 2012, Pufe et al., 2003, Albright, 1947b, Riggs and Melton, 1986, Parfitt, 1994), the current studies demonstrated that $_{Ocn}$VEGFKO in males and females had minimal effect on trabecular bone phenotype. Striking phenotypes like those observed when analysing cortical bone were not visible and therefore it asks the question as to whether sexual dimorphisms have been missed in the past due to studies largely focussing on trabecular bone phenotypes, in which it has been suggested previously that there were no sexual dimorphisms in 8 week old mice (Liu et al., 2012). Additionally, *Vegf* has previously been deleted in immature osteoblast cells and mice aged 8-12 weeks old have been studied (Liu et al., 2012, Hu and Olsen, 2016). Perhaps the mice analysed were too young to identify any sex differences or the difference in promotor used (Osterix-Cre) has meant that the sexual dimorphic bone phenotype was not identified

following *Vegf* deletion from immature osteoblasts. Equally, information could have been missed due to the low resolution of CT used or the type of bone used for analysis. A significant amount of knowledge can therefore be gained by looking at cortical bone in the study of degenerative bone disease.

The parameters measured and discussed here were of varying n number, dependent on the bone and technique used to obtain the data. Tail length and weight were obtained directly after the mice were culled and therefore it was relatively easy to get high n numbers for this parameter. Data obtained from medium resolution scans was dependent on whether the bones were intact and therefore suitable for CT analysis. The n number of 4 used here was higher than that used for synchrotron scans, as the desktop Skyscan is readily available at the University of Southampton, whereas obtaining beamtime to use SR CT at SLS is much more difficult and therefore less bones can be scanned.

Previous studies have identified VEGF as being essential in the control of bone formation and therefore the disruption in mineralisation following OcnVEGFKO was unsurprising (Maes et al., 2012, Zelzer et al., 2002, Ferrara et al., 2003, Harada et al., 1994). The enhanced dysfunctions in mineralisation in male OcnVEGFKOs versus female OcnVEGFKOs, correlated with SR CT and histology results and once more was interesting given the previous focus on females in the study of degenerative bone disease. High levels of woven bone and osteoid were identified by BSE-SEM in male OcnVEGFKO tibia largely and to a lesser extent in female male OcnVEGFKO tibia. This data was supported by previous pentachrome histological stains presented in results chapter one, in which osteoid was present around the vascular canals and osteocyte lacunae in male OcnVEGFKOs. Woven bone is structurally brittle bone which is laid down very quickly (as reviewed by Kini and Nandeesh, 2012).

The most interesting finding from the BSE-SEM however, was the presence of osteoid deep within the male OcnVEGFKO vascular openings, visible on the endosteal surface of the femur as a result of maceration. This observation was not replicated in male WT, female WT or female OcnVEGFKO samples. In male OcnVEGFKO mice, an incomplete mineralised surface was present and mineralisation appeared to have arrested, with the beginnings of mineral depositions present around the vascular inlets. This phenotype corresponds to previous studies which have described patchy osteomalacia as a result of a *Phospho1* knockout in mice. The male OcnVEGFKO femur used here

therefore shows a rickets tendency, where there is a failure to mineralise on the forward facing surface of the osteocyte (Boyde et al., 2017, Steendijk and Boyde, 1973). Rickets is typically associated with increased levels of osteoid and a reduced mineralising front, which perfectly describes this phenotype observed by BSE-SEM (Marie and Glorieux, 1981). Phenotypes such as these, which show alterations in mineralisation and bone quality, have been characterised extensively for many years by Professor Alan Boyde (Boyde, 1980a). For years, Professor Boyde has suggested that osteocytes are not involved in the degradation of bone but instead, they are able to reduce mineralisation. In the case of bone diseases such as rickets, mineralisation is reduced so much that it becomes arrested and this is why phenotypes such as the one presented in this chapter are observed (Boyde, 1980b). It has been suggested that the production of matrix extracellular phosphoglycoprotein and osteopontin by osteocytes not only regulates and prevents over-mineralisation, but is also up-regulated in diseases such as rickets and subsequently prevents mineralisation entirely (McKee et al., 2013). It would be interesting to measure the expression of these proteins in future studies.

With the phenotype and physical traits following the deletion of osteoblast-VEGF deletion in 16 week old animals characterised, a number of issues remained: i) it was unclear what the mechanisms involved in causing this bone phenotype and physical traits were in $_{Ocn}$VEGFKO mice and, ii) it was unclear what was influencing the sexual dimorphisms which had been quantified. In subsequent chapters, a focus will be put on investigations into the potential mechanisms behind the bone phenotypes and sex differences which have been identified. The role of autocrine signalling pathways, paracrine signalling pathways and the potential role of sex hormones in the occurrence of these traits will therefore be fully investigated.

Chapter 5 Results III – Investigating the role of VEGF expression in prepubertal development and osteoblast function

5.1 Introduction

Previously, a sexually dimorphic role of VEGF in the maintenance of bone integrity was identified, where the porous and vascular phenotype was surprisingly particularly severe in male OcnVEGFKOs versus females. In attempt to assess hormone independent signalling of VEGF in the maintenance of bone health, experiments were performed using both young pre-pubertal mice with a much lower levels of sex hormones than adult mice and by using isolated long bone osteoblasts for *in vitro* studies. Cell culture experiments were performed in a dish and therefore, the effect of circulating hormones on the occurrence of a phenotype was removed as much as possible.

Following fertilisation, embryos are female by default and it is the SRY gene present on the Y chromosome in males that triggers this differentiation of the male testes (Koopman et al., 1991). Post-natal levels of both oestrogen and testosterone remain low during early development, until puberty. In mice, the onset of puberty occurs at 8.5-9 weeks of age and it has been reported that just prior to this at 5-7 weeks of age, the bioactivity levels of androgen and oestrogen in C57BL6 male and female mice begin to increase (Drickamer, 1981, Callewaert et al., 2010b). It has also been identified that oestrogen has an inhibitory effect on skeletal growth in females during the early stages of puberty. Conversely, oestrogens have been shown to upregulate skeletal production during early puberty in males and testosterone is involved in the upregulation of bone growth in late puberty in males (Callewaert et al., 2010b). Based on this, 4 week old mice with comparatively lower levels of sex hormones than adult 16 week old mice were used for this subsequent analysis.

In 1947 the role of oestrogen on the regulation of bone health was first identified and it was found to be important in the maintenance of osteoblast activity. After the menopause in females, levels of oestrogen are shown to be greatly reduced and this is associated with a reduction in bone mass and the quality of bone that constitutes the skeleton. Testosterone has shown to play a similar role in men. Here however, age-related decline in

testosterone levels is slow and happens later than it does in females. Nevertheless, orchidectomies have shown that testosterone is required for the maintenance of bone mass (Albright, 1947b, Albright, 1947a, Lindsay, 1982, Lindsay, 1987, Riggs and Melton, 1995). Oestrogen has since been shown to play an important role in the tight regulation of bone remodelling. It does this by inhibition of osteoclast differentiation and there is therefore a disruption in the tight balance between bone production and bone breakdown in post-menopausal women over the age of 50, who have reducing levels of oestrogen (Hughes et al., 1996). Although sex hormones are undoubtably responsible for a wide range of divergences seen in males and females, it has previously been shown that dimorphisms in gene expression exist soon after fertilisation (Bermejo-Alvarez et al., 2010). Therefore, an investigation into the genetic and hormonal regulation involved in the onset of the diverse bone phenotypes observed in males and females must be undertaken to improve understanding.

Additionally, *in vitro* experiments were performed to look at the at the influence of sex hormones on bone and vasculature phenotypes. When osteoblast cells are removed from a living organism, the effect of circulating hormones is removed. Phenol red is often present in the cell media and has been known for many years to be a weak oestrogen (Berthois et al., 1986). It was therefore imperative for this study to use culture media without phenol red in it. Despite the fact that dimorphisms have been seen even in the bones of healthy males and females (Seeman, 2001, Martin, 2002, Seeman, 2002, Callewaert et al., 2010a), *in vitro* experiments in which primary cells are separated into individual flasks of males and females are rare. By grouping male and female cells together, it is therefore possible that sex differences could have been missed in past *in vitro* studies.

Angiogenic VEGF signalling pathways play a known role in both haematopoietic stem cell survival and in the maintenance of vascular homeostasis (Gerber et al., 2002, Lee et al., 2007). The direct effect of VEGF on the osteoblast cell that produced it however, remains debated in the literature. Where some studies suggest that VEGF does indeed regulate its own function (Hu and Olsen, 2016), others suggest that osteoblast cells are reliant on the presence of endothelial cells to alter their differentiation in response to different osteoblastic-mediators and therefore suggest that paracrine signalling pathways predominate (Clarkin et al., 2008b). Looking at the angiogenic effect of osteoblast-derived *Vegf* deletion on osteoblast cells directly in both males and females will therefore improve

our understanding of any potential mechanisms involved in the expression of both bone phenotypes and sexual dimorphisms. If there is no direct effect on osteoblast cells, it will suggest that other signalling pathways must be involved in the control of healthy levels of bone porosity, angiogenesis and mineralisation.

Therefore, this chapter aims to look at the role of sex hormones in the regulation of VEGF signalling by both studying pre-pubertal animals and by performing *in vitro* studies in the absence of circulating sex hormones, which will look at the direct effects of osteoblast-derived *Vegf* deletion. It is hoped that this might help us to understand more about the signalling of VEGF in the maintenance of bone health and to explain the phenotype observed previously by SR CT, histology and BSE-SEM.

The third aim of this PhD project was to investigate the role of *Vegf* expression in prepubertal development and osteoblast function

Whole tibial analysis of $_{Ocn}$VEGFKO at 4 weeks of age

- High resolution micro-CT in *4 week old prepubertal mice*
- Trabecular bone analysis using medium-resolution micro-CT
- Whole Geometry measurements of the tibia

Osteoblast-derived *Vegf* will be deleted in male and female long bone osteoblasts (OB) *in vitro* (OBVEGFKO).

- *In vitro* effects of *Vegf* deletion in male and female osteoblasts (VEGF ELISA to confirm knockdown, ALP, viability, qPCR, western blot)

5.2 Methodology

5.2.1 Pre-pubertal *Vegf* knockout mice

4 week old mice were used for investigations into the effect of sex hormones on the presence of both long bone (cortical porosity, trabecular bone and whole bone geometry) and vascular (separation of intracortical canals and lacunae from SR CT data) phenotypes. Mice were derived and bred in the same way as 16 week old mice, but instead culled by schedule 1 cervical dislocation at 4 weeks of age. SR CT (chapter 3.2.1) and medium resolution CT data (chapter 4.2.3 and 4.2.4) was used to interrogate potential phenotypes in males and females, as per 16 week old mice.

5.2.2 Osteoblast extraction

Postnatal day 4/5 *Vegf* $^{fl/fl}$ mice were used for the extraction of osteoblasts. Prior to their arrival at the holding room, sex was determined by physical examination at the Biomedical Research Facility in the Faculty of Medicine at the University of Southampton. The anogenital distance was used to determine sex as this measurement is sexually dimorphic in mice, with the distance in males being twice as long as that in females. *Vegf* $^{fl/fl}$ mice were sacrificed using schedule 1 procedures, specific for mouse pups of this age. Long bones were dissected from *Vegf* $^{fl/fl}$ mice and cut into small pieces to facilitate digestion. The skin and knee joint was removed, separating the tibia and femur. Male and female long bones were separated into individual universal tubes of 6ml Hanks buffered saline solution prior to digestion. At least three male and female P4/5 mice were needed to produce sufficient numbers of cells per flask.

LOBs were isolated in a 4 step digestion process using the collagenase (10 minutes), collagenase (1 hour), EDTA (10 minutes), collagenase (30 minutes; CCEC) osteoblast isolation method, in which 10mg/ml collagenase and 4mM EDTA was added to the long bones sequentially (Taylor et al., 2014). Digestion was performed on a shaker at 37°C and from the second collagenase digestion step onwards, collagenase and EDTA supernatants were retained for further use. Once all digestion stages had been performed, the resulting male and female fractions in individual tubes were spun down at 470 *x g* for 5 minutes. The pellet was subsequently resuspended in media, before the fractions from the three different stages of digestion were combined into individual male and female universals.

Osteoblast cells were cultured in two T75 flasks containing male and female LOBs, as well as 12ml of 488ml Alpha minimum essential media (MEM) culture medium with 10% (v/v) heat inactivated Fetal Bovine Serum (FBS), 0.5% (v/v) gentamycin, 100µg/ml penicillin streptomycin. Due to the inherent interest in the effect of sex hormones on phenotypes expressed, the media used was phenol red free. Media was changed twice per week, until cells reached 90% confluence. The appearance of LOBs reaching confluence can be seen in figure 5.1.

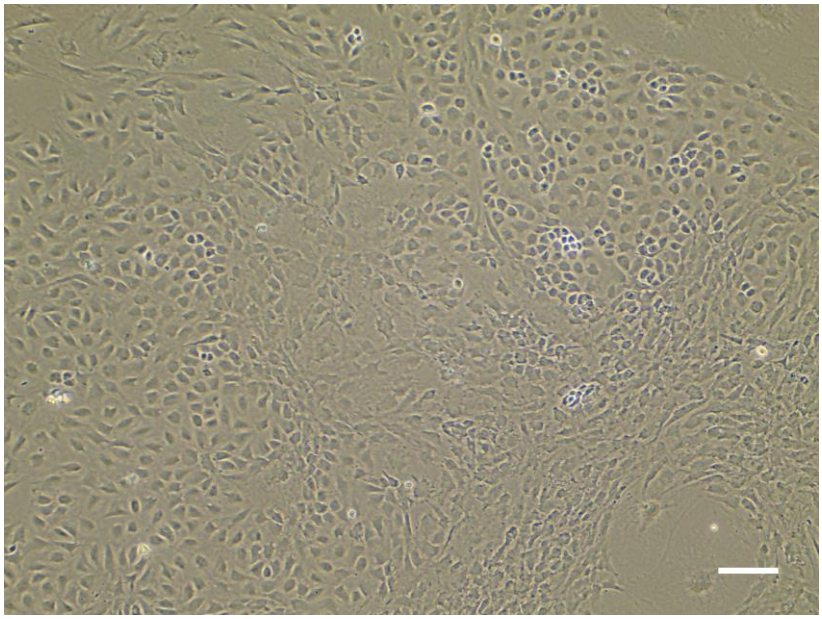

Figure 5.1: Confluent LOBs extracted from P4 *Vegf*$^{fl/fl}$ C57BL6 mice in a T75 flask, prior to plating. Image taken using the EVOS microscope (10X magnification). Scale bar = 200µm.

5.2.3 Treatment with VEGF or SU5416

1% (v/v) FBS alpha MEM was used to starve the cells of growth media for 24 hours prior to treatment. LOBs were subsequently treated with VEGF (5ng/ml and 50ng/ml) or semaxanib tyrosine kinase inhibitor (SU5416; 10µM) in 1% (v/v) FBS media for 24 hours. DMSO was 1% (v/v) FBS media as a control. Cell viability assays were performed as detailed in the main methods (chapter 2.6.3).

5.2.4 Deletion of osteoblast-derived *Vegf*

All procedures involving the use of adenoviruses were carried out in a category two, viral lab. The adenoviral constructs were purchased from Vector Biolabs due to their proven success in the knockout of *Vegf* in osteoblasts, referred to here as OBVEGFKO (Hu and Olsen, 2016). *Vegf* $^{fl/fl}$ male and female LOBs were transfected with Adv-Cre GFP and Adv-GFP to act as a control, at a multiplicity of infection (MOI) of 100 (Zhang et al., 2014). Adenovirus dilutions were made with 10% (v/v) FBS Alpha MEM media. Cells were left to recover for 6 days, unless otherwise stated. Ahead of CM collection on day 7, cells were treated with low serum growth media containing 1% (v/v) FBS for 24 hours. WT and knockout (OBVEGFKO) conditioned media was stored at -80°C for future use. For viability, WNT3a (75ng/ml) was used as a positive control and β-glycerol-phosphate (2mM) was used as a positive control for ALP experiments following OBVEGFKO in LOBs.

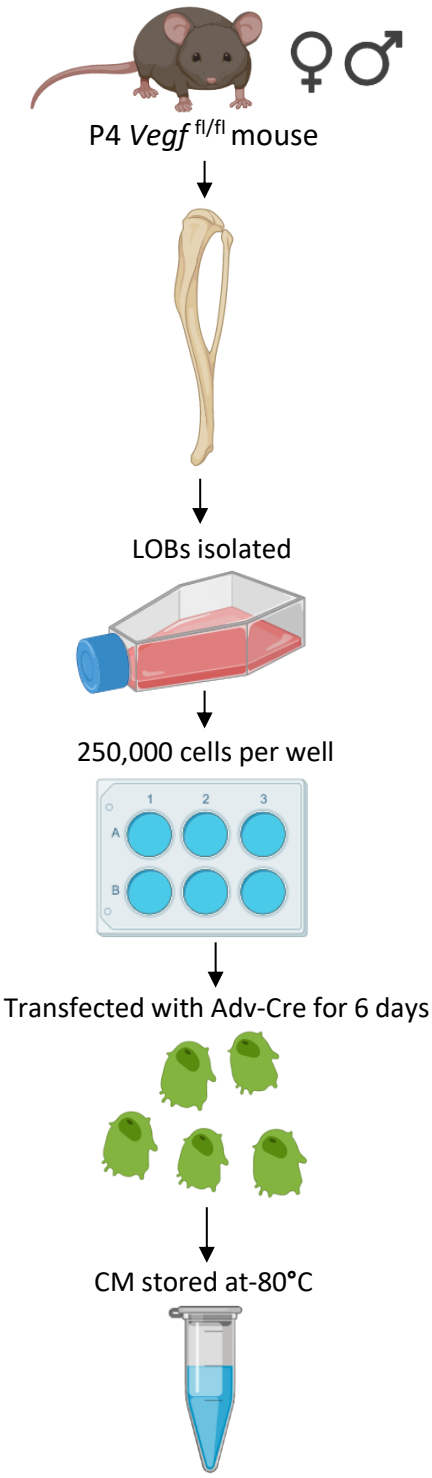

Figure 5.2: Methodology schematic, showing the process of *in vitro* OBVEGFKO. LOBs are isolated from the long bones of postnatal day 4 *Vegf* $^{fl/fl}$ mice. Once confluent, LOBs are plated in a 6 well plate. After leaving them for 48 hours to settle, they are treated with adenovirus-cre for the deletion of VEGF and adenovirus GFP as a control for 6 days. Following this, LOBs are stepped down for 24 hours with 1% (v/v) FBS media and CM stored at -80°C until further use.

5.2.5 VEGF ELISA

A mouse VEGF-A ELISA kit was used to determine whether deletion of osteoblast-derived *Vegf* was successful. The conditioned media was collected from male and female LOBs which had been treated with adenovirus was used for this assay, following the Invitrogen protocol. Replicates of samples and standards were plated. A spectrophotometer with a 405nm filter was used to measure the absorbance and unknown concentrations were calculated using a standard curve, plotted using the known concentrations and absorbencies of the eight standards. The concentrations of VEGF calculated using the standard curve (mg/mL) were normalised using results from the protein assay, described previously (chapter 2.6.2). The percentage knockdown was then calculated in males and females by quantifying the percentage decrease in VEGF (pg/mL/mg/mL) when comparing Adv-Cre with Adv-GFP.

5.3 Results

5.3.1 Conditional deletion of *Vegf* does not significantly influence cortical porosity in male and female pre-pubertal mice

In order to look at the effect of OcnVEGFKO on pre-pubertal mice, SR CT of 4 week old male and female mice was performed (figure 5.3a; 0.65µm voxel size). Here the levels of sex hormones in males and females is comparatively low as the mice are not yet sexually mature (Callewaert et al., 2010b). Unlike in 16 week old mice, where intracortical porosity was significantly increased in male OcnVEGFKOs versus WT, here there were no significant differences in % volume cortical porosity observed in either sex as a result of *Vegf* deletion. Following quantification, it was evident that intracortical porosity was increased in both male and female OcnVEGFKOs, however variation in OcnVEGFKO repeats meant that standard error was reasonably large and therefore this finding deemed insignificant (figure 5.3b). Equally, there were no quantifiable differences between male and female mice of 4 weeks of age. Visibly, SR CT scans showed high levels of porosity present in the posterior region particularly, in both males and females following conditional deletion of *Vegf*.

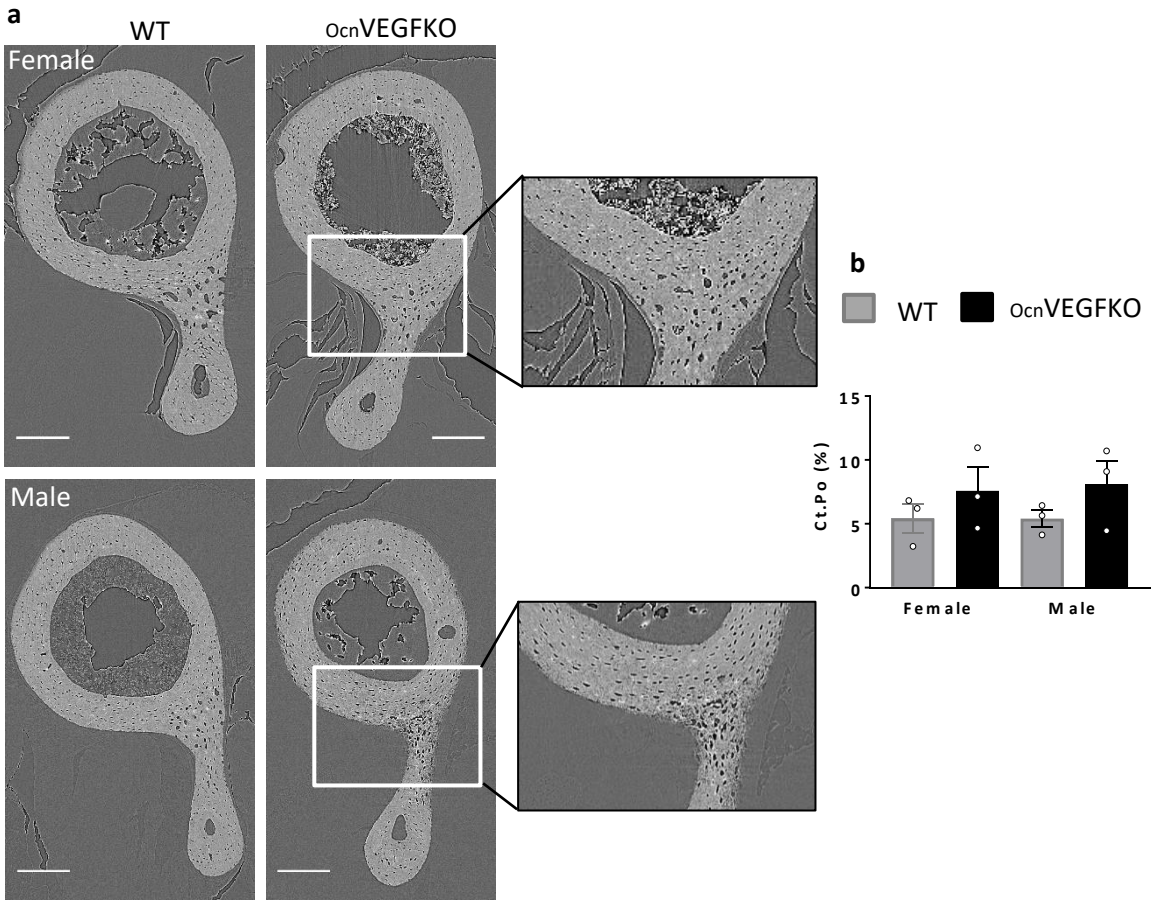

Figure 5.3: No significant differences in intracortical porosity following conditional deletion of VEGF in 4 week old mice. High resolution, synchrotron X-ray computed tomography (SR CT; g; 0.65µm voxel size) slices from 4 week old female and male WT and OcnVEGFKO mice (a) revealed poorly mineralised areas of cortical bone at the tibiofibular junction (white square). The % cortical porosity was not significantly changed in both males and females following OcnVEGFKO (b). Error bars indicate mean value ± SEM, n=3 females and 3 males from 2 individual litters $p<0.05$*, using two way ANOVA.

5.3.2 High-resolution SR CT revealed sex differences in vascular canals following deletion of bone-derived *Vegf* in 4 week old pre-pubertal mice

Following the separation and quantification of osteocyte lacunae (yellow) and intracortical canal fractions (red), some sexual dimorphism was identified (figure 5.4a). No differences in proportions of lacunae and intracortical canals as a percentage of the total porosity were seen between female OcnVEGFKO and WTs (figure 5.4b). As seen in adult mice however, in 4 week old mice there was a significant increase in the intracortical canal fraction and a significant decrease in osteocyte lacunae fraction (% volume of total porosity) in male OcnVEGFKOs versus WT littermate controls (figure 5.4). In both sexes, lacunae and canal density (figure 5.5a; Lc.Dn/5.5; Ca.Dn) and diameter (figure 5.5b; Lc.Dm/5.5e; Ca.Dm) were not significantly altered. The most notable finding was a significant increase in intracortical canal volume in 4 week old males following the conditional deletion of *Vegf*. There were no significant changes in intracortical canal volume in female OcnVEGFKO versus WT. This correlates data obtained from 16 week old mice and measurements of intracortical porosity are summarised within appendix D.3.

In 4 week old animals, the average density of intracortical canals was greater than in 16 week old male and female mice, however this was not a significant finding. A similar observation was noted with regards to intracortical canal volume, where the average canal volume was once more higher in 4 week old male and female WT animals in comparison to 16 week old WT animals. In females, this was significant ($p<0.05$) and could perhaps be explained by the fact that 4 week old bones are still undergoing development and therefore need a copious blood supply to facilitate growth.

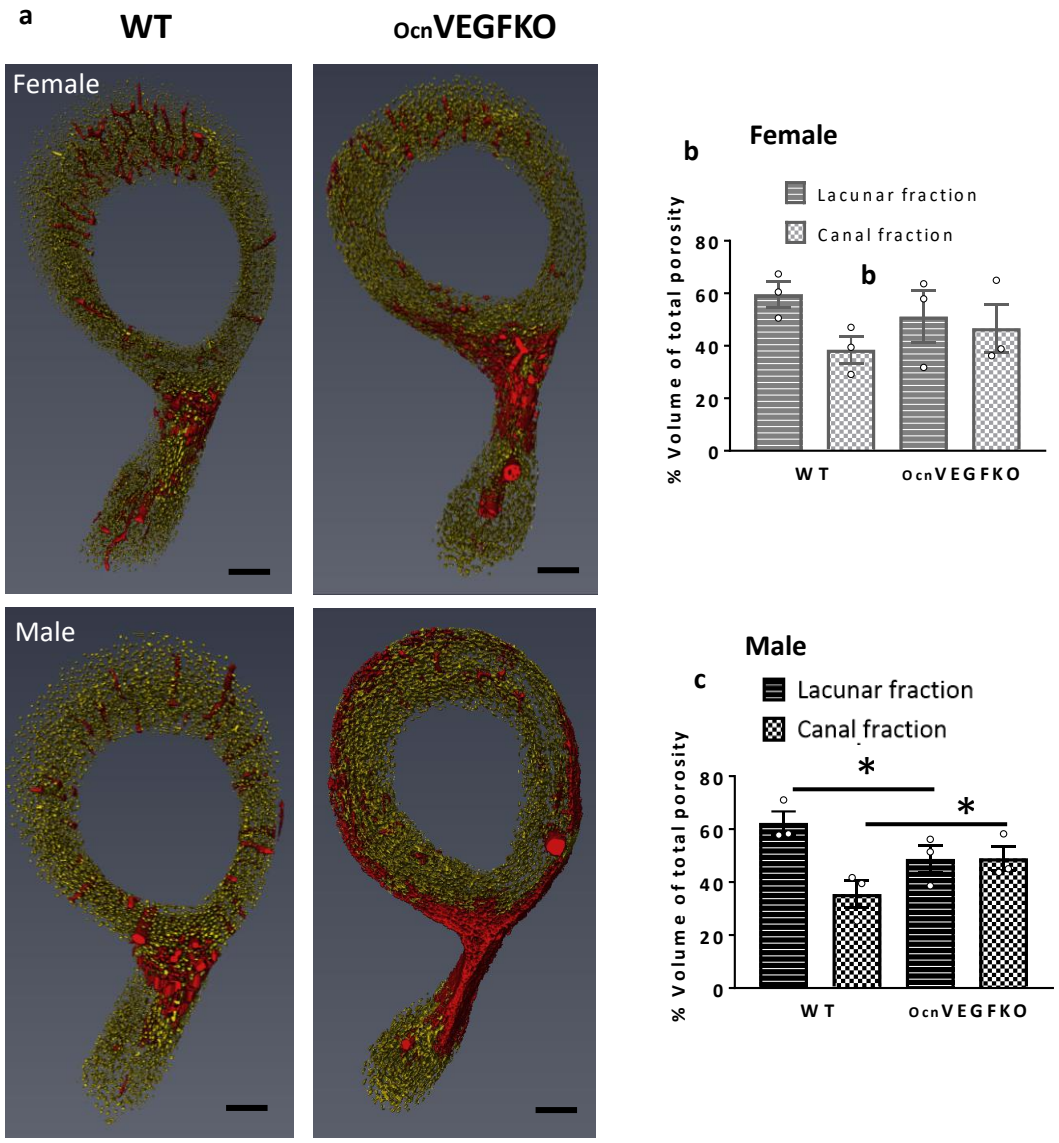

Figure 5.4: Significant increase in proportion of canals following OcnVEGFKO in male pre-pubertal mice. Aviso 9.0 was utilised for separation of osteocyte lacunae (yellow) from intracortical canals (red) in male and female mice (a). In females, there were no significant changes in the % of porosity constituting the intracortical canals and osteocyte lacunae (b). In males, there was a significant increase in % porosity in the intracortical canal fraction as a result of a conditional deletion of *Vegf*. The lacunae fraction was significantly decreased in male OcnVEGFKO mice versus WT controls (c). Error bars indicate mean value ± SEM, n=3 females and 3 males from 2 individual litters $p<0.05$*, using two way ANOVA. Scale bar = 200µm.

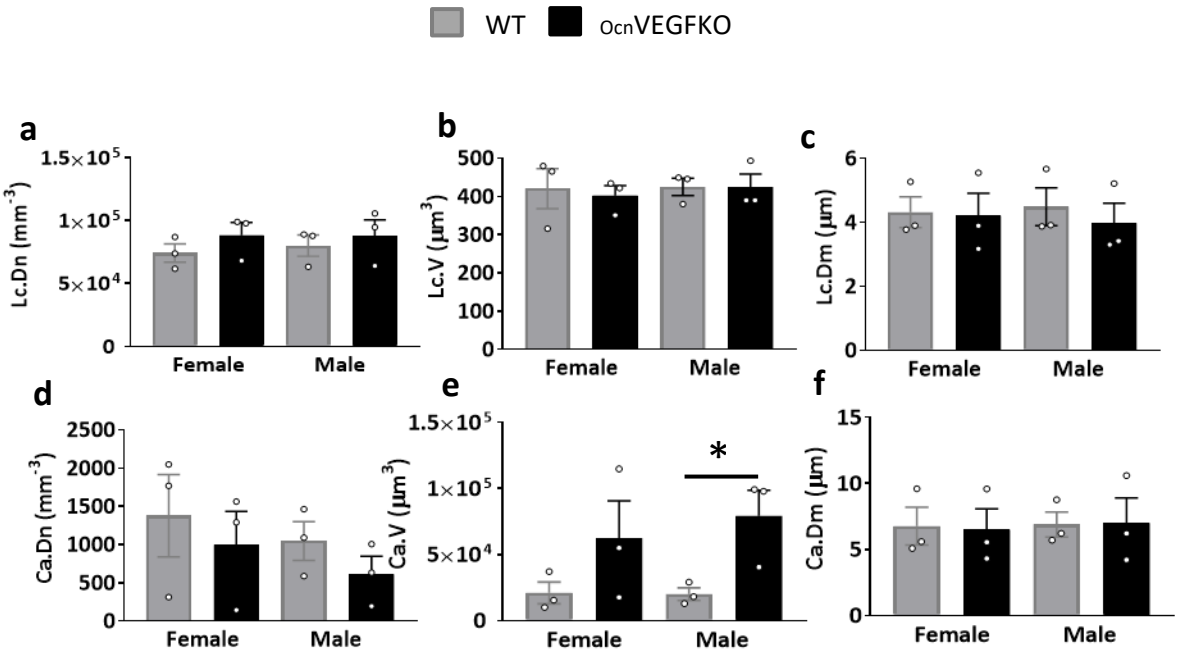

Figure 5.5: Increase in canal volume in 4 week old male mice as a result of OcnVEGFKO. Measurements taken of regularly sized osteocyte lacunae show no significant differences in lacunae number density (Lc.Dn; a), mean lacunar volume Lc.V; b) or (Lc.Dm; c) in males or females following knockout of *Vegf* versus WT. Number of intracortical canals greater than the lacunar threshold (see methods) was not significantly changed in OcnVEGFKO (Ca.Dn; d), however there was a significant change in mean canal volume (Ca.V; e) versus WT in male OcnVEGFKO. Mean canal diameter was not significantly altered in male OcnVEGFKO (Ca.Dm; f). Error bars indicate mean value ± SEM, n=3 females and 3 males from 2 individual litters $p<0.05$*, using two way ANOVA.

5.3.3 Deletion of VEGF in osteocalcin expressing osteoblasts has no effect on trabecular bone parameters in male and female 4 week old mice

For completeness and to enable comparisons between immature (4 week old) and mature mice (16 week old), well known measures of trabecular bone morphometry were quantified (figure 5.6; BV/TV, bone volume; BS/TV, bone surface area; Tb.Th, trabecular thickness; Tb.N, trabecular number). In 4 week old mice, no sexual divergences were observed in any of these trabecular bone parameters in OcnVEGFKO animals versus WT.

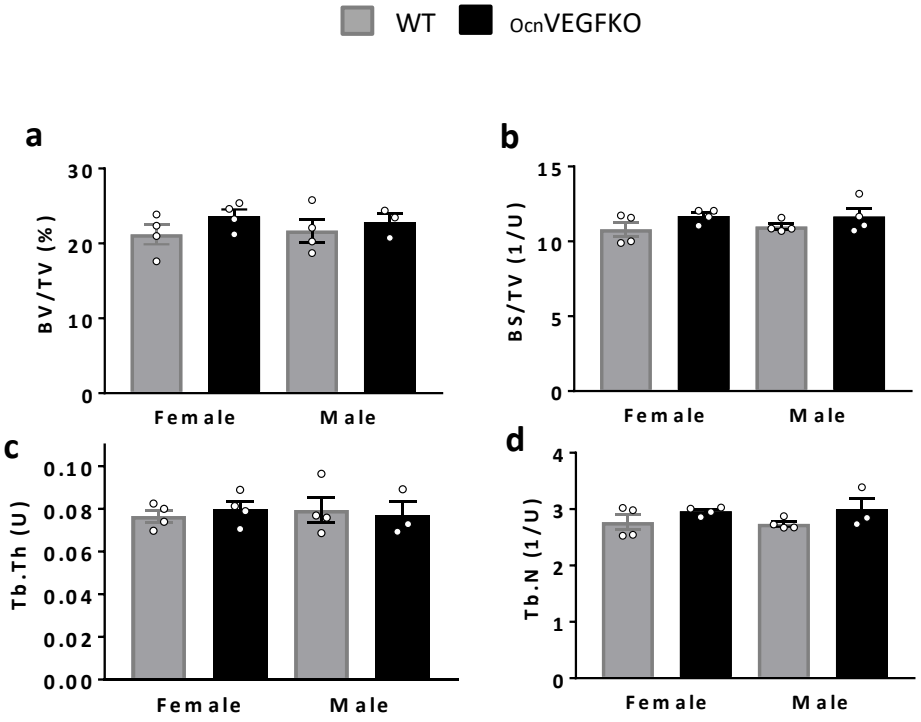

Figure 5.6: No changes in trabecular measurements in 4 week old male and female mice following OcnVEGFKO. No differences in % bone volume (a; BV/TV), bone surface area (b; BS/TV), trabecular thickness (c; Tb.Th) or trabecular number were identified in 4 week old animals following OcnVEGFKO. Error bars indicate mean value ± SEM, $p<0.05$*, using two way ANOVA. N=4 female WT, female OcnVEGFKO, male WT and n=3 male OcnVEGFKO.

5.3.4 4 week old males compromise tibial geometry and shape following the deletion of bone-derived VEGF

Following the identification of sex differences in intracortical canal parameters by SR CT in 4 week old male OcnVEGFKO mice, measurements of geometry along the entire tibial length were also assessed in 4 week old animals (figure 5.7a). This included measures of CSA, Imin, Imax, Ct.Th, Ellipticity and J. Significant differences in CSA, Imax Ct.Th and Ellipticity (figure 5.7b) at numerous locations along the length of the tibia in male OcnVEGFKO versus WT were observed. Here, male OcnVEGFKO measurements were significantly lower than WT controls. In contrast to results collected from geometrical analysis of 16 week old bones where female bone geometry was severely compromised, the only significant difference in 4 week old bones was observed in ellipticity at ~75% along the length of the tibia. No significant changes in tibia length in males or females were observed (appendix D.5).

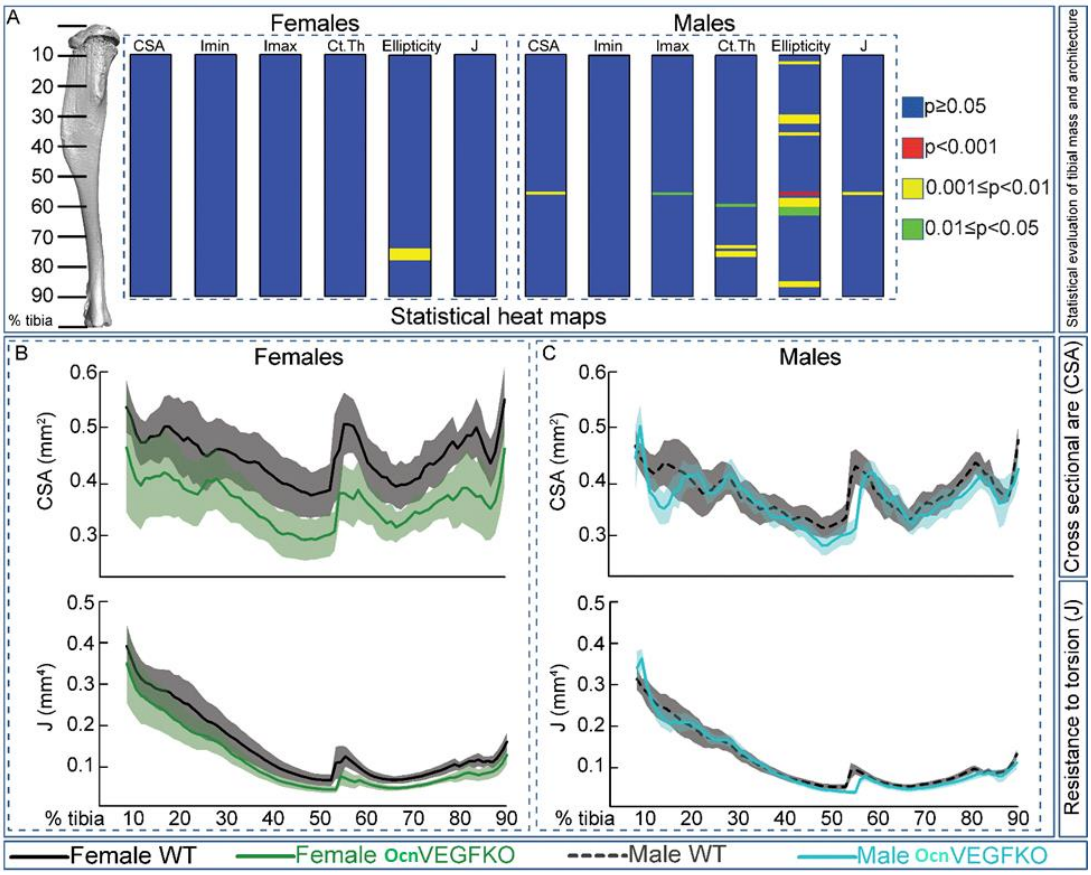

Figure 5.7: Geometrical alterations present in 4 week old male tibia following OcnVEGFKO. Graphical heat map summarises statistical differences between OcnVEGFKO versus WT mice within female and male groups at specific matched locations along the tibial length (a). Red p≤0.0001, yellow p≤0.001-0.01, green p≤0.01-0.05 and blue ≥0.05. Line graphs represent means for female (b) and male (c) WT versus OcnVEGFKO ± SEM (n=4 males and females from 2 individual litters). Statistics performed using ANOVA.

5.3.5 Exogenous VEGF has no direct effect on the viability of male or female long bone osteoblast cells

In order to investigate the potential mechanisms which might be responsible for the expression of phenotypes and gender dimorphisms seen in 16 week old mice predominantly, *in vitro* experiments were carried out using LOBs isolated from 4 day old *Vegf* $^{fl/fl}$ mice.

LOBs were treated with two different concentrations of VEGF (5ng/ml and 50ng/ml) in 1% (v/v) FBS media for 24 hours and viability assays were run to look into whether VEGF was able to interact directly with LOBs via autocrine signalling pathways to alter osteoblast viability. Results have shown no significant changes in ATP release following the addition of endogenous VEGF (figure 5.8). Therefore, endogenous VEGF does not appear to be having a direct effect on osteoblast viability at either concentration.

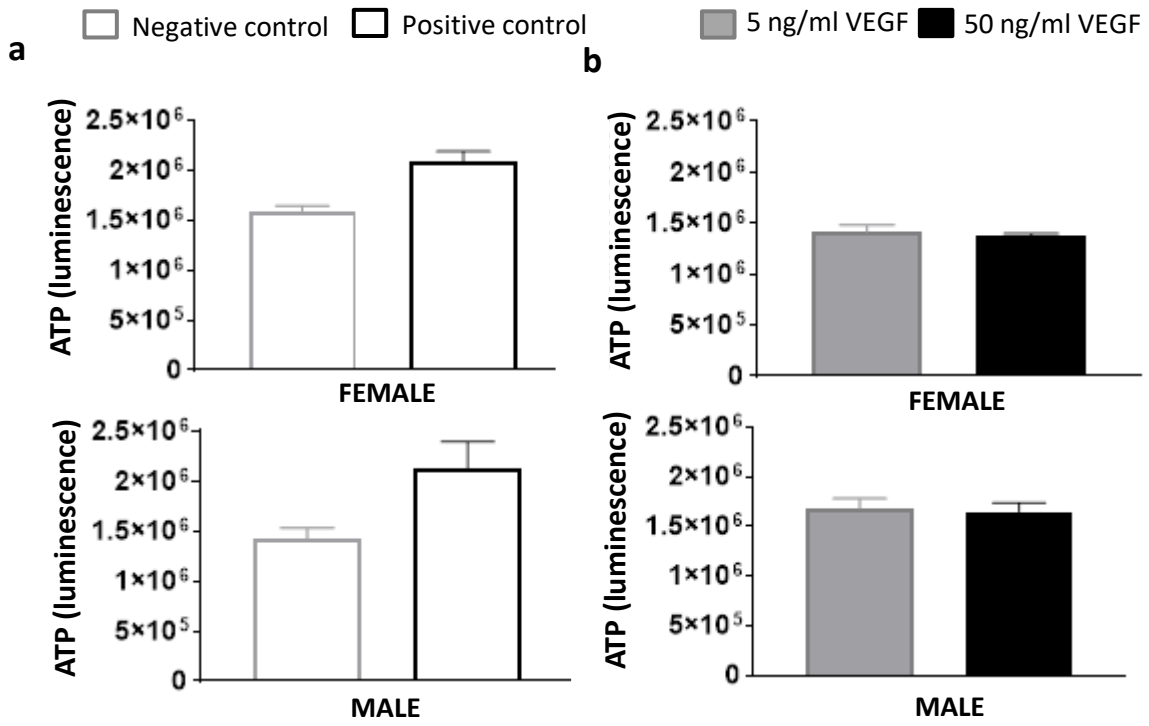

Figure 5.8: LOBs do not respond directly to addition of two different concentrations of VEGF. Osteoblast cells extracted from 4 day old *Vegf* $^{fl/fl}$ wild type mice. Male and female LOBS were cultured separately and each well containing 2,500 cells was exposed to endogenous VEGF (5ng/ml and 50ng/ml) diluted in 1% (v/v) FBS alpha MEM media for 24 hours. Male and female control cells were treated with 1% (negative control) and 10% (v/v) FBS (positive control) media (a). There was no significant difference in males or females following the addition of VEGF (b). Viability quantified using Cell Titer-Glo 2.0 Assay protocol on plate reader. Each bar represents the average of six individual treatment repeats ± SEM using t test.

5.3.6 No significant decrease in viability in male and female long bone osteoblast cells following VEGFR2 blockade

SU5416 was added to LOBs isolated from P4 *Vegf* $^{fl/fl}$ mice for 24 hours. Addition of the SU5416 tyrosine kinase inhibitor to LOBs blocks the binding of VEGF to any VEGF receptors on the surface of the osteoblast cells. This therefore provided another way of investigating whether VEGF is signalling via autocrine pathways and binding to receptors on the surface of the cells that produced it here. As shown below in figure 5.9, addition of SU5416 tyrosine kinase inhibitor did not significantly decrease the viability and ATP release of LOBs versus controls (figure 5.9b). In fact, in the case of male LOBs, the viability was significantly increased versus controls. This suggests that VEGF-VEGFR2 receptor binding and autocrine signalling with osteoblast cells is not required for the maintenance of osteoblast viability.

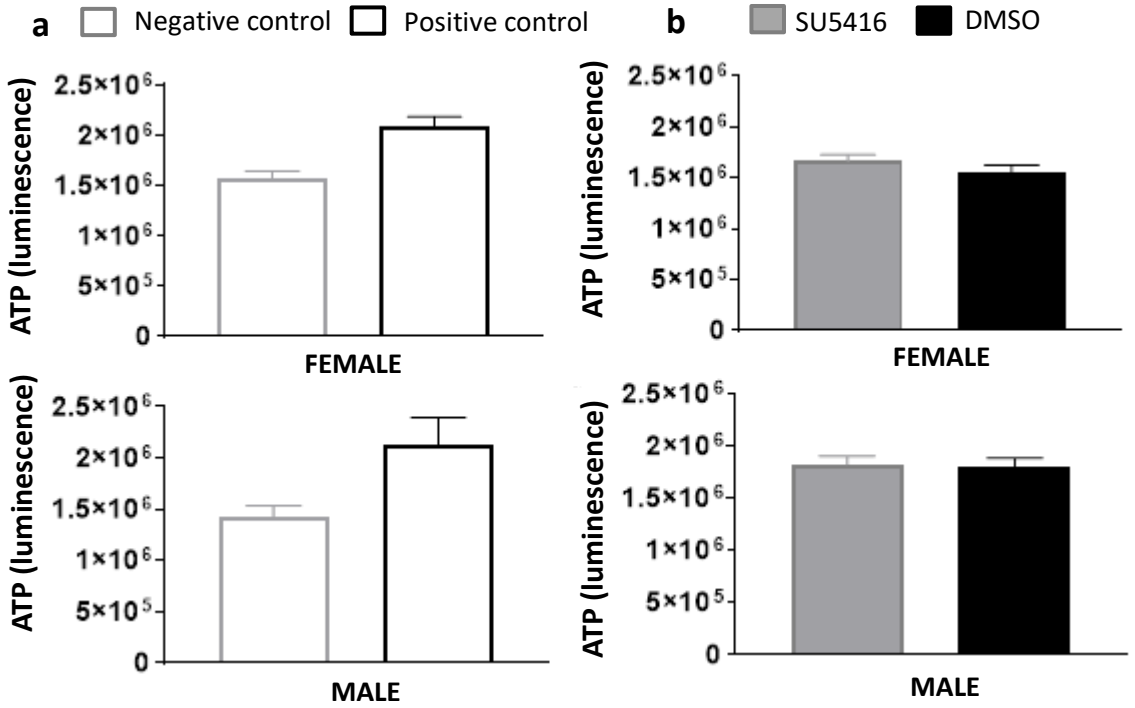

Figure 5.9: Addition of SU5416 tyrosine kinase VEGF receptor inhibitor does not significantly decrease viability in long bone osteoblast cells. Osteoblast cells extracted from 4 day old *Vegf* $^{fl/fl}$ wild type mice. Male and female LOBS were cultured separately, as described in section 2.6. Each well containing 2,500 cells was exposed to tyrosine kinase inhibitor SU5416 diluted in 1% (v/v) FBS alpha MEM media for 24 hours. Male and female control cells were treated with 1% (negative control) and 10% (positive control) (v/v) FBS media (a). Addition of SU5416 did not significantly alter osteoblast viability versus the DMSO control (b). Viability assay quantified using Cell Titer-Glo 2.0 Assay protocol on plate reader. Each bar represents the average of six repeats ± SEM (**P<0.01) using t test.

5.3.7 Deletion of osteoblast-derived VEGF does not directly affect long bone osteoblast cell viability, but significantly increases ALP elution

To examine the role of autocrine signalling pathways in the observed abnormalities in porosity, the vasculature and mineralisation presented previously, *Vegf* was deleted from osteoblasts *in vitro*. In order to do this, LOBs were treated with adenovirus-Cre-GFP as previously described (Zhang et al., 2014) and the knockout confirmed by VEGF ELISA. In both males (90% knockdown; n=3) and females (96% knockdown; n=3), there was a significant decrease in concentration of VEGF following treatment with adenovirus-Cre, when normalised to protein concentration and compared to WT controls (Figure 5.10a). Throughout repeats, VEGF concentrations in male WTs was basally slightly lower than in female WTs, however this was non-significant (p=0.09). Levels of protein were not significantly altered following OBVEGFKO and therefore the decrease in concentration of VEGF following osteoblast derived-*Vegf* deletion was not influenced greatly by normalisation (appendix D.6).

Following extraction of RNA from OBVEGFKO and WT osteoblasts, it was also possible to confirm VEGF deletion in mRNA by qPCR. Results were normalised to *Gapdh* and showed an 82% knockdown in female OBVEGFKO versus WT and a 72% knockdown in male OBVEGFKO versus WT (figure 5.10b). The protein expression of Cre recombinase was investigated by western blot, in which there was a band present in both female OBVEGFKO and male OBVEGFKO (figure 5.10c). This was further validation of the efficiency of the *Vegf* knockdown in Cre positive osteoblast cells. Transfected GFP-expressing LOBs were visualised under a fluorescence microscope for additional examination (figure 5.10d).

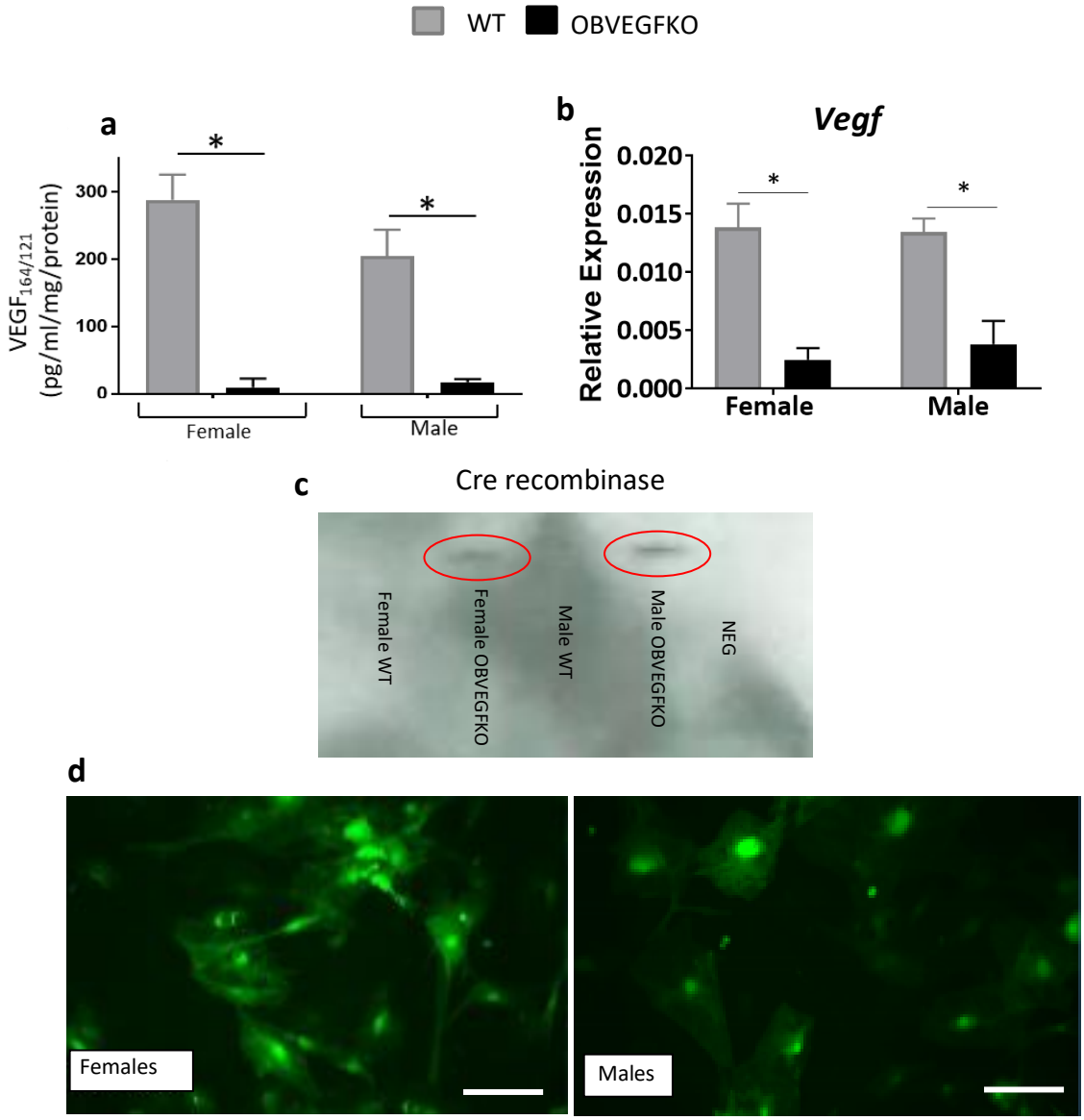

Figure 5.10: Confirmation of *Vegf* knockdown in male and female LOBs following treatment with adenovirus-Cre for 6 days. CM was used for VEGF ELISA (a) and RNA used for qPCR (b) to confirm sufficient deletion of *Vegf in vitro.* Mean is representative of three separate experiments ± SEM, $p<0.05$* using t-test. Western blot was used to investigate the protein expression of cre recombinase and a band was present in both female and male OBVEGFKO (c). LOBs were imaged using the Zeiss Axioplan fluorescent microscope at 40X magnification, to visualise GFP-expressing transfected cells (d). Scale bar = 100µm.

To study the effect of OBVEGFKO *in vitro*, it was first important to ensure that treating the cells with adenovirus-Cre did not cause osteoblast cell apoptosis. This was investigated using a viability assay and results obtained following OBVEGFKO were compared with WT levels of ATP (adenovirus-GFP). Following OBVEGFKO, there was no significant change in viability in male or female osteoblasts in comparison to WT osteoblasts (figure 5.11a). The adenovirus therefore does not cause osteoblast apoptosis or affect osteoblast proliferation and any significant results following the usage of this conditioned media to treat other cell types can be directly linked to the knockdown of *Vegf* in these osteoblast cells.

In order to look at the potential role of osteoblast-derived VEGF in the regulation of osteoblast cell differentiation via autocrine pathways, an ALP elution assay and stain was used. Deletion of *Vegf* in both male and female LOBs significantly increased ALP activity (figure 5.11b). With the known role of osteoblast-derived VEGF in the regulation of osteoblast differentiation, this increase in ALP elution was surprising and was suggestive of autocrine or intracrine regulation.

On further inspection by western blot, it was shown that both male and female WT and OBVEGFKO did not express detectable protein levels of on VEGFR2 on their cell surface (figure 5.12a). No loading control is shown in this western blot, however the same protein samples were used with different primary antibodies in subsequent westerns (MAPK; data not shown) and showed detectable, consistent levels of protein for both male and female WT and OBVEGFKO. This finding was confirmed by qPCR in which only very low levels of *Vegfr2* mRNA were detected in male and female osteoblasts, in comparison to the MBMEC positive control in which there were very high levels of *Vegfr2* mRNA expressed (figure 5.12b). Therefore, these results suggested that autocrine signalling of osteoblast-derived VEGF was not taking place here and highlighted the growing importance of additional investigations into the directionality of VEGF signalling.

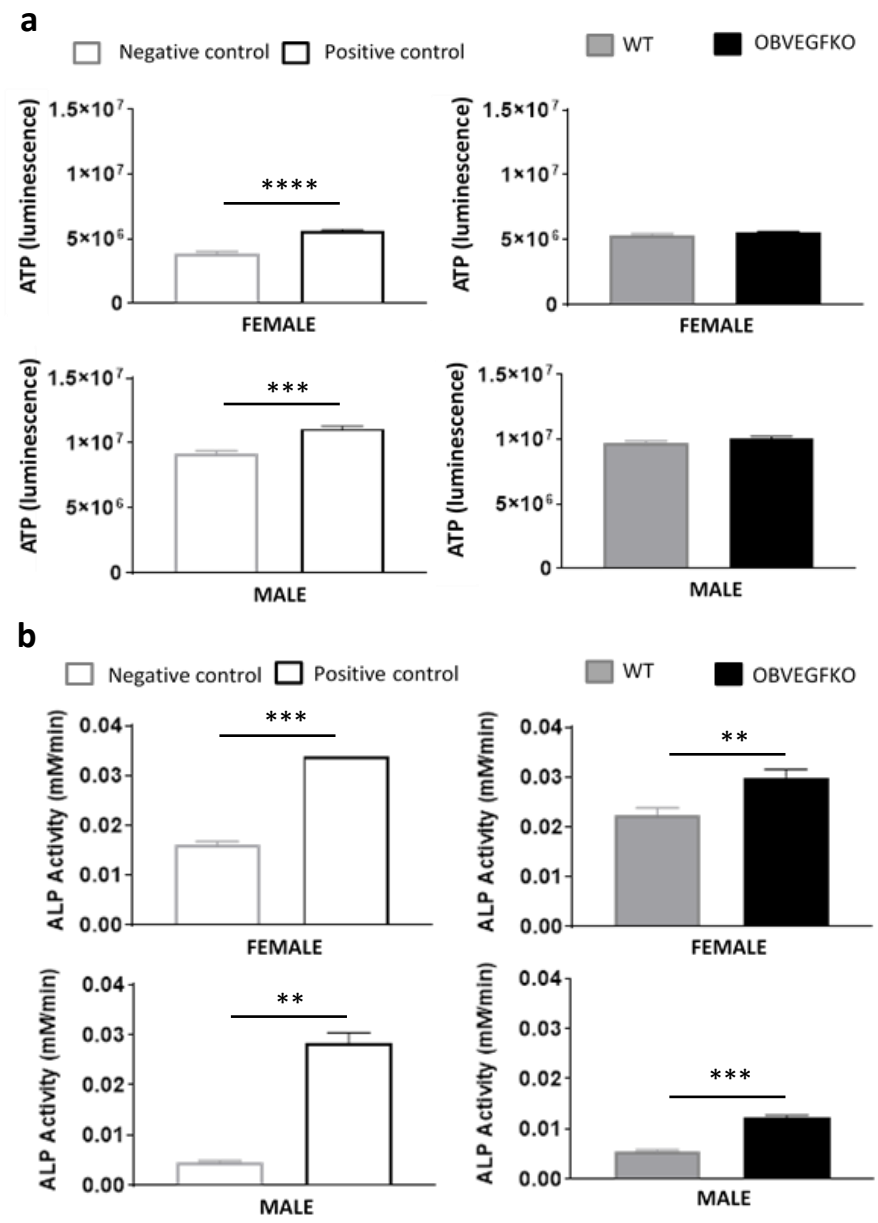

Figure 5.11: Deletion of *Vegf* in male and female osteoblasts does not influence osteoblast viability. Long bone osteoblast cells (LOBs) extracted from the long bones of 4 day old male and female *Vegf* $^{fl/fl}$ mice were infected with adenovirus-GFP or adenovirus-GFP-Cre for 24 hours (viability) in 1% (v/v) FBS low serum media or 6 days (ALP) in 10% (v/v) FBS media. No differences in viability versus WT were evident in LOBs extracted from males or females (a). Control cells received low serum (1%; v/v) media (negative control) and low serum media serum containing 75ng/ml WNT3a (positive control). Data represents mean value from six individual infections ± SEM, p<0.001***, p<0.0001**** using t-test. Significant increases were seen in ALP elution (b) following OBVEGFKO. Control cells received 10% (v/v) FBS media (negative control) and 10% (v/v) FBS containing β-glycerol-phosphate (positive control). Data represents mean value from three individual infections ± SEM, p<01**, p<0.001*** using t-test.

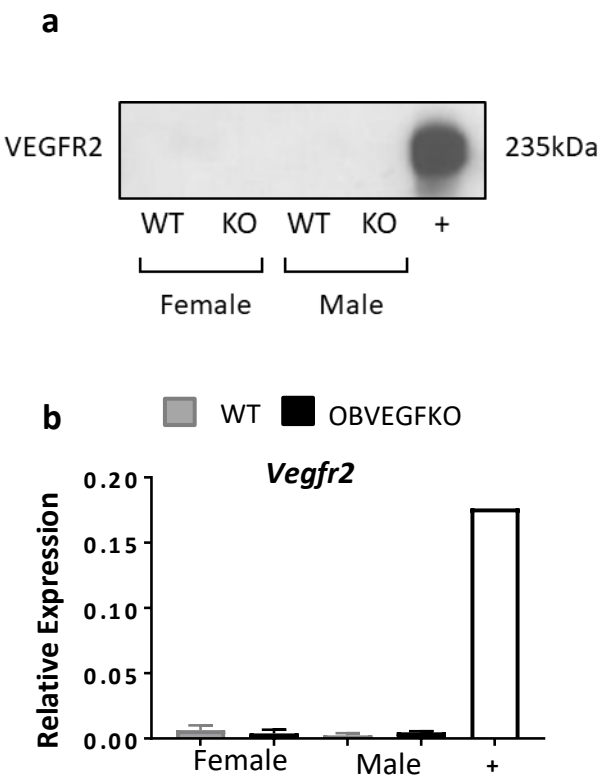

Figure 5.12: No protein and limited mRNA expression of VEGFR2 in male and female LOBs. Western blot confirms the lack of expression of VEGFR2 in osteoblast cell lysates with or without VEGF (a). Endothelial cell lysate is used here as a positive control. qPCR using cDNA reverse transcribed from both OB cell lysates (n=3) and a MBMEC cell lysate as a positive control (+), further confirmed the low levels of *Vegfr2* expression in both male and female OBs (b).

In order to further investigate any changes in osteoblast mRNA which might be contributing to the phenotype recorded following OcnVEGFKO *in vivo,* qPCR was used to look at the expression of a range of additional targets. It was first important to investigate whether the sexually dimorphic bone and vascular phenotype was driven by sex steroid signalling with respective receptors. There were no significant differences identified between sex or genotype when looking at the mRNA expression of the *Ar* (5.13a) and *Esr*1/2 (figure 5.13b; *Esr1* and figure 5.13c; *Esr2*) in male and female WT and OBVEGFKO cells.

Together, OPG and RANKL are involved in the maturation of osteoclast cells from a macrophage to a mature cell. By looking at levels of *Opg* (5.13d) and *Rankl* (5.13e) mRNA expression in both males and females following the deletion of osteoblast-derived *Vegf*, it was possible to study potential effects of OBVEGFKO on the osteoclast cell development and remodelling in both sexes. No differences in expression of either gene were identified versus WT here, however.

Sclerostin is a known negative regulator of osteogenesis and its expression was also investigated by qPCR. Although *Sost* mRNA expression appeared to be upregulated in OBVEGFKO males versus WT, in both males and females the findings were non-significant (5.13f).

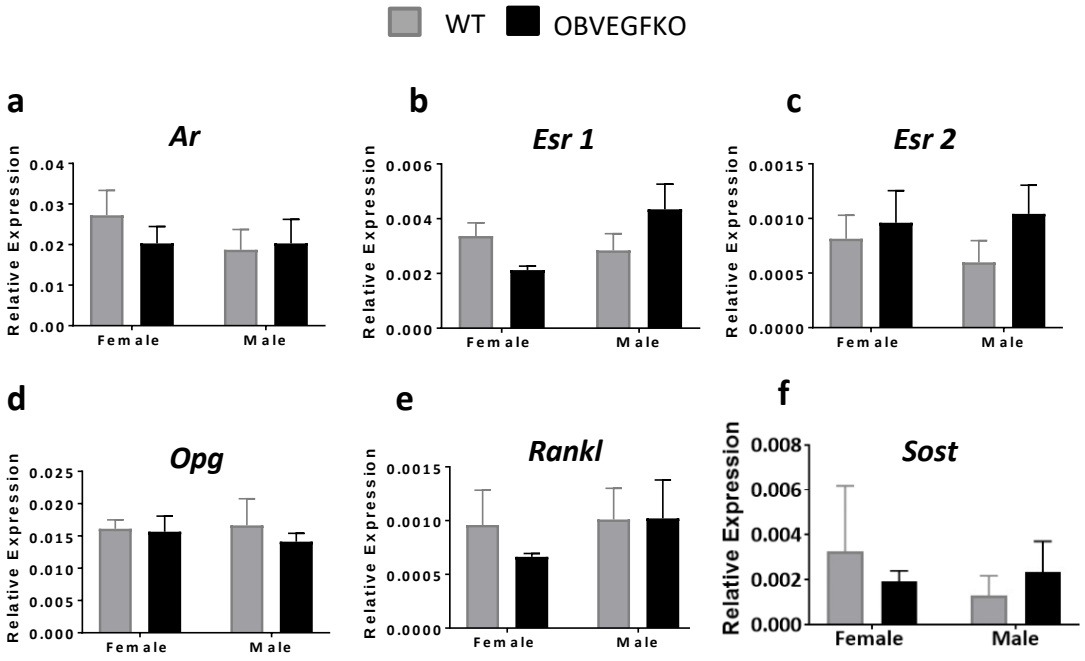

Figure 5.13: No notable changes in gene expression following OBVEGFKO. qPCR investigations also showed no significant alterations in gene expression of androgen receptor (*Ar*; a), estrogen receptor 1 (*Esr1*; b) or estrogen receptor 2 (*Esr2*; c) in male and female osteoblasts following OBVEGFKO. The involvement of osteoclasts in the phenotype was investigated by looking at relative expression of *Opg* (d) and *Rankl* (e), where no significant changes in mRNA expression were identified following OBVEGFKO. *Sost* expression was also unchanged. Data represents mean value from three individual infections ± SEM, using t-test.

5.4 Discussion

Although it is difficult to completely eliminate the effect of sex hormones without doing an ovariectomy or orchidectomy, the study of juvenile mice has provided a means of examining the bone phenotype in animals in which the concentration of sex hormones is low. Prior to puberty, oestrogen and testosterone are up-regulated first in mice between 5 and 7 weeks of age and as a result, 4 week old pre-pubertal mice were chosen for this analysis of young mice. Equally, the 16 week old mice used in previous studies were old enough to ensure that they had gone through puberty, which occurs at 8.5-9 weeks of age in mice (Drickamer, 1981, Callewaert et al., 2010b).

Using high-resolution micro-CT it was shown that following the conditional deletion of *Vegf in vivo*, there were no significant changes in volume cortical porosity. Although, as per 16 week old mice, in 4 week old mice the porosity following *Vegf* deletion was higher versus WT in males and females. When interrogating the cortical porosity further and separating the blood vessel canals from the osteocyte lacunae, the only significant difference identified in either fraction was a significant increase in the volume and proportion of intracortical canals in male OcnVEGFKO mice versus WT. This was the first indication that perhaps the control of sexual dimorphism was multi-factorial and involved other factors aside from sex hormones, as the canal phenotype that was seen in adult mice was still observed in 4 week old pre-pubertal mice. In both male and female 4 week old WT mice, the bone cortex appeared to be filled by copious levels of canals, however the intracortical canal volume was only significantly higher than that of 16 week old mice in females. This difference in canal volume was unsurprising as bone remodelling and angiogenesis is very active during development and numerous studies have shown that young animals have increased vasculature in comparison to older animals (Burkhardt et al., 1987, Lu et al., 2008).

In contrast to the changes in bone geometry identified in adult whole bone however, in 4 week old animals significant differences were observed in males along the tibia length. Where in 16 week old mice it was the females that had alterations in multiple measures of bone geometry along the tibia length following conditional *Vegf* deletion, in female 4 week old mice there was only one area of significance identified in ellipticity. The areas of significance identified for geometric measurements in female 16 week old mice, were all

insignificant in these younger animals and instead there were significant differences in CSA, Ct.Th, ellipticity, J and Imax in male knockout animals versus WT littermate controls. Many of these changes in geometry were localised to the tibiofibular junction, confirming it as being a good location for in depth phenotypic analysis of bone traits in young animals as well as older animals. This data suggested that during maturation, male knockout mice are perhaps able to 'correct' their dysfunctional bone geometry but compromise their cortical porosity as a result, whereas the alterations in bone geometry are intensified with in females with increased age.

With the study of juvenile mice still showing that OcnVEGFKO initiates some forms of sexual divergence, albeit on a lesser scale that in adult mice, *in vitro* studies enabled experiments to be carried out in the absence of the circulating sex hormones that would be present *in vivo.* Here, adenovirus-Cre was used to delete *Vegf* from primary male and female *Vegf*$^{fl/fl}$ osteoblasts (OBVEGFKO). The direct effect of VEGF on osteoblast cells was examined here and results obtained suggested that VEGF does not signal directly with osteoblasts, consistent with previous studies (Clarkin et al., 2008b). The lack of VEGFR2 on osteoblast cells also confirmed that VEGF must interact with other cell types in a paracrine manner, or indeed via intracrine pathways in the control of osteogenesis (Liu et al., 2012). In both males and females it was also proven that there were no significant changes in the mRNA expression of *Ar* or *Esr1 and Esr2* following OBVEGFKO, which provided further evidence to suggest that additional factors other than sex hormones were responsible for sexual dimorphisms observed *in vivo*.

Supplementing these *in vitro* studies and also the preliminary investigations into bone mineralisation in male and female WT and OcnVEGFKO bones during this PhD, complementary research using Raman spectroscopy (Raman and Krishnan, 1928) has been performed in our lab (Goring et al., 2019). This has enabled investigations into the effect of osteoblast-specific *in vitro* OBVEGFKO on mineral matrix composition. Raman is a highly sensitive fingerprinting technique that has been used in the past in our lab to analyse primary bone cell cultures (Smith et al., 2017). *Vegf* was deleted *in vitro* here from *Vegf*$^{fl/fl}$ LOBs in males and females, as described in this chapter. Here, deletion of *Vegf* in LOBs resulted in a large-scale upregulation of the immature calcium species amorphous calcium phosphate (Figure 5.14a ACP; +23.6 fold). Conversely in females, there was the largest upregulation in carbonated appetite (Figure 5.14c CAP; +10.5 fold), a mature calcium

species. Equally, mineral/matrix levels were significantly increased (figure 5.14d) in females and significantly decreased in males after OBVEGFKO (Goring et al., 2019). This suggested that females were able to compensate for the loss of *Vegf* by increasing the production of CAP, but males are not (figure 5.14e) and these changes observed were independent of cell number (figure 5.14f). This adds value to the results presented in this thesis as these effects were present despite the fact this study was also performed *in vitro*, in the absence of circulating sex hormones. The fact that defects in mineralisation in OBVEGFKO males were present both *in vitro* and *in vivo* suggested that although sex hormones must play a part in some of the sexual dimorphisms observed, it is incredibly likely that other factors must also be contributing to this divergence.

Based on these studies in which sexual dimorphisms have been identified in the matrix mineral *in vitro* following OBVEGFKO (Goring et al., 2019) and on the fact sexual dimorphisms in vascular canals do exist in OcnVEGFKO pre-pubertal mice, it can be ascertained that the sex-specific effects of VEGF deletion identified in adult mice are not purely regulated by sex hormones. Although hormones may play a role in this process, there must be alternative genes or factors regulating this bone phenotype in addition. Total removal of the effect of sex hormones via an ovariectomy or orchidectomy (Kodama et al., 2004, Pufe et al., 2007, Yeh et al., 1996) would be beneficial in order to define the absolute role of sex hormones in the expression of this vascular phenotype. However, the cost and licenses required to do this sort of experiment were not feasible for this PhD project and therefore, alternative methods such as those detailed within this chapter were utilised.

Following investigations into the direct effects of VEGF on osteoblast cells in both males and females within this chapter, the next and final chapter will look at the paracrine interactions of osteoblast-derived VEGF with endothelial cells. This will attempt to identify alterations in endothelial cell gene expression following the deletion of osteoblast-derived *Vegf* and potentially pinpoint specific targets in both sexes, which could be used for therapeutics in the future.

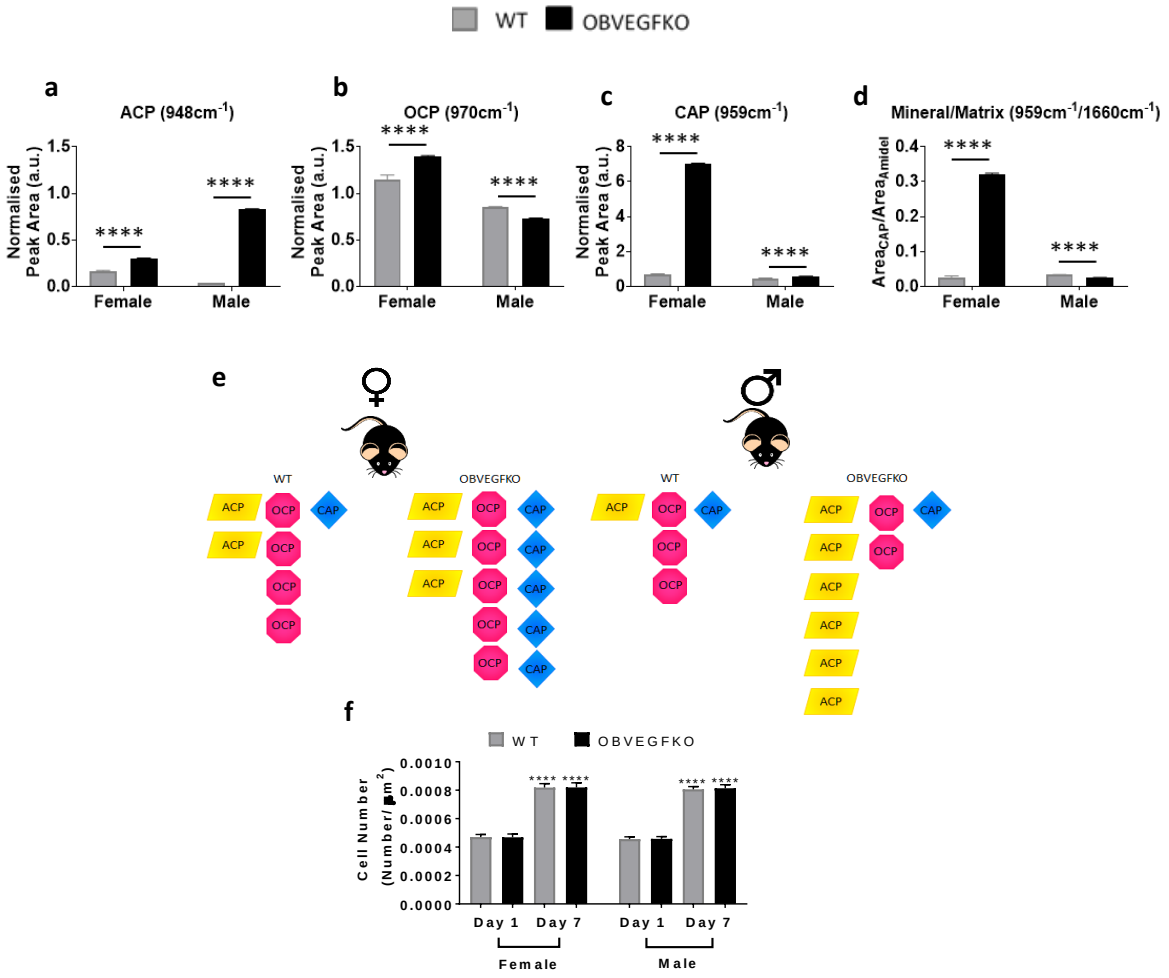

Figure 5.14: Deletion of *Vegf* in male and female osteoblasts compromises matrix mineralisation. Raman spectroscopy was able to detect clear and significant gender differences (between immature (ACP; a), intermediate (OCP; b) and mature (CAP; c) calcium species in WT and OBVEGFKO cells. Mineral/matrix ratio also shows a significant increase in matrix maturity following OBVEGFKO in females whereas the converse is exhibited in males (d). Schematic representation of the changes in calcium phosphate species in WT and OBVEGFKO cells are shown (e). Error bars indicate mean value ± SEM, p<0.01**, p<0.0001**** using t-test, n=50 spectra from each treatment group. For investigations into the effect of transfection on cell number, cells were infected with adenovirus-GFP or adenovirus-Cre-GFP for 6 days and fixed with 4% (w/v) paraformaldehyde. Hoechst 33342 was used to stain cells to highlight cell nuclei, prior to counting (f). Data represents mean number of nuclei per µm^2 ± SEM, p<0.0001**** using Two-Way ANOVA, n=20 fields of view per group. **Raman performed by Aikta Sharma (Goring et al., 2019).**

Chapter 6 Results IV – Investigating indirect effects of osteoblast *Vegf* deletion in males and females on endothelial cell function

6.1 Introduction

The paracrine interactions between osteoblast-VEGF and vascular endothelial cells in the promotion of angiogenesis have been recognised for many years (Carmeliet et al., 1996, Ferrara et al., 1996, Harada et al., 1994). *In vitro*, endothelial cells have shown to express high protein levels of VEGFR2 and it has been suggested that OBs and vascular endothelial cells communicate with each other, as well as VEGF having an indirect effect on osteoblast cells via the vascular endothelium (Clarkin et al., 2008a). Therefore, it was important to investigate whether any of the sexually dimorphic mechanisms regulating the bone phenotype distinctly in males and females were driven indirectly by vascular endothelial cells. These additional *in vitro* studies enabled further analysis of the role of sex hormones in the presence of the sexual divergences observed in the *in vivo* phenotype, as circulating sex hormones are characteristically low *in vitro*.

One of the main functions of VEGF is in the upregulation of vasculogenesis and angiogenesis. In many biological processes such as endochondral ossification, bone remodelling and fracture healing, the action of VEGF is therefore essential. Recent work has suggested that it is predominantly VEGF-A from early osteoblast lineage cells (osterix positive) that is essential for both angiogenesis and the rapid formation of immature woven bone post-fracture (Buettmann et al., 2019). However, over-production or under-production of osteoblast derived VEGF can have severe consequences and is often associated with the onset of pathologies. Bone diseases such as osteoporosis have been associated with a diminished level of haematopoiesis and a decrease in the number of arterial capillaries for many years (Burkhardt et al., 1987). On the contrary, proliferation of vascular endothelial cells as a result of an up-regulation in the levels of VEGF has been associated with tumour formation and the onset of cancer (Morikawa et al., 2002, McDonald and Foss, 2000). These new blood vessels produced are non-typical to those

produced during healthy angiogenesis and promote both resistance to chemotherapy and the spreading of the cancer around the body (as reviewed by Schito, 2019). Therefore, functional VEGF signalling with vascular endothelial cell receptors is essential for the maintenance of health.

Given the proven association with differential gene expression and the presence of sexual dimorphisms from a very early stage in development (Bermejo-Alvarez et al., 2010), identifying changes in gene expression in endothelial cells following OBVEGFKO in males and females enables examination of potential mechanisms involved in the onset of this vascular phenotype. The vasculature has already been proven to be dysfunctional in terms of morphology in the male OcnVEGFKO mouse model and therefore it was predicted that that endothelial genes which are up or down regulated following OBVEGFKO may then signal back to osteoblast cells to indirectly affect osteogenesis in a pathogenic manner.

As previously discussed, the isolation of primary endothelial cells from bone is challenging and therefore MBMECs are commonly used as a substitute (Liu et al., 2014, Masek and Sweetenham, 1994). The study of the indirect effect of OBVEGFKO in males and females on changes in MBMEC mRNA expression is facilitated by using gene profiler arrays. The arrays selected enabled the study of a large subset of genes, including those implicated in skeletal development, bone mineral metabolism, the maintenance of the extracellular matrix, angiogenesis, inflammation, apoptosis, cell adhesion, growth factors and transcription factors. This large-scale screening of 164 genes in total therefore facilitated the identification of specific endothelial cell targets which were regulated in a sex-specific manner and may be responsible for the observed phenotype *in vivo.* Identification of specific targets which are altered in endothelial cells following OBVEGFKO and understanding the mechanisms involved could prove to be instrumental in the development of therapeutics for the treatment of degenerative bone diseases in the future.

The final aim was to investigate the indirect effects of osteoblast *Vegf* deletion in males and females on endothelial cell function.

OBVEGFKO cell media from male and female bones will be collected and added to endothelial cell cultures

CM experiments

- Viability, BrdU, gene expression, angiogenic array and osteogenic array

Osteoblast-derived Vegf will be deleted in vivo (Ocn VEGFKO) and CD31/sclerostin/VEGFR2 expressing cells immunolabelled

6.2 Methodology

6.2.1 MBMEC culture

Primary C57BL/6 MBMEC's from Generon were cultured in T75 flasks until confluent, after following the protocols provided. Endothelial cell basal media was used to resuspend the cells, with growth factors and supplements provided by Generon. Cells were split (see methods 2.6.1) and grown until reaching 90% confluence.

6.2.1.1 Treatment with conditioned media

Male and female WT and OBVEGFKO conditioned media collected from adenoviral treated LOBs was used to treat the MBMECs (Figure 6.1).

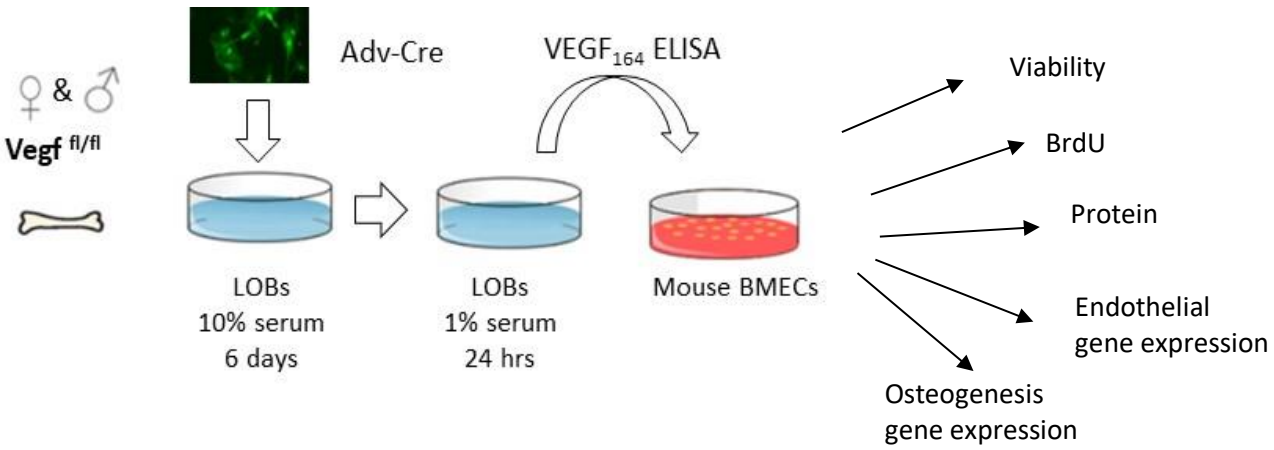

Figure 6.1: Schematic detailing the methodology used to investigate the indirect effect of deleting osteoblast-derived *Vegf*. *Vegf* was deleted from LOBs, extracted from P4 *Vegf*$^{fl/fl}$ mice. LOBs were treated with Adenovirus-Cre (Adv-Cre) for 6 days, prior to being stepped down in 1% FBS (v/v) media for 24 hours. Conditioned media was collected and once *Vegf* deletion was confirmed, it was used to treat MBMECs for 24 hours. These MBMECs were then used to analyse the effect on viability, protein expression and gene expression (qPCR).

6.2.1.2 MBMEC proliferation assay

BrdU Cell Proliferation ELISA kit was used for quantification of mouse bone marrow endothelial MBMEC cell proliferation. 20µl BrdU was added to each well for 6 hours, in order for proliferating cells to incorporate BrdU into their DNA. To allow the antibody to bind to BrdU incorporated cells, they were fixed, permeabilized and their DNA denatured

by the 'fixing solution'. This solution is part of the BrdU kit containing ethanol and sodium hydroxide, allowing these three phases to be carried out in one singular step. Each well was washed and incubated with anti-BrdU primary detector antibody at room temperature for one hour. The wells were washed again and 100µl of goat anti-mouse IgG HRP conjugate antibody was added to each well for 30 minutes at room temperature. Following an additional wash, 100µl of tetra-methylbenzidine (TMB) solution was added to each well and incubated for 30 minutes in the dark, until wells which contained BrdU positive cells were visible as a blue colour. 100µl stop solution was then added to each well and the colour of positive wells changed from blue to yellow. The plate was read in the spectrophotometer at 450nm.

6.2.2 Endothelial cell gene arrays

Qiagen RT^2 profiler PCR Arrays for Mouse Endothelial Cell Biology (figure 6.2) and Mouse Osteogenesis (figure 6.3) were used and the manufacturer's instructions followed. Analysis was performed using Opticon Monitor 3 and the Qiagen analysis centre was used to calculate fold changes in comparison to the control. Housekeeping genes *Gapdh,* beta actin (*Actb)*, beta glucuronidase (*Gusb*), heat shock protein 90 alpha (*Hsp90ab1)* and beta-2 microglobulin (*B2m)* were utilised by the Qiagen analysis centre to normalise the data to. One biological repeat was carried out for male and female WTs and OBVEGFKOs, as well as controls. Further detail on the genes studied in both arrays are listed in appendix C.3.

	1	2	3	4	5	6	7	8	9	10	11	12
A	Ace	Adam17	Agt	Agtr1a	Angpt1	Anxa5	Apoe	Bax	Bcl2	Bcl2l1	Casp1	Casp3
B	Cav1	Ccl2	Ccl5	Cdh5	Cflar	Col18a1	Cradd	Cx3cl1	Cxcl1	Cxcl2	Cxcr5	Edn1
C	Edn2	Ednra	Eng	F2r	F2rl1	F3	Fas	Fasl	Fgf1	Fgf2	Flt1	Fn1
D	Hif1a	Icam1	Il11	Il1b	Il3	Il6	Il7	Itga5	Itgav	Itgb1	Itgb3	Kdr
E	Kit	Mmp1a	Mmp2	Mmp9	Nos3	Nppb	Npr1	Ocln	Pdgfra	Pecam1	Pf4	Pgf
F	Plat	Plau	Plg	Procr	Ptgis	Ptgs2	Sele	Sell	Selp	Selplg	Serpine1	Sod1
G	Tek	Tfpi	Tgfb1	Thbd	Thbs1	Timp1	Tnf	Tnfsf10	Tymp	Vcam1	Vegfa	Vwf
H	Actb	B2m	Gapdh	Gusb	Hsp90ab1	MGDC	RTC	RTC	RTC	PPC	PPC	PPC

Figure 6.2: Gene layout for the mouse endothelial RT^2 profiler PCR Array. 96 well plate containing 84 endothelial genes selected by Qiagen, 5 housekeeping genes and 6 controls.

	1	2	3	4	5	6	7	8	9	10	11	12
A	Acvr1	Ahsg	Alpl	Anxa5	Bglap	Bgn	Bmp1	Bmp2	Bmp3	Bmp4	Bmp5	Bmp6
B	Bmp7	Bmpr1a	Bmpr1b	Bmpr2	Cd36	Cdh11	Chrd	Col10a1	Col14a1	Col1a1	Col1a2	Col2a1
C	Col3a1	Col4a1	Col5a1	Comp	Csf1	Csf2	Csf3	Ctsk	Dlx5	Egf	Fgf1	Fgf2
D	Fgfr1	Fgfr2	Flt1	Fn1	Gdf10	Gli1	Icam1	Igf1	Igf1r	Ihh	Itga2	Itga2b
E	Itga3	Itgam	Itgav	Itgb1	Mmp10	Mmp2	Mmp8	Mmp9	Nfkb1	Nog	Pdgfa	Phex
F	Runx2	Serpinh1	Smad1	Smad2	Smad3	Smad4	Smad5	Sost	Sox9	Sp7	Spp1	Tgfb1
G	Tgfb2	Tgfb3	Tgfbr1	Tgfbr2	Tgfbr3	Tnf	Tnfsf11	Twist1	Vcam1	Vdr	Vegfa	Vegfb
H	Actb	B2m	Gapdh	Gusb	Hsp90ab1	MGDC	RTC	RTC	RTC	PPC	PPC	PPC

Figure 6.3: Gene layout for the mouse osteogenesis RT^2 profiler PCR Array. 96 well plate containing 84 endothelial genes selected by Qiagen, 5 housekeeping genes and 6 controls.

6.2.3 Immunostaining

In order to further interrogate the vasculature (CD31), VEGFR2 and sclerostin (negative regulator of osteogenesis) expression in 16 week old mice, cryo-sections of bone were immunolabelled.

6.2.3.1 Sample preparation

Tibiae were harvested from adult mice and muscle gently removed. Bones were fixed in pre-chilled methanol-free 4% (w/v) PFA for 4 hours (4 °C) and agitated on a tube roller. Fixative was removed and bones washed twice in PBS for 30 minutes each time. Bones were then washed in dH_2O twice for 5 minutes. 0.5M EDTA solution was used to initiate the decalcification of the tibiae (4**°**C with continuous shaking). After 24 hours, bones were washed with dH_2O and PBS. They were then treated with a solution of 20% (w/v) sucrose, 2% (w/v) Polyvinylpyrrolidone in PBS at 4 °C. Tibiae were cryo-embedded and thick cryo sections of 30µm cut. Solutions used for this process are documented in appendix B.

6.2.3.2 Antibody incubation

Immunostaining was performed in a humid chamber. Sections were air dried for an hour and permeabilised for 10 minutes (0.3% (w/v) triton PBS). They were then blocked for 1 hour with 5% (v/v) goat serum for CD31 and VEGFR2 and 5% (v/v) donkey serum for sclerostin. A PAP water-resistant pen was used to draw around bone sections and rat anti-mouse CD31 primary antibody (1:40) was added to each section, excluding the negative control. For sclerostin, the goat anti-mouse primary antibody was diluted 1:50 and for VEGFR2, the rabbit IgG primary antibody was diluted 1:800. Sections were incubated with

the respective antibody overnight at 4°C. Sections were washed in PBS three times and Alexa Fluor 488 goat anti-rat (1:400), Alexa Fluor 555 donkey anti-goat (1:300) and Alexa Fluor 488 goat anti-rabbit (1:300) were used as secondary antibodies for CD31, sclerostin and VEGFR2 respectively. Following PBS washes, nuclei were stained with Hoechst 33342 (1:10000) and sections mounted using FluoromountG. Imaging was performed using a Zeiss Axioplan2 microscope.

6.3 Results

6.3.1 Deletion of osteoblast-derived *Vegf in vitro* does not affect mouse bone marrow endothelial cell viability or proliferation

By performing an *in vitro* deletion of *Vegf* in male and female osteoblast cells and subsequently treating MBMECs with the conditioned media collected from WT and OBVEGFKO cells (figure 6.4), it was possible to investigate the indirect paracrine effect of VEGF on MBMECs.

Despite there being a high level of OBVEGF deletion in both male and female LOBs of above 90% on average in males and females, treatment of MBMEC with male and female OBVEGFKO conditioned media did not significantly affect either MBMEC proliferation (figure 6.5a) or cell viability (figure 6.5b) when compared to WT controls.

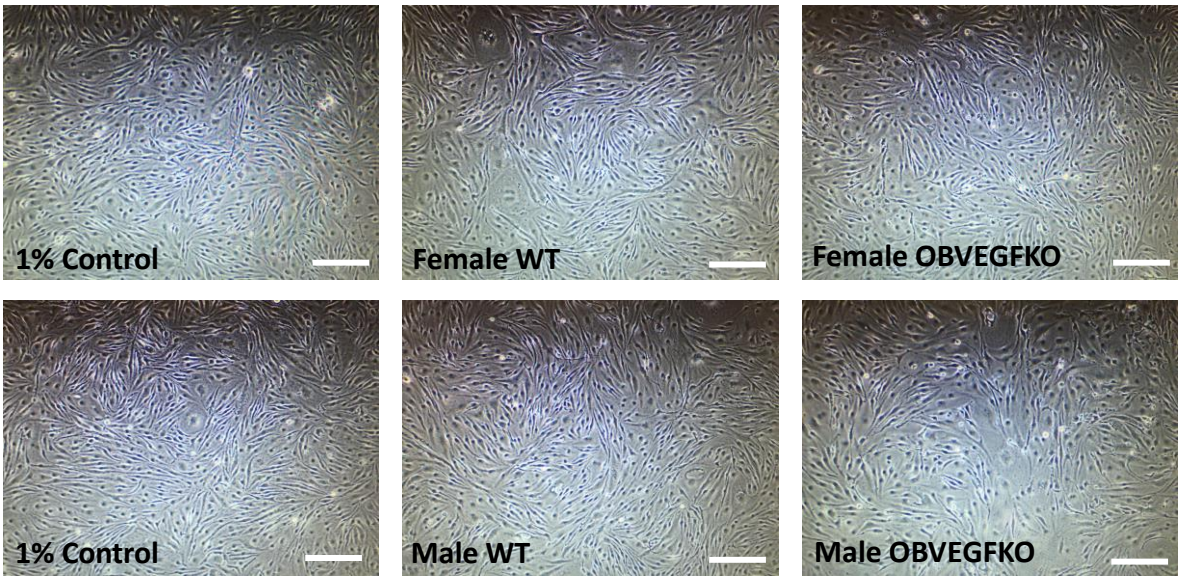

Figure 6.4: No differences observed in MBMECs treated with conditioned media collected from WT and VEGFKO LOBs. Following confirmation of VEGF deletion in OBVEGFKO cells, WT (adenovirus-GFP treated LOBs) and OBVEGFKO (adenovirus-Cre treated LOBs) conditioned media was collected and used to treat MBMECs for 24 hours. 1% (v/v) FBS media was used as a control. Images were taken with the EVOS microscope (10X). Scale bar = 500µm.

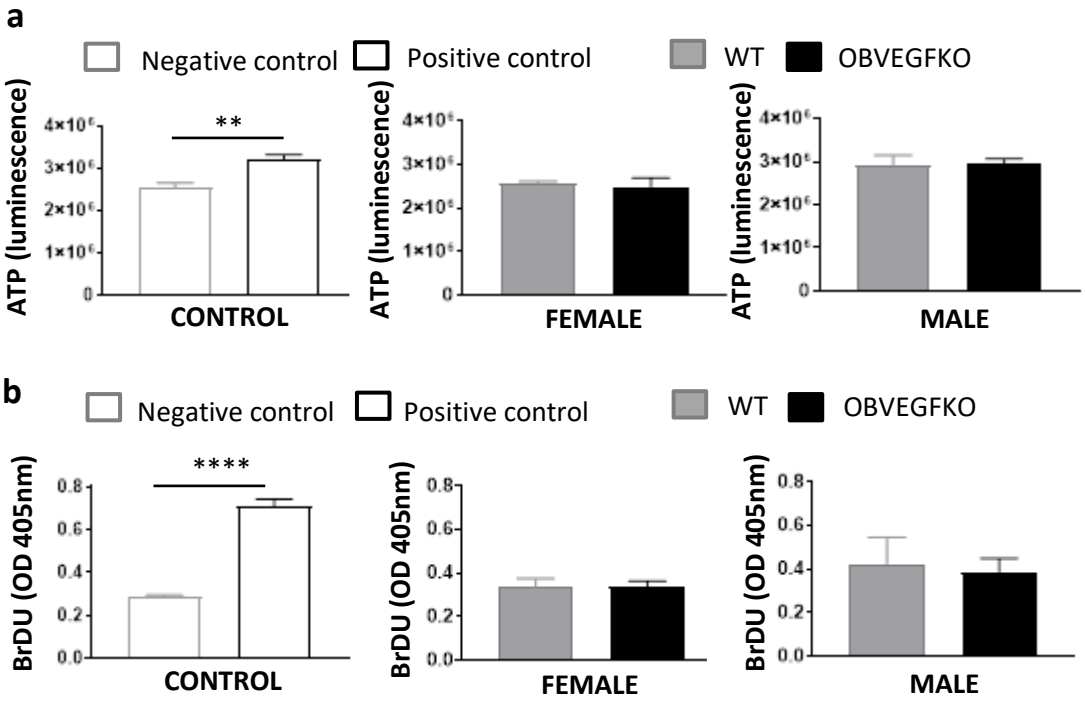

Figure 6.5: Deletion of *Vegf* in male and female osteoblasts does not influence endothelial cell viability or proliferation. MBMECs) were treated with conditioned media collected from male and female WT and OBVEGFKO LOBs for 24 hours. Viability (ATP; a) and proliferation (BrDU; b) assays were carried out. Low serum (1% v/v; negative control) and high serum (10% v/v; positive control) media was used as controls. Data represents n=6 replicates ± SEM, $p<0.01$**, $p<0.0001$**** using t-test.

6.3.2 High levels of VEGFR2 expression in bone marrow derived endothelial cells

In LOBs, the lack of VEGFR2 protein expression detected by western blot suggested that osteoblasts do not have VEGFR2 on their cell surface. Therefore, the expression of VEGFR2 in MBMECs which had been treated with WT and OBVEGFKO conditioned media collected from osteoblast cells was investigated. This enabled investigations into potential paracrine effects of VEGF on endothelial cells.

Unlike in LOBs, high levels of VEGFR2 protein expression were identified in all MBMEC lysates. Following the treatment of MBMECs with OBVEGFKO conditioned media for 5 minutes, higher levels of VEGFR2 protein expression was evident in OBVEGFKO in comparison to WT controls in the results presented below. In MBMECs treated for 24 hours with OBVEGFKO conditioned media however, the levels of VEGFR2 protein expression were reduced below versus WT controls (figure 6.6).

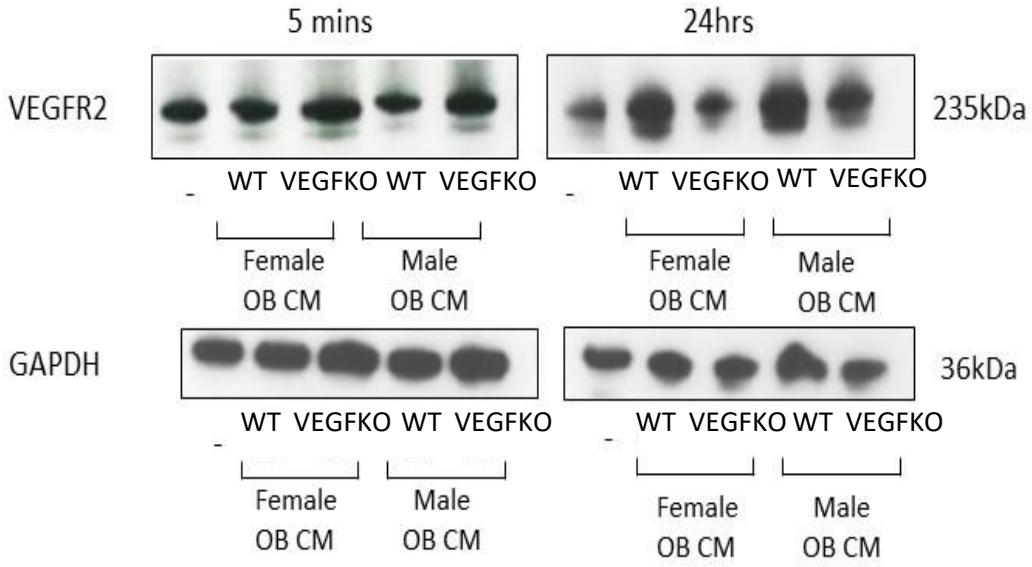

Figure 6.6: VEGFR2 protein is expressed by MBMECs, but not long bone derived osteoblast cells. For investigation into VEGFR2 expression, MBMECs were treated for either 5 minutes or 24hrs with OBVEGFKO conditioned media, WT osteoblast conditioned media or 1% (v/v) low serum media (-). Total VEGFR2 protein was assessed by Western blotting. GAPDH expression was measured as a loading control. Data representative of one biological repeat.

6.3.3 Sexually dimorphic expression of endothelial and osteogenic genes in MBMECs following *Vegf* knockout in male and female long bone osteoblast cells

To further investigate the indirect effect of OBVEGFKO in males and females on endothelial cell function *in vitro*, an 'endothelial' and 'osteogenesis' qPCR array was carried out. This enabled identification of any alterations in MBMEC gene expression as a result of *Vegf* deletion in osteoblast cells. In addition, comparisons were also made between MBMECs treated with male and female WT conditioned media versus those treated with 1% (v/v) FBS basal media (control). This acted as a control and enabled evaluation of the effect of the addition of adenovirus-GFP to male and female LOBs (WT; without Cre) on endothelial cells. A list of genes studied and abbreviations are listed in appendix C.3 and C.4.

Following treatment of MBMEC with OBVEGFKO and WT conditioned media for 24 hours, osteogenic and endothelial cell biology gene arrays showed major upregulations and downregulations in many genes produced by endothelial cells, which may be linked to the phenotype that has been observed in the *in vivo* VEGF knockout studies (table 6.1). Many of these changes in gene expression were sex-specific, which was of particular interest to this study given the previously identified sexual dimorphisms *in* vivo. When comparing MBMECs treated with male and female WT LOB conditioned media with those treated with 1% (v/v) FBS control media, levels of Insulin-like growth factor-1 (*Igf1)* expression were upregulated in male (+1.05 fold) and downregulated in female WTs (-4.01 fold) versus those treated with 1% (v/v) control media. In contrast and consistent with an indirect effect of VEGF on bone existing via the vasculature, endothelial cells treated with conditioned medium from male OBVEGFKO cells showed decreased levels of *Igf1* expression (-2.33 fold) versus WT, in contrast to the MBMEC treated with conditioned medium from female OBVEGFKO in which *Igf1* mRNA expression was increased versus WT (+3.07 fold). IGF-1 has previously been identified as a primary factor involved in the expression of skeletal dimorphism and therefore, changes in endothelial cell gene expression such as this following OBVEGFKO could be potentially contributing to the skeletal phenotype observed following in vitro OcnVEGFKO.

Other genes differentially expressed in MBMEC following OBVEGFKO in males and females included angiogenic growth factors such as Transforming Growth Factor-β1 (*Tgf-β1*) and

placental growth factor (*Pgf*). In MBMECs treated with male OBVEGFKO conditioned media, both of these factors were upregulated in comparison to WT controls (+1.5 fold and +2.26 fold respectively). When MBMECs were treated with female OBVEGFKO conditioned media however, both of these angiogenic factors were downregulated versus WT (-1.01 fold and -1.46 fold respectively). In endothelial cells treated with male OBVEGFKO conditioned media, the mRNA expression of numerous other adhesion molecules such as vascular cell adhesion protein 1 (*Vcam*; +1.43 fold) and platelet cell adhesion molecule (*Pecam* or CD31; +2.03 fold) was also upregulated. Additionally, the endothelial cell expression of genes with a role in angiogenesis such as *P-selectin* (-1.42 fold) and Thymidine Phosphorylase (*Tymp*), *Fgf1* (-1.13 fold) and *Fgf2* (-1.01 fold) was downregulated versus WT following treatment with male OBVEGFKO conditioned media. The combined effect of the differential expression of multiple genes therefore may be responsible for the increased vasculature seen in male OcnVEGFKO mice *in vivo*.

The osteogenesis genetic profile array also indicated an upregulation of sclerostin (*Sost*), a negative regulator of osteogenesis, following OBVEGFKO in both females (+6.58 fold) and males (+3.21 fold). Following OBVEGFKO, endothelial cell expression of pro-osteogenic genes such as Bone Gamma-carboxyglutamic Acid-containing Protein (*Bglap; Ocn*), Biglycan (*Bgn*), Distal-Less Homeobox 5 (*Dlx5*), Runt Transcription Factor 2 (*Runx2*) and osterix (*Sp7; Osx*) were more highly upregulated in females than in males versus WT. It is possible therefore that females are able to counteract the higher endothelial cell mRNA expression of *Sost* by upregulating the expression of other genes which are vital in bone development, therefore meaning that their bone phenotype is less severe.

Data was plotted as graphical heat maps to compare the control study (WT versus 1% (v/v) control), as well as OBVEGFKO versus WT in females (figure 6.7) and males (figure 6.8). In the control, for both the osteogenesis and angiogenesis gene array, the heat maps for males and females was largely dominated by down regulated gene expression in endothelial cells (green). In contrast in both males and females there was generally large levels of upregulation, with heat maps predominantly red when comparing OBVEGFKO with WT treated MBMECs.

Table 6.1: Summary of key changes in MBMEC gene expression following treatment with male and female OBVEGFKO and WT CM. Endothelial and osteogenesis gene array utilised for analysis. Results displayed as fold change, showing genes upregulated (red) and downregulated (green) versus WT.

Gene	Female KO vs WT OB CM (fold change)	Male KO vs WT OB CM (fold change)	Function
Igf1	3.07	-2.33	Bone growth and development
Fgf2	1.11	-1.01	Angiogenic factor
Fgf1	1.09	-1.13	Angiogenic factor
Flt1 (VEGFR1)	-1.01	-1.09	Vasculogenesis and angiogenesis
Hif1-alpha	1.22	-1.32	Response to hypoxia, upregulates VEGF
Pdgfra	1.22	-1.08	Tyrosine kinase, binds PDGF
Kdr/VEGFR2	1.04	-1.32	Predominant VEGF receptor
Tymp	1.19	-2.13	Promotes angiogenesis
Selpg/P-selectin	3.52	-1.42	Cell adhesion molecule important in angiogenesis
Bglap (Ocn)	3.48	1.06	Secreted by OB regulates remodelling
Bgn	2.16	1.45	Proteoglycan playing a role in bone growth
Bmp6	-1.14	3.21	Induces cartilage and bone formation
Dlx5	4.95	1.92	Bone development, fracture healing, triggers OB development
Nppb	2.94	-2.87	Cardiovascular homeostasis, mutations associated with osteoporosis
Tgf-beta 1	-1.01	1.25	Angiogenic growth factor
Runx2	3.43	-1.55	Osteoblast differentiation and skeletal morphogenesis.
Sost	6.58	3.21	Produced by osteocytes, inhibits bone formation
Sox9	5.54	4.01	Important in skeletal development and sex determination
Sp7 (Osx)	2.26	1.5	Needed for osteoblast differentiation and bone formation
Pcam	1.07	2.05	Cell adhesion molecule
Vcam	-1.07	1.43	Cell adhesion molecule
Pgf	-1.46	2.26	Angiogenic growth factor
Twist1	5.06	1.53	Early development
Vdr	2.1	1.47	Encodes receptor for vit D3, formation of bones and teeth

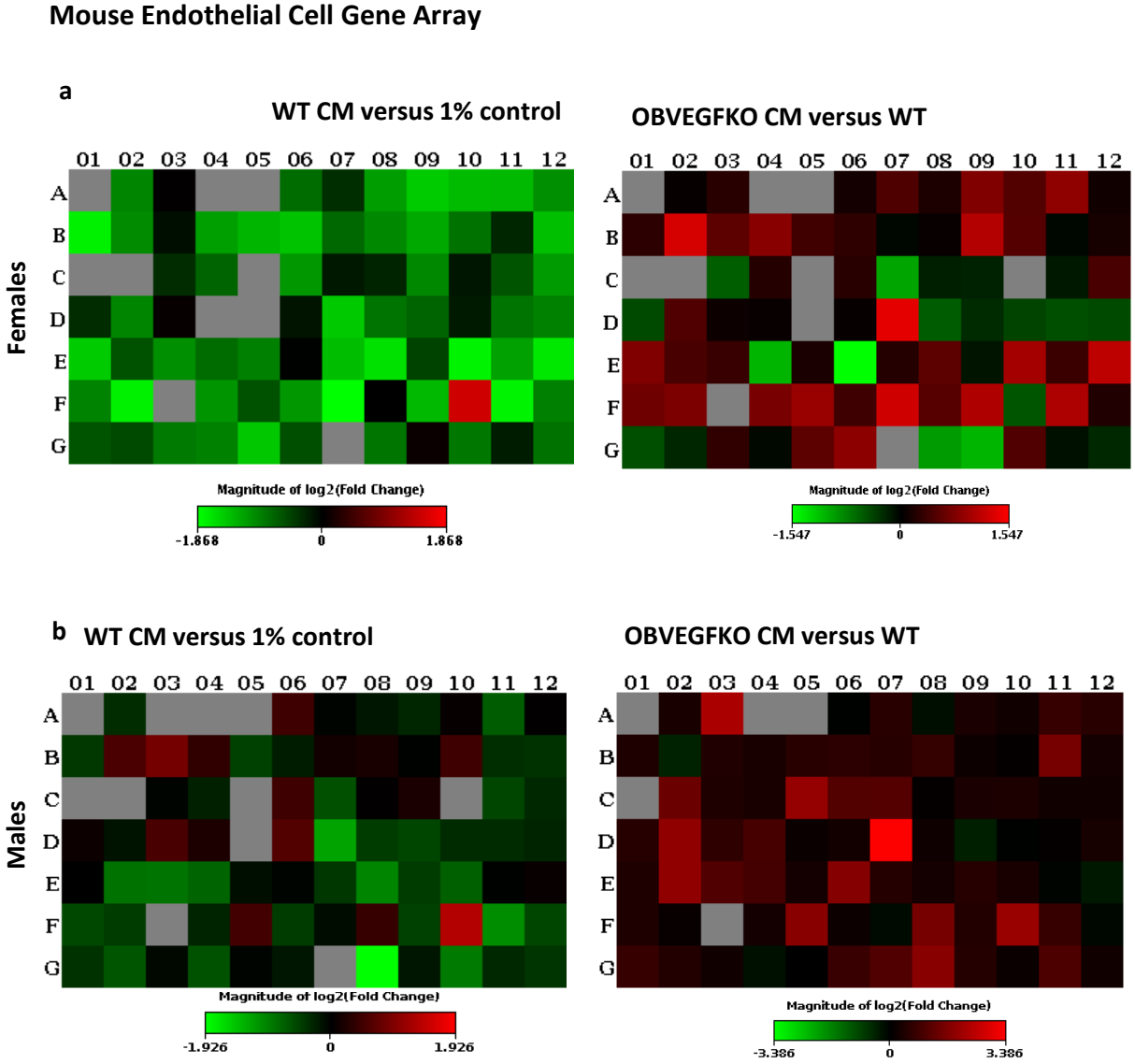

Figure 6.7: Heat map representation of changes in gene expression in MBMECs shown in the endothelial cell gene array following OBVEGFKO in males and females. Heat maps represent the expression of 84 different endothelial cell genes, following the treatment of MBMEC with female (a) and male (b) OBVEGFKO and WT conditioned media. Data is plotted as fold change, with red being upregulation and green downregulation of gene expression. Both WT versus 1% (v/v) FBS control and OBVEGFKO versus WT data recorded.

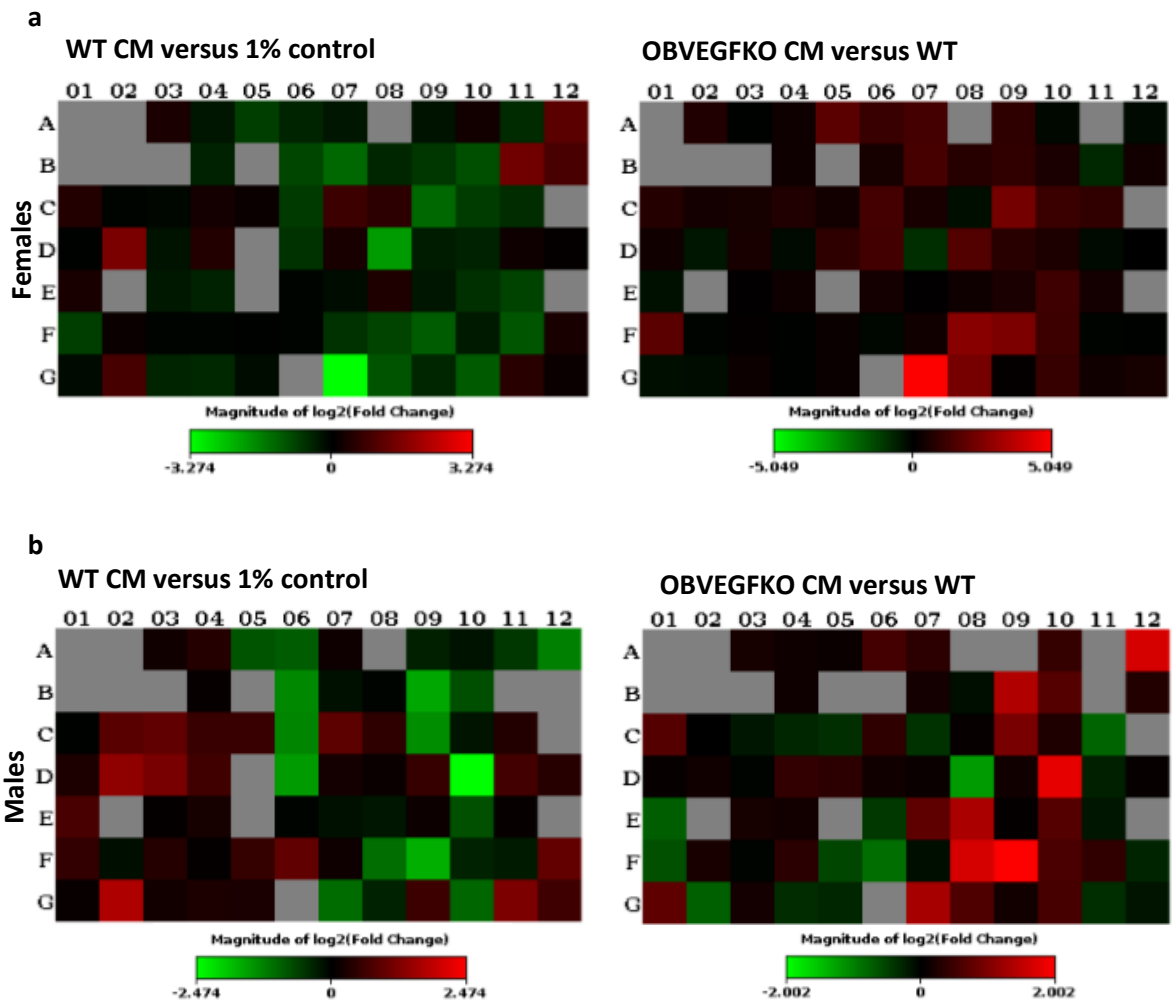

Figure 6.8: Heat map representation of changes in gene expression in MBMECs shown in the osteogenesis gene array following OBVEGFKO in males and females. Heat maps represent the expression of 84 different genes which are implicated in osteogenesis, following the treatment of MBMEC with female (a) and male (b) OBVEGFKO and WT conditioned media. Data is plotted as fold change, with red being upregulation and green downregulation of gene expression. Both WT versus 1% (v/v) FBS control and KO versus WT data recorded.

6.3.4 Deletion of bone-derived *Vegf* increases the expression of sclerostin at the tibiofibular junction in 16 week old male bones

Following the identification of *Sost* as being a key gene which was upregulated in male and female endothelial cells as a result of osteoblast-derived VEGF deletion and given its known role as a negative regulator of osteogenesis, the expression of sclerostin following *in vivo* OcnVEGFKO was investigated further. With sclerostin also known to have an inhibitory role on mineralisation, this study was equally especially of interest due to the dysfunctional mineralisation which was characterised in previous sections. As a result, cryo cross-sections of male and female WT and OBVEGFKO 16 week old tibia were cut at the tibiofibular junction region.

Immunostaining showed that following OcnVEGFKO in females, there was no obvious difference in sclerostin expression compared to the WT (figure 6.9a). In males however, there was a dramatic increase in sclerostin expression across the entire bone cross-section (figure 6.9b, 6.10a) in OcnVEGFKO tibia sections versus WT. Levels of sclerostin expression in male OcnVEGFKO mice were consistently high for each mouse examined (n=3). The localisation of sclerostin staining on the bone cortex was investigated further and on closer inspection of consecutive slices at the tibiofibular junction (figure 6.10b,d,f), it appeared that sclerostin expression correlated with the expression of CD31 positive endothelial cells (figure 6.10c,e,g). Osteocytes did also appear to stain for sclerostin, however they did not stain for CD31.

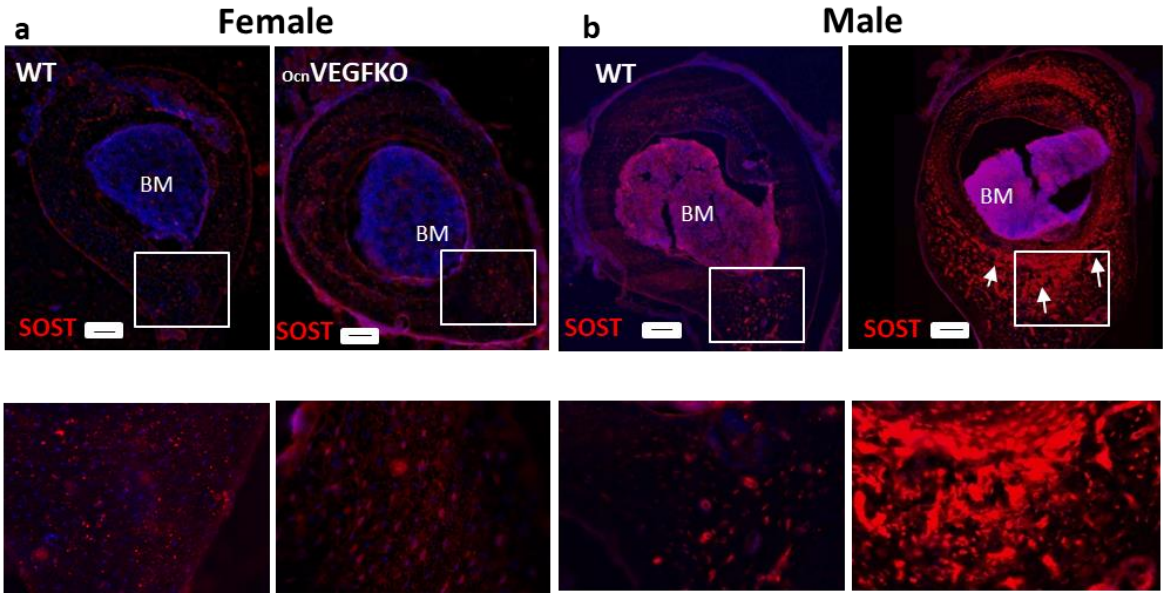

Figure 6.9: Sexual dimorphic alterations in protein expression of sclerostin following VEGF deletion are evident in whole bone sections. Cryosections from female (a) and male (b) WT and OBVEGF tibiofibular junction were stained with Sclerostin primary antibody and Hoechst to stain the nuclei. Increases in sclerostin levels were visible following OcnVEGFKO in males (Alexa Fluor 555), specifically in the posterior region (arrows) below the bone marrow (BM). White box represents the region of cortical bone magnified below. Scale bar = 100µm.

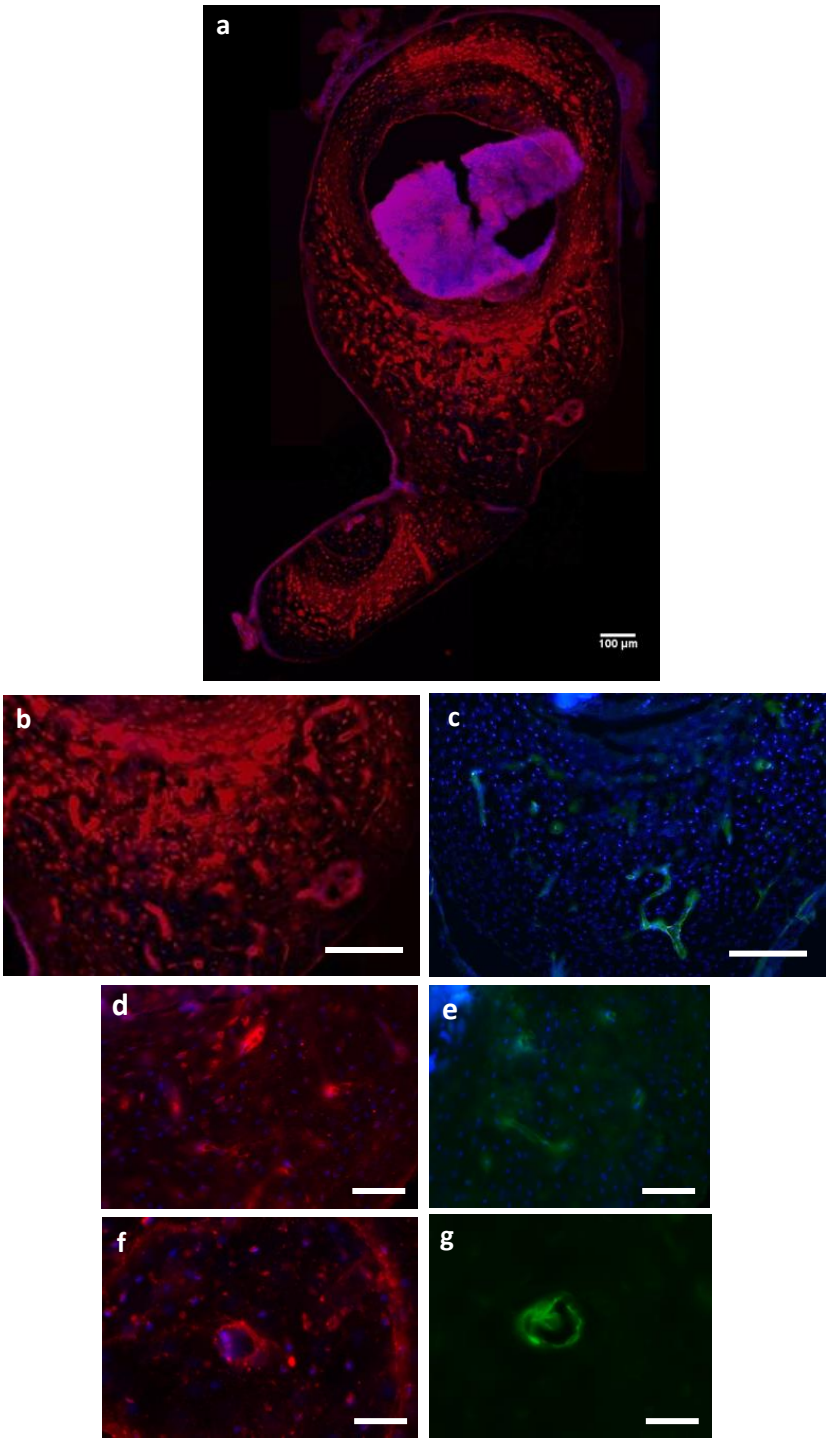

Figure 6.10: Increased levels of sclerostin in male OcnVEGFKO mice localised to CD31 positive cells. Following OcnVEGFKO, immunohistochemistry of cryo sections identified increased levels of sclerostin expression present in males especially (a; red). On closer inspection of sclerostin stained sections (b, d, f) and following the staining of consecutive slices with CD31 (Alexa Fluor 488; green), it was found that sclerostin expression was localised to CD31+ endothelial cells (c, e, g). Osteocytes can be seen to stain for sclerostin, but not CD31. Scale bar = 100µm.

6.3.5 VEGFR2 expression is co-localised to CD31 endothelial cells

As further validation for the expression of VEGFR2 in endothelial cells specifically, immunohistochemistry using VEGFR2 (figure 6.11a) and CD31 (figure 6.11b) primary antibodies was performed on cryo sections taken from the tibiofibular junction. VEGFR2 labelling of sections showed that VEGFR2 was co-localised only with CD31 positive endothelial cells, supporting the results from the previous western blot which showed that VEGFR2 was only present on endothelial cells, not osteoblast cells.

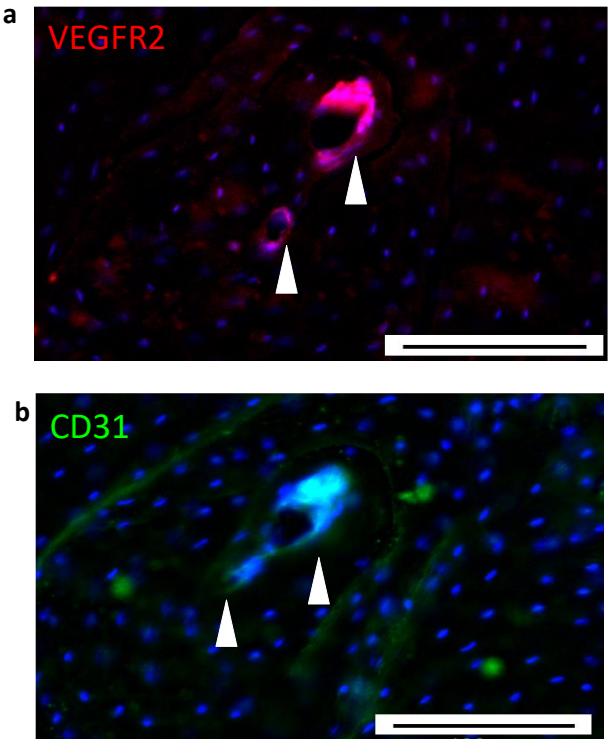

Figure 6.11: High expression levels of VEGFR2 in endothelial cells, validated by immunohistochemistry. Immunohistochemistry of cryo sections staining for both VEGFR2 (Alexa Fluor 555; a) and CD31 (Alexa Fluor 488; b) confirmed the co-localisation of VEGFR2 with the bone vasculature (white arrows; CD31+ endothelial cells). Scale bar = 100µm

6.4 Discussion

Initial results which showed that viability and proliferation of MBMECs was not altered following OBVEGFKO in males or females were somewhat surprising. Given what is known about osteoblast-VEGF signalling with endothelial cells for the close coupling of osteogenesis and angiogenesis (Wang et al., 2007, Liu et al., 2012), it was expected that deletion of *Vegf* would reduce the viability and proliferation of endothelial cells as a result of the lack of interactions between VEGF and VEGFR2 on the endothelial cell surface. This was not the case however and endothelial cells were able to maintain their viability and proliferation in the absence of *Vegf*. The sexual dimorphic effect observed in the vasculature *in vivo,* following OBVEGFKO is therefore either i) not linked to altered endothelial cell viability or proliferation and/or ii) sex steroids, genetic, mechanical or environmental factors are required to induce the vascular effects seen *in vivo*.

Preliminary investigations into protein expression in MBMECs following OBVEGFKO in males and females showed differential expression of VEGFR2 in MBMECs treated with conditioned media for 5 minutes, in comparison to MBMECs treated with conditioned media for 24 hours. It was thought that perhaps this could be reflective of increased levels of VEGF existing in WT LOBs, prompting the internalisation of VEGFR2 in these osteoblast cells after a 5 minute treatment with conditioned media. This is a theory which has been discussed in previous studies, which predict that within the first 5 minutes of treatment with VEGF, there is 60% internalisation of VEGFR2 (Bazzazi et al., 2017). In contrast, these initial results suggested that prolonged deletion of osteoblast-derived *Vegf* in both males and females could have the potential to influence the sensitivity of endothelial cells to VEGF, thus reducing VEGFR2 protein expression. Subsequent repeats would strengthen this finding further. Linking this with the viability results it can be suggested that the lack of VEGFR2 present in these MBMECs following prolonged exposure to osteoblast-derived VEGF did not influence MBMEC proliferation or viability. Therefore, MBMECs must be compensating for the loss of VEGF via alternative mechanisms. As a result, changes in endothelial cell gene expression were subsequently investigated.

Sexual dimorphisms in endothelial cell gene expression as a result of depletion of OBVEGF were identified in a number of genes known to be instrumental in the maintenance of angiogenesis, osteogenesis and cell adhesion. One of these genes was interestingly *Igf-1*,

which has been linked to sex-hormone independent expression of skeletal sexual dimorphisms. Serum levels of *Igf-1* have been shown to be unaltered as a result of an ovariectomy or an orchidectomy, but upregulated in males during times of times of peak growth and therefore pivotal in skeletal development (Callewaert et al., 2009). Interestingly, levels of *Igf-1* mRNA in endothelial cells were downregulated following OBVEGFKO in males, but upregulated following OBVEGFKO in females versus WT. IGF-1 plays an important role in bone growth and sex steroids and IGF-1 have been shown to closely interact during puberty (Mauras et al., 1996), with IGF-1 playing a role in the upregulation of radial expansion during the development of the skeleton. Therefore this could be contributing to the significant differences observed in the male and female bone phenotypes observed previously. Complementing this finding, there were greater levels of upregulation in several pro-osteogenic genes in females versus males (*Bglap*, *Runx2* and *Osx*) as a result of OBVEGFKO. There was also differential expression of angiogenic genes between sexes (*P-selectin*, *tymp*, *Fgf1* and *Fgf2*) which were all upregulated in MBMECs following OBVEGFKO in females, but downregulated following OBVEGFKO in males. Therefore, perhaps differential expression of mRNA in male and female MBMECs is contributing to the skeletal and vascular phenotype observed.

Sclerostin is a well-known negative regulator of osteogenesis and is thought to act via its inhibitory effect on the Wnt pathway, preventing efficient mineralisation and osteoblast differentiation (Winkler et al., 2003, Joeng et al., 2017). In this study, endothelial mRNA expression was shown to be up-regulated in both male and female MBMECs following VEGF deletion. Sclerostin has a proven involvement in bone remodelling and low levels have been associated with diseases where sufferers phenotypically have high bone mineral density and a low risk of fractures (Lewiecki, 2014). Therefore, the upregulation of sclerostin here correlated with the previously examined increase in intracortical porosity seen *in vivo,* where adult OcnVEGFKO male bones especially had an osteoporotic-like phenotype. Although there was a higher fold change versus WT following female OBVEGFKO in comparison to male OBVEGFKO, it was thought that a combined action of a multitude of genes and other factors was influencing the male and female bone phenotypes observed *in vivo*, not just changes in *Sost* mRNA expression. Equally, the gene array provided information on one population of cells and purely described the levels of mRNA expression within that one population, so further analysis was required.

Following *in vivo* deletion of *Vegf* and by performing immunohistochemistry, it was identified that there was a much higher protein expression of sclerostin in male OcnVEGFKO mice versus WT and also in comparison to females. Immunohistochemistry enabled the study of multiple cells within a cross-section of bone and therefore gave further insight into the effect of bone-derived *Vegf* deletion. The sclerostin expression was localised to CD31 positive vascular endothelial cells and therefore pinpointed as an interesting target for future therapeutics. It was thought that differential expression of sclerostin protein levels in endothelial cells could be associated with the severe increase in porosity and poor mineralisation seen following OcnVEGFKO in males.

Due to its role as an antagonist of the Wnt pathway and inhibitory effects on osteogenesis, anti-sclerostin (Sc1-mAb) antibodies have previously been identified as a potential target for the treatment of degenerative bone diseases such as osteoporosis, upregulating bone formation (Lewiecki, 2011, Clarke, 2014, MacNabb et al., 2016). The concept of sex-specific medicine however is novel and given the sexual dimorphisms identified in this study, it would be beneficial to explore this further. It is clear that males and females regulate their bone morphology and geometry in different ways and that this is at least in part regulated by the differential expression of osteogenic genes by endothelial cells. Therefore, perhaps males and females should not be considered as one entity when it comes to therapeutics. Importantly, from this chapter it was evident that the sexually dimorphic mechanisms responsible for the bone and vascular phenotype identified in males are largely driven indirectly by vascular endothelial cells. The signalling of VEGF via paracrine signalling pathways is therefore very important in the maintenance of bone health and the development of the vasculature.

Chapter 7 General discussion

7.1 What can the deletion of *Vegf* from mature osteoblasts tell us about degenerative bone disease?

The OcnVEGFKO mouse model described could be utilised as a model of age related osteoporosis, as a reduction in VEGF has been described with age (Ryan et al., 2006, Wang et al., 1997). Consistent with VEGF playing a role in osteoporosis it has been described in previous studies that deletion of early stage osteoblast-derived *Vegf* induces an osteoporotic-like phenotype, where there is reduced trabecular bone, alterations in bone morphology due to a decrease in osteoblast activity and upregulated adipogenesis (Liu et al., 2012, Kanis, 1994). Supporting the use of *Vegf* conditional knockout models for investigations into osteoporosis, it has been found that there is a 60% reduction in levels of circulating VEGF in post-menopausal women (Senel et al., 2013). Removal of the ovaries in miniature pigs in order to mimic post-menopausal osteoporosis in which levels of oestrogen are greatly reduced, has also found that there was a 27% decrease in vertebral concentrations of VEGF (Pufe et al., 2007). Adding to these findings, it has been shown by the results presented in this thesis that deletion of OcnVEGF leads to the expression of a highly porous and poorly mineralised bone phenotype and that the expression of this phenotype is particularly severe in males. This suggests that VEGF controls the age-induced increase in intracortical porosity and regulates healthy bone mineralisation distinctly in males and females. Prior to this study, the role of VEGF was considered to be comparative between sexes, but mostly studied in aged females due to changes described during the menopause in which there is a reduction in oestrogen which correlates with a reduction in VEGF. Therefore, this study has induced a novel way of thinking when it comes to approaching research into the functionality of VEGF in bone in the future, with studying males and females individually being a key factor.

It has been found previously that increased cortical porosity in human femurs results in a 76% decrease in bone strength (Schneider et al., 2007b). Increased cortical porosity has been observed in patients with fractured forearms (Bala et al., 2014) and it is known that 80% of total osteoporotic fractures are non-vertebral, affecting mainly cortical bone (Zebaze and Seeman, 2015, Riggs and Melton, 1986, F, 1947). The tibiofibular junction was

subsequently used as the region of interest for this study as it is a region which predominantly consists of cortical bone and is a well cited location for the occurrence of fracture (Sferopoulos, 2010, Sundaram et al., 2018, Jianhong Pan, 2018). In this current study and comparative to the rest of the tibial length, whole bone analysis identified that a significant proportion of geometric changes were localised to the tibiofibular junction, the region of interest. Results suggested that VEGF regulates bone architecture distinctly in males and females at this location, with VEGF being vital for the maintenance of bone geometry at the tibiofibular junction during early development in males (4 week old mice) and important during adulthood in females (16 week old mice). It is well known that changes in geometry during development are more pronounced in males than in females and therefore perhaps males rely on VEGF more heavily than females during development, thus deletion of osteoblast-*Vegf* has a greater effect (Hu and Olsen, 2016, Kusumbe et al., 2014a, Costa et al., 2009, Martin, 2002).

Finite element analysis and digital volume correlation of the entire mouse tibia has found that compressive strain is greatest at the antero-medial surface just below the tibiofibular junction and at the postero-lateral surface just above the junction (Oliviero et al., 2018). Therefore, with the tibiofibular junction being the location in which the tibia and fibular separate and sitting centrally between the areas of the tibia in which there is most strain during three point bending, it is quite possible that the male bones used in this study which are increasingly porous as a result of OcnVEGFKO would be more prone to fracture than WT controls at this region specifically and should be investigated in the future. If this was the case it would suggest that there is sexual divergence in the regulation of bone integrity by VEGF at the tibiofibular junction.

The effect of ageing on mechanical strength has been studied previously using BALB/c mice, in which three-point bending tests have been utilised to examine the mechanical and material properties of male and female femur, vertebrae and radius throughout development (from 2 to 20 months). Here, sexual dimorphism in bone strength, energy to fracture and ultimate force have been identified with ageing, which appear to go hand in hand with a reduction in bone volume fraction with age in males and females. Interestingly, it has been found that at several points during ageing male bones had a lower moment of inertia, ultimate stress, bone volume and strength at different regions of the femur versus females. Ultimate force and trabecular bone volume fraction measures of the vertebrae

were also lower in males versus females from 7 to 20 months (Willinghamm et al., 2010). Given the sexually divergent role of VEGF in the regulation of bone microstructure and mineralisation identified in this project and the known age-related decline in VEGF, it therefore would be of great interest to look at the role of VEGF in the control of the changes in these sex-specific mechanical properties of bone at consecutive points in development and throughout ageing. Although not the focus of this PhD project, studies into the effect of OcnVEGFKO on the mechanical and material properties of bone in males and females would therefore be of great interest in the future, with a specific interest in the mechanical properties of the tibiofibular junction. The prediction would be that male bones depleted of VEGF would have lower strength, ultimate force and ultimate stress, making them more prone to fracture. Although VEGF from cells of early osteoblast lineage has already been shown to be instrumental during fracture healing (Buettmann et al., 2019), results could be used to interpret whether the VEGF is likely to have a role in the prevention of fracture in healthy males and females.

In 2012 in the EU, the economic impact of fragility and incident fractures was at £27.1 billion and by 2025 it has been estimated that this value is set to rise by 25% (Hernlund et al., 2013). The use of models of osteoporosis such as the mouse model used in this study is therefore hugely important in the understanding of mechanisms regulating osteoporotic phenotypes and subsequently finding a treatment for osteoporosis which could greater reduce the risk of fragility fracture, reduce bone turnover and increase BMD with minimal side effects in the future.

As VEGF is known to be a potent inducer of angiogenesis and implicated in the coupling of angiogenesis and osteogenesis (Muller et al., 1997, Breier and Risau, 1996, Gerstenfeld and Einhorn, 2006), the effect of bone-derived *Vegf* deletion on the bone vasculature in both males and females was of significant interest in this study. *In vitro* results suggested that in healthy humans, osteoblast-derived VEGF does not signal directly with VEGFR2 via autocrine pathways on the osteoblast cell surface to regulate the structural properties of bone or in the control of mineralisation. Instead it was found that osteoblast-derived VEGF signals with vascular endothelial cells via paracrine pathways, altering the gene expression of key regulators of osteogenesis and angiogenesis in a sex-specific manner, to in turn regulate adult bone morphology.

Key genes identified to be altered divergently in endothelial cells and are regulated by osteoblast-VEGF signalling in males and females distinctly include *Igf-1, Fgf, Hif1-α, Tymp, Selpg, Bmp6, Tgfb-1, Sost, Vcam* and *Pgf*. An elegant recent study has shown that by using monoclonal antibodies which bind to IGF-1R, it is possible to delay ageing in aged female, but not male mice (Mao et al., 2018). This therefore suggests that the role of IGF-1 in the regulation of health profiles is sexually dimorphic in other systems too, rather than this finding being specific to the skeleton. Not only this, IGF-1 appears to have additional divergence at different stages of development and ageing. IGF-1 has been shown to be vitally important in the skeleton during bone growth, especially in males (Callewaert et al., 2010a) and this is a finding which is supported by studies using Ames dwarf mice. Interestingly however, although treatment with IGF-1 enhanced bone growth in dwarf mice, the life span of male mice specifically was reduced by 20% in males only (Sun et al., 2017). Where an IGF-1R antibody would be likely to reduce the growth of long bones and a reduction in IGF-1 in males has been associated with a severe osteoporotic phenotype in the OcnVEGFKO mice, this treatment would be seemingly detrimental for the reversal of this bone phenotype. IGF-1R has huge potential as a therapeutic for a wide range of cancers and has undergone successful clinical trials (Tolcher et al., 2009). This shows the importance of treating males and females as individual entities when considering potential therapies for osteoporosis and how it is imperative to look at the bigger picture when investigating potential targets for disease in general and not just look at the effect that an antibody would have on one individual developmental process or disease.

In order to take the experiments presented in this thesis using the OcnVEGFKO mouse model further to investigate potential therapeutics for the treatment degenerative bone diseases such as osteoporosis, preliminary investigations could involve *in vitro* experiments in which VEGF was deleted in male and female LOBs with adenovirus-Cre as described. Here, agonists and antagonists for genes (*Igf-1, Fgf, Hif1-alpha, Kdr, Tymp, Selpg, Bmp6, Tgfb-1, Runx2, Sost, Vcam* and *Pgf*) identified to be expressed in a sexual divergent manner in this study, as well genes identified in future studies to be involved in poorly mineralised bone phenotype observed *in vivo,* would be used to treat co-cultures of osteoblasts and endothelial cells. The effect of targeting these factors on LOB matrix mineral composition would then be quantified by Raman spectroscopy, used previously in complementary studies (Goring et al., 2019). Successful targets could then be validated *in vivo* in the

OcnVEGFKO pre-clinical mouse model of osteoporosis. Therefore, the use of this mouse model and the ability to link *in vitro* and *in vivo* results could assist with the identification of novel treatments for osteoporosis in the future.

It is also advantageous to use other well characterised pathologies of bone and mineralisation to learn more about changes identified in the results presented in this thesis. Both histology and BSE-SEM identified high levels of osteoid surrounding the osteocyte lacunae and blood vessel canals in OcnVEGFKO males. As well as this, BSE-SEM was able to identify an arrested mineral front in OcnVEGFKO males, with small depositions of mineral surrounding the canals and osteoid embedded deep within the canals. Having identified comparable phenotypes in rachitic bones to the phenotype observed in this study (Marie and Glorieux, 1981, Boyde et al., 2017, Boyde, 1980a, Steendijk and Boyde, 1973), it was therefore possible to use this knowledge on bone mineralisation defects in rickets and relate it to this model of osteoporosis (OcnVEGFKO), learning more about the osteoporotic phenotype based on previous findings. Past studies have found that vitamin D induces angiogenesis in endothelial cells and it is thought that an upregulation of VEGF is responsible for this (Grundmann et al., 2012). Therefore, it is not entirely surprising that the phenotype of vitamin-D deficient rickets bones and *Vegf* deficient osteoporotic bones are comparable and this enables the sharing of knowledge between two bone pathologies.

7.2 Sex differences following deletion of bone-derived *Vegf*; what about the joints and osteoarthritis?

It is clear from the literature that sex differences do exist in other degenerative diseases of the bones and joints and studies which focus on sexual divergences identified in different pathologies could therefore help to provide information on how to interpret these divergences and inspire potential approaches moving forwards. Where osteoporosis is a disease in which there are degenerative changes in bone mass, osteoarthritis (OA) is characterised by irreversible and detrimental remodelling of joint tissues, particularly articular cartilage and subchondral bone (Martel-Pelletier et al., 2008). The role of VEGF in the progression of OA has been identified by the deletion of *Vegf* in chondrocytes under the control of a Col2-Cre promotor. Converse to this study in which the deletion of *Vegf* induced an osteoporotic-like phenotype, it has been suggested that the deletion of VEGF in chondrocytes reduces the severity of induced OA. Therefore, it appears that VEGF has differing effects in the maintenance of bone and cartilage health. Comparatively however, in the Col2-Cre *Vegf* knockout model, there was reduced thickening of the subchondral bone, which would correlate with previous known effects of VEGF on the maintenance of bone density (Nagao et al., 2017, Liu et al., 2012). Interestingly, it has been previously identified that deletion of chondrocyte derived VEGF using males as a Col2-Cre transgene carrier results in post-natal lethality of the offspring (Haigh et al., 2000). When females were used as the carrier, offspring were infertile but survived long enough to be studied (Nagao et al., 2017).

Further sexual dimorphisms in OA have been identified in two well characterised models of the disease; surgical destabilising of the medial meniscus (DMM) (Ma et al., 2007) and the STR/ort model (Uchida et al., 2012, Staines et al., 2017). Using these models it has been reported that the OA phenotype was most severe in males, with more severe degenerative changes in the knee joint observed in males versus females. A difference in pain symptoms was also reported between sexes (Mahr et al., 2003, Ma et al., 2007). Pain has not been measured in the OcnVEGFKO model, however similarly to these OA studies, the phenotype was more severe in males than females in 16 week old OcnVEGFKO bones.

In order to determine the potential mechanisms behind these sex differences produced in the DMM model, ovariectomy and orchidectomy studies have been performed prior to the

induction of OA. Following the removal of the gonads, the sexual dimorphisms observed previously were reversed and females displayed greater OA severity following DMM than males in the absence of sex hormones (Ma et al., 2007). Therefore, in this instance it was found that sex hormones were largely responsible for the divergent severity of OA.

An ovariectomy or orchidectomy would have been a valuable experiment to undertake in this project using OcnVEGFKO mice. This would provide further validation that the sex-specific bone traits regulated by VEGF are independent of sex hormones and significantly controlled by the upregulation and downregulation of the angiogenic and osteogenic genes identified by gene array in males and females. In order to perform an experiment such as this, the gonads and ovaries would have to be removed from the OcnVEGFKO mice prior to puberty. The bioactivity levels of oestrogen and androgens increase between 5 and 7 weeks in males and females, therefore the removal of the gonads would have to be before 4 weeks of age, to ensure that levels of circulating hormones were low at the time of surgery (Drickamer, 1981, Callewaert et al., 2010b). SR CT, histology and BSE-SEM as described previously could then be to analyse these mice at 16 weeks of age and results compared to those generated from this study.

As it was not possible to do such an experiment in the work presented in this thesis, experiments using both young pre-pubertal animals and *in vitro* studies were performed, where the contribution of circulating sex hormones would be less. Unlike in the male DMM model of OA, the phenotype observed following OcnVEGFKO in 16 week old mice was not reversed in sex-hormone depleted conditions. Instead, there was still a visible phenotype identified in 4 week old male OcnVEGFKOs using SR CT, an increase in intracortical canal volume and upregulation in immature mineral matrix species following the *in vitro* deletion of VEGF in males (Goring et al., 2019). There were also dimorphic changes in the mRNA expression of key genes implicated in skeletal development and angiogenesis *in vitro* as previously mentioned. This suggested that although it is never possible to completely eliminate the effect of sex hormones, in healthy bone VEGF is able to regulate bone health indirectly via sex-specific changes in endothelial cell gene expression.

The lack of studies in which both males and females are compared appears to be a recurring downfall in investigations into a wide range of different degenerative diseases of the bones and joints. In rheumatoid arthritis (RA), it has been highlighted that although males are more predisposed to RA onset, females suffer from greater

intensities of joint destruction (Jawaheer et al., 2006). In osteoporosis, there are similar differences between sexes when looking at the statistics of the prevalence of the disease and the subsequent death rates as a result of fracture, although osteoporosis is conversely more common in females. In osteoporosis, the mortality rate within a year of osteoporotic fracture is much higher in males than females (Cooper et al., 1992, Jones et al., 1996, O'Neill et al., 1996). In the current study, deletion of bone-derived *Vegf* has been found to increase levels of osteoid, woven bone and immature matrix components in males. This therefore has suggested that VEGF controls bone mineralisation distinctly in males and females, with a particularly important role in the adult male skeleton.

During healing and following chondrocyte differentiation, there is mineralisation of the callus (reviewed by Einhorn and Gerstenfeld, 2015). The results from this study suggest that adequate mineralisation of the callus in these male bones would not be possible during fracture healing, meaning that bones would not able to heal properly and there could be further complications. This is demonstrated in figure 4.5, a rotating video of a fractured male OcnVEGFKO tibia which has failed to heal sufficiently. Subsequently, dysfunctional mineralisation in male OcnVEGFKOs could explain the high level (37.5%) mortality rate post hip fracture in males which has been recorded previously (Cooper et al., 1992, Jones et al., 1996, O'Neill et al., 1996). A potential hypothesis therefore would be that VEGF plays a more pivotal role in fracture healing and mineralisation in male adults than it does in females. This could be tested by surgically creating a bone defect of known diameter at tibiofibular junction in male and female WT and OcnVEGFKO bones. Healing could be measured by micro-CT analysis, comparing the size of the defect in WT and OcnVEGFKO bones of each sex.

A multitude of differences between males and females have been identified in models of OA, which further justifies the importance of studying both males and females when looking at models of degenerative disease. Although differences in incident rates and severity of the disease phenotypes have been identified in diseases of the bones and joints, the mechanisms responsible for dimorphisms that might occur between males and females are frequently unknown. Despite these observed differences and similar to the study of osteoporosis, it has been acknowledged at scientific meetings that there is a clinical need for the study of both sexes in arthritis research, particularly OA.

7.3 Sex-specific medicines; a feasible approach for the future stratified treatment of bone pathology

Sexual dimorphisms exist between males and females basally; males characteristically have a larger skeleton, which is thought to protect them from fracture during ageing (Seeman, 2001, Martin, 2002, Seeman, 2002, Callewaert et al., 2010a) and their bones are characteristically longer and thicker (Joakimsen et al., 1998). Despite these well known basal sex differences in the skeletal composition of healthy humans and the high incidence rates of osteoporosis in females, males and females are still considered as one entity when it comes to diagnosis and treatment of the disease. In fact men, who typically suffer from symptoms of osteoporosis up to 10 years later than females (Campion and Maricic, 2003) and are at a greater risk of mortality post-fracture (Cooper et al., 1992, Jones et al., 1996, O'Neill et al., 1996), are known to be underdiagnosed when it comes to osteoporosis (Jennings et al., 2010, Laurent et al., 2019). For the first time, the research presented in this thesis has identified that VEGF regulates bone microstructure, geometry and mineralisation distinctly in males and females. It seems appropriate therefore that males and females should be considered as individuals when it comes to designing novel therapeutics for osteoporosis.

The most common drugs currently used to treat osteoporosis are bisphosphonates, which inhibit bone resorption by mimicking pyrophosphate and bind to locations in which bone remodelling is especially dynamic (Keen, 2007). Bisphosphonates which are known to have a particularly strong effect in the treatment of osteoporosis include alendronate, ibandronate and risedronate. More recently zoledronate has been identified as a particularly powerful option and one treatment can inhibit osteoclast activity and increase bone density for up to one year. Bisphosphonates can be given orally or intravenously, but carry renal side effects and prolonged usage have more severe side effects such as osteonecrosis of the jaw (Reid et al., 2002, Rawlins and Dillon, 2005). With the growing population which is set to be 10 times larger than the population in the 1800s by 2070 (Bongaarts, 2009) and with the number of elderly people therefore increasing in size exponentially, the need for sufficient therapeutics and a different approach for the treatment of osteoporosis is evident.

Sclerostin antibodies have shown promise for the treatment of osteoporosis. Experiments have shown that monoclonal antibodies are able to upregulate the mineralising surface and bone formation rate (Li et al., 2011). In the current study, VEGF is shown to control sclerostin protein expression and mineralisation distinctly in males and females, with higher levels of sclerostin protein expression correlating with the failure to sufficiently mineralise in males as a result of OcnVEGFKO in males. With this knowledge, perhaps drugs such as anti-sclerostin would have a higher efficacy in males than in females. Romosozumab is an inhibitor of sclerostin and has passed phase three clinical trials which assessed the effectiveness of the drug on post-menopausal women only. Although it decreased vertebral fractures by 75% in the patient subgroup, the effect of this drug on men was not considered in this trial and therefore it has not been considered here that males and females may respond differently to treatment (Rachner et al., 2019).

Personalised medicine conceptualises the idea of individualising medicine and given the sex differences identified in bone development, would seem a fitting approach for the treatment of osteoporosis. It has been found that many differences in disease phenotypes occur between individuals and these may include differences which are due to sex, genetics, age or lifestyle (Jain, 2002). Therefore, by treating individuals based on their disease phenotype rather than a generic diagnosis, it is suggested that responses to treatment will improve and cost health services less money in the long run. Personalised medicine is now a recognised approach for cancer, in which there is known to be large variations in individual responses to specific therapies. It has been identified in cancer that clinical outcome can be predicted by the gene expression profile of tumours (Carter et al., 2006) and therefore this facilitates individual treatment approaches. Personalised medicine is an accepted concept for the treatment of breast cancer, where patients are genotyped for CYP2D6, which is involved in the activation of the cancer drug tamoxifen. Variations in CYP2D6 are associated with returning occurrences of breast cancer. If a dysfunctional variant form of CYP2D6 is detected, treatment is personalised as the patient will be treated with an alternative drug such as raloxifene instead (Skaar and Desta, 2018, de Souza and Olopade, 2011).

For osteoporosis, the potential divergences in the effectiveness of drugs such as anti-sclerostin on males and females could be evaluated *in vitro* pre-clinically as previously described, before performing *in vivo* experiments to validate the response to the drug in

both sexes, based on measures of cortical porosity (SR CT), mineralisation (BSE-SEM) and histology at the tibiofibular junction. The ability of the drug to reverse the vascular phenotype *in vivo* would be of particular relevance to this study and help to define the role that sclerostin, as an example, has on the presence of abnormal vasculature which is seen in this animal model. The effect of the osteoporotic drug in males and females could additionally be tested by comparing the mechanical properties of the bones in knockout mice, knockout mice treated with the drug and WT mice. Three point bending experiments would therefore be a valuable way of testing this.

With increased interest in the study of epigenetics in bone pathologies and dimorphic results identified in studies such as this one where males and females have individual phenotypic disease profiles, it is hoped that the personalised medicine will become more readily recognised in the bone field in the future. Reversal experiments using targets shown to be differentially expressed in males and females and subsequently producing diverse responses to antibody therapies between sexes could be the first step in increasing acceptance of the concept.

7.4 Study limitations and future work

The severity of the disease phenotype identified in this mouse model in males in particular, created various challenges, all of which were endeavoured to be overcome in this PhD. The mouse tibia used for the majority of this study were very delicate and thus, careful attention was given to the handling of these long bones. At the time of dissection and analysis of gross measurements, genotyping had been blinded and therefore equal care was taken with all bones. It was not possible to use bones such as the male OcnVEGFKO bone identified as being fractured in figure 4.5 for analysis. The aforementioned challenges in the separation of intracortical canals and osteocyte lacunae in the SR CT scans were overcome by the use of individual thresholding and the categorisation of the larger fraction of porosity as intracortical canals, but nevertheless the analysis of the intracortical canal fraction produced interesting data which correlated with the signs of poor mineralisation which were identified by histology and BSE-SEM. The use of a bone cutter for accessing the region of interest prior to histological analysis of the contralateral limb to those used for micro-CT meant that many of the bones developed microfractures and thus, for subsequent studies it would be advisable to embed the entire tibia prior to exposing the region of interest. This did not alter results however, as bones which were particularly badly damaged were not used for analysis.

Due to the need to use litter mate controls for experimentation and the fragility of some of the OcnVEGFKO bones which meant that some tibia were fractured and could not be used for further analysis, n numbers of n=3 or n=4 biological repeats were often used in this thesis. Occasionally there was not both a male and female OcnVEGFKO mouse present within one litter and therefore none of the mice from these specific litters could be used for analysis due to a lack of male and female litter mate pairs. Although it was hoped that these numbers would be higher, they are in line with power calculations which suggest that n=3 or higher would be sufficient to detect significant changes in OcnVEGFKO versus WT (chapter 3.1). N numbers of n=3 or n=4 also correlate with publications using comparable strains of transgenic animals, which are costly to breed in large quantities (Liu et al., 2012, Nagao et al., 2017, Duan et al., 2016, Duan et al., 2015) and were based on ARRIVE guidelines.

The fidelity of the *in vivo Vegf* deletion was also carefully investigated. It was acknowledged that osteoblasts are not the only bone cell expressing osteocalcin and thus the knockout mice were defined as OcnVEGFKO for the *in vivo* studies, as opposed to OBVEGFKO. Using the Cre-Lox system to specifically delete a gene from osteoblast lineage cells is well cited in the literature, with a high knockout specificity (Hu and Olsen, 2016, Buettmann et al., 2019, Liu et al., 2012, Zhang et al., 2002). Both the genotyping of samples using genomic DNA and the combined qPCR results using *Vegf* primers were able to show that the OcnVEGFKO was both effective and specific to bone. Although due to time limitations, the qPCR investigating the efficiency of the *Vegf* deletion was only n=3, the supporting literature is extensive (chapter 3.1) and the % knockdown was sufficiently high in these repeats performed to be confident that the deletion of *Vegfa* was specific to osteocalcin expressing bone cells.

Comparatively, relatively few challenges and limitations arose from the *in vitro* studies. The OBVEGFKO was successful on the first attempt, which was hugely instrumental to the progression of this part of the project. You can never totally remove the effect of hormones, but nevertheless the *in vitro* studies provided an environment in which lower levels of sex hormones would be present than in post-pubertal mice *in vivo*, enabling the effect of circulating hormones on the OBVEGFKO phenotype to be tested as much as possible without performing a gonadectomy. The use of phenol red free media for *in vitro* experiments was an important detail to enable the study of the effect of sex hormones, due to the fact that phenol red is known to be a weak oestrogen (Berthois et al., 1986) and therefore could have altered the results. It must be noted however, that charcoal stripped FBS was not used for these *in vitro* experiments and its use in future *in vitro* experiments which investigate sexual dimorphisms would strengthen them further. Charcoal treated with Dextran is used to selectively remove any hormones present without affecting the ability of the FBS to support healthy cell growth and thus would be a valuable addition to studies such as this.

Additional points to consider in terms of *in vitro* experiments include that due to the vast expense of gene microarrays, only one biological repeat of the endothelial and osteogenesis gene arrays was carried out. In subsequent experiments it would be of great value to increase the number of biological repeats or confirm the findings by running qPCR of individual genes, using RNA isolated from MBMECs treated with WT and OBVEGFKO

conditioned media. In this study, genes of interest such as *Sost* were singled out and levels of gene and protein expression investigated further, however with additional time a greater number of individual genes would be singled out for further investigations.

Going forward and as previously mentioned, it would additionally be interesting to perform an ovariectomy or orchidectomy on these mice and look at the mechanical properties of the bones using three point bending experiments, as well as finite element analysis to tell us more about the role of hormones in the progression of this disease phenotype. Three point bending is a recognised way of simulating the damage process that occurs during fracture and combined with finite element analysis it has been found to be possible to analyse the damage behaviour of the bone (Ridha and Thurner, 2013). Mechanical strain could also be measured *in vitro* and *in vivo*. It has been found *in vitro* previously that mechanical strain applied using a loading jig, induces the differentiation of LOBs via the oestrogen receptor. In this study, there were no differences in *Esr1* and *Esr2* mRNA expression in males or female LOBs and expression was not altered following the deletion of *Vegf*. Therefore it is possible that strain would not alter osteoblast differentiation here, however it would be interesting to investigate regardless of this (Damien et al., 2000). *In vivo,* strain could be applied to the tibia of male and female WT and OcnVEGFKO bones. Here, the bone would not undergo natural loading and therefore strain would be controlled by rate and magnitude, inducing remodelling and an increase in porosity. The effect could therefore be measured by SR CT and BSE-SEM, with a particular interest in sex differences (Rubin and Lanyon, 1985).

Equally, it would be interesting to expand this research and quantify pain in these mice. This could be a blinded study pre-genotyping and would therefore enable subsequent bone phenotypes to be directly correlated with pain. Quantification of gait asymmetries is a measure of pain which is frequently used in models of OA (Poulet et al., 2014). Although the male OcnVEGFKO mice did not appear to be in any pain outwardly, this has not been thoroughly investigated and given their severe bone and vascular phenotype would be a valuable experiment.

Equally, measures of skull and long bone phenotypes suggest that the changes identified in male OcnVEGFKOs are specific to loaded bones. Measures of movement and behaviour of the mice within their cages would therefore enable comparisons between male and female WT and OcnVEGFKO bone phenotypes, to determine whether there is a correlation

between movement and the increased cortical porosity in males. This has been facilitated in the past by the use of ethovision camera software (Noldus et al., 2001). It has been suggested that males that live in groups are more prone to fighting and thus the loading is greater on their skeleton. The male mice in this study were also housed in groups, so using the ethovision would also allow this sort of activity to be monitored (Meakin et al., 2013).

mRNA expression of androgen and oestrogen receptors in male and female LOBs was quantified using qPCR, however levels of hormones have not been measured *in vivo*. Circulating levels of hormones could be measured *in vivo* by the collection of blood samples, the serum could then be used for a sex hormone ELISA to determine the concentrations present in 4 week old and 16 week old mice. This would validate that the levels of sex hormones were lower in 4 week old mice than in adult mice.

Additionally, systemic circulation and blood pressure have not been measured in this study and neither has cardiac function. Given the role of VEGF as an inducer of angiogenesis and the fact that there are more vessels in OcnVEGFKO males which are abnormal in morphology, this would be interesting to investigate further. Vascular function could also be interrogated in depth within the bone using perfusion studies. Injection of a contrast agent such as barium sulphate could facilitate the examination of the blood vessels along the whole tibial length using a much lower resolution desktop micro-CT than the high resolution scans used in this project (Sider et al., 2010). This would allow the vasculature at the tibiofibular junction which has been well characterised in this study, to be compared and contrasted at other sites along the length of the tibia.

Given the deficiencies in mineralisation identified in male OcnVEGFKO mice by histology, BSE-SEM and *in vitro* studies (Goring et al., 2019) it would also be valuable to look at any changes of expression in PHOSPHO1, MEPE, DMP1 or osteopontin. These proteins have been found to play a vital role in the regulation of healthy bone mineralisation (Fisher and Fedarko, 2003, Qin et al., 2001, Boyde et al., 2017) and therefore it is predicted that their expression may be altered in male versus female OcnVEGFKO mice. Considering the similarities of the OcnVEGFKO bone phenotype to *Phospho1* knockout mice and the fact that low levels of DMP1 are associated with rickets, a depletion in PHOSPHO1 and DMP1 in the male OcnVEGFKO mice would be predicted and would be interesting to investigate. A summary schematic highlighting potential mechanisms underlying skeletal sexual

dimorphism of osteoblast-derived VEGF signalling, as well as future discussion points is included in figure 7.1.

7.5 General conclusion

For the first time in this study, high resolution micro-CT has facilitated the interrogation of intracortical porosity in both male and female OcnVEGFKO mice, enabling the in depth scrutiny of the resulting bone and vascular phenotype. From the results obtained, it can be suggested that the systemic loss of VEGF with ageing or as a result of age-induced degenerative bone diseases could differentially impact bone structure, vascular morphology, mineralisation and subsequent genetic expression in males and females. By future targeting of sex-specific regulators of bone mineralisation or angiogenesis which are altered in male and female OcnVEGFKOs in *in vivo* and *in vitro* studies, novel therapeutics could become accessible. With the population of ageing individuals rapidly increasing and bearing a huge economic burden, this is particularly timely for the treatment of degenerative bone diseases such as osteoporosis.

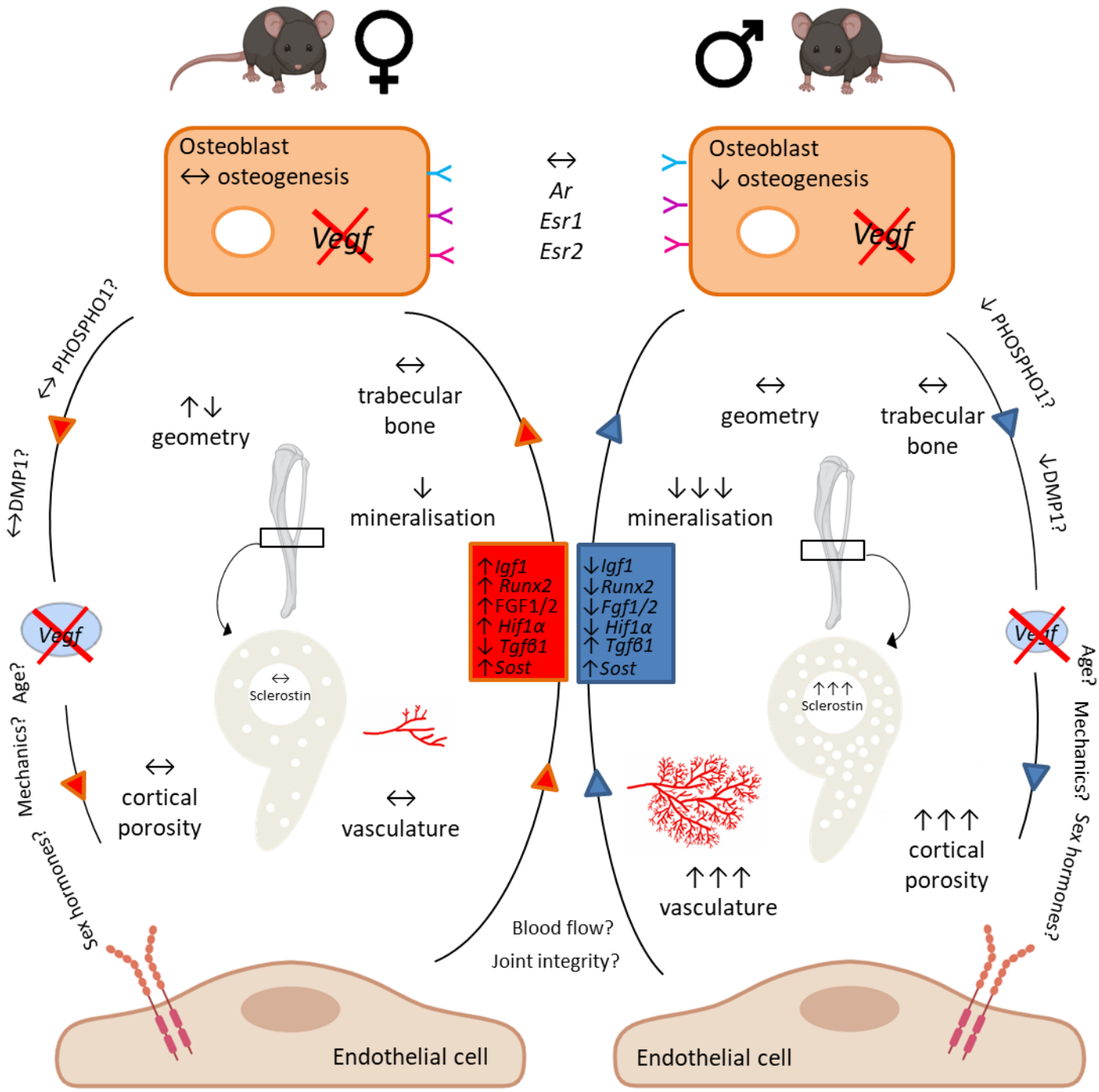

Figure 7.1: Summary schematic highlighting potential mechanisms and environmental influences underlying skeletal sexual dimorphism of osteoblast derived VEGF signalling.

Appendix A Materials

GENOTYPING

Genomic DNA

20mg/ml proteinase K was bought from Thermo Scientific (EO0491). Agarose was bought from Melford (MB1200), GoTaq Flexi DNA polymerase from Promega (M7801) and dNTPs from Promega (U1330).

cDNA

The RNeasy RNA isolation kit was purchased from Qiagen (74104). The reverse transcriptase kit (5003) and the Oligo(dT) (C1101) were from Promega. For qPCR, the Luna qPCR mastermix was from New England BioLabs M3003.

HISTOLOGY

For production of MMA for the embedding of tibia, MMA was bought from Merck (8.00590) and destabilised using aluminium oxide 60 active basic from Merck (1.01067). Benzoyl peroxide from was also obtained from Merck (801641). Nonylphenol came from Sigma (74432) and N-N Dimethyl-P-toluidine from Merck (8.00590). Isopropanol was purchased from Sigma (278475).

Giemsa and Pentachrome stain

For the Giemsa stain, Giemsa stock solution was bought from Merck (1.09204). Cellosolve (128082), acetic acid (A6283), xylene (534056) and DPX mountant (06522) were all obtained from Sigma.

For the Pentachrome stain, Alician Blue (A3157), iron haematoxylin (HT1079) and phosphotungstic acid (HT152) were all obtained from Sigma. Brilliant Crocein was bought from Santa Cruz Biotechnology (sc-214624).

SEM

Ammonium iodide (203467) and iodine (207772) was purchased from Sigma.

IMMUNOSTAINING

EDTA powder (EDS-1KG), sucrose (S7903), triton (X100) and PVP (PVP40) were all bought from Sigma.

CD31, VEGFR2 and Sclerostin staining

CD31 primary rat anti-mouse antibody was bought from BD bioscience (550274). The secondary antibody, Alexa Fluor 488 goat anti-rat (A-11006) and Hoechst 33342 (H3570) utilised for staining the nuclei, was purchased from Invitrogen. Goat serum for blocking (G9023) and the PAP pen for drawing around the sections was obtained from sigma (Z672548). FluoromountG for mounting the coverslip was from Southern Biotech (0100-01).

The VEGFR2 primary antibody (2479) was bought from Cell Signalling Technologies. Goat anti-rabbit 488 was used as the secondary antibody and purchased from Invitrogen (A-11008).

Donkey serum for blocking prior to sclerostin immunostaining was purchased from Sigma (D9663). Sclerostin primary antibody was obtained from R&D Systems (MAB1589). Alexa Fluor 555 donkey anti-goat secondary antibody from Invitrogen was used (A-21432).

CELL CULTURE

Osteoblast cells

Collagenase (C0130) and EDTA powder (EDS-1KG) were ordered from Sigma. For culturing osteoblast cells, Gibco Alpha MEM media (12492013) and fetal bovine serum (10082147) was used. Nunc flasks with filter caps were bought from Thermo Fisher (156499). Gentamicin (G1397) and penicillin streptomycin (P4333) was added to the culture media as an antibacterial. Trypsin EDTA was used for splitting osteoblast cells (Gibco; R001100) and endothelial cells (Generon; 6915).

For deletion of osteoblast-derived VEGF, adenovirus-Cre was purchased from Vector Biolabs (1045). Adenovirus GFP was used as a control (1060). A VEGF ELISA kit from abcam (ab209882) was used to confirm the knockdown of VEGF.

A Pierce BCA protein assay kit was purchased from Thermofisher (23225) and for protein lysis tris, glycerol SDS and Na3VO4 were purchased from Sigma.

Endogenous VEGF and tyrosine kinase inhibitor SU5416 (S8442) were ordered from Sigma, along with DMSO which was used as a control (W387520).

In order to measure cell viability, a Cell Titer-Glo 2.0 Assay from Promega (G9242) was used.

For the ALP elution assay, P-Nitrophenol solution (N7660) from Sigma was used. P-Nitrophenyl phosphate was purchased from Thermo Fisher (34045).

Mouse Bone Marrow Endothelial Cells (MBMECs)

MBMECs (C57-6221), basal media and growth supplements (M1168) were ordered from Generon. The BrdU Cell Proliferation ELISA kit was purchased from Abcam (126556).

For qPCR the RNeasy kit from Qiagen (74104) and the Promega GoScript Reverse Transcriptase kit (A5003) was used to make cDNA. All custom-designed primers were ordered from Sigma.

For the endothelial cell gene arrays, the Qiagen RT2 first strand kit was used (330404). Qiagen RT2 profiler PCR Arrays for Mouse Endothelial Cell Biology (PAMM-015ZA) and Mouse Osteogenesis (PAMM-026ZA) were purchased for analysis of gene expression in MBMEC following OBVEGFKO.

WESTERN BLOT

10µl of 6x blue/orange loading dye was bought from Promega (G1881) and 2-Mercaptoethanol from Sigma (M6250). MOPS SDS running buffer from Thermo Fisher (NP0001) was used here, as well as 4-12% (w/v) NuPAGE protein gels (NP0321). Amersham™ Hybond® membranes for the transfer of protein were purchased from Fisher Scientific (45-000-850). NuPAGE transfer buffer 20X, was ordered from Thermo Fisher (NP00061). Western blotting sponge pads were ordered from VWR (103254-872), as was the filter paper (PIER88620).

The VEGFR2 primary antibody (2479) was from Cell Signalling Technologies. The secondary antibody used for both was goat anti-rabbit IgG HRP from Thermo Fisher (65-6120).

Tween-20 (P1379) and TBS (T5912) were both ordered from Sigma. ECL western blotting substrate kit was purchased from abcam (ab65623). Polymax developer (100488-220), fixer (102098-110) and Amersham hyperfilm ECL (28-9068-36) from VWR was used for producing images of protein expression.

Appendix B Solutions

ALP ELUTION

Working solution: 70% dH_20 + 20% 0.1M NaHCO3 + 10% 30 mM MgCl2 pH9.5

IMMUNOHISTOCHEMISTRY

EDTA

Mix 146.12g of EDTA powder with miliQ water up to 1000ml. Put NaOH tablets in to increase the pH to 7.4. The solution will become clear at about pH8 and you will then have to add HCl until pH 7.4 is reached.

20% Sucrose 2% PVP

Put 40g of sucrose into a beaker with 4g polyvinylpyrrolidone (PVP) and fill beaker up to 200ml with PBS. Mix with a mixer and with parafilm on lid. Once dissolved leave at 4°C.

0.3% Triton

900UL of triton topped up to 300ml with PBS. Cut the end of tip off for viscous liquid to flow through and pipette 910UL to allow for this. Stir with stirrer until dissolved.

4% PFA

50ml of 16% PFA and 150ml of cold PBS that has been in the fridge overnight are mixed to make 4% PFA on the morning that the dissection is performed.

Appendix C Methods

Table Appendix C.1: Primers used for genotyping, using genomic DNA. DNA is extracted from ear tips for the genotyping of first generation Ocn-Cre mice using Cre forward and reverse primers and from tail tips for the genotyping of second generation mice using Cre and VEGF forward and reverse primers. An annealing temperature of 55°C was used for all primers.

Target	Forward 5'-3'	Reverse 5'-3'	Annealing Temp (°C)
Cre	CAAATAGCCCTGGCAGATTC	TGATACAAGGGACATCTTCC	55
VEGF	CCTGGCCCTCAAGTACACCTT	TCCGTACGACGCATTTCTAG	55

Table Appendix C.2: Target genes used for qPCR. mRNA was extracted from OB and MBMEC, before being reverse transcribed. cDNA was used to look at the expression of target genes detailed below. An annealing temperature of 60°C was used for all primers.

Target	Forward 5'-3'	Reverse 5'-3'
Bmp1	TTGTACGCGAGAACATACAGC	CTGAGTCGGGTCCTTTGGC
Opg	AGTCCGTGAAGCAGGAGT	CCATCTGGACATTTTTTGCAAA
Rankl	CACAGCGCTTCTCAGGAGCT	CATCCAACCATGAGCCTTCC
Ar	GGACCATGTTTTACCCATCG	TCGTTTCTGCTGGCACATAG
Esr1	TTCTCCCTTTGCTACGTCAC	ATCGCTTTGTCAACGACTTC
Esr2	TGGTCATCAAATCGACCTTT	GGAACAAGGTCACATCCAAG
Vegfr2	TCTGTGGTTCTGCGTGGAGA	GTATCATTTCCAACCACCCT
Osteocalcin	CCTGAGTCTGACAAAGCCTTCA	GCCGGAGTCTGTTCACTACCTT
Sost	CTACTTGTGCACGCTGCCTT	TTTGGCGTCATAGGGATGGT
Gapdh	TGTGTCCGTCGTGGATCTGA	CCTGCTTCACCACCTTCTTGA
Vegf	ATCTTCAAGCCGTCCTGTGT	CTGCATGGTGATGTTGCTCT

Table appendix C.3: List of genes present in the Endothelial cell RT^2 Gene Profiler array from Qiagen.

Position	UniGene	GenBank	Symbol	Description
A01	Mm.754	NM_009598	*Ace*	Angiotensin I converting enzyme (peptidyl-dipeptidase A) 1
A02	Mm.27681	NM_009615	*Adam17*	A disintegrin and metallopeptidase domain 17
A03	Mm.301626	NM_007428	*Agt*	Angiotensinogen (serpin peptidase inhibitor, clade A, member 8)
A04	Mm.35062	NM_177322	*Agtr1a*	Angiotensin II receptor, type 1a
A05	Mm.309336	NM_009640	*Angpt1*	Angiopoietin 1
A06	Mm.1620	NM_009673	*Anxa5*	Annexin A5
A07	Mm.305152	NM_009696	*Apoe*	Apolipoprotein E
A08	Mm.19904	NM_007527	*Bax*	Bcl2-associated X protein
A09	Mm.257460	NM_009741	*Bcl2*	B-cell leukemia/lymphoma 2
A10	Mm.238213	NM_009743	*Bcl2l1*	Bcl2-like 1
A11	Mm.1051	NM_009807	*Casp1*	Caspase 1
A12	Mm.34405	NM_009810	*Casp3*	Caspase 3
B01	Mm.28278	NM_007616	*Cav1*	Caveolin 1, caveolae protein
B02	Mm.290320	NM_011333	*Ccl2*	Chemokine (C-C motif) ligand 2
B03	Mm.284248	NM_013653	*Ccl5*	Chemokine (C-C motif) ligand 5
B04	Mm.21767	NM_009868	*Cdh5*	Cadherin 5
B05	Mm.336848	NM_009805	*Cflar*	CASP8 and FADD-like apoptosis regulator
B06	Mm.4352	NM_009929	*Col18a1*	Collagen, type XVIII, alpha 1
B07	Mm.218009	NM_009950	*Cradd*	CASP2 and RIPK1 domain containing adaptor with death domain
B08	Mm.103711	NM_009142	*Cx3cl1*	Chemokine (C-X3-C motif) ligand 1
B09	Mm.21013	NM_008176	*Cxcl1*	Chemokine (C-X-C motif) ligand 1
B10	Mm.4979	NM_009140	*Cxcl2*	Chemokine (C-X-C motif) ligand 2
B11	Mm.6246	NM_007551	*Cxcr5*	Chemokine (C-X-C motif) receptor 5
B12	Mm.14543	NM_010104	*Edn1*	Endothelin 1
C01	Mm.284855	NM_007902	*Edn2*	Endothelin 2
C02	Mm.283168	NM_010332	*Ednra*	Endothelin receptor type A
C03	Mm.225297	NM_007932	*Eng*	Endoglin
C04	Mm.24816	NM_010169	*F2r*	Coagulation factor II (thrombin) receptor
C05	Mm.1614	NM_007974	*F2rl1*	Coagulation factor II (thrombin) receptor-like 1
C06	Mm.273188	NM_010171	*F3*	Coagulation factor III
C07	Mm.1626	NM_007987	*Fas*	Fas (TNF receptor superfamily member 6)
C08	Mm.3355	NM_010177	*Fasl*	Fas ligand (TNF superfamily, member 6)
C09	Mm.241282	NM_010197	*Fgf1*	Fibroblast growth factor 1
C10	Mm.473689	NM_008006	*Fgf2*	Fibroblast growth factor 2
C11	Mm.389712	NM_010228	*Flt1*	FMS-like tyrosine kinase 1
C12	Mm.193099	NM_010233	*Fn1*	Fibronectin 1
D01	Mm.3879	NM_010431	*Hif1a*	Hypoxia inducible factor 1, alpha subunit
D02	Mm.435508	NM_010493	*Icam1*	Intercellular adhesion molecule 1
D03	Mm.35814	NM_008350	*Il11*	Interleukin 11
D04	Mm.222830	NM_008361	*Il1b*	Interleukin 1 beta
D05	Mm.983	NM_010556	*Il3*	Interleukin 3
D06	Mm.1019	NM_031168	*Il6*	Interleukin 6
D07	Mm.3825	NM_008371	*Il7*	Interleukin 7
D08	Mm.16234	NM_010577	*Itga5*	Integrin alpha 5 (fibronectin receptor alpha)
D09	Mm.227	NM_008402	*Itgav*	Integrin alpha V
D10	Mm.263396	NM_010578	*Itgb1*	Integrin beta 1 (fibronectin receptor beta)
D11	Mm.87150	NM_016780	*Itgb3*	Integrin beta 3
D12	Mm.285	NM_010612	*Kdr*	Kinase insert domain protein receptor
E01	Mm.247073	NM_021099	*Kit*	Kit oncogene

E02	Mm.156952	NM_032006	*Mmp1a*	Matrix metallopeptidase 1a (interstitial collagenase)
E03	Mm.29564	NM_008610	*Mmp2*	Matrix metallopeptidase 2
E04	Mm.4406	NM_013599	*Mmp9*	Matrix metallopeptidase 9
E05	Mm.258415	NM_008713	*Nos3*	Nitric oxide synthase 3, endothelial cell
E06	Mm.2740	NM_008726	*Nppb*	Natriuretic peptide type B
E07	Mm.4627	NM_008727	*Npr1*	Natriuretic peptide receptor 1
E08	Mm.4807	NM_008756	*Ocln*	Occludin
E09	Mm.221403	NM_011058	*Pdgfra*	Platelet derived growth factor receptor, alpha polypeptide
E10	Mm.343951	NM_008816	*Pecam1*	Platelet/endothelial cell adhesion molecule 1
E11	Mm.332490	NM_019932	*Pf4*	Platelet factor 4
E12	Mm.4809	NM_008827	*Pgf*	Placental growth factor
F01	Mm.154660	NM_008872	*Plat*	Plasminogen activator, tissue
F02	Mm.4183	NM_008873	*Plau*	Plasminogen activator, urokinase
F03	Mm.971	NM_008877	*Plg*	Plasminogen
F04	Mm.3243	NM_011171	*Procr*	Protein C receptor, endothelial
F05	Mm.2339	NM_008968	*Ptgis*	Prostaglandin I2 (prostacyclin) synthase
F06	Mm.292547	NM_011198	*Ptgs2*	Prostaglandin-endoperoxide synthase 2
F07	Mm.5245	NM_011345	*Sele*	Selectin, endothelial cell
F08	Mm.1461	NM_011346	*Sell*	Selectin, lymphocyte
F09	Mm.3337	NM_011347	*Selp*	Selectin, platelet
F10	Mm.332590	NM_009151	*Selplg*	Selectin, platelet (p-selectin) ligand
F11	Mm.250422	NM_008871	*Serpine1*	Serine (or cysteine) peptidase inhibitor, clade E, member 1
F12	Mm.276325	NM_011434	*Sod1*	Superoxide dismutase 1, soluble
G01	Mm.14313	NM_013690	*Tek*	Endothelial-specific receptor tyrosine kinase
G02	Mm.124316	NM_011576	*Tfpi*	Tissue factor pathway inhibitor
G03	Mm.248380	NM_011577	*Tgfb1*	Transforming growth factor, beta 1
G04	Mm.24096	NM_009378	*Thbd*	Thrombomodulin
G05	Mm.4159	NM_011580	*Thbs1*	Thrombospondin 1
G06	Mm.8245	NM_011593	*Timp1*	Tissue inhibitor of metalloproteinase 1
G07	Mm.1293	NM_013693	*Tnf*	Tumor necrosis factor
G08	Mm.1062	NM_009425	*Tnfsf10*	Tumor necrosis factor (ligand) superfamily, member 10
G09	Mm.287977	NM_138302	*Tymp*	Thymidine phosphorylase
G10	Mm.76649	NM_011693	*Vcam1*	Vascular cell adhesion molecule 1
G11	Mm.282184	NM_009505	*Vegfa*	Vascular endothelial growth factor A
G12	Mm.22339	NM_011708	*Vwf*	Von Willebrand factor homolog
H01	Mm.328431	NM_007393	*Actb*	Actin, beta
H02	Mm.163	NM_009735	*B2m*	Beta-2 microglobulin
H03	Mm.343110	NM_008084	*Gapdh*	Glyceraldehyde-3-phosphate dehydrogenase
H04	Mm.3317	NM_010368	*Gusb*	Glucuronidase, beta
H05	Mm.2180	NM_008302	*Hsp90ab1*	Heat shock protein 90 alpha (cytosolic), class B member 1
H06	N/A	SA_00106	MGDC	Mouse Genomic DNA Contamination
H07	N/A	SA_00104	RTC	Reverse Transcription Control
H08	N/A	SA_00104	RTC	Reverse Transcription Control
H09	N/A	SA_00104	RTC	Reverse Transcription Control
H10	N/A	SA_00103	PPC	Positive PCR Control
H11	N/A	SA_00103	PPC	Positive PCR Control
H12	N/A	SA_00103	PPC	Positive PCR Control

Table appendix C.4: List of genes present in the Osteogenic RT^2 Gene Profiler array from Qiagen.

Position	UniGene	GenBank	Symbol	Description
A01	Mm.689	NM_007394	*Acvr1*	Activin A receptor, type 1
A02	Mm.197554	NM_013465	*Ahsg*	Alpha-2-HS-glycoprotein
A03	Mm.288186	NM_007431	*Alpl*	Alkaline phosphatase, liver/bone/kidney
A04	Mm.1620	NM_009673	*Anxa5*	Annexin A5
A05	Mm.389459	NM_007541	*Bglap*	Bone gamma carboxyglutamate protein
A06	Mm.2608	NM_007542	*Bgn*	Biglycan
A07	Mm.27757	NM_009755	*Bmp1*	Bone morphogenetic protein 1
A08	Mm.103205	NM_007553	*Bmp2*	Bone morphogenetic protein 2
A09	Mm.209571	NM_173404	*Bmp3*	Bone morphogenetic protein 3
A10	Mm.6813	NM_007554	*Bmp4*	Bmp4 Bone morphogenetic protein 4
A11	Mm.428950	NM_007555	*Bmp5*	Bone morphogenetic protein 5
A12	Mm.385759	NM_007556	*Bmp6*	Bone morphogenetic protein 6
B01	Mm.595	NM_007557	*Bmp7*	Bone morphogenetic protein 7
B02	Mm.237825	NM_009758	*Bmpr1a*	Bone morphogenetic protein receptor, type 1A
B03	Mm.39089	NM_007560	*Bmpr1b*	Bone morphogenetic protein receptor, type 1B
B04	Mm.7106	NM_007561	*Bmpr2*	Bone morphogenic protein receptor, type II (serine/threonine kinase)
B05	Mm.18628	NM_007643	*Cd36*	CD36 antigen
B06	Mm.1571	NM_009866	*Cdh11*	Cadherin 11
B07	Mm.20457	NM_009893	*Chrd*	Chordin
B08	Mm.443177	NM_009925	*Col10a1*	Collagen, type X, alpha 1
B09	Mm.297859	M_181277	*Col14a1*	Collagen, type XIV, alpha 1
B10	Mm.277735	NM_007742	*Col1a1*	Collagen, type I, alpha 1
B11	Mm.277792	NM_007743	*Col1a2*	Collagen, type I, alpha 2
B12	Mm.2423	NM_031163	*Col2a1*	Collagen, type II, alpha 1
C01	Mm.249555	NM_009930	*Col3a1*	Collagen, type III, alpha 1
C02	Mm.738	NM_009931	*Col4a1*	Collagen, type IV, alpha 1
C03	Mm.7281	NM_015734	*Col5a1*	Collagen, type V, alpha 1
C04	Mm.45071	NM_016685	*Comp*	Cartilage oligomeric matrix protein
C05	Mm.795	NM_007778	*Csf1*	Colony stimulating factor 1 (macrophage)
C06	Mm.4922	NM_009969	*Csf2*	Colony stimulating factor 2 (granulocyte-macrophage)
C07	Mm.1238	NM_009971	*Csf3*	Colony stimulating factor 3 (granulocyte)
C08	Mm.272085	NM_007802	*Ctsk*	Cathepsin K
C09	Mm.4873	NM_198854	*Dlx5*	Distal-less homeobox 5
C10	Mm.252481	NM_010113	*Egf*	Epidermal growth factor
C11	Mm.241282	NM_010197	*Fgf1*	Fibroblast growth factor 1
C12	Mm.473689	NM_008006	*Fgf2*	Fibroblast growth factor 2
D01	Mm.265716	NM_010206	*Fgfr1*	Fibroblast growth factor receptor 1
D02	Mm.16340	NM_010207	*Fgfr2*	Fibroblast growth factor receptor 2
D03	Mm.389712	NM_010228	*Flt1*	FMS-like tyrosine kinase 1
D04	Mm.193099	NM_010233	*Fn1*	Fibronectin 1
D05	Mm.432071	NM_145741	*Gdf10*	Growth differentiation factor 10
D06	Mm.391450	NM_010296	*Gli1*	GLI-Kruppel family member GLI1
D07	Mm.435508	NM_010493	*Icam1*	Intercellular adhesion molecule 1
D08	Mm.268521	NM_010512	*Igf1*	Insulin-like growth factor 1
D09	Mm.275742	NM_010513	*Igf1r*	Insulin-like growth factor I receptor
D10	Mm.439736	NM_010544	*Ihh*	Indian hedgehog
D11	Mm.5007	NM_008396	*Itga2*	Integrin alpha 2
D12	Mm.26646	NM_010575	*Itga2b*	Integrin alpha 2b
E01	Mm.57035	NM_013565	*Itga3*	Integrin alpha 3
E02	Mm.262106	NM_008401	*Itgam*	Integrin alpha M
E03	Mm.227	NM_008402	*Itgav*	Integrin alpha V
E04	Mm.263396	NM_010578	*Itgb1*	Integrin beta 1 (fibronectin receptor beta)
E05	Mm.14126	NM_019471	*Mmp10*	Matrix metallopeptidase 10
E06	Mm.29564	NM_008610	*Mmp2*	Matrix metallopeptidase 2
E07	Mm.16415	NM_008611	*Mmp8*	Matrix metallopeptidase 8
E08	Mm.4406	NM_013599	*Mmp9*	Matrix metallopeptidase 9
E09	Mm.256765	NM_008689	*Nfkb1*	Nuclear factor of kappa light polypeptide gene enhancer in B-cells 1, p105
E10	Mm.135266	NM_008711	*Nog*	Noggin

E11	Mm.2675	NM_008808	*Pdgfa*	Platelet derived growth factor, alpha
E12	Mm.2529	NM_011077	*Phex*	Phosphate regulating gene with homologies to endopeptidases on the X chromosome (hypophosphatemia, vitamin D resistant rickets)
F01	Mm.391013	NM_009820	*Runx2*	Runt related transcription factor 2
F02	Mm.22708	NM_009825	*Serpinh1*	Serine (or cysteine) peptidase inhibitor, clade H, member 1
F03	Mm.223717	NM_008539	*Smad1*	MAD homolog 1 (Drosophila)
F04	Mm.391091	NM_010754	*Smad2*	MAD homolog 2 (Drosophila)
F05	Mm.7320	NM_016769	*Smad3*	MAD homolog 3 (Drosophila)
F06	Mm.100399	NM_008540	*Smad4*	MAD homolog 4 (Drosophila)
F07	Mm.272920	NM_008541	*Smad5*	MAD homolog 5 (Drosophila)
F08	Mm.265602	NM_024449	*Sost*	Sclerostin
F09	Mm.286407	NM_011448	*Sox9*	SRY-box containing gene 9
F10	Mm.263284	NM_130458	*Sp7*	Sp7 transcription factor 7
F11	Mm.288474	NM_009263	*Spp1*	Secreted phosphoprotein 1
F12	Mm.248380	NM_011577	*Tgfb1*	Transforming growth factor, beta 1
G01	Mm.18213	NM_009367	*Tgfb2*	Transforming growth factor, beta 2
G02	Mm.3992	NM_009368	*Tgfb3*	Transforming growth factor, beta 3
G03	Mm.197552	NM_009370	*Tgfbr1*	Transforming growth factor, beta receptor I
G04	Mm.172346	NM_009371	*Tgfbr2*	Transforming growth factor, beta receptor II
G05	Mm.200775	NM_011578	*Tgfbr3*	Transforming growth factor, beta receptor III
G06	Mm.1293	NM_013693	*Tnf*	Tumor necrosis factor
G07	Mm.249221	NM_011613	*Tnfsf11*	Tumor necrosis factor (ligand) superfamily, member 11
G08	Mm.3280	NM_011658	*Twist1*	Twist homolog 1 (Drosophila)
G09	Mm.76649	NM_011693	*Vcam1*	Vascular cell adhesion molecule 1
G10	Mm.245084	NM_009504	*Vdr*	Vitamin D receptor
G11	Mm.282184	NM_009505	*Vegfa*	Vascular endothelial growth factor A
G12	Mm.15607	NM_011697	*Vegfb*	Vascular endothelial growth factor B
H01	Mm.328431	NM_007393	*Actb*	Actin, beta
H02	Mm.163	NM_009735	*B2m*	Beta-2 microglobulin
H03	Mm.343110	NM_008084	*Gapdh*	Glyceraldehyde-3-phosphate dehydrogenase
H04	Mm.3317	NM_010368	*Gusb*	Glucuronidase, beta
H05	Mm.2180	NM_008302	*Hsp90ab1*	Heat shock protein 90 alpha (cytosolic), class B member 1
H06	N/A	SA_00106	MGDC	Mouse Genomic DNA Contamination
H07	N/A	SA_00104	RTC	Reverse Transcription Control
H08	N/A	SA_00104	RTC	Reverse Transcription Control
H09	N/A	SA_00104	RTC	Reverse Transcription Control
H10	N/A	SA_00103	PPC	Positive PCR Control
H11	N/A	SA_00103	PPC	Positive PCR Control
H12	N/A	SA_00103	PPC	Positive PCR Control

Appendix D Results

a

WT (%)	OcnVEGFKO (%)
100	35
100	VEGF undetectably low
100	20

b

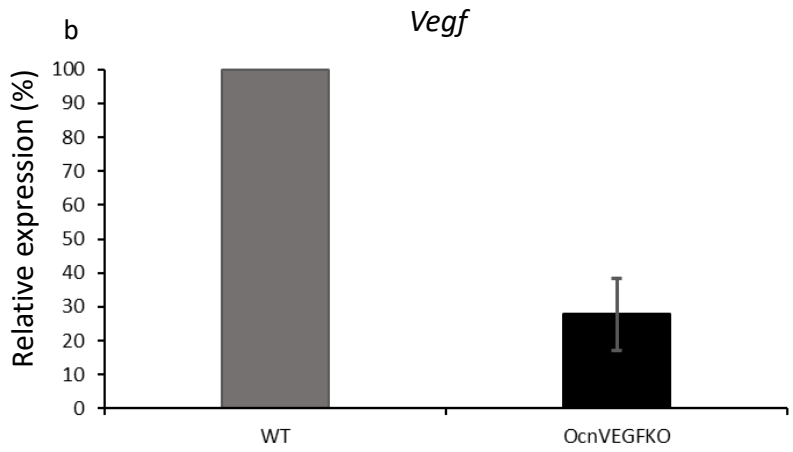

Figure Appendix D.1: Relative expression of *Vegf* in OcnVEGFKO versus WT control shows successful deletion of *Vegf*. RNA was extracted from 16 week old snap frozen calvaria and reverse transcribed. qPCR determined the relative expression of *Vegf* following the bone specific deletion of *Vegf.* Raw data represented in a table format and WT normalised to 100% to calculate the relative % of *Vegf* following conditional deletion (n=3; a). Significant decrease in *Vegf* expression is demonstrated in graphical format following OcnVEGFKO. Data is represented as mean value ± SEM, (n=2; b).

Table Appendix D.2: Proportions of lacunae above/below the threshold of small osteocyte lacunae, for each individual animal.

Sex	Mutation	Repeat	Num.High	Num.Low	Num.Total	Low.Propor	High.Propor
Female	WT	1	7348	1175	8523	0.1378623	0.8621377
Female	WT	2	9391	721	10112	0.0713014	0.9286986
Female	WT	3	8416	733	9149	0.080118	0.919882
Female	OcnVEGFKO	1	7393	1465	8858	0.1653872	0.8346128
Female	OcnVEGFKO	2	7397	1504	8901	0.1689698	0.8310302
Female	OcnVEGFKO	3	8215	1405	9620	0.1460499	0.8539501
Male	WT	1	10522	1417	11939	0.1186867	0.8813133
Male	WT	2	9709	1182	10891	0.10853	0.89147
Male	WT	3	7519	1495	9014	0.1658531	0.8341469
Male	OcnVEGFKO	1	7526	7466	14992	0.4979989	0.5020011
Male	OcnVEGFKO	2	8953	6213	15166	0.4096664	0.5903336
Male	OcnVEGFKO	3	7693	9775	17468	0.5595947	0.4404053

Table Appendix D.3: Quantitative morphometric measures for intracortical vascular canals and osteocyte lacunae of 4 and 16-week-old WT and $_{Ocn}$VEGFKO mice. Intracortical canals and osteocyte lacunae have been defined using individual thresholds for each animal. Quantification is performed using 300 slices per dataset.

	4 week old						16 week old					
	Female			Male			Female			Male		
	WT	$_{Ocn}$VEGFKO	p	WT	$_{Ocn}$VEGFKO	p	WT	$_{Ocn}$VEGFKO	p	WT	$_{Ocn}$VEGFKO	p
Lc.V (μm^3)	421±52	403±26	NS	425±23	425±34	NS	363±24	423±33	p<0.05	423±21	421±19	NS
Ca.V (μm^3)	21023±8262	62560±28310	NS	20189±4737	79296±19376	p<0.05	16794±8598	35362±14434	NS	11144±3749	862208±374663	P<0.01
Lc.Dm (µm)	4.32±0.48	4.21±0.70	NS	4.49±0.59	3.99±0.6	NS	3.27±0.20	3.69±0.10	p<0.05	3.78±0.09	3.25±0.05	p<0.001
Ca.Dm (µm)	6.77±1.43	6.49±1.59	NS	6.90±0.94	7.02±1.88	NS	5.90±1.13	6.63±0.94	NS	5.60±0.52	6.17±0.48	NS
Number of Osteocyte Lacunae (# per mm3)	74265±7267	88399±10108	NS	80104±8404	88219±12472	NS	66339±857	73645±1472	p<0.05	64364±2238	70130±3822	NS
Number of Blood Vessel Canals (# per mm3)	1379±538	1001±435	NS	1050±254	614±235	NS	682±390	625±228	NS	819±103	170±62	p<0.01

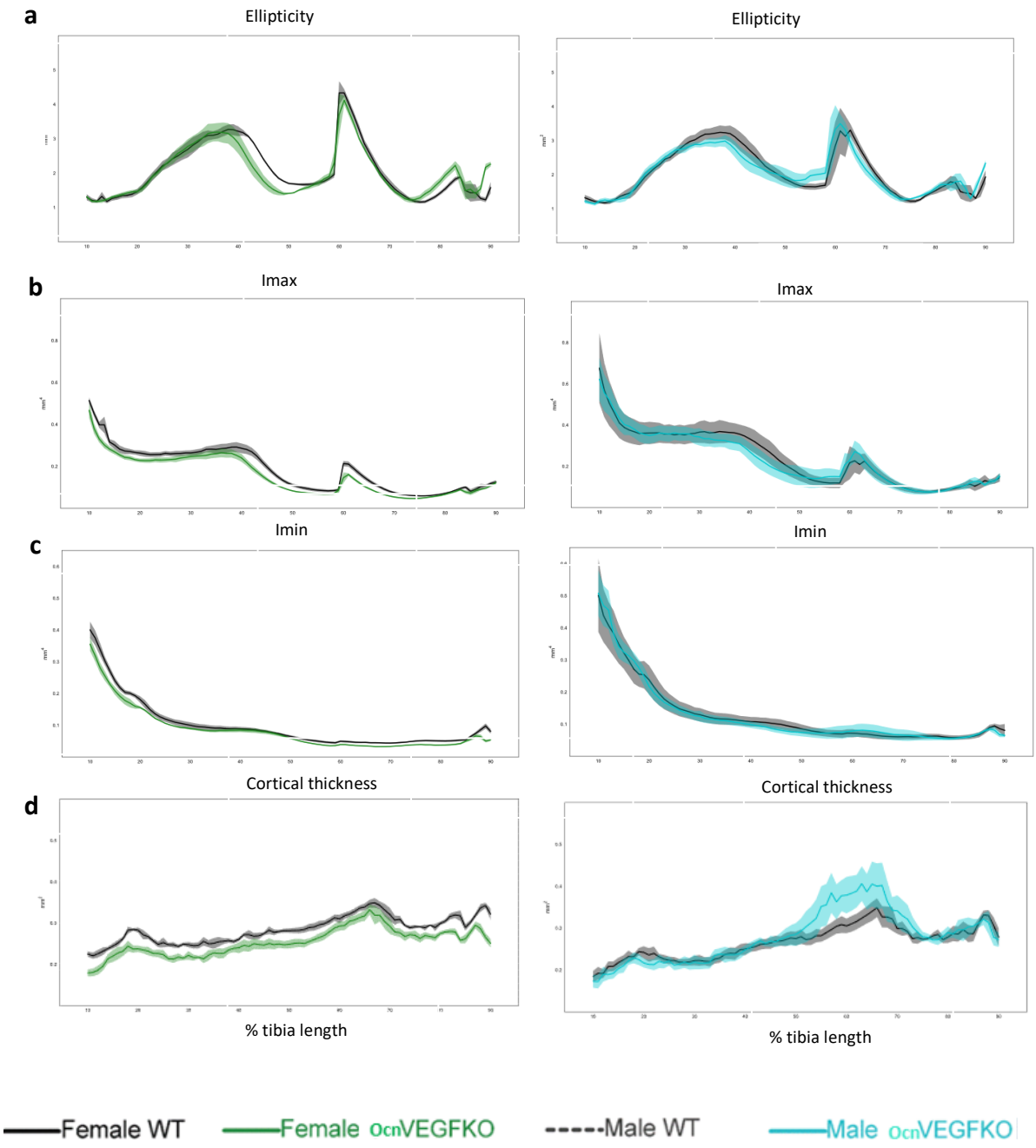

Figure appendix D.4: Changes in ellipticity, Imax, Imin and thickness along the tibial length following OcnVEGFKO. Line graphs represent means for female and male WT versus OcnVEGFKO ± SEM (n=4 female and 4 male mice from individual litters). Data plotted for measurements along the tibial length (10 to 90%), representative of overall effect of genotype.

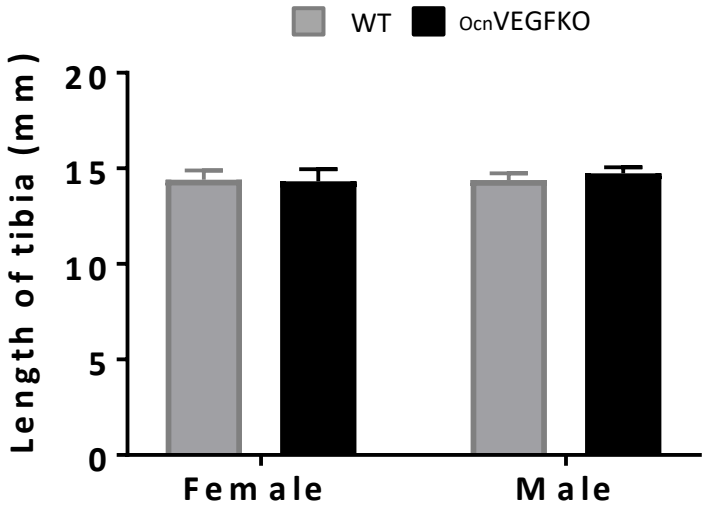

Figure appendix D.5: No significant difference in tibia length of 4 week old mice following OcnVEGFKO. The length of the tibia was assessed using the slice number taken from medium resolution scans (18µm voxel size). No significant differences were identified in males or females. Data is represented as mean value ± SEM, n=3.

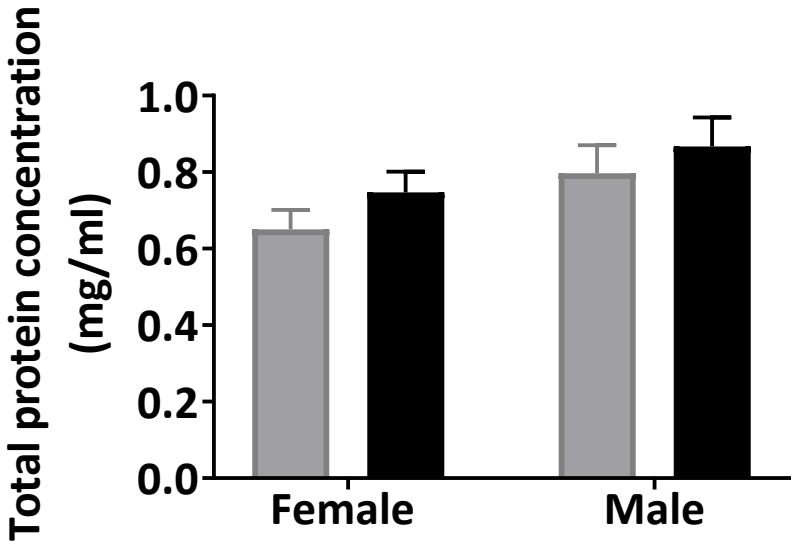

Figure appendix D.6: No change in total protein concentration following OBVEGFKO in male and female LOBs. Cells were plated at 500,000 cells per well and LOBs were treated with Adenovirus-GFP (WT) and Adenovirus-Cre (OBVEGFKO) for 6 days, followed by treatment with low serum media for 24 hours. Protein was lysed and protein concentrations recorded using a BCA assay. WT versus OBVEGFKO ± SEM (n=4 individual LOB isolations).

List of References

ACHEN, M. G., JELTSCH, M., KUKK, E., MÄKINEN, T., VITALI, A., WILKS, A. F., ALITALO, K. & STACKER, S. A. 1998. Vascular endothelial growth factor D (VEGF-D) is a ligand for the tyrosine kinases VEGF receptor 2 (Flk1) and VEGF receptor 3 (Flt4). *Proc Natl Acad Sci U S A,* 95**,** 548-53.

ADDISON, W. N., NAKANO, Y., LOISEL, T., CRINE, P. & MCKEE, M. D. 2008. MEPE-ASARM peptides control extracellular matrix mineralization by binding to hydroxyapatite: an inhibition regulated by PHEX cleavage of ASARM. *J Bone Miner Res,* 23**,** 1638-49.

AGNA, J. W., KNOWLES, H. C. & ALVERSON, G. 1958. The mineral content of normal human bone. *J Clin Invest,* 37**,** 1357-61.

AKIYAMA, H., LYONS, J. P., MORI-AKIYAMA, Y., YANG, X., ZHANG, R., ZHANG, Z., DENG, J. M., TAKETO, M. M., NAKAMURA, T., BEHRINGER, R. R., MCCREA, P. D. & DE CROMBRUGGHE, B. 2004. Interactions between Sox9 and beta-catenin control chondrocyte differentiation. *Genes Dev,* 18**,** 1072-87.

ALBRIGHT, F. 1947a. The effect of hormones on osteogenesis in man. *Recent Prog Horm Res,* 1**,** 293-353.

ALBRIGHT, F. 1947b. Osteoporosis. *Ann Intern Med,* 27**,** 861-82.

ALT, V., THORMANN, U., RAY, S., ZAHNER, D., DÜRSELEN, L., LIPS, K., EL KHASSAWNA, T., HEISS, C., RIEDRICH, A., SCHLEWITZ, G., IGNATIUS, A., KAMPSCHULTE, M., VON DEWITZ, H., HEINEMANN, S., SCHNETTLER, R. & LANGHEINRICH, A. 2013. A new metaphyseal bone defect model in osteoporotic rats to study biomaterials for the enhancement of bone healing in osteoporotic fractures. *Acta Biomater,* 9**,** 7035-42.

ANDERSON, H. C. 2003. Matrix vesicles and calcification. *Curr Rheumatol Rep,* 5**,** 222-6.

ANDERSON, H. C., SIPE, J. B., HESSLE, L., DHANYAMRAJU, R., ATTI, E., CAMACHO, N. P., MILLÁN, J. L. & DHAMYAMRAJU, R. 2004. Impaired calcification around matrix vesicles of growth plate and bone in alkaline phosphatase-deficient mice. *Am J Pathol,* 164**,** 841-7.

ANDERSON, P. H., SAWYER, R. K., MOORE, A. J., MAY, B. K., O'LOUGHLIN, P. D. & MORRIS, H. A. 2008. Vitamin D depletion induces RANKL-mediated osteoclastogenesis and bone loss in a rodent model. *J Bone Miner Res,* 23**,** 1789-97.

ANDERSSON, G. & EK-RYLANDER, B. 1995. The tartrate-resistant purple acid phosphatase of bone osteoclasts--a protein phosphatase with multivalent substrate specificity and regulation. *Acta Orthop Scand Suppl,* 266**,** 189-94.

ANDRAE, J., GALLINI, R. & BETSHOLTZ, C. 2008. Role of platelet-derived growth factors in physiology and medicine. *Genes Dev,* 22**,** 1276-312.

ATKINS, G. J., ROWE, P. S., LIM, H. P., WELLDON, K. J., ORMSBY, R., WIJENAYAKA, A. R., ZELENCHUK, L., EVDOKIOU, A. & FINDLAY, D. M. 2011. Sclerostin is a locally acting regulator of late-osteoblast/preosteocyte differentiation and regulates mineralization through a MEPE-ASARM-dependent mechanism. *J Bone Miner Res,* 26**,** 1425-36.

AUGAT, P. & SCHORLEMMER, S. 2006. The role of cortical bone and its microstructure in bone strength. *Age Ageing,* 35 Suppl 2**,** ii27-ii31.

AVIOLI, L. V. & KRANE, S. M. 1998. *Metabolic bone disease and clinically related disorders,* San Diego ; London, Academic.

BAGI, C. M., BERRYMAN, E. & MOALLI, M. R. 2011. Comparative bone anatomy of commonly used laboratory animals: implications for drug discovery. *Comp Med,* 61**,** 76-85.

BALA, Y., ZEBAZE, R., GHASEM-ZADEH, A., ATKINSON, E. J., IULIANO, S., PETERSON, J. M., AMIN, S., BJØRNEREM, Å., MELTON, L. J., JOHANSSON, H., KANIS, J. A., KHOSLA, S. & SEEMAN, E. 2014. Cortical porosity identifies women with osteopenia at increased risk for forearm fractures. *J Bone Miner Res,* 29**,** 1356-62.

BALASCH, J. 2003. Sex steroids and bone: current perspectives. *Hum Reprod Update,* 9**,** 207-22.

BARON, R. 1989. Polarity and membrane transport in osteoclasts. *Connect Tissue Res,* 20**,** 109-20.

BATES, D. O., HILLMAN, N. J., WILLIAMS, B., NEAL, C. R. & POCOCK, T. M. 2002. Regulation of microvascular permeability by vascular endothelial growth factors. *J Anat,* 200**,** 581-97.

BAZZAZI, H., ISENBERG, J. S. & POPEL, A. S. 2017. Inhibition of VEGFR2 Activation and Its Downstream Signaling to ERK1/2 and Calcium by Thrombospondin-1 (TSP1):. *Front Physiol,* 8**,** 48.

BELL, K. L., LOVERIDGE, N., POWER, J., GARRAHAN, N., MEGGITT, B. F. & REEVE, J. 1999. Regional differences in cortical porosity in the fractured femoral neck. *Bone,* 24**,** 57-64.

BELLOMO, D., HEADRICK, J. P., SILINS, G. U., PATERSON, C. A., THOMAS, P. S., GARTSIDE, M., MOULD, A., CAHILL, M. M., TONKS, I. D., GRIMMOND, S. M., TOWNSON, S., WELLS, C., LITTLE, M., CUMMINGS, M. C., HAYWARD, N. K. & KAY, G. F. 2000. Mice lacking the vascular endothelial growth factor-B gene (Vegfb) have smaller hearts, dysfunctional coronary vasculature, and impaired recovery from cardiac ischemia. *Circ Res,* 86**,** E29-35.

BERENDSEN, A. D. & OLSEN, B. R. 2014. How vascular endothelial growth factor-A (VEGF) regulates differentiation of mesenchymal stem cells. *J Histochem Cytochem,* 62**,** 103-8.

BERENDSEN, A. D. & OLSEN, B. R. 2015. Bone development. *Bone,* 80**,** 14-18.

BERMEJO-ALVAREZ, P., RIZOS, D., RATH, D., LONERGAN, P. & GUTIERREZ-ADAN, A. 2010. Sex determines the expression level of one third of the actively expressed genes in bovine blastocysts. *Proc Natl Acad Sci U S A,* 107**,** 3394-9.

BERSE, B., BROWN, L. F., VAN DE WATER, L., DVORAK, H. F. & SENGER, D. R. 1992. Vascular permeability factor (vascular endothelial growth factor) gene is expressed differentially in normal tissues, macrophages, and tumors. *Mol Biol Cell,* 3**,** 211-20.

BERTHOIS, Y., KATZENELLENBOGEN, J. A. & KATZENELLENBOGEN, B. S. 1986. Phenol red in tissue culture media is a weak estrogen: implications concerning the study of estrogen-responsive cells in culture. *Proc Natl Acad Sci U S A,* 83**,** 2496-500.

BERWICK, D. C., JAVAHERI, B., WETZEL, A., HOPKINSON, M., NIXON-ABELL, J., GRANNÒ, S., PITSILLIDES, A. A. & HARVEY, K. 2017. Pathogenic LRRK2 variants are gain-of-function mutations that enhance LRRK2-mediated repression of β-catenin signaling. *Mol Neurodegener,* 12**,** 9.

BIEWENER, A. A., SWARTZ, S. M. & BERTRAM, J. E. 1986. Bone modeling during growth: dynamic strain equilibrium in the chick tibiotarsus. *Calcif Tissue Int,* 39**,** 390-5.

BILEZIKIAN, J. P., RAISZ, L. G. & MARTIN, T. J. 2008. *Principles of bone biology,* Amsterdam ; London, Elsevier.

BILTZ, R. M. & PELLEGRINO, E. D. 1977. The nature of bone carbonate. *Clin Orthop Relat Res*, 279-92.

BINGHAM, P. J. & RAISZ, L. G. 1974. Bone growth in organ culture: effects of phosphate and other nutrients on bone and cartilage. *Calcif Tissue Res,* 14, 31-48.

BIRO, F. M., PINNEY, S. M., HUANG, B., BAKER, E. R., WALT CHANDLER, D. & DORN, L. D. 2014. Hormone changes in peripubertal girls. *J Clin Endocrinol Metab,* 99, 3829-35.

BLAKEMORE, S. J., BURNETT, S. & DAHL, R. E. 2010. The role of puberty in the developing adolescent brain. *Hum Brain Mapp,* 31, 926-33.

BLUMER, M. J., HAUSOTT, B., SCHWARZER, C., HAYMAN, A. R., STEMPEL, J. & FRITSCH, H. 2012. Role of tartrate-resistant acid phosphatase (TRAP) in long bone development. *Mech Dev,* 129, 162-76.

BONEWALD, L. F. 1999. Establishment and characterization of an osteocyte-like cell line, MLO-Y4. *J Bone Miner Metab,* 17, 61-5.

BONEWALD, L. F. 2004. Osteocyte biology: its implications for osteoporosis. *J Musculoskelet Neuronal Interact,* 4, 101-4.

BONEWALD, L. F. 2011. The amazing osteocyte. *J Bone Miner Res,* 26, 229-38.

BONEWALD, L. F. & WACKER, M. J. 2013. FGF23 production by osteocytes. *Pediatr Nephrol,* 28, 563-8.

BONGAARTS, J. 2009. Human population growth and the demographic transition. *Philos Trans R Soc Lond B Biol Sci,* 364, 2985-90.

BOSKEY, A. L., GADALETA, S., GUNDBERG, C., DOTY, S. B., DUCY, P. & KARSENTY, G. 1998. Fourier transform infrared microspectroscopic analysis of bones of osteocalcin-deficient mice provides insight into the function of osteocalcin. *Bone,* 23, 187-96.

BOSWORTH, L. A. & DOWNES, S. 2011. *Electrospinning for tissue regeneration,* Oxford, Woodhead Publishing.

BOYCE, B. F. & XING, L. 2008. Functions of RANKL/RANK/OPG in bone modeling and remodeling. *Arch Biochem Biophys,* 473, 139-46.

BOYDE, A. 1980a. Electron microscopy of the mineralising front. Metab Bone Dis Rel Res.

BOYDE, A. 1980b. Evidence against osteocytic osteolysis. In: Bone histomorphometry. . Metab Bone Dis Rel Res: Societe Nouvelle de Publications Medicales et Dentaires Paris.

BOYDE, A., MCCORKELL, F. A., TAYLOR, G. K., BOMPHREY, R. J. & DOUBE, M. 2014. Iodine vapor staining for atomic number contrast in backscattered electron and X-ray imaging. *Microsc Res Tech,* 77, 1044-51.

BOYDE, A., STAINES, K. A., JAVAHERI, B., MILLAN, J. L., PITSILLIDES, A. A. & FARQUHARSON, C. 2017. A distinctive patchy osteomalacia characterises Phospho1-deficient mice. *J Anat,* 231, 298-308.

BREELAND, G. 2019. Embryology, Bone Ossification. *In:* MENEZES, R. (ed.). StatPearls.

BREIER, G. & RISAU, W. 1996. The role of vascular endothelial growth factor in blood vessel formation. *Trends Cell Biol,* 6, 454-6.

BRITZ, H. M., JOKIHAARA, J., LEPPANEN, O. V., JARVINEN, T. & COOPER, D. M. 2010. 3D visualization and quantification of rat cortical bone porosity using a desktop micro-CT system: a case study in the tibia. *J Microsc,* 240**,** 32-7.

BRITZ, H. M., JOKIHAARA, J., LEPPANEN, O. V., JARVINEN, T. L. & COOPER, D. M. 2012. The effects of immobilization on vascular canal orientation in rat cortical bone. *J Anat,* 220**,** 67-76.

BROOKES, M. 1963. BLOOD SUPPLY OF LONG BONES. *Br Med J,* 2**,** 1064-5.

BROOKES, M. & HARRISON, R. G. 1957. The vascularization of the rabbit femur and tibio-fibula. *J Anat,* 91**,** 61-72.

BUETTMANN, E. G., MCKENZIE, J. A., MIGOTSKY, N., SYKES, D. A. W., HU, P., YONEDA, S. & SILVA, M. J. 2019. VEGFA from Early Osteoblast Lineage Cells (Osterix+) is Required in Mice for Fracture Healing. *J Bone Miner Res*.

BURGHARDT, A. J., KAZAKIA, G. J., RAMACHANDRAN, S., LINK, T. M. & MAJUMDAR, S. 2010. Age- and gender-related differences in the geometric properties and biomechanical significance of intracortical porosity in the distal radius and tibia. *J Bone Miner Res,* 25**,** 983-93.

BURKHARDT, R., KETTNER, G., BOHM, W., SCHMIDMEIER, M., SCHLAG, R., FRISCH, B., MALLMANN, B., EISENMENGER, W. & GILG, T. 1987. Changes in trabecular bone, hematopoiesis and bone marrow vessels in aplastic anemia, primary osteoporosis, and old age: a comparative histomorphometric study. *Bone,* 8**,** 157-64.

BURNS, E. R., STEVENS, J. A. & LEE, R. 2016. The direct costs of fatal and non-fatal falls among older adults - United States. *J Safety Res,* 58**,** 99-103.

BURR, D. B. 2010. Cortical bone: a target for fracture prevention? *Lancet,* 375**,** 1672-3.

BURR, D. B., MARTIN, R. B., SCHAFFLER, M. B. & RADIN, E. L. 1985. Bone remodeling in response to in vivo fatigue microdamage. *J Biomech,* 18**,** 189-200.

CALLEWAERT, F., SINNESAEL, M., GIELEN, E., BOONEN, S. & VANDERSCHUEREN, D. 2010a. Skeletal sexual dimorphism: relative contribution of sex steroids, GH-IGF1, and mechanical loading. *J Endocrinol,* 207**,** 127-34.

CALLEWAERT, F., VENKEN , K., KOPCHICK , J., TORCASIO , A., VAN LENTHE , G., BOONEN , S. & VANDERSCHUERE , D. 2009. Sexual dimorphism in cortical bone size and strength but not density is determined by independent and time-specific actions of sex steroids and IGF-1: Evidence from pubertal mouse models. *Journal of Bone and Mineral Research,* 25**,** 617-626.

CALLEWAERT, F., VENKEN, K., KOPCHICK, J. J., TORCASIO, A., VAN LENTHE, G. H., BOONEN, S. & VANDERSCHUEREN, D. 2010b. Sexual dimorphism in cortical bone size and strength but not density is determined by independent and time-specific actions of sex steroids and IGF-1: evidence from pubertal mouse models. *J Bone Miner Res,* 25**,** 617-26.

CAMPION, J. M. & MARICIC, M. J. 2003. Osteoporosis in men. *Am Fam Physician,* 67**,** 1521-6.

CARMELIET, P., FERREIRA, V., BREIER, G., POLLEFEYT, S., KIECKENS, L., GERTSENSTEIN, M., FAHRIG, M., VANDENHOECK, A., HARPAL, K., EBERHARDT, C., DECLERCQ, C., PAWLING, J., MOONS, L., COLLEN, D., RISAU, W. & NAGY, A. 1996. Abnormal blood vessel development and lethality in embryos lacking a single VEGF allele. *Nature,* 380**,** 435-9.

CARRIERO, A., DOUBE, M., VOGT, M., BUSSE, B., ZUSTIN, J., LEVCHUK, A., SCHNEIDER, P., MULLER, R. & SHEFELBINE, S. J. 2014. Altered lacunar and vascular porosity in osteogenesis imperfecta mouse bone as revealed by synchrotron tomography contributes to bone fragility. *Bone,* 61**,** 116-24.

CARTER, D. R. & HAYES, W. C. 1977. The compressive behavior of bone as a two-phase porous structure. *J Bone Joint Surg Am,* 59**,** 954-62.

CARTER, S. L., EKLUND, A. C., KOHANE, I. S., HARRIS, L. N. & SZALLASI, Z. 2006. A signature of chromosomal instability inferred from gene expression profiles predicts clinical outcome in multiple human cancers. *Nat Genet,* 38**,** 1043-8.

CHAI, Y. E. 2015. *Craniofacial development*.

CHAMBERS, T. J. 2000. Regulation of the differentiation and function of osteoclasts. *J Pathol,* 192**,** 4-13.

CHARLES, J. F. & ALIPRANTIS, A. O. 2014. Osteoclasts: more than 'bone eaters'. *Trends Mol Med,* 20**,** 449-59.

CHEN, L., ADAR, R., YANG, X., MONSONEGO, E. O., LI, C., HAUSCHKA, P. V., YAYON, A. & DENG, C. X. 1999. Gly369Cys mutation in mouse FGFR3 causes achondroplasia by affecting both chondrogenesis and osteogenesis. *J Clin Invest,* 104**,** 1517-25.

CINES, D. B., POLLAK, E. S., BUCK, C. A., LOSCALZO, J., ZIMMERMAN, G. A., MCEVER, R. P., POBER, J. S., WICK, T. M., KONKLE, B. A., SCHWARTZ, B. S., BARNATHAN, E. S., MCCRAE, K. R., HUG, B. A., SCHMIDT, A. M. & STERN, D. M. 1998. Endothelial cells in physiology and in the pathophysiology of vascular disorders. *Blood,* 91**,** 3527-61.

CLARKE, B. 2008. Normal bone anatomy and physiology. *Clin J Am Soc Nephrol,* 3 Suppl 3**,** S131-9.

CLARKE, B. L. 2014. Anti-sclerostin antibodies: utility in treatment of osteoporosis. *Maturitas,* 78**,** 199-204.

CLARKIN, C. & OLSEN, B. R. 2010. On bone-forming cells and blood vessels in bone development. *Cell Metab,* 12**,** 314-316.

CLARKIN, C. E., EMERY, R. J., PITSILLIDES, A. A. & WHEELER-JONES, C. P. 2008a. Evaluation of VEGF-mediated signaling in primary human cells reveals a paracrine action for VEGF in osteoblast-mediated crosstalk to endothelial cells. *J Cell Physiol,* 214**,** 537-44.

CLARKIN, C. E., GARONNA, E., PITSILLIDES, A. A. & WHEELER-JONES, C. P. 2008b. Heterotypic contact reveals a COX-2-mediated suppression of osteoblast differentiation by endothelial cells: A negative modulatory role for prostanoids in VEGF-mediated cell: cell communication? *Exp Cell Res,* 314**,** 3152-61.

CLAXTON, S. & FRUTTIGER, M. 2004. Periodic Delta-like 4 expression in developing retinal arteries. *Gene Expr Patterns,* 5**,** 123-7.

COHEN, J. & HARRIS, W. H. 1958. The three-dimensional anatomy of haversian systems. *J Bone Joint Surg Am,* 40-A**,** 419-34.

COHEN, T., GITAY-GOREN, H., SHARON, R., SHIBUYA, M., HALABAN, R., LEVI, B. Z. & NEUFELD, G. 1995. VEGF121, a vascular endothelial growth factor (VEGF) isoform lacking heparin binding ability, requires cell-surface heparan sulfates for efficient binding to the VEGF receptors of human melanoma cells. *J Biol Chem,* 270**,** 11322-6.

COLLERAN, P. N., WILKERSON, M. K., BLOOMFIELD, S. A., SUVA, L. J., TURNER, R. T. & DELP, M. D. 2000. Alterations in skeletal perfusion with simulated microgravity: a possible mechanism for bone remodeling. *J Appl Physiol (1985),* 89**,** 1046-54.

COLLIN-OSDOBY, P. 1994. Role of vascular endothelial cells in bone biology. *J Cell Biochem,* 55**,** 304-9.

COLLIN-OSDOBY, P., ROTHE, L., ANDERSON, F., NELSON, M., MALONEY, W. & OSDOBY, P. 2001. Receptor activator of NF-kappa B and osteoprotegerin expression by human microvascular endothelial cells, regulation by inflammatory cytokines, and role in human osteoclastogenesis. *J Biol Chem,* 276**,** 20659-72.

COOKE, J. P., CREAGER, M. A., OSMUNDSON, P. J. & SHEPHERD, J. T. 1990. Sex differences in control of cutaneous blood flow. *Circulation,* 82**,** 1607-15.

COOPER, C., ATKINSON, E. J., O'FALLON, W. M. & MELTON, L. J. 1992. Incidence of clinically diagnosed vertebral fractures: a population-based study in Rochester, Minnesota, 1985-1989. *J Bone Miner Res,* 7**,** 221-7.

COOPER, D., TURINSKY, A., SENSEN, C. & HALLGRIMSSON, B. 2007. Effect of voxel size on 3D micro-CT analysis of cortical bone porosity. *Calcif Tissue Int,* 80**,** 211-9.

COOPER, D. M., KAWALILAK, C. E., HARRISON, K., JOHNSTON, B. D. & JOHNSTON, J. D. 2016. Cortical Bone Porosity: What Is It, Why Is It Important, and How Can We Detect It? *Curr Osteoporos Rep,* 14**,** 187-98.

COOPER, D. M., TURINSKY, A. L., SENSEN, C. W. & HALLGRIMSSON, B. 2003. Quantitative 3D analysis of the canal network in cortical bone by micro-computed tomography. *Anat Rec B New Anat,* 274**,** 169-79.

CORRAL, D. A., AMLING, M., PRIEMEL, M., LOYER, E., FUCHS, S., DUCY, P., BARON, R. & KARSENTY, G. 1998. Dissociation between bone resorption and bone formation in osteopenic transgenic mice. *Proc Natl Acad Sci U S A,* 95**,** 13835-40.

COSTA, N., PARAMANATHAN, S., MAC DONALD, D., WIERZBICKI, A. S. & HAMPSON, G. 2009. Factors regulating circulating vascular endothelial growth factor (VEGF): association with bone mineral density (BMD) in post-menopausal osteoporosis. *Cytokine,* 46**,** 376-81.

CRAMER, T., SCHIPANI, E., JOHNSON, R. S., SWOBODA, B. & PFANDER, D. 2004. Expression of VEGF isoforms by epiphyseal chondrocytes during low-oxygen tension is HIF-1 alpha dependent. *Osteoarthritis Cartilage,* 12**,** 433-9.

CURREY, J. 1960. Differences in the blood-supply of bone of different histological types. *Quart J Microspical Sci,* 101**,** 351-370.

D'ALESSIO, S., CORREALE, C., TACCONI, C., GANDELLI, A., PIETROGRANDE, G., VETRANO, S., GENUA, M., ARENA, V., SPINELLI, A., PEYRIN-BIROULET, L., FIOCCHI, C. & DANESE, S. 2014. VEGF-C-dependent stimulation of lymphatic function ameliorates experimental inflammatory bowel disease. *J Clin Invest,* 124**,** 3863-78.

DAMIEN, E., PRICE, J. S. & LANYON, L. E. 2000. Mechanical strain stimulates osteoblast proliferation through the estrogen receptor in males as well as females. *J Bone Miner Res,* 15**,** 2169-77.

DANIELSEN, C. C., MOSEKILDE, L. & ANDREASSEN, T. T. 1992. Long-term effect of orchidectomy on cortical bone from rat femur: bone mass and mechanical properties. *Calcif Tissue Int,* 50**,** 169-74.

DE CROMBRUGGHE, B., LEFEBVRE, V., BEHRINGER, R. R., BI, W., MURAKAMI, S. & HUANG, W. 2000. Transcriptional mechanisms of chondrocyte differentiation. *Matrix Biol,* 19**,** 389-94.

DE SOUZA, J. A. & OLOPADE, O. I. 2011. CYP2D6 genotyping and tamoxifen: an unfinished story in the quest for personalized medicine. *Semin Oncol,* 38**,** 263-73.

DE WIJS-MEIJLER, D. P. M., DANSER, A. H. J., REISS, I. K. M., DUNCKER, D. J. & MERKUS, D. 2017. Sex differences in pulmonary vascular control: focus on the nitric oxide pathway. *Physiol Rep,* 5.

DECKERS, M. M., KARPERIEN, M., VAN DER BENT, C., YAMASHITA, T., PAPAPOULOS, S. E. & LÖWIK, C. W. 2000. Expression of vascular endothelial growth factors and their receptors during osteoblast differentiation. *Endocrinology,* 141**,** 1667-74.

DEMPSTER, D. 2006. Anatomy and Functions of the Adult Skeleton. A*SBMR Primer*.

DIAS, S., HATTORI, K., HEISSIG, B., ZHU, Z., WU, Y., WITTE, L., HICKLIN, D. J., TATENO, M., BOHLEN, P., MOORE, M. A. & RAFII, S. 2001. Inhibition of both paracrine and autocrine VEGF/ VEGFR-2 signaling pathways is essential to induce long-term remission of xenotransplanted human leukemias. *Proc Natl Acad Sci U S A,* 98**,** 10857-62.

DILLING, C. F., WADA, A. M., LAZARD, Z. W., SALISBURY, E. A., GANNON, F. H., VADAKKAN, T. J., GAO, L., HIRSCHI, K., DICKINSON, M. E., DAVIS, A. R. & OLMSTED-DAVIS, E. A. 2010. Vessel formation is induced prior to the appearance of cartilage in BMP-2-mediated heterotopic ossification. *J Bone Miner Res,* 25**,** 1147-56.

DING, W. G., YAN, W. H., WEI, Z. X. & LIU, J. B. 2012. Difference in intraosseous blood vessel volume and number in osteoporotic model mice induced by spinal cord injury and sciatic nerve resection. *J Bone Miner Metab,* 30**,** 400-7.

DONALDSON, L. J., COOK, A. & THOMSON, R. G. 1990. Incidence of fractures in a geographically defined population. *J Epidemiol Community Health,* 44**,** 241-5.

DONG, P., PACUREANU, A., ZULUAGA, M. A., OLIVIER, C., FROUIN, F., GRIMAL, Q. & PEYRIN, F. 2013. A new quantitative approach for estimating bone cell connections from nano-CT images. *Conf Proc IEEE Eng Med Biol Soc,* 2013**,** 3694-7.

DOTY, S. B. 1981. Morphological evidence of gap junctions between bone cells. *Calcif Tissue Int,* 33**,** 509-12.

DOUGALL, W. C., GLACCUM, M., CHARRIER, K., ROHRBACH, K., BRASEL, K., DE SMEDT, T., DARO, E., SMITH, J., TOMETSKO, M. E., MALISZEWSKI, C. R., ARMSTRONG, A., SHEN, V., BAIN, S., COSMAN, D., ANDERSON, D., MORRISSEY, P. J., PESCHON, J. J. & SCHUH, J. 1999. RANK is essential for osteoclast and lymph node development. *Genes Dev,* 13**,** 2412-24.

DRICKAMER, L. C. 1981. Selection for age of sexual maturation in mice and the sequences for population regulation. *Behav Neural Biol,* 31**,** 82-9.

DUAN, X., BRADBURY, S. R., OLSEN, B. R. & BERENDSEN, A. D. 2016. VEGF stimulates intramembranous bone formation during craniofacial skeletal development. *Matrix Biol,* 52-54**,** 127-140.

DUAN, X., MURATA, Y., LIU, Y., NICOLAE, C., OLSEN, B. R. & BERENDSEN, A. D. 2015. Vegfa regulates perichondrial vascularity and osteoblast differentiation in bone development. *Development,* 142**,** 1984-91.

DUCY, P. 2000. Cbfa1: a molecular switch in osteoblast biology. *Dev Dyn,* 219**,** 461-71.

DUCY, P., DESBOIS, C., BOYCE, B., PINERO, G., STORY, B., DUNSTAN, C., SMITH, E., BONADIO, J., GOLDSTEIN, S., GUNDBERG, C., BRADLEY, A. & KARSENTY, G. 1996. Increased bone formation in osteocalcin-deficient mice. *Nature,* 382**,** 448-452.

DUCY, P. & KARSENTY, G. 1995. Two distinct osteoblast-specific cis-acting elements control expression of a mouse osteocalcin gene. *Mol Cell Biol,* 15**,** 1858-69.

DUCY, P., ZHANG, R., GEOFFROY, V., RIDALL, A. L. & KARSENTY, G. 1997. Osf2/Cbfa1: A transcriptional activator of osteoblast differentiation. *Cell,* 89**,** 747-754.

DUONG, L. T., LAKKAKORPI, P., NAKAMURA, I. & RODAN, G. A. 2000. Integrins and signaling in osteoclast function. *Matrix Biol,* 19**,** 97-105.

DURANOVA, H., MARTINIAKOVA, M., OMELKA, R., GROSSKOPF, B., BOBONOVA, I. & TOMAN, R. 2014. Changes in compact bone microstructure of rats subchronically exposed to cadmium. *Acta Vet Scand,* 56**,** 64.

ECAROT-CHARRIER, B., SHEPARD, N., CHARETTE, G., GRYNPAS, M. & GLORIEUX, F. H. 1988. Mineralization in osteoblast cultures: a light and electron microscopic study. *Bone,* 9**,** 147-54.

EINHORN, T. A. & GERSTENFELD, L. C. 2015. Fracture healing: mechanisms and interventions. *Nat Rev Rheumatol,* 11**,** 45-54.

ENGSIG, M. T., CHEN, Q. J., VU, T. H., PEDERSEN, A. C., THERKIDSEN, B., LUND, L. R., HENRIKSEN, K., LENHARD, T., FOGED, N. T., WERB, Z. & DELAISSE, J. M. 2000. Matrix metalloproteinase 9 and vascular endothelial growth factor are essential for osteoclast recruitment into developing long bones. *J Cell Biol,* 151**,** 879-89.

ENLOW, D. H. 1962. Functions of the Haversian system. *Am J Anat,* 110**,** 269-305.

EVERTS, V., DELAISSÉ, J. M., KORPER, W., JANSEN, D. C., TIGCHELAAR-GUTTER, W., SAFTIG, P. & BEERTSEN, W. 2002. The bone lining cell: its role in cleaning Howship's lacunae and initiating bone formation. *J Bone Miner Res,* 17**,** 77-90.

F, A. 1947. Trabecular bone research for OP *Ann Intern Med,* 27**,** 861 – 882.

FEI, J., JIA, F., PEYRIN, F., FRANÇOISE, P., MALAVAL, L., VICO, L., LAURENCE, V., LAFAGE-PROUST, M. H. & MARIE-HÉLÈNE, L. P. 2010. Imaging and quantitative assessment of long bone vascularization in the adult rat using microcomputed tomography. *Anat Rec (Hoboken),* 293**,** 215-24.

FENG, J. Q., WARD, L. M., LIU, S., LU, Y., XIE, Y., YUAN, B., YU, X., RAUCH, F., DAVIS, S. I., ZHANG, S., RIOS, H., DREZNER, M. K., QUARLES, L. D., BONEWALD, L. F. & WHITE, K. E. 2006. Loss of DMP1 causes rickets and osteomalacia and identifies a role for osteocytes in mineral metabolism. *Nat Genet,* 38**,** 1310-5.

FENG, X. & MCDONALD, J. M. 2011. Disorders of bone remodeling. *Annu Rev Pathol,* 6**,** 121-45.

FERRARA, N., CARVER-MOORE, K., CHEN, H., DOWD, M., LU, L., O'SHEA, K. S., POWELL-BRAXTON, L., HILLAN, K. J. & MOORE, M. W. 1996. Heterozygous embryonic lethality induced by targeted inactivation of the VEGF gene. *Nature,* 380**,** 439-42.

FERRARA, N., GERBER, H. P. & LECOUTER, J. 2003. The biology of VEGF and its receptors. *Nat Med,* 9**,** 669-76.

FERRARA, N. & HENZEL, W. J. 1989. Pituitary follicular cells secrete a novel heparin-binding growth factor specific for vascular endothelial cells. *Biochem Biophys Res Commun,* 161**,** 851-8.

FISHER, L. W. & FEDARKO, N. S. 2003. Six genes expressed in bones and teeth encode the current members of the SIBLING family of proteins. *Connect Tissue Res,* 44 Suppl 1**,** 33-40.

FLICK, L. M., WEAVER, J. M., ULRICH-VINTHER, M., ABUZZAHAB, F., ZHANG, X., DOUGALL, W. C., ANDERSON, D., O'KEEFE, R. J. & SCHWARZ, E. M. 2003. Effects of receptor activator of NFkappaB (RANK) signaling blockade on fracture healing. *J Orthop Res,* 21**,** 676-84.

FLORENCIO-SILVA, R., SASSO, G. R., SASSO-CERRI, E., SIMÕES, M. J. & CERRI, P. S. 2015. Biology of Bone Tissue: Structure, Function, and Factors That Influence Bone Cells. *Biomed Res Int,* 2015**,** 421746.

FLOREY 1966. The endothelial cell. *Br Med J,* 2**,** 487-90.

FONG, G. H., ROSSANT, J., GERTSENSTEIN, M. & BREITMAN, M. L. 1995. Role of the Flt-1 receptor tyrosine kinase in regulating the assembly of vascular endothelium. *Nature,* 376**,** 66-70.

FORWOOD, M. R. & TURNER, C. H. 1995. Skeletal adaptations to mechanical usage: results from tibial loading studies in rats. *Bone,* 17**,** 197S-205S.

FROST, H. 1963. *Bone remodelling dynamics*, Charles C Thomas Company.

FROST, H. M. 1961. Halo volume. IV. Measurement of the diffusion pathway between osteocyte lacuna and blood. *Henry Ford Hosp Med Bull,* 9**,** 137-44.

FROST, H. M. 1969. Tetracycline-based histological analysis of bone remodeling. *Calcif Tissue Res,* 3**,** 211-37.

FROST, H. M. 1987. The mechanostat: a proposed pathogenic mechanism of osteoporoses and the bone mass effects of mechanical and nonmechanical agents. *Bone Miner,* 2**,** 73-85.

GALLI, C., FU, Q., WANG, W., OLSEN, B. R., MANOLAGAS, S. C., JILKA, R. L. & O'BRIEN, C. A. 2009. Commitment to the osteoblast lineage is not required for RANKL gene expression. *J Biol Chem,* 284**,** 12654-62.

GENGE, B. R., WU, L. N. & WUTHIER, R. E. 2008. Mineralization of annexin-5-containing lipid-calcium-phosphate complexes: modulation by varying lipid composition and incubation with cartilage collagens. *J Biol Chem,* 283**,** 9737-48.

GERBER, H. P. & FERRARA, N. 2000. Angiogenesis and bone growth. *Trends Cardiovasc Med,* 10**,** 223-8.

GERBER, H. P., HILLAN, K. J., RYAN, A. M., KOWALSKI, J., KELLER, G. A., RANGELL, L., WRIGHT, B. D., RADTKE, F., AGUET, M. & FERRARA, N. 1999a. VEGF is required for growth and survival in neonatal mice. *Development,* 126**,** 1149-59.

GERBER, H. P., MALIK, A. K., SOLAR, G. P., SHERMAN, D., LIANG, X. H., MENG, G., HONG, K., MARSTERS, J. C. & FERRARA, N. 2002. VEGF regulates haematopoietic stem cell survival by an internal autocrine loop mechanism. *Nature,* 417**,** 954-8.

GERBER, H. P., VU, T. H., RYAN, A. M., KOWALSKI, J., WERB, Z. & FERRARA, N. 1999b. VEGF couples hypertrophic cartilage remodeling, ossification and angiogenesis during endochondral bone formation. *Nat Med,* 5**,** 623-8.

GERHARDT, H., GOLDING, M., FRUTTIGER, M., RUHRBERG, C., LUNDKVIST, A., ABRAMSSON, A., JELTSCH, M., MITCHELL, C., ALITALO, K., SHIMA, D. & BETSHOLTZ, C. 2003. VEGF guides angiogenic sprouting utilizing endothelial tip cell filopodia. *J Cell Biol,* 161**,** 1163-77.

GERSTENFELD, L. & EINHORN, T. 2006. Fracture Healing: The Biology of Bone Repair and Regeneration. *ASBMR Primer*.

GIBSON, G. 1998. Active role of chondrocyte apoptosis in endochondral ossification. *Microsc Res Tech,* 43**,** 191-204.

GÓMEZ-BARRENA, E., ROSSET, P., LOZANO, D., STANOVICI, J., ERMTHALLER, C. & GERBHARD, F. 2015. Bone fracture healing: cell therapy in delayed unions and nonunions. *Bone,* 70**,** 93-101.

GONZALEZ, T. L., SUN, T., KOEPPEL, A. F., LEE, B., WANG, E. T., FARBER, C. R., RICH, S. S., SUNDHEIMER, L. W., BUTTLE, R. A., CHEN, Y. I., ROTTER, J. I., TURNER, S. D., WILLIAMS, J., GOODARZI, M. O. & PISARSKA, M. D. 2018. Sex differences in the late first trimester human placenta transcriptome. *Biol Sex Differ,* 9**,** 4.

GORING, A., SHARMA, A., JAVAHERI, B., SMITH, R. C., KANCZLER, J. M., BOYDE, A., HESSE, E., MAHAJAN, S., OLSEN, B. R., PITSILLIDES, A. A., SCHNEIDER, P., OREFFO, R. O. & CLARKIN, C. E. 2019. Regulation of the bone vascular network is sexually dimorphic. *J Bone Miner Res*.

GROSS, P. M., HEISTAD, D. D. & MARCUS, M. L. 1979. Neurohumoral regulation of blood flow to bones and marrow. *Am J Physiol,* 237**,** H440-8.

GROSSO, A., BURGER, M. G., LUNGER, A., SCHAEFER, D. J., BANFI, A. & DI MAGGIO, N. 2017. It Takes Two to Tango: Coupling of Angiogenesis and Osteogenesis for Bone Regeneration. *Front Bioeng Biotechnol,* 5**,** 68.

GRUNDMANN, M., HAIDAR, M., PLACZKO, S., NIENDORF, R., DARASHCHONAK, N., HUBEL, C. A. & VON VERSEN-HÖYNCK, F. 2012. Vitamin D improves the angiogenic properties of endothelial progenitor cells. *Am J Physiol Cell Physiol,* 303**,** C954-62.

GRÜNEBOOM, A., HAWWARI, I., WEIDNER, D., CULEMANN, S., MÜLLER, S., HENNEBERG, S., BRENZEL, A., MERZ, S., BORNEMANN, L., ZEC, K., WUELLING, M., KLING, L., HASENBERG, M., VOORTMANN, S., LANG, S., BAUM, W., OHS, A., KRAFF, O., QUICK, H. H., JÄGER, M., LANDGRAEBER, S., DUDDA, M., DANUSER, R., STEIN, J. V., ROHDE, M., GELSE, K., GARBE, A. I., ADAMCZYK, A., WESTENDORF, A. M., HOFFMANN, D., CHRISTIANSEN, S., ENGEL, D. R., VORTKAMP, A., KRÖNKE, G., HERRMANN, M., KAMRADT, T., SCHETT, G., HASENBERG, A. & GUNZER, M. 2019. A network of trans-cortical capillaries as mainstay for blood circulation in long bones. *Nature Metabolism,* 1**,** 236-250.

GULLBERG, B., JOHNELL, O. & KANIS, J. A. 1997. World-wide projections for hip fracture. *Osteoporos Int,* 7**,** 407-13.

HAIGH, J. J., GERBER, H. P., FERRARA, N. & WAGNER, E. F. 2000. Conditional inactivation of VEGF-A in areas of collagen2a1 expression results in embryonic lethality in the heterozygous state. *Development,* 127**,** 1445-53.

HAMLAT, A., ADN, M., PASQUALINI, E., BRASSIER, G. & ASKAR, B. 2005. Pathophysiology of capillary haemangioma growth after birth. *Med Hypotheses,* 64**,** 1093-6.

HANNAH, K. M., THOMAS, C. D., CLEMENT, J. G., DE CARLO, F. & PEELE, A. G. 2010. Bimodal distribution of osteocyte lacunar size in the human femoral cortex as revealed by micro-CT. *Bone,* 47**,** 866-71.

HARADA, S., NAGY, J. A., SULLIVAN, K. A., THOMAS, K. A., ENDO, N., RODAN, G. A. & RODAN, S. B. 1994. Induction of vascular endothelial growth factor expression by prostaglandin E2 and E1 in osteoblasts. *J Clin Invest,* 93**,** 2490-6.

HARMEY, D., HESSLE, L., NARISAWA, S., JOHNSON, K. A., TERKELTAUB, R. & MILLÁN, J. L. 2004. Concerted regulation of inorganic pyrophosphate and osteopontin by akp2, enpp1, and ank: an integrated model of the pathogenesis of mineralization disorders. *Am J Pathol,* 164**,** 1199-209.

HAUGE, E. M., QVESEL, D., ERIKSEN, E. F., MOSEKILDE, L. & MELSEN, F. 2001. Cancellous bone remodeling occurs in specialized compartments lined by cells expressing osteoblastic markers. *J Bone Miner Res,* 16**,** 1575-82.

HAUSMAN, M. R., SCHAFFLER, M. B. & MAJESKA, R. J. 2001. Prevention of fracture healing in rats by an inhibitor of angiogenesis. *Bone,* 29**,** 560-4.

HAVERS, C. *Osteologia nova: or, some new observations of the bones, and the parts belonging to them; with the manner of their accretion and nutrition: communicated to the Royal Society in several discourses ... To which is added, a fifth discourse, of the cartilages. The second edition. By Clopton Havers*.

HAVILL, L. M., ALLEN, M. R., HARRIS, J. A., LEVINE, S. M., COAN, H. B., MAHANEY, M. C. & NICOLELLA, D. P. 2013. Intracortical bone remodeling variation shows strong genetic effects. *Calcif Tissue Int,* 93**,** 472-80.

HAYWARD, C. 2003. *Gender differences at puberty,* Cambridge, Cambridge University Press.

HE, G. & GEORGE, A. 2004. Dentin matrix protein 1 immobilized on type I collagen fibrils facilitates apatite deposition in vitro. *J Biol Chem,* 279**,** 11649-56.

HERNLUND, E., SVEDBOM, A., IVERGARD, M., COMPSTON, J., COOPER, C., STENMARK, J., MCCLOSKEY, E. V., JONSSON, B. & KANIS, J. A. 2013. Osteoporosis in the European Union: medical management, epidemiology and economic burden. A report prepared in collaboration with the International Osteoporosis Foundation (IOF) and the European Federation of Pharmaceutical Industry Associations (EFPIA). *Arch Osteoporos,* 8**,** 136.

HILL, T. P., SPÄTER, D., TAKETO, M. M., BIRCHMEIER, W. & HARTMANN, C. 2005. Canonical Wnt/beta-catenin signaling prevents osteoblasts from differentiating into chondrocytes. *Dev Cell,* 8**,** 727-38.

HOCHBERG, M., SILMAN, A., SMOLEN, J., WEINBLATT, M. & WEISMAN, M. 2014. *Rheumatology*.

HOEBEN, A., LANDUYT, B., HIGHLEY, M. S., WILDIERS, H., VAN OOSTEROM, A. T. & DE BRUIJN, E. A. 2004. Vascular endothelial growth factor and angiogenesis. *Pharmacol Rev,* 56**,** 549-80.

HOLASH, J., WIEGAND, S. J. & YANCOPOULOS, G. D. 1999. New model of tumor angiogenesis: dynamic balance between vessel regression and growth mediated by angiopoietins and VEGF. *Oncogene,* 18**,** 5356-62.

HOLMES, D. I. & ZACHARY, I. 2005. The vascular endothelial growth factor (VEGF) family: angiogenic factors in health and disease. *Genome Biol,* 6**,** 209.

HOLSTEIN, J. H., KARABIN-KEHL, B., SCHEUER, C., GARCIA, P., HISTING, T., MEIER, C., BENNINGER, E., MENGER, M. D. & POHLEMANN, T. 2013. Endostatin inhibits Callus remodeling during fracture healing in mice. *J Orthop Res,* 31**,** 1579-84.

HU, K. & OLSEN, B. R. 2016. Osteoblast-derived VEGF regulates osteoblast differentiation and bone formation during bone repair. *J Clin Invest,* 126**,** 509-26.

HUANG, A., SUN, D., CARROLL, M. A., JIANG, H., SMITH, C. J., CONNETTA, J. A., FALCK, J. R., SHESELY, E. G., KOLLER, A. & KALEY, G. 2001a. EDHF mediates flow-induced dilation in

skeletal muscle arterioles of female eNOS-KO mice. *Am J Physiol Heart Circ Physiol,* 280**,** H2462-9.

HUANG, A., WU, Y., SUN, D., KOLLER, A. & KALEY, G. 2001b. Effect of estrogen on flow-induced dilation in NO deficiency: role of prostaglandins and EDHF. *J Appl Physiol (1985),* 91**,** 2561-6.

HUESA, C., HOUSTON, D., KIFFER-MOREIRA, T., YADAV, M. M., MILLAN, J. L. & FARQUHARSON, C. 2015. The Functional co-operativity of Tissue-Nonspecific Alkaline Phosphatase (TNAP) and PHOSPHO1 during initiation of Skeletal Mineralization. *Biochem Biophys Rep,* 4**,** 196-201.

HUESA, C., YADAV, M. C., FINNILÄ, M. A., GOODYEAR, S. R., ROBINS, S. P., TANNER, K. E., ASPDEN, R. M., MILLÁN, J. L. & FARQUHARSON, C. 2011. PHOSPHO1 is essential for mechanically competent mineralization and the avoidance of spontaneous fractures. *Bone,* 48**,** 1066-74.

HUGHES, D. E., DAI, A., TIFFEE, J. C., LI, H. H., MUNDY, G. R. & BOYCE, B. F. 1996. Estrogen promotes apoptosis of murine osteoclasts mediated by TGF-beta. *Nat Med,* 2**,** 1132-6.

INTERLICHIA, J. P., WILLIAMS, N. G. & RODGERS, B. D. 2010. A rapid, valid and inexpensive assay for measuring epiphyseal plates in mouse tibia. *Growth Horm IGF Res,* 20**,** 171-3.

ISSEMANN, I. & GREEN, S. 1990. Activation of a member of the steroid hormone receptor superfamily by peroxisome proliferators. *Nature,* 347**,** 645-50.

ITKIN, T., GUR-COHEN, S., SPENCER, J. A., SCHAJNOVITZ, A., RAMASAMY, S. K., KUSUMBE, A. P., LEDERGOR, G., JUNG, Y., MILO, I., POULOS, M. G., KALINKOVICH, A., LUDIN, A., KOLLET, O., SHAKHAR, G., BUTLER, J. M., RAFII, S., ADAMS, R. H., SCADDEN, D. T., LIN, C. P. & LAPIDOT, T. 2016. Distinct bone marrow blood vessels differentially regulate haematopoiesis. *Nature,* 532**,** 323-8.

ITO, Y., TEITELBAUM, S. L., ZOU, W., ZHENG, Y., JOHNSON, J. F., CHAPPEL, J., ROSS, F. P. & ZHAO, H. 2010. Cdc42 regulates bone modeling and remodeling in mice by modulating RANKL/M-CSF signaling and osteoclast polarization. *J Clin Invest,* 120**,** 1981-93.

IWAMOTO, J., SEKI, A., MATSUURA, M., SATO, Y., TAKEDA, T., MATSUMOTO, H. & YEH, J. K. 2009. Influence of ovariectomy on bone turnover and trabecular bone mass in mature cynomolgus monkeys. *Yonsei Med J,* 50**,** 358-67.

JAFFE, E. A., NACHMAN, R. L., BECKER, C. G. & MINICK, C. R. 1973. Culture of human endothelial cells derived from umbilical veins. Identification by morphologic and immunologic criteria. *J Clin Invest,* 52**,** 2745-56.

JAIN, K. K. 2002. Personalized medicine. *Curr Opin Mol Ther,* 4**,** 548-58.

JANSSEN, I., HEYMSFIELD, S. B., WANG, Z. M. & ROSS, R. 2000. Skeletal muscle mass and distribution in 468 men and women aged 18-88 yr. *J Appl Physiol (1985),* 89**,** 81-8.

JAVAHERI, B., CARRIERO, A., STAINES, K. A., CHANG, Y. M., HOUSTON, D. A., OLDKNOW, K. J., MILLAN, J. L., KAZERUNI, B. N., SALMON, P., SHEFELBINE, S., FARQUHARSON, C. & PITSILLIDES, A. A. 2015. Phospho1 deficiency transiently modifies bone architecture yet produces consistent modification in osteocyte differentiation and vascular porosity with ageing. *Bone,* 81**,** 277-291.

JAVAHERI, B., HOPKINSON, M., POULET, B., POLLARD, A. S., SHEFELBINE, S. J., CHANG, Y. M., FRANCIS-WEST, P., BOU-GHARIOS, G. & PITSILLIDES, A. A. 2016. Deficiency and Also

Transgenic Overexpression of Timp-3 Both Lead to Compromised Bone Mass and Architecture In Vivo. *PLoS One,* 11**,** e0159657.

JAWAHEER, D., LUM, R. F., GREGERSEN, P. K. & CRISWELL, L. A. 2006. Influence of male sex on disease phenotype in familial rheumatoid arthritis. *Arthritis Rheum,* 54**,** 3087-94.

JELTSCH, M., KAIPAINEN, A., JOUKOV, V., MENG, X., LAKSO, M., RAUVALA, H., SWARTZ, M., FUKUMURA, D., JAIN, R. K. & ALITALO, K. 1997. Hyperplasia of lymphatic vessels in VEGF-C transgenic mice. *Science,* 276**,** 1423-5.

JENNINGS, L. A., AUERBACH, A. D., MASELLI, J., PEKOW, P. S., LINDENAUER, P. K. & LEE, S. J. 2010. Missed opportunities for osteoporosis treatment in patients hospitalized for hip fracture. *J Am Geriatr Soc,* 58**,** 650-7.

JENSEN, E. D., GOPALAKRISHNAN, R. & WESTENDORF, J. J. 2010. Regulation of gene expression in osteoblasts. *Biofactors,* 36**,** 25-32.

JIA, Y., ZHU, Y., QIU, S., XU, J. & CHAI, Y. 2019. Exosomes secreted by endothelial progenitor cells accelerate bone regeneration during distraction osteogenesis by stimulating angiogenesis. *Stem Cell Res Ther,* 10**,** 12.

JIANHONG PAN, Z. Z., YAOZHANG LI 2018. Surgical effects and prognosis of non-rigid internal fixation for ankle fractures combined with tibiofibular syndesmotic injuries. *Int J Clin Exp Med* 11**,** 8370-8375

JILKA, R. L., WEINSTEIN, R. S., BELLIDO, T., ROBERSON, P., PARFITT, A. M. & MANOLAGAS, S. C. 1999. Increased bone formation by prevention of osteoblast apoptosis with parathyroid hormone. *J Clin Invest,* 104**,** 439-46.

JOAKIMSEN, R. M., FØNNEBØ, V., MAGNUS, J. H., TOLLAN, A. & SØGAARD, A. J. 1998. The Tromsø Study: body height, body mass index and fractures. *Osteoporos Int,* 8**,** 436-42.

JOENG, K. S., LEE, Y. C., LIM, J., CHEN, Y., JIANG, M. M., MUNIVEZ, E., AMBROSE, C. & LEE, B. H. 2017. Osteocyte-specific WNT1 regulates osteoblast function during bone homeostasis. *J Clin Invest,* 127**,** 2678-2688.

JOHANSEN, A., EVANS, R. J., STONE, M. D., RICHMOND, P. W., LO, S. V. & WOODHOUSE, K. W. 1997. Fracture incidence in England and Wales: a study based on the population of Cardiff. *Injury,* 28**,** 655-60.

JOHNSON, K. A., HESSLE, L., VAINGANKAR, S., WENNBERG, C., MAURO, S., NARISAWA, S., GODING, J. W., SANO, K., MILLAN, J. L. & TERKELTAUB, R. 2000. Osteoblast tissue-nonspecific alkaline phosphatase antagonizes and regulates PC-1. *Am J Physiol Regul Integr Comp Physiol,* 279**,** R1365-77.

JONES, G., WHITE, C., NGUYEN, T., SAMBROOK, P. N., KELLY, P. J. & EISMAN, J. A. 1996. Prevalent vertebral deformities: relationship to bone mineral density and spinal osteophytosis in elderly men and women. *Osteoporos Int,* 6**,** 233-9.

JOST, A. 1953 Problems of fetal endocrinology. *Recent Progr Horm Res* 8.

JOUKOV, V., PAJUSOLA, K., KAIPAINEN, A., CHILOV, D., LAHTINEN, I., KUKK, E., SAKSELA, O., KALKKINEN, N. & ALITALO, K. 1996. A novel vascular endothelial growth factor, VEGF-C, is a ligand for the Flt4 (VEGFR-3) and KDR (VEGFR-2) receptor tyrosine kinases. *EMBO J,* 15**,** 1751.

JOWSEY, J. 1966. Studies of Haversian systems in man and some animals. *J Anat,* 100**,** 857-64.

KAIPAINEN, A., KORHONEN, J., MUSTONEN, T., VAN HINSBERGH, V. W., FANG, G. H., DUMONT, D., BREITMAN, M. & ALITALO, K. 1995. Expression of the fms-like tyrosine kinase 4 gene becomes restricted to lymphatic endothelium during development. *Proc Natl Acad Sci U S A,* 92**,** 3566-70.

KAMIOKA, H., HONJO, T. & TAKANO-YAMAMOTO, T. 2001. A three-dimensional distribution of osteocyte processes revealed by the combination of confocal laser scanning microscopy and differential interference contrast microscopy. *Bone,* 28**,** 145-9.

KANEMATSU, M., SATO, T., TAKAI, H., WATANABE, K., IKEDA, K. & YAMADA, Y. 2000. Prostaglandin E2 induces expression of receptor activator of nuclear factor-kappa B ligand/osteoprotegrin ligand on pre-B cells: implications for accelerated osteoclastogenesis in estrogen deficiency. *J Bone Miner Res,* 15**,** 1321-9.

KANIS, J. A. 1994. Assessment of fracture risk and its application to screening for postmenopausal osteoporosis: synopsis of a WHO report. WHO Study Group. *Osteoporos Int,* 4**,** 368-81.

KAPUSTIN, A. N., DAVIES, J. D., REYNOLDS, J. L., MCNAIR, R., JONES, G. T., SIDIBE, A., SCHURGERS, L. J., SKEPPER, J. N., PROUDFOOT, D., MAYR, M. & SHANAHAN, C. M. 2011. Calcium regulates key components of vascular smooth muscle cell-derived matrix vesicles to enhance mineralization. *Circ Res,* 109**,** e1-12.

KEEN, R. 2007. Osteoporosis: strategies for prevention and management. *Best Pract Res Clin Rheumatol,* 21**,** 109-22.

KHURANA, J. S. 2009. *Bone pathology,* Totowa, N.J. ; London, Humana.

KIM, J. N., LEE, J. Y., SHIN, K. J., GIL, Y. C., KOH, K. S. & SONG, W. C. 2015. Haversian system of compact bone and comparison between endosteal and periosteal sides using three-dimensional reconstruction in rat. *Anat Cell Biol,* 48**,** 258-61.

KINI, U. & NANDEESH, B. N. 2012. Physiology of Bone Formation, Remodeling, and Metabolism. *Radionuclide and Hybrid Bone Imaging***,** 29–57.

KOBAYASHI, K., NOJIRI, H., SAITA, Y., MORIKAWA, D., OZAWA, Y., WATANABE, K., KOIKE, M., ASOU, Y., SHIRASAWA, T., YOKOTE, K., KANEKO, K. & SHIMIZU, T. 2015. Mitochondrial superoxide in osteocytes perturbs canalicular networks in the setting of age-related osteoporosis. *Sci Rep,* 5**,** 9148.

KOBLIZEK, T. I., WEISS, C., YANCOPOULOS, G. D., DEUTSCH, U. & RISAU, W. 1998. Angiopoietin-1 induces sprouting angiogenesis in vitro. *Curr Biol,* 8**,** 529-32.

KOCH, S. & CLAESSON-WELSH, L. 2012. Signal transduction by vascular endothelial growth factor receptors. *Cold Spring Harb Perspect Med,* 2**,** a006502.

KODAMA, I., NIIDA, S., SANADA, M., YOSHIKO, Y., TSUDA, M., MAEDA, N. & OHAMA, K. 2004. Estrogen regulates the production of VEGF for osteoclast formation and activity in op/op mice. *J Bone Miner Res,* 19**,** 200-6.

KOMORI, T., YAGI, H., NOMURA, S., YAMAGUCHI, A., SASAKI, K., DEGUCHI, K., SHIMIZU, Y., BRONSON, R. T., GAO, Y. H., INADA, M., SATO, M., OKAMOTO, R., KITAMURA, Y., YOSHIKI, S. & KISHIMOTO, T. 1997. Targeted disruption of Cbfa1 results in a complete lack of bone formation owing to maturational arrest of osteoblasts. *Cell,* 89**,** 755-764.

KOOPMAN, P., GUBBAY, J., VIVIAN, N., GOODFELLOW, P. & LOVELL-BADGE, R. 1991. Male development of chromosomally female mice transgenic for Sry. *Nature,* 351**,** 117-21.

KRONENBERG, H. M. 2003. Developmental regulation of the growth plate. *Nature,* 423**,** 332-6.

KURDY, N. M., WEISS, J. B. & BATE, A. 1996. Endothelial stimulating angiogenic factor in early fracture healing. *Injury,* 27**,** 143-5.

KUSUMBE, A. P., RAMASAMY, S. K. & ADAMS, R. H. 2014a. Coupling of angiogenesis and osteogenesis by a specific vessel subtype in bone. *Nature,* 507**,** 323-328.

KUSUMBE, A. P., RAMASAMY, S. K. & ADAMS, R. H. 2014b. Coupling of angiogenesis and osteogenesis by a specific vessel subtype in bone. *Nature,* 507**,** 323-8.

LACEY, D. L., ERDMANN, J. M., TEITELBAUM, S. L., TAN, H. L., OHARA, J. & SHIOI, A. 1995. Interleukin 4, interferon-gamma, and prostaglandin E impact the osteoclastic cell-forming potential of murine bone marrow macrophages. *Endocrinology,* 136**,** 2367-76.

LAKKAKORPI, P., TUUKKANEN, J., HENTUNEN, T., JÄRVELIN, K. & VÄÄNÄNEN, K. 1989. Organization of osteoclast microfilaments during the attachment to bone surface in vitro. *J Bone Miner Res,* 4**,** 817-25.

LANGE, T., GUTTMANN-RAVIV, N., BARUCH, L., MACHLUF, M. & NEUFELD, G. 2003. VEGF162, a new heparin-binding vascular endothelial growth factor splice form that is expressed in transformed human cells. *J Biol Chem,* 278**,** 17164-9.

LANYON 1980. The influence of function on the develop- ment of bone curvature. An experimental study on the rat tibia. *J Zool Lond,* 192**,** 457-466

LANYON, L. E. 1993. Osteocytes, strain detection, bone modeling and remodeling. *Calcif Tissue Int,* 53 Suppl 1**,** S102-6; discussion S106-7.

LANYON, L. E., HAMPSON, W. G., GOODSHIP, A. E. & SHAH, J. S. 1975. Bone deformation recorded in vivo from strain gauges attached to the human tibial shaft. *Acta Orthop Scand,* 46**,** 256-68.

LARSEN, P. R. 2003. *Williams textbook of endocrinology,* Philadelphia, Pa. ; [London], W. B. Saunders.

LAURENT, M., ANTONIO, L., SINNESAEL, M., DUBOIS, V., GIELEN, E., CLASSENS, F. & VANDERSCHUEREN, D. 2014. Androgens and estrogens in skeletal sexual dimorphism. *Asian J Androl,* 16**,** 213-22.

LAURENT, M. R., DEDEYNE, L., DUPONT, J., MELLAERTS, B., DEJAEGER, M. & GIELEN, E. 2019. Age-related bone loss and sarcopenia in men. *Maturitas,* 122**,** 51-56.

LEBLANC, A. D., SCHNEIDER, V. S., EVANS, H. J., ENGELBRETSON, D. A. & KREBS, J. M. 1990. Bone mineral loss and recovery after 17 weeks of bed rest. *J Bone Miner Res,* 5**,** 843-50.

LEE, S., CHEN, T. T., BARBER, C. L., JORDAN, M. C., MURDOCK, J., DESAI, S., FERRARA, N., NAGY, A., ROOS, K. P. & IRUELA-ARISPE, M. L. 2007. Autocrine VEGF signaling is required for vascular homeostasis. *Cell,* 130**,** 691-703.

LEUNG, D. W., CACHIANES, G., KUANG, W. J., GOEDDEL, D. V. & FERRARA, N. 1989. Vascular endothelial growth factor is a secreted angiogenic mitogen. *Science,* 246**,** 1306.

LEWIECKI, E. M. 2011. Sclerostin monoclonal antibody therapy with AMG 785: a potential treatment for osteoporosis. *Expert Opin Biol Ther,* 11**,** 117-27.

LEWIECKI, E. M. 2014. Role of sclerostin in bone and cartilage and its potential as a therapeutic target in bone diseases. *Ther Adv Musculoskelet Dis,* 6**,** 48-57.

LEWINSON, D. & SILBERMANN, M. 1992. Chondroclasts and endothelial cells collaborate in the process of cartilage resorption. *Anat Rec,* 233**,** 504-14.

LI, H., HONG, S., QIAN, J., ZHENG, Y., YANG, J. & YI, Q. 2010. Cross talk between the bone and immune systems: osteoclasts function as antigen-presenting cells and activate CD4+ and CD8+ T cells. *Blood,* 116**,** 210-7.

LI, X. & ERIKSSON, U. 2001. Novel VEGF family members: VEGF-B, VEGF-C and VEGF-D. *Int J Biochem Cell Biol,* 33**,** 421-6.

LI, X., OMINSKY, M. S., WARMINGTON, K. S., NIU, Q. T., ASUNCION, F. J., BARRERO, M., DWYER, D., GRISANTI, M., STOLINA, M., KOSTENUIK, P. J., SIMONET, W. S., PASZTY, C. & KE, H. Z. 2011. Increased bone formation and bone mass induced by sclerostin antibody is not affected by pretreatment or cotreatment with alendronate in osteopenic, ovariectomized rats. *Endocrinology,* 152**,** 3312-22.

LIN, C., MCGOUGH, R., ASWAD, B., BLOCK, J. A. & TEREK, R. 2004. Hypoxia induces HIF-1alpha and VEGF expression in chondrosarcoma cells and chondrocytes. *J Orthop Res,* 22**,** 1175-81.

LINDSAY, R. 1982. The role of sex hormones and synthetic steroids in prevention of post-menopausal osteoporosis. *Clin Invest Med,* 5**,** 189-94.

LINDSAY, R. 1987. The menopause: sex steroids and osteoporosis. *Clin Obstet Gynecol,* 30**,** 847-59.

LIPSETT, M. B., WILSON, H., KIRSCHNER, M. A., KORENMAN, S. G., FISHMAN, L. M., SARFATY, G. A. & BARDIN, C. W. 1966. Studies on Leydig cell physiology and pathology: secretion and metabolism of testosterone. *Recent Prog Horm Res,* 22**,** 245-81.

LIU, C. & CASTILLO, A. B. 2018. Targeting Osteogenesis-Angiogenesis Coupling for Bone Repair. *J Am Acad Orthop Surg,* 26**,** e153-e155.

LIU, J. F., DU, Z. D., CHEN, Z. & HE, Z. X. 2014. Whole bone marrow cell culture: A convenient protocol for the. *Exp Ther Med,* 8**,** 805-812.

LIU, Y., BERENDSEN, A. D., JIA, S., LOTINUN, S., BARON, R., FERRARA, N. & OLSEN, B. R. 2012. Intracellular VEGF regulates the balance between osteoblast and adipocyte differentiation. *J Clin Invest,* 122**,** 3101-13.

LU, C., HANSEN, E., SAPOZHNIKOVA, A., HU, D., MICLAU, T. & MARCUCIO, R. S. 2008. Effect of age on vascularization during fracture repair. *J Orthop Res,* 26**,** 1384-9.

LYTTLE, D. J., FRASER, K. M., FLEMING, S. B., MERCER, A. A. & ROBINSON, A. J. 1994. Homologs of vascular endothelial growth factor are encoded by the poxvirus orf virus. *J Virol,* 68**,** 84-92.

MA, H. L., BLANCHET, T. J., PELUSO, D., HOPKINS, B., MORRIS, E. A. & GLASSON, S. S. 2007. Osteoarthritis severity is sex dependent in a surgical mouse model. *Osteoarthritis Cartilage,* 15**,** 695-700.

MAAS, A. H. & APPELMAN, Y. E. 2010. Gender differences in coronary heart disease. *Neth Heart J,* 18**,** 598-602.

MACKIE, E. J., AHMED, Y. A., TATARCZUCH, L., CHEN, K. S. & MIRAMS, M. 2008. Endochondral ossification: how cartilage is converted into bone in the developing skeleton. *Int J Biochem Cell Biol,* 40**,** 46-62.

MACNABB, C., PATTON, D. & HAYES, J. S. 2016. Sclerostin Antibody Therapy for the Treatment of Osteoporosis: Clinical Prospects and Challenges. *J Osteoporos,* 2016**,** 6217286.

MADER, K. S., SCHNEIDER, P., MULLER, R. & STAMPANONI, M. 2013. A quantitative framework for the 3D characterization of the osteocyte lacunar system. *Bone,* 57**,** 142-54.

MAES, C., ARALDI, E., HAIGH, K., KHATRI, R., VAN LOOVEREN, R., GIACCIA, A. J., HAIGH, J. J., CARMELIET, G. & SCHIPANI, E. 2012. VEGF-independent cell-autonomous functions of HIF-1alpha regulating oxygen consumption in fetal cartilage are critical for chondrocyte survival. *J Bone Miner Res,* 27**,** 596-609.

MAES, C., CARMELIET, P., MOERMANS, K., STOCKMANS, I., SMETS, N., COLLEN, D., BOUILLON, R. & CARMELIET, G. 2002. Impaired angiogenesis and endochondral bone formation in mice lacking the vascular endothelial growth factor isoforms VEGF164 and VEGF188. *Mech Dev,* 111**,** 61-73.

MAES, C., KOBAYASHI, T., SELIG, M. K., TORREKENS, S., ROTH, S. I., MACKEM, S., CARMELIET, G. & KRONENBERG, H. M. 2010. Osteoblast precursors, but not mature osteoblasts, move into developing and fractured bones along with invading blood vessels. *Dev Cell,* 19**,** 329-44.

MAHR, S., MENARD, J., KRENN, V. & MULLER, B. 2003. Sexual dimorphism in the osteoarthritis of STR/ort mice may be linked to articular cytokines. *Ann Rheum Dis,* 62**,** 1234-7.

MAJESKA, R. J. & WUTHIER, R. E. 1975. Studies on matrix vesicles isolated from chick epiphyseal cartilage. Association of pyrophosphatase and ATPase activities with alkaline phosphatase. *Biochim Biophys Acta,* 391**,** 51-60.

MAK, K. K., CHEN, M. H., DAY, T. F., CHUANG, P. T. & YANG, Y. 2006. Wnt/beta-catenin signaling interacts differentially with Ihh signaling in controlling endochondral bone and synovial joint formation. *Development,* 133**,** 3695-707.

MANOLAGAS, S. C. 2000. Birth and death of bone cells: basic regulatory mechanisms and implications for the pathogenesis and treatment of osteoporosis. *Endocr Rev,* 21**,** 115-37.

MANOLAGAS, S. C. & PARFITT, A. M. 2010. What old means to bone. *Trends Endocrinol Metab,* 21**,** 369-74.

MAO, K., QUIPILDOR, G. F., TABRIZIAN, T., NOVAJ, A., GUAN, F., WALTERS, R. O., DELAHAYE, F., HUBBARD, G. B., IKENO, Y., EJIMA, K., LI, P., ALLISON, D. B., SALIMI-MOOSAVI, H., BELTRAN, P. J., COHEN, P., BARZILAI, N. & HUFFMAN, D. M. 2018. Late-life targeting of the IGF-1 receptor improves healthspan and lifespan in female mice. *Nat Commun,* 9**,** 2394.

MARCUS, R. 2008. *Osteoporosis,* Amsterdam ; London, Elsevier.

MARENZANA, M. & ARNETT, T. R. 2013. The key role of the blood supply to bone. *Bone Research,* 1**,** 203.

MARIE, P. J., DEBIAIS, F. & HAŸ, E. 2002. Regulation of human cranial osteoblast phenotype by FGF-2, FGFR-2 and BMP-2 signaling. *Histol Histopathol,* 17**,** 877-85.

MARIE, P. J. & GLORIEUX, F. H. 1981. Histomorphometric study of bone remodeling in hypophosphatemic vitamin D-resistant rickets. *Metab Bone Dis Relat Res,* 3**,** 31-8.

MARKS, S. C. & SEIFERT, M. F. 1985. The lifespan of osteoclasts: experimental studies using the giant granule cytoplasmic marker characteristic of beige mice. *Bone,* 6**,** 451-5.

MAROTTI, G. 1977. Decrement in volume of osteoblasts during osteon formation and its effect on the size of the corresponding osteocytes. *Bone histomorphometry***,** 385-397.

MARTEL-PELLETIER, J., BOILEAU, C., PELLETIER, J. P. & ROUGHLEY, P. J. 2008. Cartilage in normal and osteoarthritis conditions. *Best Pract Res Clin Rheumatol,* 22**,** 351-84.

MARTIN, A., DAVID, V., LAURENCE, J. S., SCHWARZ, P. M., LAFER, E. M., HEDGE, A. M. & ROWE, P. S. 2008. Degradation of MEPE, DMP1, and release of SIBLING ASARM-peptides (minhibins): ASARM-peptide(s) are directly responsible for defective mineralization in HYP. *Endocrinology,* 149**,** 1757-72.

MARTIN, R. B. 2002. Size, structure and gender: lessons about fracture risk. *J Musculoskelet Neuronal Interact,* 2**,** 209-11.

MARTIN, R. B., BURR, D. B. & SHARKEY, N. A. 1998. *Skeletal tissue mechanics,* New York ; London, Springer.

MARTÍNEZ-REINA, J., GARCÍA-RODRÍGUEZ, J., MORA-MACÍAS, J., DOMÍNGUEZ, J. & REINA-ROMO, E. 2018. Comparison of the volumetric composition of lamellar bone and the woven bone of calluses. *Proc Inst Mech Eng H,* 232**,** 682-689.

MARTINI, F., NATH, J. & BARTHOLOMEW, E. 2014. *Fundamentals of anatomy & physiology*.

MARTINIAKOVÁ , M., GROSSKOPF , B., OMELKA , R., DAMMERS , K., VONDRÁKOVÁ , M. & BAUEROVÁ , M. 2007 Histological study of compact bone tissue in some mammals: a method for species determination. *International Journal of Osteoarchaeology,* 17**,** 82-90.

MASEK, L. C. & SWEETENHAM, J. W. 1994. Isolation and culture of endothelial cells from human bone marrow. *Br J Haematol,* 88**,** 855-65.

MATSUZAKI, H., WOHL, G. R., NOVACK, D. V., LYNCH, J. A. & SILVA, M. J. 2007. Damaging fatigue loading stimulates increases in periosteal vascularity at sites of bone formation in the rat ulna. *Calcif Tissue Int,* 80**,** 391-9.

MAURAS, N., ROGOL, A. D., HAYMOND, M. W. & VELDHUIS, J. D. 1996. Sex steroids, growth hormone, insulin-like growth factor-1: neuroendocrine and metabolic regulation in puberty. *Horm Res,* 45**,** 74-80.

MAXIE, M. & JUBB, K. 2015. *Jubb, Kennedy & Palmer's Pathology of domestic animals*.

MCCREADIE, B. R., HOLLISTER, S. J., SCHAFFLER, M. B. & GOLDSTEIN, S. A. 2004. Osteocyte lacuna size and shape in women with and without osteoporotic fracture. *J Biomech,* 37**,** 563-72.

MCDONALD, D. M. & FOSS, A. J. 2000. Endothelial cells of tumor vessels: abnormal but not absent. *Cancer Metastasis Rev,* 19**,** 109-20.

MCKEE, M. D., HOAC, B., ADDISON, W. N., BARROS, N. M., MILLÁN, J. L. & CHAUSSAIN, C. 2013. Extracellular matrix mineralization in periodontal tissues: Noncollagenous matrix proteins, enzymes, and relationship to hypophosphatasia and X-linked hypophosphatemia. *Periodontol 2000,* 63**,** 102-22.

MCKEON, K. E., WRIGHT, R. W., JOHNSON, J. E., MCCORMICK, J. J. & KLEIN, S. E. 2012. Vascular anatomy of the tibiofibular syndesmosis. *J Bone Joint Surg Am,* 94**,** 931-8.

MCMAHON, G. 2000. VEGF receptor signaling in tumor angiogenesis. *Oncologist,* 5 Suppl 1**,** 3-10.

MEAKIN, L. B., SUGIYAMA, T., GALEA, G. L., BROWNE, W. J., LANYON, L. E. & PRICE, J. S. 2013. Male mice housed in groups engage in frequent fighting and show a lower response to additional bone loading than females or individually housed males that do not fight. *Bone,* 54**,** 113-7.

MELNYK, M., HENKE, T., CLAES, L. & AUGAT, P. 2008. Revascularisation during fracture healing with soft tissue injury. *Arch Orthop Trauma Surg,* 128**,** 1159-65.

MEYER, H. E., TVERDAL, A. & FALCH, J. A. 1993. Risk factors for hip fracture in middle-aged Norwegian women and men. *Am J Epidemiol,* 137**,** 1203-11.

MIKUNI-TAKAGAKI, Y., KAKAI, Y., SATOYOSHI, M., KAWANO, E., SUZUKI, Y., KAWASE, T. & SAITO, S. 1995. Matrix mineralization and the differentiation of osteocyte-like cells in culture. *J Bone Miner Res,* 10**,** 231-42.

MIRZAALI, M. J., SCHWIEDRZIK, J. J., THAIWICHAI, S., BEST, J. P., MICHLER, J., ZYSSET, P. K. & WOLFRAM, U. 2016. Mechanical properties of cortical bone and their relationships with age, gender, composition and microindentation properties in the elderly. *Bone,* 93**,** 196-211.

MOREIRA, C., DEMPSTER, D. & BARON, R. 2019. Anatomy and Ultrastructure of Bone –

Histogenesis, Growth and Remodeling.

MORIKAWA, S., BALUK, P., KAIDOH, T., HASKELL, A., JAIN, R. K. & MCDONALD, D. M. 2002. Abnormalities in pericytes on blood vessels and endothelial sprouts in tumors. *Am J Pathol,* 160**,** 985-1000.

MOSER, S. C. & VAN DER EERDEN, B. C. J. 2018. Osteocalcin-A Versatile Bone-Derived Hormone. *Front Endocrinol (Lausanne),* 9**,** 794.

MOSEY, H., NUNEZ, J. A., GORING, A., CLARKIN, C. E., STAINES, K. A., LEE, P. D., PITSILLIDES, A. A. & JAVAHERI, B. 2017. Sost Deficiency does not Alter Bone's Lacunar or Vascular Porosity in Mice. *Front Mater,* 4**,** 27.

MUKHERJEE, A. & ROTWEIN, P. 2009. Akt promotes BMP2-mediated osteoblast differentiation and bone development. *J Cell Sci,* 122**,** 716-26.

MULLER, Y. A., LI, B., CHRISTINGER, H. W., WELLS, J. A., CUNNINGHAM, B. C. & DE VOS, A. M. 1997. Vascular endothelial growth factor: crystal structure and functional mapping of the kinase domain receptor binding site. *Proc Natl Acad Sci U S A,* 94**,** 7192-7.

NAGAO, M., HAMILTON, J. L., KC, R., BERENDSEN, A. D., DUAN, X., CHEONG, C. W., LI, X., IM, H. J. & OLSEN, B. R. 2017. Vascular Endothelial Growth Factor in Cartilage Development and Osteoarthritis. *Sci Rep,* 7**,** 13027.

NAKASHIMA, K., ZHOU, X., KUNKEL, G., ZHANG, Z., DENG, J. M., BEHRINGER, R. R. & DE CROMBRUGGHE, B. 2002. The novel zinc finger-containing transcription factor osterix is required for osteoblast differentiation and bone formation. *Cell,* 108**,** 17-29.

NARISAWA, S., FRÖHLANDER, N. & MILLÁN, J. L. 1997. Inactivation of two mouse alkaline phosphatase genes and establishment of a model of infantile hypophosphatasia. *Dev Dyn,* 208**,** 432-46.

NIEDERMAIR, T., SCHIRNER, S., SEEBRÖKER, R., STRAUB, R. H. & GRÄSSEL, S. 2018. Substance P modulates bone remodeling properties of murine osteoblasts and osteoclasts. *Sci Rep,* 8**,** 9199.

NIIDA, S., KAKU, M., AMANO, H., YOSHIDA, H., KATAOKA, H., NISHIKAWA, S., TANNE, K., MAEDA, N. & KODAMA, H. 1999. Vascular endothelial growth factor can substitute for macrophage colony-stimulating factor in the support of osteoclastic bone resorption. *J Exp Med,* 190**,** 293-8.

NIIDA, S., KONDO, T., HIRATSUKA, S., HAYASHI, S., AMIZUKA, N., NODA, T., IKEDA, K. & SHIBUYA, M. 2005. VEGF receptor 1 signaling is essential for osteoclast development and bone

marrow formation in colony-stimulating factor 1-deficient mice. *Proc Natl Acad Sci U S A,* 102**,** 14016-21.

NOGUERA-TROISE, I., DALY, C., PAPADOPOULOS, N. J., COETZEE, S., BOLAND, P., GALE, N. W., LIN, H. C., YANCOPOULOS, G. D. & THURSTON, G. 2006. Blockade of Dll4 inhibits tumour growth by promoting non-productive angiogenesis. *Nature,* 444**,** 1032-7.

NOLDUS, L. P., SPINK, A. J. & TEGELENBOSCH, R. A. 2001. EthoVision: a versatile video tracking system for automation of behavioral experiments. *Behav Res Methods Instrum Comput,* 33**,** 398-414.

NORDSTRÖM, P., EKLUND, F., BJÖRNSTIG, U., NORDSTRÖM, A., LORENTZON, R., SIEVÄNEN, H. & GUSTAFSON, Y. 2011. Do both areal BMD and injurious falls explain the higher incidence of fractures in women than in men? *Calcif Tissue Int,* 89**,** 203-10.

NÚÑEZ, J. A., GORING, A., HESSE, E., THURNER, P. J., SCHNEIDER, P. & CLARKIN, C. E. 2017. Simultaneous visualisation of calcified bone microstructure and intracortical vasculature using synchrotron X-ray phase contrast-enhanced tomography. *Sci Rep,* 7**,** 13289.

NÚÑEZ, J. A., GORING, A., JAVAHERI, B., RAZI, H., GOMEZ-NICOLA, D., PITSILLIDES, A. A., THURNER, P. J., SCHNEIDER, P. & CLARKIN, C. E. 2018. Regional diversity in the murine cortical vascular network is revealed by synchrotron X-ray tomography and is amplified with age. *Eur Cell Mater,* 35**,** 281-299.

NUZZO, S., PEYRIN, F., CLOETENS, P., BARUCHEL, J. & BOIVIN, G. 2002. Quantification of the degree of mineralization of bone in three dimensions using synchrotron radiation microtomography. *Med Phys,* 29**,** 2672-81.

O'BRIEN, C. A. 2010. Control of RANKL gene expression. *Bone,* 46**,** 911-9.

O'NEILL, T. W., FELSENBERG, D., VARLOW, J., COOPER, C., KANIS, J. A. & SILMAN, A. J. 1996. The prevalence of vertebral deformity in european men and women: the European Vertebral Osteoporosis Study. *J Bone Miner Res,* 11**,** 1010-8.

OLIVEIRA, C. S., SARAIVA, N. Z., DE LIMA, M. R., OLIVEIRA, L. Z., SERAPIÃO, R. V., GARCIA, J. M., BORGES, C. A. & CAMARGO, L. S. 2016. Cell death is involved in sexual dimorphism during preimplantation development. *Mech Dev,* 139**,** 42-50.

OLIVIERO, S., GIORGI, M. & DALL'ARA, E. 2018. Validation of finite element models of the mouse tibia using digital volume correlation. *J Mech Behav Biomed Mater,* 86**,** 172-184.

OLOFSSON, B., PAJUSOLA, K., KAIPAINEN, A., VON EULER, G., JOUKOV, V., SAKSELA, O., ORPANA, A., PETTERSSON, R. F., ALITALO, K. & ERIKSSON, U. 1996. Vascular endothelial growth factor B, a novel growth factor for endothelial cells. *Proc Natl Acad Sci U S A,* 93**,** 2576-81.

OLSEN, B. 2006. Bone Embryology. *ASBMR Primer, Edition 6***,** 2-6.

OLSSON, A. K., DIMBERG, A., KREUGER, J. & CLAESSON-WELSH, L. 2006. VEGF receptor signalling - in control of vascular function. *Nat Rev Mol Cell Biol,* 7**,** 359-71.

OMINSKY, M. S., VLASSEROS, F., JOLETTE, J., SMITH, S. Y., STOUCH, B., DOELLGAST, G., GONG, J., GAO, Y., CAO, J., GRAHAM, K., TIPTON, B., CAI, J., DESHPANDE, R., ZHOU, L., HALE, M. D., LIGHTWOOD, D. J., HENRY, A. J., POPPLEWELL, A. G., MOORE, A. R., ROBINSON, M. K., LACEY, D. L., SIMONET, W. S. & PASZTY, C. 2010. Two doses of sclerostin antibody in cynomolgus monkeys increases bone formation, bone mineral density, and bone strength. *J Bone Miner Res,* 25**,** 948-59.

ORCEL, P., BIELAKOFF, J. & DE VERNEJOUL, M. C. 1990. Effects of transforming growth factor-beta on long-term human cord blood monocyte cultures. *J Cell Physiol,* 142**,** 293-8.

ORTEGA, N., BEHONICK, D. J. & WERB, Z. 2004. Matrix remodeling during endochondral ossification. *Trends Cell Biol,* 14**,** 86-93.

PACIFICI, R., RIFAS, L., MCCRACKEN, R., VERED, I., MCMURTRY, C., AVIOLI, L. V. & PECK, W. A. 1989. Ovarian steroid treatment blocks a postmenopausal increase in blood monocyte interleukin 1 release. *Proc Natl Acad Sci U S A,* 86**,** 2398-402.

PAGE, D. J., THURET, R., VENKATRAMAN, L., TAKAHASHI, T., BENTLEY, K. & HERBERT, S. P. 2019. Positive Feedback Defines the Timing, Magnitude, and Robustness of Angiogenesis. *Cell Rep,* 27**,** 3139-3151.e5.

PALACIO-MANCHENO, P. E., LARRIERA, A. I., DOTY, S. B., CARDOSO, L. & FRITTON, S. P. 2014. 3D assessment of cortical bone porosity and tissue mineral density using high-resolution µCT: effects of resolution and threshold method. *J Bone Miner Res,* 29**,** 142-50.

PARFITT, A. M. 1994. Osteonal and hemi-osteonal remodeling: the spatial and temporal framework for signal traffic in adult human bone. *J Cell Biochem,* 55**,** 273-86.

PARK, J. E., KELLER, G. A. & FERRARA, N. 1993. The vascular endothelial growth factor (VEGF) isoforms: differential deposition into the subepithelial extracellular matrix and bioactivity of extracellular matrix-bound VEGF. *Mol Biol Cell,* 4**,** 1317-26.

PATTON, D. M., BIGELOW, E. M. R., SCHLECHT, S. H., KOHN, D. H., BREDBENNER, T. L. & JEPSEN, K. J. 2019. The relationship between whole bone stiffness and strength is age and sex dependent. *J Biomech,* 83**,** 125-133.

PERRY, R. J., FARQUHARSON, C. & AHMED, S. F. 2008. The role of sex steroids in controlling pubertal growth. *Clin Endocrinol (Oxf),* 68**,** 4-15.

PETROVA, T. V., MAKINEN, T. & ALITALO, K. 1999. Signaling via vascular endothelial growth factor receptors. *Exp Cell Res,* 253**,** 117-30.

PFEILSCHIFTER, J., CHENU, C., BIRD, A., MUNDY, G. R. & ROODMAN, G. D. 1989. Interleukin-1 and tumor necrosis factor stimulate the formation of human osteoclastlike cells in vitro. *J Bone Miner Res,* 4**,** 113-8.

PIETRI, M. & LUCARINI, S. 2007. The orthopaedic treatment of fragility fractures. *Clin Cases Miner Bone Metab,* 4**,** 108-16.

POLTORAK, Z., COHEN, T., SIVAN, R., KANDELIS, Y., SPIRA, G., VLODAVSKY, I., KESHET, E. & NEUFELD, G. 1997. VEGF145, a secreted vascular endothelial growth factor isoform that binds to extracellular matrix. *J Biol Chem,* 272**,** 7151-8.

PORTAL-NÚÑEZ, S., LOZANO, D. & ESBRIT, P. 2012. Role of angiogenesis on bone formation. *Histol Histopathol,* 27**,** 559-66.

POULET, B., DE SOUZA, R., KNIGHTS, C. B., GENTRY, C., WILSON, A. M., BEVAN, S., CHANG, Y. M. & PITSILLIDES, A. A. 2014. Modifications of gait as predictors of natural osteoarthritis progression in STR/Ort mice. *Arthritis Rheumatol,* 66**,** 1832-42.

PRASADAM, I., ZHOU, Y., DU, Z., CHEN, J., CRAWFORD, R. & XIAO, Y. 2014. Osteocyte-induced angiogenesis via VEGF-MAPK-dependent pathways in endothelial cells. *Mol Cell Biochem,* 386**,** 15-25.

PUFE, T., CLAASSEN, H., SCHOLZ-AHRENS, K. E., VAROGA, D., DRESCHER, W., FRANKE, A. T., WRUCK, C., PETERSEN, W., CELLARIUS, C., SCHREZENMEIR, J. & GLUER, C. C. 2007. Influence of estradiol on vascular endothelial growth factor expression in bone: a study in Gottingen miniature pigs and human osteoblasts. *Calcif Tissue Int,* 80**,** 184-91.

PUFE, T., SCHOLZ-AHRENS, K. E., FRANKE, A. T., PETERSEN, W., MENTLEIN, R., VAROGA, D., TILLMANN, B., SCHREZENMEIR, J. & GLÜER, C. C. 2003. The role of vascular endothelial growth factor in glucocorticoid-induced bone loss: evaluation in a minipig model. *Bone,* 33**,** 869-76.

PURSIHEIMO, J. P., RANTANEN, K., HEIKKINEN, P. T., JOHANSEN, T. & JAAKKOLA, P. M. 2009. Hypoxia-activated autophagy accelerates degradation of SQSTM1/p62. *Oncogene,* 28**,** 334-44.

QIN, C., BRUNN, J. C., JONES, J., GEORGE, A., RAMACHANDRAN, A., GORSKI, J. P. & BUTLER, W. T. 2001. A comparative study of sialic acid-rich proteins in rat bone and dentin. *Eur J Oral Sci,* 109**,** 133-41.

QIU, S., RAO, D. S., PALNITKAR, S. & PARFITT, A. M. 2002. Relationships between osteocyte density and bone formation rate in human cancellous bone. *Bone,* 31**,** 709-11.

RACHNER, T. D., HOFBAUER, L. C., GÖBEL, A. & TSOURDI, E. 2019. Novel therapies in osteoporosis: PTH-related peptide analogs and inhibitors of sclerostin. *J Mol Endocrinol,* 62**,** R145-R154.

RAISZ, L. G. & BINGHAM, P. J. 1972. Effect of hormones on bone development. *Annu Rev Pharmacol,* 12**,** 337-52.

RAJENDRAN, P., RENGARAJAN, T., THANGAVEL, J., NISHIGAKI, Y., SAKTHISEKARAN, D., SETHI, G. & NISHIGAKI, I. 2013. The vascular endothelium and human diseases. *Int J Biol Sci,* 9**,** 1057-69.

RAMAN, C. & KRISHNAN, K. 1928. A New Type of Secondary Radiation. *Nature* 121.

RAMASAMY, S. K. 2017. Structure and Functions of Blood Vessels and Vascular Niches in Bone. *Stem Cells Int,* 2017**,** 5046953.

RAMASAMY, S. K., KUSUMBE, A. P., SCHILLER, M., ZEUSCHNER, D., BIXEL, M. G., MILIA, C., GAMREKELASHVILI, J., LIMBOURG, A., MEDVINSKY, A., SANTORO, M. M., LIMBOURG, F. P. & ADAMS, R. H. 2016. Blood flow controls bone vascular function and osteogenesis. *Nat Commun,* 7**,** 13601.

RAWLINS, M. & DILLON, A. 2005. NICE discrimination. *J Med Ethics,* 31**,** 683-4; discussion 685-8.

RAY, R. D., KAWABATA, M. & GALANTE, J. 1967. Experimental study of peripheral circulation and bone growth. An experimental method for the quantitative determination of bone blood flow. 3. *Clin Orthop Relat Res,* 54**,** 175-85.

REID, I. R., BROWN, J. P., BURCKHARDT, P., HOROWITZ, Z., RICHARDSON, P., TRECHSEL, U., WIDMER, A., DEVOGELAER, J. P., KAUFMAN, J. M., JAEGER, P., BODY, J. J., BRANDI, M. L., BROELL, J., DI MICCO, R., GENAZZANI, A. R., FELSENBERG, D., HAPP, J., HOOPER, M. J., ITTNER, J., LEB, G., MALLMIN, H., MURRAY, T., ORTOLANI, S., RUBINACCI, A., SAAF, M., SAMSIOE, G., VERBRUGGEN, L. & MEUNIER, P. J. 2002. Intravenous zoledronic acid in postmenopausal women with low bone mineral density. *N Engl J Med,* 346**,** 653-61.

RENDERS, G. A., MULDER, L., VAN RUIJVEN, L. J. & VAN EIJDEN, T. M. 2007. Porosity of human mandibular condylar bone. *J Anat,* 210**,** 239-48.

REY, C., KIM, H. M., GERSTENFELD, L. & GLIMCHER, M. J. 1996. Characterization of the apatite crystals of bone and their maturation in osteoblast cell culture: comparison with native bone crystals. *Connect Tissue Res,* 35**,** 343-9.

RHEES, B. K. & ATCHLEY, W. R. 2000. Body weight and tail length divergence in mice selected for rate of development. *J Exp Zool,* 288**,** 151-64.

RIDHA, H. & THURNER, P. J. 2013. Finite element prediction with experimental validation of damage distribution in single trabeculae during three-point bending tests. *J Mech Behav Biomed Mater,* 27**,** 94-106.

RIGGS, B. L. & MELTON, L. J. 1986. Involutional osteoporosis. *N Engl J Med,* 314**,** 1676-86.

RIGGS, B. L. & MELTON, L. J. 1995. *Osteoporosis : etiology, diagnosis, and management,* Philadelphia, Pa., Lippincott-Raven.

RISAU, W. 1997. Mechanisms of angiogenesis. *Nature,* 386**,** 671-4.

RISAU, W. & FLAMME, I. 1995. Vasculogenesis. *Annu Rev Cell Dev Biol,* 11**,** 73-91.

RISSANEN, T. T., MARKKANEN, J. E., GRUCHALA, M., HEIKURA, T., PURANEN, A., KETTUNEN, M. I., KHOLOVÁ, I., KAUPPINEN, R. A., ACHEN, M. G., STACKER, S. A., ALITALO, K. & YLÄ-HERTTUALA, S. 2003. VEGF-D is the strongest angiogenic and lymphangiogenic effector among VEGFs delivered into skeletal muscle via adenoviruses. *Circ Res,* 92**,** 1098-106.

ROBERTS, S., NARISAWA, S., HARMEY, D., MILLÁN, J. L. & FARQUHARSON, C. 2007. Functional involvement of PHOSPHO1 in matrix vesicle-mediated skeletal mineralization. *J Bone Miner Res,* 22**,** 617-27.

ROBERTS, S. J., STEWART, A. J., SADLER, P. J. & FARQUHARSON, C. 2004. Human PHOSPHO1 exhibits high specific phosphoethanolamine and phosphocholine phosphatase activities. *Biochem J,* 382**,** 59-65.

ROCHE, B., DAVID, V., VANDEN-BOSSCHE, A., PEYRIN, F., MALAVAL, L., VICO, L. & LAFAGE-PROUST, M. H. 2012. Structure and quantification of microvascularisation within mouse long bones: what and how should we measure? *Bone,* 50**,** 390-9.

RODRIGUEZ-FLOREZ, N., GARCIA-TUNON, E., MUKADAM, Q., SAIZ, E., OLDKNOW, K. J., FARQUHARSON, C., MILLÁN, J. L., BOYDE, A. & SHEFELBINE, S. J. 2015. An investigation of the mineral in ductile and brittle cortical mouse bone. *J Bone Miner Res,* 30**,** 786-95.

ROODMAN, G. D. 1992. Interleukin-6: an osteotropic factor? *J Bone Miner Res,* 7**,** 475-8.

ROSCHGER, P., RINNERTHALER, S., YATES, J., RODAN, G. A., FRATZL, P. & KLAUSHOFER, K. 2001. Alendronate increases degree and uniformity of mineralization in cancellous bone and decreases the porosity in cortical bone of osteoporotic women. *Bone,* 29**,** 185-91.

ROWE, P. S., DE ZOYSA, P. A., DONG, R., WANG, H. R., WHITE, K. E., ECONS, M. J. & OUDET, C. L. 2000. MEPE, a new gene expressed in bone marrow and tumors causing osteomalacia. *Genomics,* 67**,** 54-68.

RUBANYI, G. M. & VANHOUTTE, P. M. 1986. Superoxide anions and hyperoxia inactivate endothelium-derived relaxing factor. *Am J Physiol,* 250**,** H822-7.

RUBIN, C. T. & LANYON, L. E. 1984. Regulation of bone formation by applied dynamic loads. *J Bone Joint Surg Am,* 66**,** 397-402.

RUBIN, C. T. & LANYON, L. E. 1985. Regulation of bone mass by mechanical strain magnitude. *Calcif Tissue Int,* 37**,** 411-7.

RYAN, N. A., ZWETSLOOT, K. A., WESTERKAMP, L. M., HICKNER, R. C., POFAHL, W. E. & GAVIN, T. P. 2006. Lower skeletal muscle capillarization and VEGF expression in aged vs. young men. *J Appl Physiol (1985),* 100**,** 178-85.

RYU, S. J., RYU, D. S., KIM, J. Y., PARK, J. Y., KIM, K. H., CHIN, D. K., KIM, K. S., CHO, Y. E. & KUH, S. U. 2015. Bone Mineral Density Changes after Orchiectomy using a Scrotal Approach in Rats. *Korean J Spine,* 12**,** 55-9.

SAINSON, R. C., AOTO, J., NAKATSU, M. N., HOLDERFIELD, M., CONN, E., KOLLER, E. & HUGHES, C. C. 2005. Cell-autonomous notch signaling regulates endothelial cell branching and proliferation during vascular tubulogenesis. *FASEB J,* 19**,** 1027-9.

SAITO, H., GASSER, A., BOLAMPERTI, S., MAEDA, M., MATTHIES, L., JÄHN, K., LONG, C. L., SCHLÜTER, H., KWIATKOWSKI, M., SAINI, V., PAJEVIC, P. D., BELLIDO, T., VAN WIJNEN, A. J., MOHAMMAD, K. S., GUISE, T. A., TAIPALEENMÄKI, H. & HESSE, E. 2019. TG-interacting factor 1 (Tgif1)-deficiency attenuates bone remodeling and blunts the anabolic response to parathyroid hormone. *Nat Commun,* 10**,** 1354.

SALOMÉ, M., PEYRIN, F., CLOETENS, P., ODET, C., LAVAL-JEANTET, A. M., BARUCHEL, J. & SPANNE, P. 1999. A synchrotron radiation microtomography system for the analysis of trabecular bone samples. *Med Phys,* 26**,** 2194-204.

SCHITO, L. 2019. Hypoxia-Dependent Angiogenesis and Lymphangiogenesis in Cancer. *Adv Exp Med Biol,* 1136**,** 71-85.

SCHITO, L. & SEMENZA, G. L. 2016. Hypoxia-Inducible Factors: Master Regulators of Cancer Progression. *Trends Cancer,* 2**,** 758-770.

SCHNEIDER, P., KRUCKER, T., MEYER, E., ULMANN-SCHULER, A., WEBER, B., STAMPANONI, M. & MULLER, R. 2009a. Simultaneous 3D visualization and quantification of murine bone and bone vasculature using micro-computed tomography and vascular replica. *Microsc Res Tech,* 72**,** 690-701.

SCHNEIDER, P., KRUCKER, T., MEYER, E., ULMANN-SCHULER, A., WEBER, B., STAMPANONI, M. & MÜLLER, R. 2009b. Simultaneous 3D visualization and quantification of murine bone and bone vasculature using micro-computed tomography and vascular replica. *Microsc Res Tech,* 72**,** 690-701.

SCHNEIDER, P., STAUBER, M., VOIDE, R., STAMPANONI, M., DONAHUE, L. R. & MULLER, R. 2007a. Ultrastructural properties in cortical bone vary greatly in two inbred strains of mice as assessed by synchrotron light based micro- and nano-CT. *J Bone Miner Res,* 22**,** 1557-70.

SCHNEIDER, P., STAUBER, M., VOIDE, R., STAMPANONI, M., DONAHUE, L. R. & MÜLLER, R. 2007b. Ultrastructural properties in cortical bone vary greatly in two inbred strains of mice as assessed by synchrotron light based micro- and nano-CT. *J Bone Miner Res,* 22**,** 1557-70.

SCHNEIDER, P., VOIDE, R., STAMPANONI, M., DONAHUE, L. R. & MULLER, R. 2013. The importance of the intracortical canal network for murine bone mechanics. *Bone,* 53**,** 120-8.

SCHUIT, S. C., VAN DER KLIFT, M., WEEL, A. E., DE LAET, C. E., BURGER, H., SEEMAN, E., HOFMAN, A., UITTERLINDEN, A. G., VAN LEEUWEN, J. P. & POLS, H. A. 2004. Fracture incidence and association with bone mineral density in elderly men and women: the Rotterdam Study. *Bone,* 34**,** 195-202.

SEEMAN, E. 2001. Clinical review 137: Sexual dimorphism in skeletal size, density, and strength. *J Clin Endocrinol Metab,* 86**,** 4576-84.

SEEMAN, E. 2002. Pathogenesis of bone fragility in women and men. *Lancet,* 359**,** 1841-50.

SENEL, K., BAYKAL, T., SEFEROGLU, B., ALTAS, E. U., BAYGUTALP, F., UGUR, M. & KIZILTUNC, A. 2013. Circulating vascular endothelial growth factor concentrations in patients with postmenopausal osteoporosis. *Archives of medical science : AMS,* 9**,** 709-712.

SENGER, D. R., GALLI, S. J., DVORAK, A. M., PERRUZZI, C. A., HARVEY, V. S. & DVORAK, H. F. 1983. Tumor cells secrete a vascular permeability factor that promotes accumulation of ascites fluid. *Science,* 219**,** 983-5.

SFEROPOULOS, N. K. 2010. Synostosis of the proximal tibiofibular joint. *Case Rep Med,* 2010**,** 794594.

SHALABY, F., HO, J., STANFORD, W. L., FISCHER, K. D., SCHUH, A. C., SCHWARTZ, L., BERNSTEIN, A. & ROSSANT, J. 1997. A requirement for Flk1 in primitive and definitive hematopoiesis and vasculogenesis. *Cell,* 89**,** 981-90.

SHALABY, F., ROSSANT, J., YAMAGUCHI, T. P., GERTSENSTEIN, M., WU, X. F., BREITMAN, M. L. & SCHUH, A. C. 1995. Failure of blood-island formation and vasculogenesis in Flk-1-deficient mice. *Nature,* 376**,** 62-6.

SHAPIRO, I. M., GOLUB, E. E., CHANCE, B., PIDDINGTON, C., OSHIMA, O., TUNCAY, O. C., FRASCA, P. & HASELGROVE, J. C. 1988. Linkage between energy status of perivascular cells and mineralization of the chick growth cartilage. *Dev Biol,* 129**,** 372-9.

SHIBUYA, M. 1995. Role of VEGF-flt receptor system in normal and tumor angiogenesis. *Adv Cancer Res,* 67**,** 281-316.

SHIBUYA, M., YAMAGUCHI, S., YAMANE, A., IKEDA, T., TOJO, A., MATSUSHIME, H. & SATO, M. 1990. Nucleotide sequence and expression of a novel human receptor-type tyrosine kinase gene (flt) closely related to the fms family. *Oncogene,* 5**,** 519-24.

SIDER, K. L., SONG, J. & DAVIES, J. E. 2010. A new bone vascular perfusion compound for the simultaneous analysis of bone and vasculature. *Microsc Res Tech,* 73**,** 665-72.

SIETSEMA, W. K. 1995. Animal models of cortical porosity. *Bone,* 17**,** 297S-305S.

SILBERMANN, M. & FROMMER, J. 1972. The nature of endochondral ossification in the mandibular condyle of the mouse. *Anat Rec,* 172**,** 659-67.

SILVESTRINI, G., BALLANTI, P., PATACCHIOLI, F., LEOPIZZI, M., GUALTIERI, N., MONNAZZI, P., TREMANTE, E., SARDELLA, D. & BONUCCI, E. 2005. Detection of osteoprotegerin (OPG) and its ligand (RANKL) mRNA and protein in femur and tibia of the rat. *J Mol Histol,* 36**,** 59-67.

SINGER, F. R. 2009. Paget disease: when to treat and when not to treat. *Nat Rev Rheumatol,* 5**,** 483-9.

SIRIS, E. S. & FELDMAN, F. 1997. Natural history of untreated Paget's disease of the tibia. *J Bone Miner Res,* 12**,** 691-2.

SISON, K., EREMINA, V., BAELDE, H., MIN, W., HIRASHIMA, M., FANTUS, I. G. & QUAGGIN, S. E. 2010. Glomerular structure and function require paracrine, not autocrine, VEGF-VEGFR-2 signaling. *J Am Soc Nephrol,* 21**,** 1691-701.

SIVARAJ, K. K. & ADAMS, R. H. 2016. Blood vessel formation and function in bone. *Development,* 143**,** 2706-15.

SKAAR, T. C. & DESTA, Z. 2018. CYP2D6 and Endoxifen in Tamoxifen Therapy: A Tribute to David A. Flockhart. *Clin Pharmacol Ther,* 103**,** 755-757.

SMAIL, P. J., REYES, F. I., J.S.D, W. & FAIMAN, C. 1981. *The Fetal Hormonal Environment and its Effect on the Morphogenesis of the Genital System*, Springer, Dordrecht.

SMIT, T. H., BURGER, E. H. & HUYGHE, J. M. 2002. A case for strain-induced fluid flow as a regulator of BMU-coupling and osteonal alignment. *J Bone Miner Res,* 17**,** 2021-9.

SMITH, S. J., EMERY, R., PITSILLIDES, A., CLARKIN, C. E. & MAHAJAN, S. 2017. Detection of early osteogenic commitment in primary cells using Raman spectroscopy. *Analyst,* 142**,** 1962-1973.

SOLTANOFF, C. S., YANG, S., CHEN, W. & LI, Y. P. 2009. Signaling networks that control the lineage commitment and differentiation of bone cells. *Crit Rev Eukaryot Gene Expr,* 19**,** 1-46.

SPECTOR, J. A., MEHRARA, B. J., GREENWALD, J. A., SAADEH, P. B., STEINBRECH, D. S., BOULETREAU, P. J., SMITH, L. P. & LONGAKER, M. T. 2001. Osteoblast expression of vascular endothelial growth factor is modulated by the extracellular microenvironment. *Am J Physiol Cell Physiol,* 280**,** C72-80.

ST-JACQUES, B., HAMMERSCHMIDT, M. & MCMAHON, A. P. 1999. Indian hedgehog signaling regulates proliferation and differentiation of chondrocytes and is essential for bone formation. *Genes Dev,* 13**,** 2072-86.

STAINES, K. A., MACKENZIE, N. C., CLARKIN, C. E., ZELENCHUK, L., ROWE, P. S., MACRAE, V. E. & FARQUHARSON, C. 2012. MEPE is a novel regulator of growth plate cartilage mineralization. *Bone,* 51**,** 418-30.

STAINES, K. A., POULET, B., WENTWORTH, D. N. & PITSILLIDES, A. A. 2017. The STR/ort mouse model of spontaneous osteoarthritis - an update. *Osteoarthritis Cartilage,* 25**,** 802-808.

STEENBOCK, H. & HERTING, D. C. 1955. Vitamin D and growth. *J Nutr,* 57**,** 449-68.

STEENDIJK, R. & BOYDE, A. 1973. Scanning electron microscopic observations on bone from patients with hypophosphataemic (vitamin D resistant) rickets. *Calcif Tissue Res,* 11**,** 242-50.

STEFANINI, M. O., WU, F. T., MAC GABHANN, F. & POPEL, A. S. 2009. The presence of VEGF receptors on the luminal surface of endothelial cells affects VEGF distribution and VEGF signaling. *PLoS Comput Biol,* 5**,** e1000622.

STENBECK, G. & HORTON, M. A. 2000. A new specialized cell-matrix interaction in actively resorbing osteoclasts. *J Cell Sci,* 113 (Pt 9)**,** 1577-87.

STOUT, S. D., BRUNSDEN, B. S., HILDEBOLT, C. F., COMMEAN, P. K., SMITH, K. E. & TAPPEN, N. C. 1999. Computer-assisted 3D reconstruction of serial sections of cortical bone to determine the 3D structure of osteons. *Calcif Tissue Int,* 65**,** 280-4.

STREETEN, E. A. & BRANDI, M. L. 1990. Biology of bone endothelial cells. *Bone Miner,* 10**,** 85-94.

STUERMER, E. K., SEHMISCH, S., RACK, T., WENDA, E., SEIDLOVA-WUTTKE, D., TEZVAL, M., WUTTKE, W., FROSCH, K. H. & STUERMER, K. M. 2010. Estrogen and raloxifene improve metaphyseal fracture healing in the early phase of osteoporosis. A new fracture-healing model at the tibia in rat. *Langenbecks Arch Surg,* 395**,** 163-72.

STUTTFELD, E. & BALLMER-HOFER, K. 2009. Structure and function of VEGF receptors. *IUBMB Life,* 61**,** 915-22.

SUGIYAMA, T., MEAKIN, L. B., GALEA, G. L., JACKSON, B. F., LANYON, L. E., EBETINO, F. H., RUSSELL, R. G. & PRICE, J. S. 2011. Risedronate does not reduce mechanical loading-related increases in cortical and trabecular bone mass in mice. *Bone,* 49**,** 133-9.

SUN, D., HUANG, A., SMITH, C. J., STACKPOLE, C. J., CONNETTA, J. A., SHESELY, E. G., KOLLER, A. & KALEY, G. 1999. Enhanced release of prostaglandins contributes to flow-induced arteriolar dilation in eNOS knockout mice. *Circ Res,* 85**,** 288-93.

SUN, L. Y., FANG, Y., PATKI, A., KOOPMAN, J. J., ALLISON, D. B., HILL, C. M., MASTERNAK, M. M., DARCY, J., WANG, J., MCFADDEN, S. & BARTKE, A. 2017. Longevity is impacted by growth hormone action during early postnatal period. *Elife,* 6.

SUNDARAM, K., KLARE, C. M. & MOSCHETTI, W. E. 2018. Proximal tibiofibular osteoarthritis presenting as pain after total knee arthroplasty treated successfully with fusion of the proximal tibial-fibular joint. *Arthroplast Today,* 4**,** 139-142.

TAGUE, R. G. 1992. Sexual dimorphism in the human bony pelvis, with a consideration of the Neandertal pelvis from Kebara Cave, Israel. *Am J Phys Anthropol,* 88**,** 1-21.

TAICHMAN, R. S. 2005. Blood and bone: two tissues whose fates are intertwined to create the hematopoietic stem-cell niche. *Blood,* 105**,** 2631-9.

TAKAHASHI, H. & SHIBUYA, M. 2005. The vascular endothelial growth factor (VEGF)/VEGF receptor system and its role under physiological and pathological conditions. *Clin Sci (Lond),* 109**,** 227-41.

TAKAHASHI, N., YAMANA, H., YOSHIKI, S., ROODMAN, G. D., MUNDY, G. R., JONES, S. J., BOYDE, A. & SUDA, T. 1988. Osteoclast-like cell formation and its regulation by osteotropic hormones in mouse bone marrow cultures. *Endocrinology,* 122**,** 1373-82.

TAMAMURA, Y., OTANI, T., KANATANI, N., KOYAMA, E., KITAGAKI, J., KOMORI, T., YAMADA, Y., COSTANTINI, F., WAKISAKA, S., PACIFICI, M., IWAMOTO, M. & ENOMOTO-IWAMOTO, M. 2005. Developmental regulation of Wnt/beta-catenin signals is required for growth plate assembly, cartilage integrity, and endochondral ossification. *J Biol Chem,* 280**,** 19185-95.

TAPPEN, N. C. 1977. Three-dimensional studies on resorption spaces and developing osteons. *Am J Anat,* 149**,** 301-17.

TAYLOR, S. E., SHAH, M. & ORRISS, I. R. 2014. Generation of rodent and human osteoblasts. *Bonekey Rep,* 3**,** 585.

TEAM, R. D. C. 2011. *R: A Language and Environment for Statistical Computing* [Online]. Available: http://www.R-project.org/ [Accessed 28.09.2018].

TERMAN, B. I., CARRION, M. E., KOVACS, E., RASMUSSEN, B. A., EDDY, R. L. & SHOWS, T. B. 1991. Identification of a new endothelial cell growth factor receptor tyrosine kinase. *Oncogene,* 6**,** 1677-83.

TERMAN, B. I., DOUGHER-VERMAZEN, M., CARRION, M. E., DIMITROV, D., ARMELLINO, D. C., GOSPODAROWICZ, D. & BÖHLEN, P. 1992. Identification of the KDR tyrosine kinase as a receptor for vascular endothelial cell growth factor. *Biochem Biophys Res Commun,* 187**,** 1579-86.

THORMANN, U., EL KHAWASSNA, T., RAY, S., DUERSELEN, L., KAMPSCHULTE, M., LIPS, K., VON DEWITZ, H., HEINEMANN, S., HEISS, C., SZALAY, G., LANGHEINRICH, A. C., IGNATIUS, A., SCHNETTLER, R. & ALT, V. 2014. Differences of bone healing in metaphyseal defect fractures between osteoporotic and physiological bone in rats. *Injury,* 45**,** 487-93.

THURNER, P. J., CHEN, C. G., IONOVA-MARTIN, S., SUN, L., HARMAN, A., PORTER, A., AGER, J. W., 3RD, RITCHIE, R. O. & ALLISTON, T. 2010. Osteopontin deficiency increases bone fragility but preserves bone mass. *Bone,* 46**,** 1564-73.

TIEDE-LEWIS, L. M., XIE, Y., HULBERT, M. A., CAMPOS, R., DALLAS, M. R., DUSEVICH, V., BONEWALD, L. F. & DALLAS, S. L. 2017. Degeneration of the osteocyte network in the C57BL/6 mouse model of aging. *Aging (Albany NY),* 9**,** 2190-2208.

TOBIUME, H., KANZAKI, S., HIDA, S., ONO, T., MORIWAKE, T., YAMAUCHI, S., TANAKA, H. & SEINO, Y. 1997. Serum bone alkaline phosphatase isoenzyme levels in normal children and children with growth hormone (GH) deficiency: a potential marker for bone formation and response to GH therapy. *J Clin Endocrinol Metab,* 82**,** 2056-61.

TOLAR, J., TEITELBAUM, S. L. & ORCHARD, P. J. 2004. Osteopetrosis. *N Engl J Med,* 351**,** 2839-49.

TOLCHER, A. W., SARANTOPOULOS, J., PATNAIK, A., PAPADOPOULOS, K., LIN, C. C., RODON, J., MURPHY, B., ROTH, B., MCCAFFERY, I., GORSKI, K. S., KAISER, B., ZHU, M., DENG, H., FRIBERG, G. & PUZANOV, I. 2009. Phase I, pharmacokinetic, and pharmacodynamic study of AMG 479, a fully human monoclonal antibody to insulin-like growth factor receptor 1. *J Clin Oncol,* 27**,** 5800-7.

TOMBRAN-TINK, J. & BARNSTABLE, C. J. 2004. Osteoblasts and osteoclasts express PEDF, VEGF-A isoforms, and VEGF receptors: possible mediators of angiogenesis and matrix remodeling in the bone. *Biochem Biophys Res Commun,* 316**,** 573-9.

TONG, X., CHEN, X., ZHANG, S., HUANG, M., SHEN, X., XU, J. & ZOU, J. 2019. The Effect of Exercise on the Prevention of Osteoporosis and Bone Angiogenesis. *Biomed Res Int,* 2019**,** 8171897.

TORTORA, G. & DERRICKSON, B. 2014. *Principles of anatomy & physiology*.

TROUILLET-ASSANT, S., GALLET, M., NAUROY, P., RASIGADE, J. P., FLAMMIER, S., PARROCHE, P., MARVEL, J., FERRY, T., VANDENESCH, F., JURDIC, P. & LAURENT, F. 2015. Dual impact of live Staphylococcus aureus on the osteoclast lineage, leading to increased bone resorption. *J Infect Dis,* 211**,** 571-81.

TRUETA, J. & BUHR, A. J. 1963. THE VASCULAR CONTRIBUTION TO OSTEOGENESIS. V. THE VASCULATURE SUPPLYING THE EPIPHYSIAL CARTILAGE IN RACHITIC RATS. *J Bone Joint Surg Br,* 45**,** 572-81.

TRUETA, J. & HARRISON, M. H. 1953. The normal vascular anatomy of the femoral head in adult man. *J Bone Joint Surg Br,* 35-B**,** 442-61.

TRUETA, J. & TRIAS, A. 1961. The vascular contribution to osteogenesis. IV. The effect of pressure upon the epiphysial cartilage of the rabbit. *J Bone Joint Surg Br,* 43-B**,** 800-13.

TSUJI-TAMURA, K. & OGAWA, M. 2018. Morphology regulation in vascular endothelial cells. *Inflamm Regen,* 38**,** 25.

UCHIDA, K., URABE, K., NARUSE, K., KOZAI, Y., ONUMA, K., MIKUNI-TAKAGAKI, Y., KASHIMA, I., UENO, M., SAKAI, R., ITOMAN, M. & TAKASO, M. 2012. Differential age-related bone architecture changes between female and male STR/Ort mice. *Exp Anim,* 61**,** 59-66.

VAN DER GEER, P., HUNTER, T. & LINDBERG, R. A. 1994. Receptor protein-tyrosine kinases and their signal transduction pathways. *Annu Rev Cell Biol,* 10**,** 251-337.

VAUPEL, P., MAYER, A. & HÖCKEL, M. 2004. Tumor hypoxia and malignant progression. *Methods Enzymol,* 381**,** 335-54.

VEVERKA, V., HENRY, A. J., SLOCOMBE, P. M., VENTOM, A., MULLOY, B., MUSKETT, F. W., MUZYLAK, M., GREENSLADE, K., MOORE, A., ZHANG, L., GONG, J., QIAN, X., PASZTY, C., TAYLOR, R. J., ROBINSON, M. K. & CARR, M. D. 2009. Characterization of the structural features and interactions of sclerostin: molecular insight into a key regulator of Wnt-mediated bone formation. *J Biol Chem,* 284**,** 10890-900.

VRAHNAS, C., BLANK, M., DITE, T. A., TATARCZUCH, L., ANSARI, N., CRIMEEN-IRWIN, B., NGUYEN, H., FORWOOD, M. R., HU, Y., IKEGAME, M., BAMBERY, K. R., PETIBOIS, C., MACKIE, E. J., TOBIN, M. J., SMYTH, G. K., OAKHILL, J. S., MARTIN, T. J. & SIMS, N. A. 2019. Increased autophagy in EphrinB2-deficient osteocytes is associated with elevated secondary mineralization and brittle bone. *Nature Communications,* 10**,** 3436.

WALLACE, I. J., RUBIN, C. T. & LIEBERMAN, D. E. 2015. Osteoporosis. *Evol Med Public Health,* 2015**,** 343.

WAN, C., GILBERT, S. R., WANG, Y., CAO, X., SHEN, X., RAMASWAMY, G., JACOBSEN, K. A., ALAQL, Z. S., EBERHARDT, A. W., GERSTENFELD, L. C., EINHORN, T. A., DENG, L. & CLEMENS, T. L. 2008. Activation of the hypoxia-inducible factor-1alpha pathway accelerates bone regeneration. *Proc Natl Acad Sci U S A,* 105**,** 686-91.

WANG, D. S., YAMAZAKI, K., NOHTOMI, K., SHIZUME, K., OHSUMI, K., SHIBUYA, M., DEMURA, H. & SATO, K. 1996. Increase of vascular endothelial growth factor mRNA expression by 1,25-dihydroxyvitamin D3 in human osteoblast-like cells. *J Bone Miner Res,* 11**,** 472-9.

WANG, J., BINGAMAN, S. & HUXLEY, V. H. 2010. Intrinsic sex-specific differences in microvascular endothelial cell phosphodiesterases. *Am J Physiol Heart Circ Physiol,* 298**,** H1146-54.

WANG, L., ZHOU, F., ZHANG, P., WANG, H., QU, Z., JIA, P., YAO, Z., SHEN, G., LI, G., ZHAO, G., LI, J., MAO, Y., XIE, Z., XU, W. & XU, Y. 2017. Human type H vessels are a sensitive biomarker of bone mass. *Cell Death Dis,* 8**,** e2760.

WANG, X., MABREY, J. D. & AGRAWAL, C. M. 1998. An interspecies comparison of bone fracture properties. *Biomed Mater Eng,* 8**,** 1-9.

WANG, Y., WAN, C., DENG, L., LIU, X., CAO, X., GILBERT, S. R., BOUXSEIN, M. L., FAUGERE, M. C., GULDBERG, R. E., GERSTENFELD, L. C., HAASE, V. H., JOHNSON, R. S., SCHIPANI, E. & CLEMENS, T. L. 2007. The hypoxia-inducible factor alpha pathway couples angiogenesis to osteogenesis during skeletal development. *J Clin Invest,* 117**,** 1616-26.

WANG, Y. X., CROFTON, J. T., BEALER, S. L. & SHARE, L. 1997. Sexual dimorphism in regional blood flow responses to vasopressin in conscious rats. *Am J Physiol,* 273**,** R1126-31.

WHEATLEY, C. M., SNYDER, E. M., JOHNSON, B. D. & OLSON, T. P. 2014. Sex differences in cardiovascular function during submaximal exercise in humans. *Springerplus,* 3**,** 445.

WHITE, T. D. & FOLKENS, P. A. 2005. *The human bone manual,* Oxford, Academic.

WICKHAM, H. 2016. ggplot2: Elegant Graphics for Data Analysis. *Springer-Verlag New York*.

WILLINGHAMM, M. D., BRODT, M. D., LEE, K. L., STEPHENS, A. L., YE, J. & SILVA, M. J. 2010. Age-related changes in bone structure and strength in female and male BALB/c mice. *Calcif Tissue Int,* 86**,** 470-83.

WINKLER, D. G., SUTHERLAND, M. K., GEOGHEGAN, J. C., YU, C., HAYES, T., SKONIER, J. E., SHPEKTOR, D., JONAS, M., KOVACEVICH, B. R., STAEHLING-HAMPTON, K., APPLEBY, M., BRUNKOW, M. E. & LATHAM, J. A. 2003. Osteocyte control of bone formation via sclerostin, a novel BMP antagonist. *EMBO J,* 22**,** 6267-76.

WITZENBICHLER, B., MAISONPIERRE, P. C., JONES, P., YANCOPOULOS, G. D. & ISNER, J. M. 1998. Chemotactic properties of angiopoietin-1 and -2, ligands for the endothelial-specific receptor tyrosine kinase Tie2. *J Biol Chem,* 273**,** 18514-21.

WOOLARD, J., WANG, W. Y., BEVAN, H. S., QIU, Y., MORBIDELLI, L., PRITCHARD-JONES, R. O., CUI, T. G., SUGIONO, M., WAINE, E., PERRIN, R., FOSTER, R., DIGBY-BELL, J., SHIELDS, J. D., WHITTLES, C. E., MUSHENS, R. E., GILLATT, D. A., ZICHE, M., HARPER, S. J. & BATES, D. O. 2004. VEGF165b, an inhibitory vascular endothelial growth factor splice variant: mechanism of action, in vivo effect on angiogenesis and endogenous protein expression. *Cancer Res,* 64**,** 7822-35.

WU, Y., HUANG, A., SUN, D., FALCK, J. R., KOLLER, A. & KALEY, G. 2001. Gender-specific compensation for the lack of NO in the mediation of flow-induced arteriolar dilation. *Am J Physiol Heart Circ Physiol,* 280**,** H2456-61.

XIONG, J., CAWLEY, K., PIEMONTESE, M., FUJIWARA, Y., ZHAO, H., GOELLNER, J. J. & O'BRIEN, C. A. 2018. Soluble RANKL contributes to osteoclast formation in adult mice but not ovariectomy-induced bone loss. *Nat Commun,* 9**,** 2909.

XIONG, J., PIEMONTESE, M., ONAL, M., CAMPBELL, J., GOELLNER, J. J., DUSEVICH, V., BONEWALD, L., MANOLAGAS, S. C. & O'BRIEN, C. A. 2015. Osteocytes, not Osteoblasts or Lining Cells, are the Main Source of the RANKL Required for Osteoclast Formation in Remodeling Bone. *PLoS One,* 10**,** e0138189.

YADAV, M. C., SIMAO, A. M., NARISAWA, S., HUESA, C., MCKEE, M. D., FARQUHARSON, C. & MILLAN, J. L. 2011. Loss of skeletal mineralization by the simultaneous ablation of PHOSPHO1 and alkaline phosphatase function: a unified model of the mechanisms of initiation of skeletal calcification. *J Bone Miner Res,* 26**,** 286-97.

YANG, Y. Q., TAN, Y. Y., WONG, R., WENDEN, A., ZHANG, L. K. & RABIE, A. B. 2012. The role of vascular endothelial growth factor in ossification. *Int J Oral Sci,* 4**,** 64-8.

YASUI, T., KADONO, Y., NAKAMURA, M., OSHIMA, Y., MATSUMOTO, T., MASUDA, H., HIROSE, J., OMATA, Y., YASUDA, H., IMAMURA, T., NAKAMURA, K. & TANAKA, S. 2011. Regulation of RANKL-induced osteoclastogenesis by TGF-β through molecular interaction between Smad3 and Traf6. *J Bone Miner Res,* 26**,** 1447-56.

YEH, J. K., CHEN, M. M. & ALOIA, J. F. 1996. Ovariectomy-induced high turnover in cortical bone is dependent on pituitary hormone in rats. *Bone,* 18**,** 443-50.

YING, C., HSU, W. L., HONG, W. F., CHENG, W. T. & YANG, Y. 2000. Estrogen receptor is expressed in pig embryos during preimplantation development. *Mol Reprod Dev,* 55**,** 83-8.

YOSHIDA, H., HAYASHI, S., KUNISADA, T., OGAWA, M., NISHIKAWA, S., OKAMURA, H., SUDO, T. & SHULTZ, L. D. 1990. The murine mutation osteopetrosis is in the coding region of the macrophage colony stimulating factor gene. *Nature,* 345**,** 442-4.

YOUNG, K., WOMBLE, M., WISE, J., DESAIX, P., KRUSE, D., POE, B., JOHNSON, E., JOHNSON, J., KOROL, O. & BETTS, J. 2003. *Anatomy & Physiology*, Open Stax College.

ZEBAZE, R. & SEEMAN, E. 2015. Cortical bone: a challenging geography. *J Bone Miner Res,* 30**,** 24-9.

ZEBAZE, R. M., GHASEM-ZADEH, A., BOHTE, A., IULIANO-BURNS, S., MIRAMS, M., PRICE, R. I., MACKIE, E. J. & SEEMAN, E. 2010. Intracortical remodelling and porosity in the distal radius and post-mortem femurs of women: a cross-sectional study. *Lancet,* 375**,** 1729-36.

ZELZER, E., MAMLUK, R., FERRARA, N., JOHNSON, R. S., SCHIPANI, E. & OLSEN, B. R. 2004. VEGFA is necessary for chondrocyte survival during bone development. *Development,* 131**,** 2161-71.

ZELZER, E., MCLEAN, W., NG, Y. S., FUKAI, N., REGINATO, A. M., LOVEJOY, S., D'AMORE, P. A. & OLSEN, B. R. 2002. Skeletal defects in VEGF(120/120) mice reveal multiple roles for VEGF in skeletogenesis. *Development,* 129**,** 1893-904.

ZHANG, L. F., QI, J., ZUO, G., JIA, P., SHEN, X., SHAO, J., KANG, H., YANG, H. & DENG, L. 2014. Osteoblast-secreted factors promote proliferation and osteogenic differentiation of bone marrow stromal cells via VEGF/heme-oxygenase-1 pathway. *PLoS One,* 9**,** e99946.

ZHANG, M., XUAN, S., BOUXSEIN, M. L., VON STECHOW, D., AKENO, N., FAUGERE, M. C., MALLUCHE, H., ZHAO, G., ROSEN, C. J., EFSTRATIADIS, A. & CLEMENS, T. L. 2002. Osteoblast-specific knockout of the insulin-like growth factor (IGF) receptor gene reveals an essential role of IGF signaling in bone matrix mineralization. *J Biol Chem,* 277**,** 44005-12.

ZHAO, W., BYRNE, M. H., WANG, Y. & KRANE, S. M. 2000. Osteocyte and osteoblast apoptosis and excessive bone deposition accompany failure of collagenase cleavage of collagen. *J Clin Invest,* 106**,** 941-9.

ZHU, Y., RUAN, Z., LIN, Z., LONG, H., ZHAO, R., SUN, B., CHENG, L., TANG, L., XIA, Z., LI, C. & ZHAO, S. 2019. The association between CD31. *J Bone Miner Metab*.

ZOCH, M. L., CLEMENS, T. L. & RIDDLE, R. C. 2016. New insights into the biology of osteocalcin. *Bone,* 82**,** 42-9.